

MODELING AND EXPERIMENTAL ANALYSIS OF MULTIFAULTS IN A TAPERED ROLLER BEARING SYSTEM

**Thesis Submitted
in Partial Fulfilment of the Requirements for the
Degree of**

DOCTOR OF PHILOSOPHY

**in
Mechanical Engineering**

by

ABDUL KHALIQ ANSARI

(Roll No. :- 2K18/Ph.D/ME/04)

Under the Supervision of

Dr. Paras Kumar

Associate Professor

Mechanical Engineering Department

Delhi Technological University,

Delhi-42



DELHI TECHNOLOGICAL UNIVERSITY

(Formerly Delhi College of Engineering)

Main Bawana Road, Shahabad Daultapur, New Delhi, Delhi 110042 India

June 2025



DELHI TECHNOLOGICAL UNIVERSITY

(Formerly Delhi College of Engineering)

Shahbad Daultpur, Main Bawana Road, Delhi-42

CANDIDATE'S DECLARATION

I Abdul Khaliq Ansari hereby certify that the work which is being presented in the thesis entitled Modeling and Experimental Analysis of Multifaults in a Tapered Roller Bearing System in partial fulfillment of the requirements for the award of the Degree of Doctor of Philosophy, submitted in the Department of Mechanical Engineering, Delhi Technological University is an authentic record of my own work carried out during the period from August 2018 To June 2025 under the supervision of Dr. Paras Kumar.

The matter presented in the thesis has not been submitted by me for the award of any other degree of this or any other Institute.

Candidate's Signature

Abdul Khaliq Ansari

(2K18/PHDME/04)

DTU, New Delhi

Place:

Date:



DELHI TECHNOLOGICAL UNIVERSITY

(Formerly Delhi College of Engineering)

Shahbad Daulatpur, Main Bawana Road, Delhi-42

CERTIFICATE BY THE SUPERVISOR

Certified that Mr. Abdul Khaliq Ansari (2K18/PHDME/04) has carried out their search work presented in this thesis entitled “Modeling and Experimental Analysis of Multifaults in a Tapered Roller Bearing System” for the award of Doctor of Philosophy from Department of Mechanical Engineering, Delhi Technological University, Delhi, under my supervision. The thesis embodies results of original work, and studies are carried out by the student himself and the contents of the thesis do not form the basis for the award of any other degree to the candidate or to anybody else from this or any other University/Institution.

Signature

Dr. Paras Kumar
Associate Professor
Department of Mechanical Engineering
Delhi Technological University

Date:

ACKNOWLEDGEMENT

I am greatly indebted to my supervisor **Dr. Paras Kumar**, Department of Mechanical Engineering, Delhi Technological University, Delhi, for their invaluable guidance, constant inspiration, numerous suggestions and continued support throughout this research work. I am profoundly grateful to them with reverence for helping me with the necessary information and equipments.

I would like to express my sincere gratitude to **Prof. Atul Kumar Agrawal**, DRC Chairman, **Prof. B.B. Arora**, Head, Mechanical Engineering Department, **Prof. S.K. Garg**, Former Head, Mechanical Engineering Department, Delhi Technological University, for their valuable help, motivation and extending all the necessary processing and experimental facilities during my research work. I am very thankful to **Prof. Ahmad Ali Khan (AMU)**, **Prof. Ajeet Kumar (IIT-D)**, **Prof. R.C. Singh (DTU)** and **Prof. A.S. Rao (DTU)** for being members of my SRC committee.

I would like to thank my fellow lab mates Dr. Anuj, Aakash, Dr. Yamika, Dr. Pooja, Dr. Gaurav and Dr. Ratnesh for helping and encouraging me throughout my research. A special thanks to my friend Dr. Deepak who enlightened me with a different approach to tackling the process of publication.

I would like to thank Mr. Narendra Bisht and Dr. Phool Singh for helping me during lab engagements.

I am greatly indebted to my parents for their love and blessings to see me scaling greater heights of life. Without their motivation and encouragement, the pursuit of this PhD work would have never been possible.

With immense pleasure and delight, I would like to thank my wife Sumaira for giving me moral support in the highs and lows of this PhD journey. I appreciate my son Arsalan for showering her love and affection during my PhD work.

I would like to express my deepest gratitude to my late supervisor, **Prof. Vikas Rastogi**, for his unwavering mental and moral support throughout the highs and lows of my Ph.D. journey. It was under his vision and guidance that I embarked on this doctoral path. If today I stand proud of this achievement, it is undoubtedly his mentorship that laid the foundation. It was both an honour and a privilege to have been under his tutelage. I dedicate this thesis to his cherished memory with profound respect and gratitude.

Abdul Khaliq Ansari
(2K18/PHDME/04)

Date:

ABSTRACT

Rolling element bearings are widely employed in the industrial and domestic machines and appliances due to their ease in mounting and efficient operational features. About 80% bearings found in the industrial machines happens to be the rolling bearings. Numerous factors contribute to the deterioration of these bearings, primarily including wear, ageing, environmental influences, improper installation, inadequate lubrication, and material fatigue. A defective bearing frequently leads to reduced efficiency or, in some instances, significant injury to the machine. Consequently, health monitoring and fault diagnosis have gained significant attention in recent years, and they can be performed utilising various information, including acoustic emission, stress waveforms, oil analysis, temperature, and vibration. The prevalent method employed for defect detection is vibration monitoring and analysis, which provides critical insights into anomalies occurring within the internal structure of bearings.

This study investigates the vibration-damping behaviour of four different types of antifriction bearings through experimental and computational analyses. Experiments are conducted on a customized rotor-bearing test rig with data acquisition through the OROS NV-Gate software at both the drive end (DE) and non-drive end (NDE). The damping characteristics are evaluated through static and dynamic analyses. Additionally, the study employs Taguchi and ANOVA methods to assess the effects of load and rotational speed on the vibrations and noise of healthy tapered roller bearings (SKF30206). The Taguchi method, which integrates statistical and mathematical techniques, is used to establish relationships between input parameters and system response. Twenty-seven experiments have been performed using the L27 design of experiments (DOE) approach, considering two factors (speed and load) at three levels.

Further experiments are conducted on tapered roller bearings with inner race, outer race, roller, and compound defects. A DOE framework comprising 64 experiments is designed by incorporating two continuous and one categorical factor at four levels. Beyond traditional signal processing techniques, soft computing methods are explored

to automate defect detection partially. The efficiency and relevance of this study are significantly enhanced by integrating machine learning and classifier algorithms for automated fault diagnosis. Time and frequency domain features were extracted from 800 signal datasets to ensure optimal model performance and ranked using one-way ANOVA and Kruskal-Wallis selection techniques. Initially, machine learning models are trained and tested for automated defect classification, followed by a comparative analysis of different classifiers available in MATLAB.

The results indicate that tapered roller bearings exhibit superior damping capacity compared to cylindrical, spherical, and self-aligned bearings. The contact between rolling elements and raceways played a crucial role in the damping behaviour of antifriction bearings. For both healthy and defective TRBs, vibration response data—measured in terms of root mean square (RMS), kurtosis, and noise levels (Leq) are analyzed to evaluate performance. The study highlights the effectiveness of combined parametric effect analysis with DOE and the Taguchi method in predicting the behaviour of tapered roller bearings within rotor-bearing systems. Furthermore, computational analysis demonstrates that feature selection through ranking mechanisms significantly enhances machine learning model efficiency. Among various classifiers, the highest defect classification accuracy is achieved using the top 10 features ranked by the Kruskal–Wallis test with classification accuracies of 79.0%, 86.6%, 92.9%, 97.6%, 81.9%, and 64.4% for linear, quadratic, cubic, fine, medium, and coarse models, respectively. The Kruskal–Wallis test outperforms the One-way ANOVA in feature selection and further improves the classification accuracy. This integrated approach offers a robust predictive framework for assessing the performance of TRB (tapered roller bearings) and automating defect diagnosis in rotor-bearing systems.

LIST OF PUBLICATIONS

The work conducted in this research has resulted in the following major publications:

Research Papers Published/ Accepted in Journals

- 1) Ansari, Abdul Khaliq, and Paras Kumar. "Vibration and acoustics analyses of tapered roller bearing." *Journal of Vibration Engineering & Technologies* 12.2 (2024): 2467-2484. <https://doi.org/10.1007/s42417-023-00991-9> (SCIE, IF-2.7).
- 2) Ansari, Abdul Khaliq, and Paras Kumar. "Experimental investigation of the static and dynamic damping behaviour of antifriction bearings." *Nondestructive Testing and Evaluation* (2024): 1-22. <https://doi.org/10.1080/10589759.2024.2322658> (SCIE, IF-4.2).
- 3) Ansari, Abdul Khaliq, and Paras Kumar. "Vibro-acoustic analysis of defective taper roller bearings." *Tribology International*. 199 (2024): 110044. <https://doi.org/10.1016/j.triboint.2024.110044> (SCIE, IF-6.9).
- 4) Ansari, Abdul Khaliq, and Paras Kumar. "Enhancing Machine Learning Classifier Performance in Bearing Fault Diagnosis through Feature-Based Ranking." *Mesurement*. 257 (2025): 118661 <https://doi.org/10.1016/j.measurement.2025.118661> (SCIE, IF- 5.6).

Research Papers Presented in International Conferences

- 1) Ansari, A.K., Kumar, P. and Rastogi, V., 2022. Dynamic behavior of aluminium matrix composite rotor on bearing vibration. *Materials Today: Proceedings*, 62, pp.233-238. <https://doi.org/10.1016/j.matpr.2022.03.026> "International Conference on Advances in Materials and Mechanical Engineering (ICAMME – 2022) held on 18th -19th Feb 2022 at AKJEC, UP, India. (Scopus Index)
- 2) Ansari, A.K., Kumar, P. and Rastogi, V., 2024. Machine Learning Algorithms for Multi-Defect Bearing Analysis. "International Conference on Manufacturing, Material Science and Engineering (ICMMSE-2024), held on 16th -17th August 2024 at Vignan Institute of Technology, Hyderabad, Telangana, India. (Scopus Index) (AIP conference proceedings)

TABLE OF CONTENTS

ACKNOWLEDGEMENT	iv
ABSTRACT	vi
LIST OF PUBLICATIONS	viii
TABLE OF CONTENTS	ix
LIST OF TABLES	xiv
LIST OF FIGURES	xvi
LIST OF ABBREVIATIONS	xx
LIST OF SYMBOLS	xxiii
Chapter 1 Introduction	1
1.1 Background and Motivation.....	1
1.2 Tapered Roller Bearing	6
1.3 General Causes of Bearing Defects.....	9
1.4 Defects in Bearings	10
1.4.1 Localized Defects.....	10
1.4.2 Distributed Defects.....	12
1.4.3 Defect in Bearing Elements	12
1.5 Maintenance Strategies	14
1.6 Machine Health Monitoring Techniques	15
1.6.1 Acoustic Emission.....	16

1.6.2 Thermography	16
1.6.3 Oil Debris	17
1.6.4 Vibration Analysis	17
1.7 Vibration Signal Processing and Data Analysis.....	19
1.8 Structure of the Thesis	21
Chapter 2 Literature Review	23
2.1 Introduction	23
2.2 Literature Survey on the Damping of the Rotor Bearing System	24
2.3 Literature Survey on Rotor Bearing Fault Detection and Diagnosis	27
2.4 Automated Fault Detection using Machine Learning Techniques.....	36
2.5 Research Gaps Based on Literature Review	38
2.6 Objectives of this Research	39
Chapter 3 Design and Development of an Experimental Framework for a Tapered Roller Bearing System	40
3.1 Introduction	40
3.2 Experimental Test Rig.....	40
3.2.1 Tapered Roller Bearing System and its Metallic Structure.....	41
3.2.2 D.C. Motor and Speed Controller	42
3.2.3 Flexible Coupling.....	42
3.2.4 Signal Acquisition and Display System.....	43
3.3 Experimental Arrangement for Impact Testing or Damping Analysis	45
3.4 Experimental Arrangement for Bearing Analysis.....	47
3.4.1 Test Rig	48
3.4.2 Sound Level Meter	49
3.4.3 Bearings Under Study	49

3.4.4 Defects Creation in Test Bearings	49
3.5 Summary of the Chapter	52
Chapter 4 Damping Analysis of Anti-friction Bearings	53
4.1 Introduction	53
4.2 Damping Identification Methods	55
4.2.1 Static Condition.....	56
4.2.2 Dynamic Condition	58
4.3 Results and Discussion.....	59
4.3.1 Static Condition.....	59
4.3.2 Dynamic Condition	70
4.4 Summary of the Chapter	72
Chapter 5 Vibration Behaviour of Healthy Tapered Roller Bearing at Different Operating Load and Speed	75
5.1 Introduction	75
5.2 Design of Experiment using the Taguchi Technique	77
5.3 Results and Discussion.....	81
5.3.1 Effect of Process Parameters on L_{eq}	81
5.3.2 Effect of Process Parameters on RMS	85
5.3.3 Contour and Response Surface Plot.....	90
5.4 Summary of the Chapter	91
Chapter 6 Vibration Behaviour of Faulty Tapered Roller-Bearing	93
6.1 Introduction	93
6.2 Experimental Methodology.....	94
6.3 Results and Discussion.....	100
6.3.1 Effect of Process Parameters on RMS	101

6.3.2 Effect of Process Parameters on Leq	105
6.3.3 Effect of Process Parameters on Kurtosis	109
6.3.4 Response Surface Plot.....	113
6.4 Summary of the Chapter	116
Chapter 7 Automated Fault Diagnosis for a Tapered Roller-Bearing System using a Machine Learning Approach.....	119
7.1 Introduction	119
7.2 Machine Learning Approaches	121
7.3 Hyperparameter Tuning for Machine Learning Models	124
7.4 Feature Ranking Techniques.....	126
7.4.1 One-way ANOVA.....	126
7.4.2 Kruskal-Wallis test.....	127
7.5 Experimental Methodology.....	128
7.6 Data set for Fault Classification.....	129
7.7 Results and Discussion.....	130
7.7.1 Raw data.....	131
7.7.2 Feature Ranking	132
7.7.3 Feature Selection and Model Training.....	134
7.8 Summary of the Chapter	149
Chapter 8 Conclusions, Future Scope and Implications	150
8.1 Contributions of the Work	150
8.2 Conclusions	151
8.3 Future Scope of Work	153
8.4 Implication of Work.....	154
REFERENCES.....	155

LIST OF PUBLICATIONS AND THEIR PROOFS	177
CURRICULUM VITAE/BRIEF PROFILE	180

LIST OF TABLES

Table 2.1 Literature review	32
Table 3.1 Shaft details.....	41
Table 3.2 Antifriction bearing's specification	46
Table 3.3 Tapered roller bearing specifications	51
Table 4.1 Damping coefficients of different bearings	61
Table 4.2. RMS (m/s^2) value of the acceleration of tapered roller bearing	70
Table 4.3. RMS (m/s^2) value of the acceleration of cylindrical roller bearing	70
Table 4.4. RMS (m/s^2) value of the acceleration of spherical roller bearing	70
Table 4.5. RMS (m/s^2) value of the acceleration of self-aligned bearing	71
Table 5.1 Input parameters and their level.....	78
Table 5.2 I/P (uncoded form) and O/P (or response) parameters as per DOE and experiment results	79
Table 5.3 Signal-to-noise ratio for RMS DE, RMS NDE, Leq DE and Leq NDE	80
Table 5.4 Response table for signal-to-noise ratio.....	80
Table 5.5 ANOVA effect for S/N Ratios of Leq (DE)	82
Table 5.6 ANOVA effect for S/N Ratios of Leq (NDE).....	85
Table 5.7 ANOVA effect for S/N Ratios for RMS DE.....	87
Table 5.8 ANOVA effect for S/N Ratios for RMS NDE.....	88
Table 5.9 Kurtosis value at different RPM and different loading conditions	91
Table 6.1 Input parameters and levels for experimental design.....	97
Table 6.2 Experimental design matrix	98
Table 6.3 Regression values of response parameters.....	100
Table 6.4 Model significance of RMS using ANOVA	102
Table 6.5 Model significance of Leq using ANOVA	106
Table 6.6 Model significance of kurtosis using ANOVA.....	110
Table 7.1 Description of tapered bearing dataset chosen for fault diagnosis.....	129
Table 7.2 Time-domain and frequency-domain features used for fault classification	131

Table 7.3 Features ranked by Ow-A and KW Test.....	132
Table 7.4 Performance metrics of ML models with and without using feature ranking for test data.....	146

LIST OF FIGURES

Figure 1.1 Important elements of a typical rolling element bearing	2
Figure 1.2 Bearing market share	3
Figure 1.3 Leeds bradford airport site	4
Figure 1.4 Huntly derailment site	5
Figure 1.5 Tapered roller bearing	6
Figure 1.6 Internal dimension for tapered roller bearing performance analysis	7
Figure 1.7 Schematic drawing of a tapered roller bearing indicating nomenclature ..	8
Figure 1.8 Subsurface-initiated spall at a hard inclusion (top) and Surface-initiated crack network from a surface defect	11
Figure 1.9 Localised bearing defects: (a) outer-race defect, (b) inner-race defect, and (c) roller element defect	11
Figure 1.10 Images of naturally born distributed faults (a) Outer and (b) Inner race	12
Figure 1.11 Abrased outer ring raceway of spherical roller bearing	12
Figure 1.12 Components of condition-based maintenance	14
Figure 3.1 Line diagram of test rig.....	41
Figure 3.2 DC Motor with speed controller	42
Figure 3.3 Flexible coupling	42
Figure 3.4 Front panel of Oros	43
Figure 3.5 Back panel of Oros	44
Figure 3.6 Display of signal	44
Figure 3.7 Experimental test rig for damping analysis	46
Figure 3.8 Different rolling element or antifriction bearings.....	47
Figure 3.9 Experimental test rig for bearing analysis	48
Figure 3.10 (a) Sound level meter (b) CAD model of TRB (c) Healthy TRB (d) Prefabricated faults in different parts of TRB (e) Dimensions of faults	51
Figure 4.1 Areas of damping application.....	54
Figure 4.2 Methods for experimental identification of damping	55
Figure 4.3 Zoomed view of cylindrical bearing graphs for damping calculation.....	60
Figure 4.4 Tapered roller bearing.....	64

Figure 4.5 Cylindrical roller bearing.....	65
Figure 4.6 Spherical roller bearing.....	66
Figure 4.7 Self-aligned bearing.....	67
Figure 4.8 Combined free decay graph for all bearings.....	68
Figure 4.9 Combined FRFs for all bearings.....	69
Figure 4.10 RMS value of acceleration at a different speed under different loading conditions	72
Figure 5.1 Flowchart of the proposed methodology	77
Figure 5.2 Effect of process parameter on Leq DE.....	83
Figure 5.3 Effect of process parameter on Leq NDE.....	83
Figure 5.4 Residual plot of Leq DE	84
Figure 5.5 Residual plot of Leq NDE	84
Figure 5.6 Residual plot for RMS DE.....	86
Figure 5.7 Effect of process parameter on RMS DE	87
Figure 5.8 Effect of process parameter on RMS NDE.....	87
Figure 5.9 Residual plot for RMS NDE.....	88
Figure 5.10 Pareto chart	89
Figure 5.11 Contour and Surface plot of interaction.....	90
Figure 6.1 Flowchart of the proposed methodology	95
Figure 6.2 Effect of process parameters on RMS	104
Figure 6.3 Residual plot for RMS	104
Figure 6.4 Pareto chart for RMS	105
Figure 6.5 Effect of process parameter on Leq	108
Figure 6.6 Residual plot for Leq	108
Figure 6.7 Pareto chart for Leq	109
Figure 6.8 Effect of process parameters in kurtosis	112
Figure 6.9 Residual plot for kurtosis.....	112
Figure 6.10 Pareto chart for kurtosis.....	113
Figure 6.11 Surface plot of interaction for RMS	115
Figure 6.12 Surface plot of interaction for Leq.....	116
Figure 6.13 Surface plot of interaction for kurtosis	116
Figure 7.1 Two sets of data points are divided by distinct hyperplanes in SVM ...	124

Figure 7.2 Methodology flowchart	128
Figure 7.3 Collective vibration raw data of 20 faults from test bearing	131
Figure 7.4 Collective Power Spectrum density data of 20 faults from test bearing.	132
Figure 7.5 Normalized results of OwA and KW test for test bearing data	134
Figure 7.6 Fault classification by SVM model for all features without ranking (i) SP linear kernel (ii) CM for linear kernel (iii) SP quadratic kernel (iv) CM quadratic kernel (v) SP for cubic kernel (vi) CM for cubic kernel (vii) SP for fine kernel (viii) CM for fine kernel (ix) SP for medium kernel (x) CM for medium kernel (xi) SP for coarse kernel (xii) CP for coarse kernel	137
Figure 7.7 Fault classification by SVM model for top five features of OwA test (i) SP linear kernel (ii) CM for linear kernel (iii) SP quadratic kernel (iv) CM quadratic kernel (v) SP for cubic kernel (vi) CM for cubic kernel (vii) SP for fine kernel (viii) CM for fine kernel (ix) SP for medium kernel (x) CM for medium kernel (xi) SP for coarse kernel (xii) CP for coarse kernel	139
Figure 7.8 Fault classification by SVM model for top five features of KW test) (i) SP linear kernel (ii) CM for linear kernel (iii) SP quadratic kernel (iv) CM quadratic kernel (v) SP for cubic kernel (vi) CM for cubic kernel (vii) SP for fine kernel (viii) CM for fine kernel (ix) SP for medium kernel (x) CM for medium kernel (xi) SP for coarse kernel (xii) CP for coarse kernel	141
Figure 7.9 Fault classification by SVM model for top 10 features of OwA test) (i) SP linear kernel (ii) CM for linear kernel (iii) SP quadratic kernel (iv) CM quadratic kernel (v) SP for cubic kernel (vi) CM for cubic kernel (vii) SP for fine kernel (viii) CM for fine kernel (ix) SP for medium kernel (x) CM for medium kernel (xi) SP for coarse kernel (xii) CP for coarse kernel	143
Figure 7.10 Fault classification by SVM model for top 10 features of KW test) (i) SP linear kernel (ii) CM for linear kernel (iii) SP quadratic kernel (iv) CM quadratic kernel (v) SP for cubic kernel (vi) CM for cubic kernel (vii) SP for fine kernel (viii) CM for fine kernel (ix) SP for medium kernel (x) CM for medium kernel (xi) SP for coarse kernel (xii) CP for coarse kernel	145
Figure 7.11 Influence of feature ranking on classification accuracy of SVM models with different kernels	147

Figure 7.12 Influence of feature ranking on training time of SVM models with different kernels	148
Figure 7.13 Influence of feature ranking on speed of SVM models with different kernels	148

LIST OF ABBREVIATIONS

AE	Acoustic Emission
ANOVA	Analysis of variance
ANN	Artificial neural network
ANN	Artificial neural networks
CF	Cage fault
CWRU	Case Western Reserve University
CA	Classification Accuracy
CD	Combined fault
CI	Confidence Interval
CM	Confusion Matrix
CWT	Continuous Wavelet Transform
CWT	Continuous Wavelet Transform
DOE	Design of experiment
DWT	Discrete Wavelet Transform
DE	Drive End
EDM	Electrical discharge machining
EMD	Empirical Mode Decomposition
EMD	Empirical Mode Decomposition
EWT	Empirical Wavelet Transform
EEMD	Ensemble empirical mode decomposition
FFT	Fast Fourier transform
FFT	Fast Fourier transform
FD	Fault Diagnosis
FI	Fault Identification
FVRP	Frequency versus residual plot
GA	Genetic algorithm
HMM	Hidden Markov Mode
HMM	Hidden Markov model

HMM	Hidden Markov modelling
HHT	Hilbert–Huang Transform
HHT	Hilbert–Huang transform
IWPT	Improve wavelet package transform
IR	Inner race
IMF	Intrinsic mode functions
IFFT	Inverse fast Fourier transform
IFFT	Inverse fast Fourier transform
INF	Inverse filtering
KNN	k-nearest neighbours
KNN	K-nearest neighbours
KW	Kruskal-Wallis
ML	Machine Learning
MEPFM	Main effect plot for means
MAE	Mean absolute error
MED	Minimum entropy deconvolution
MCSA	Motor Current Signature Analysis
MKACNN	Multi-kernel attention convolutional neural network
MKACNN	Multi-kernel attention convolutional neural network
MOMEDA	Multipoint optimal minimum entropy deconvolution adjusted
MOMEDA	Multipoint optimal minimum entropy deconvolution adjusted
MSSRS	Multi-scale SR spectrogram
MSMFIF	Multi-sensor based multi-frequency information fusion
MSMFIF	Multi-sensor based multi-frequency information fusion
NHLC	Non- Hertzian line contact stiffness
NDE	Non-Drive End
OwA	One-Way Anova
OR	Outer race
PS	Prediction Speed
PSVM	Proximal Support Vector Machine
RBF	Radial Basis Function

RVM	Relevance Vector Machine
RVFV	Residuals versus fitted value
RVOP	Residuals versus order plot
RSM	Response surface methodology
RSM	Response surface methodology
RPM	Revolution per minute
RMS	Root Mean Square
RMSE	Root mean square error
SP	Scatter Plot
STFT	Short-Time Fourier Transform
SINAD	Signal to Noise and Distortion Ratio
SNR	Signal to Noise Ratio
SD	Standard deviation
SWT	Stationary Wavelet Transform
SVM	Support vector machine
SVM	Support vector machine
SVR	Support Vector Regression
TRB	Tapered Roller Bearing
THD	Total Harmonic Distortion
TT	Training Time
WPD	Wavelet Packet Decomposition

LIST OF SYMBOLS

ϕ	Angle of the load
$\Delta\omega$	Bandwidth of the vibration amplitude peak
ζ	Damping ratio
ϵ	Error observed in the response.
ω_n	First Natural frequency
α_i	Lagrange multipliers
δ	Logarithmic decrement
ω_1 and ω_2	Minimum and maximum frequencies at half-power amplitude
α	Significance level
σ	Standard deviation
λ	Transformation parameter

Chapter 1 Introduction

This chapter deals with the introduction of rolling element bearings. It briefly describes different types of defects in rolling element bearings and commonly available techniques for diagnosing the bearing defects. It also provides a basic understanding of bearing dynamics and the motivation of the present research work.

1.1 Background and Motivation

A bearing is a component that limits the relative movement between two machine elements and facilitates friction reduction to ensure smooth motion.

Bearings support and guide, with minimal friction, rotating or oscillating machine elements such as shafts, axles or wheels and transfer loads between machine components. They provide high precision and low friction, enabling high rotational speeds while reducing noise, heat, energy consumption and wear. Bearings are classified based on the nature of operation, permitted motions, and the directions of loads exerted on the components. They are broadly categorised into two types: rolling contact bearings and sliding contact bearings, based on their operational mechanism [1].

- 1) Plain/ Sliding bearing
 - a) Plain bearings
 - b) Fluid bearings
- 2) Rolling Element /Antifriction bearings
 - a) Ball-bearings
 - i. Deep-groove ball bearings
 - ii. Self-aligned ball bearings
 - iii. Angular contact ball bearings
 - b) Roller bearing
 - i. Cylindrical bearing
 - ii. Tapered roller bearing
 - iii. Spherical roller bearing

iv. Needle roller bearing

All rotating components in an engineering system need a machine element that maintains system configuration, provides support and direction, and uses minimal energy. In Rolling Element Bearings (REBs), the direct sliding of the shaft against the support is substituted by the rolling motion of the balls or rollers, which markedly diminishes friction.

A REB, regardless of its type, generally consists of four primary components, as illustrated in Fig. 1.1. Two rings, specifically an inner ring and an outer ring, a collection of rolling devices in the shape of balls or rollers, and a cage or retainer. The inner ring is securely affixed to the shaft, while the outer ring is typically supported within the housing or structure. The rolling elements are situated between the two rings, and the cage maintains uniform spacing among these rolling elements. The load from the shaft is sent to the inner ring, which is subsequently shared by several rolling elements, and from there it is conveyed to the outer ring and ultimately to the structure or housing.

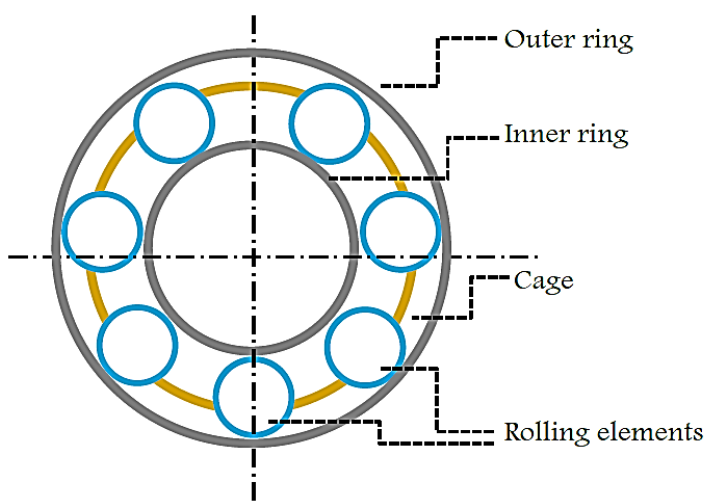


Figure 1.1 Important elements of a typical rolling element bearing [2]

Bearings are virtually used in every piece of equipment or machinery, ranging from automobile parts, farm equipment, and household appliances to defence and aerospace equipment. This factor is projected to drive market growth shortly. There has been a rising demand for bearings with lower maintenance requirements, higher efficiency,

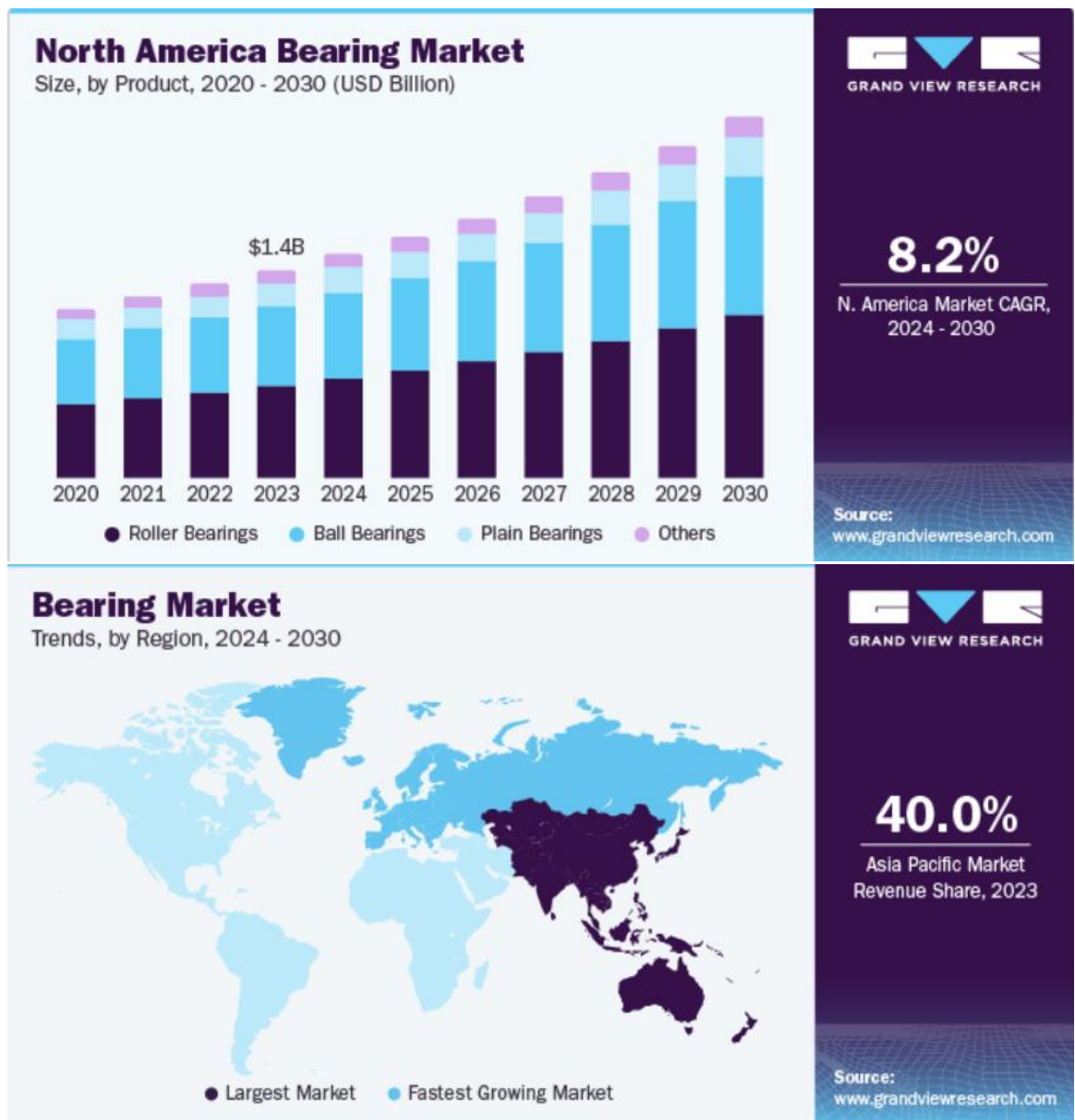


Figure 1.2 Bearing market share [3]

and longer service life. Moreover, a rise in demand for specialised bearing solutions that meet different industry-specific requirements and challenges is projected to boost the market. For instance, the rising application of high-capacity products in wind turbines is expected to catapult the demand. Wind turbines utilise these products to enhance performance and reliability, increase energy production, and reduce lubricant consumption. The energy sector poses application-specific bearings. For instance, the growth in the usage of bearings in the wind energy sector encourages suppliers to focus on the bearing products required to support wind energy applications.

The global bearings market was valued at USD 102.2 billion in 2018 and is anticipated to expand at a CAGR of 8.1% from 2019 to 2025 and 9.1% till 2030 [3]. Most global bearings market vendors have introduced sensor components in ball bearings. These elements help digitally monitor revolution speed, axial movement, deceleration, acceleration, and weight-carrying capacity. These bearings are used in road rollers, conveyors, and electric motors. Therefore, technical developments and innovations drive the growth of the global bearings market.



Figure 1.3 Leeds bradford airport site [4]

Typical varieties of rotating machinery include turbines, generators, compressors, pumps, motors, and engines. The malfunction of such equipment can result in considerable economic losses and, in extreme instances, threaten human safety. Research indicates that bearing failures are the predominant cause of malfunction in rotating machinery. A bearing malfunction enhances the rotational friction of the rotor. Consequently, the detection and identification of mechanical problems in rolling element bearings are essential for the reliability of the systems. Diagnosing the condition of a bearing can prevent unscheduled machinery failures and the expensive damage resulting from bearing failure.

In October 2007, a significant wheel-bearing failure caused a goods train to derail near Huntly, leading to eleven additional incidents in the following year—some

resulting in fires and infrastructure damage, yet astonishingly, no injuries were reported [4].

On 20 October 2023, as Storm Babet impacted the UK, a TUI flight with nearly 200 passengers deviated from the runway at Leeds Bradford Airport—its pilots surprised by an abrupt shaking from the aircraft’s nose gear. The underlying issue: a severe bearing failure, undetectable through standard inspection methods. Although there were no casualties, the event highlighted a significant weakness in contemporary aviation systems [5].



Figure 1.4 Huntly derailment site [5]

The incidents disrupted operations and posed risks to lives, highlighting a significant deficiency in our predictive maintenance capabilities. This thesis addresses the critical necessity of closing the existing gap through the creation of a comprehensive, sensor-driven, and intelligent diagnostic framework designed to detect early-stage bearing faults. With this endeavour, we strive to enhance the safety and reliability of transport systems, ensuring that potential failures are detected proactively rather than reactively, thereby safeguarding lives.

Two fundamental approaches for bearing maintenance are: statistical methods for bearing life estimation and condition monitoring coupled with diagnosis. The previous method depends on the projected lifespan derived from statistical analyses conducted

on laboratory testing. This projected lifespan may not correspond with the actual lifespan due to potential post-manufacturing defects and real-world operating situations that may not have been considered during laboratory evaluations. Consequently, due to this and the advancement of novel and effective signal processing techniques, the latter way emerged as the preferred option [6].

1.2 Tapered Roller Bearing

Tapered roller bearings shown in Fig. 1.5 can accommodate substantial axial forces, making them effective thrust bearings, while enduring significant radial forces. Tapered roller bearings (TRBs) can accommodate a combination of substantial radial and axial forces, making them prevalent in heavy-load applications. Misalignment in tapered roller bearings (TRBs) results in significant roller-edge loadings and unequal load distribution, rendering it more crucial than misalignment in other bearing types due to the tapered design and extended contact lines between the rollers and raceways.



Figure 1.5 Tapered roller bearing [7]

Description: The inner and outer ring raceways are cone segments, and the rollers are tapered so that the conical surfaces of the raceways and the roller axes, if projected, all meet at the same location on the bearing's main axis. The raceways' projection lines meet at a common point on the bearing axis (apex point), resulting in true rolling action and reduced frictional moments during operation. Tapered roller bearings' axial load carrying capacity improves with increasing contact angle ' α '. The contact angle is typically between 10° and 30° , as shown in Fig. 1.6.

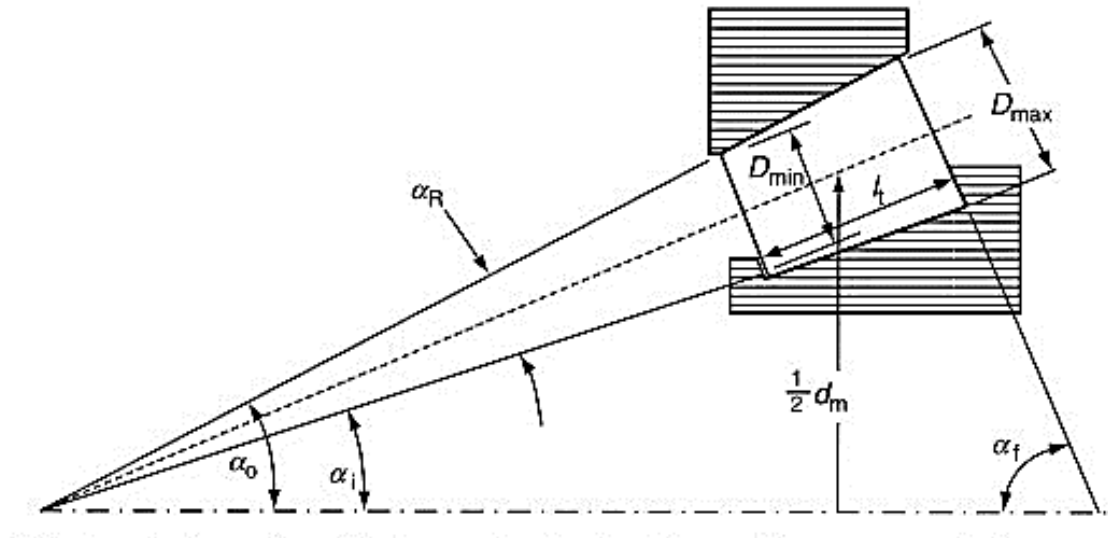


Figure 1.6 Internal dimension for tapered roller bearing performance analysis [8]

This conical geometry is used because it provides a larger contact patch, allowing for greater loads to be carried than with spherical (ball) bearings. Additionally, the geometry ensures that the tangential speeds of each roller's surfaces are the same as their raceways along the entire length of the contact patch, preventing differential scrubbing. A roller slides rather than rolls can cause wear at the roller-to-race interface, resulting in a scrubbing action due to surface speed variations. Wear degenerates the close tolerances generally held in the bearing, which might lead to other issues. A tapered roller bearing allows for much closer to pure rolling, avoiding quick wear. The inner ring has a flange that guides the rollers. This prevents the rollers from sliding out at high speeds due to momentum. The larger the half angles of these cones, the greater the axial force the bearing can withstand.

The nomenclature for tapered roller bearings differs from other roller bearing types. As illustrated in Fig. 1.7, the inner ring of the bearing is referred to as the cone, while the outer ring is termed the cup. The bearing's operation is linked to a pitch cone. Figure 1.6 also shows the dimensions and angles requisite for the performance study of tapered roller bearings. From Fig. 1.6, it can be seen that α_i , the inner raceway–roller contact angle = $\frac{1}{2}$ (cone-included angle); α_o , the outer raceway–roller contact angle = $\frac{1}{2}$ (cup-included angle); α_f , the roller large end-flange contact angle = $\frac{1}{2}$ (cone back face rib angle); and α_R is the roller-included angle. D_{max} is the large-end diameter of the roller and D_{min} is the small-end diameter of the roller, which has the end-to-end

length. Tapered roller bearings are frequently employed in back-to-back pairs to support axial forces in both directions equally. Tapered roller bearing pairs are utilised in automotive wheel bearings to concurrently withstand substantial vertical (radial) and horizontal (axial) strains.

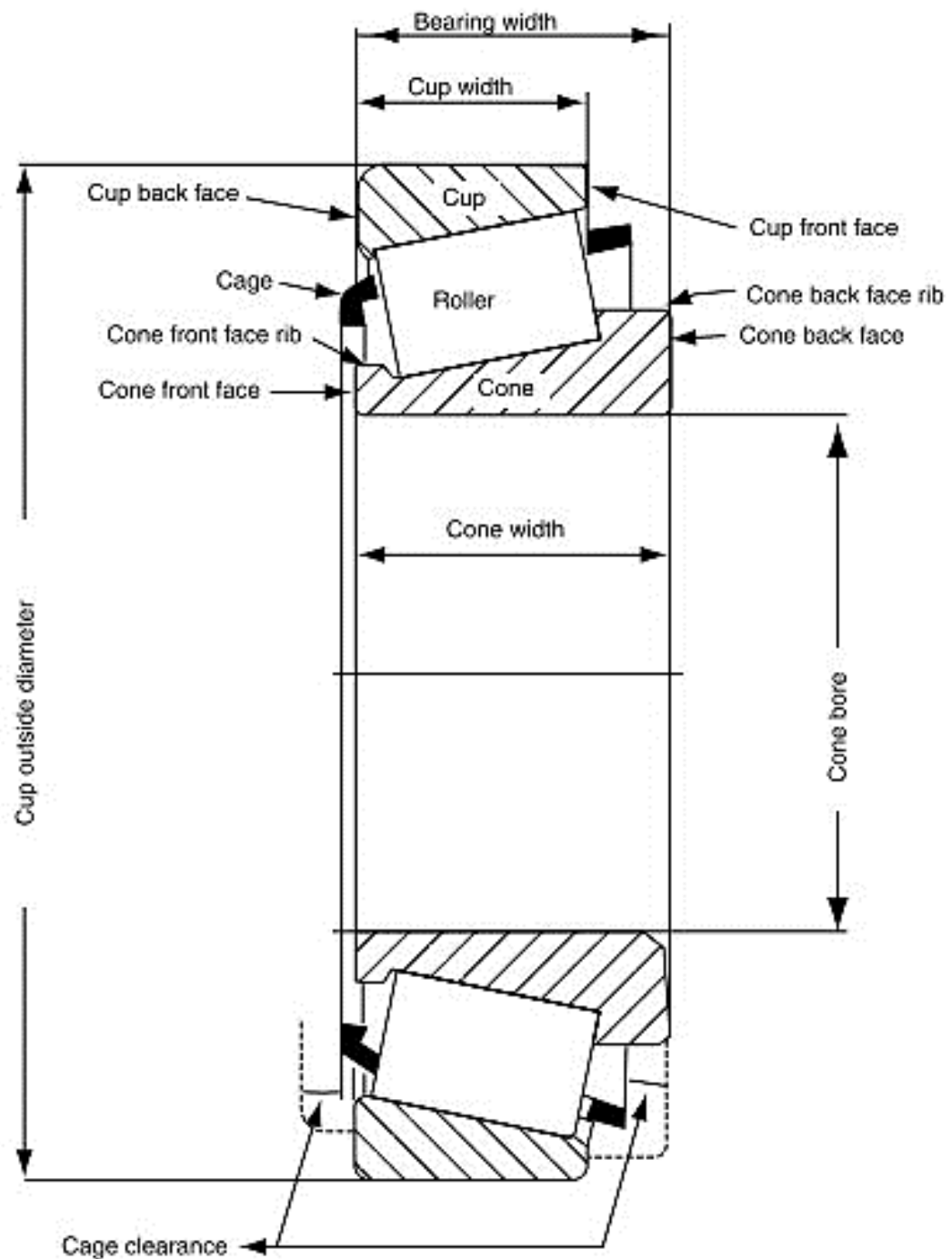


Figure 1.7 Schematic drawing of a tapered roller bearing indicating nomenclature [8]

1.3 General Causes of Bearing Defects

The causes of bearing failures are numerous. Although it isn't always easy to determine the precise cause, most bearing failures can be linked to at least one of the following important causes [8–10]:

- a) **Foreign matter:** Particles like dust, dirt, or metal can infiltrate the bearing, resulting in surface damage that contributes to heightened wear and vibration. This frequently arises due to inadequate sealing or unsanitary assembly conditions.
- b) **Incorrect mounting:** Incorrect installation techniques—like applying too much force or disregarding manufacturer instructions—can lead to internal stresses, misalignment, or harm to the bearing raceways and rolling elements.
- c) **Bearing misalignment:** When there is a misalignment between the shaft and housing, it can result in uneven load distribution, heightened friction, and localised stress. This situation accelerates wear and has the potential to lead to premature bearing failure.
- d) **Electrical damage:** Uncontrolled electric currents traversing the bearing can lead to the formation of pitting and fluting on the raceways. This form of damage frequently occurs in electric motors lacking adequate grounding or insulation.
- e) **Improper lubrication:** Employing an inappropriate lubricant, inadequate lubrication, or contaminated grease or oil can result in metal-to-metal contact, excessive heat production, and hastened wear of the bearing components.
- f) **Bearing fatigue and corrosion:** Extended exposure to cyclic loads results in material fatigue, which can lead to the spalling or flaking of the bearing surface. Furthermore, the presence of moisture or chemical exposure leads to corrosion, which compromises the integrity of the metal and shortens the lifespan of the bearing.
- g) **Defective sealing:** Defective or aged seals are ineffective in preventing contaminants from entering and maintaining lubrication, leading to dirt infiltration and lubricant depletion, which hastens deterioration and eventual failure.

- h) **High temperature:** High operating temperatures can deteriorate lubricants, modify material characteristics, and induce dimensional alterations in bearing components, potentially resulting in failure if not managed effectively.

1.4 Defects in Bearings

Bearing faults usually start as small pits or spalls and give sharp impulses in the early stages, covering a very wide frequency range (even in the ultrasonic frequency range of 100 kHz). However, for some faults such as brinelling, where a race is indented by the rolling elements, giving a permanent plastic deformation, the entry and exit events are not so sharp, and the range of excited frequencies is not so wide.

However, they would still generally be detected by envelope analysis. Several researchers have explained the mechanism of vibration in the bearings. Even a healthy bearing generates vibration, but the presence of defects increases vibration levels significantly. Many factors, the most common of which are fatigue, wear, plastic deformation, corrosion, brinelling, poor lubrication, faulty installation and incorrect design, can cause premature bearing failures. Identifying these defects and their vibration is important for the condition monitoring of bearings. The bearing defects are broadly classified into two categories: i.e. localized and distributed [11].

1.4.1 Localized Defects

A localised defect in the context of mechanical systems refers to a specific, confined area of damage or irregularity on a component's surface. This type of defect is typically not spread uniformly but occurs in a specific region, leading to distinct impacts on system behavior. This category of defects includes pits, cracks, and spalls that may develop over the rolling surfaces. Of these, spalling is the dominant mode of failure. Fatigue crack begins below the surface, propagating towards the surface until the material fails and leaves localised defects. Bentley in his paper showed that 90% of the total bearing faults involve damage to the inner ring, outer ring and rolling elements due to localised defects. The spall can have a surface or subsurface origin. A spall originating at the surface usually begins as a crack at a surface defect or at a debris dent that propagates into a crack network to form a spall. A crack that begins at a stress

riser, such as a hard inclusion below the running track in the region of the maximum shearing stress, also propagates into a crack network to form a spall [11]

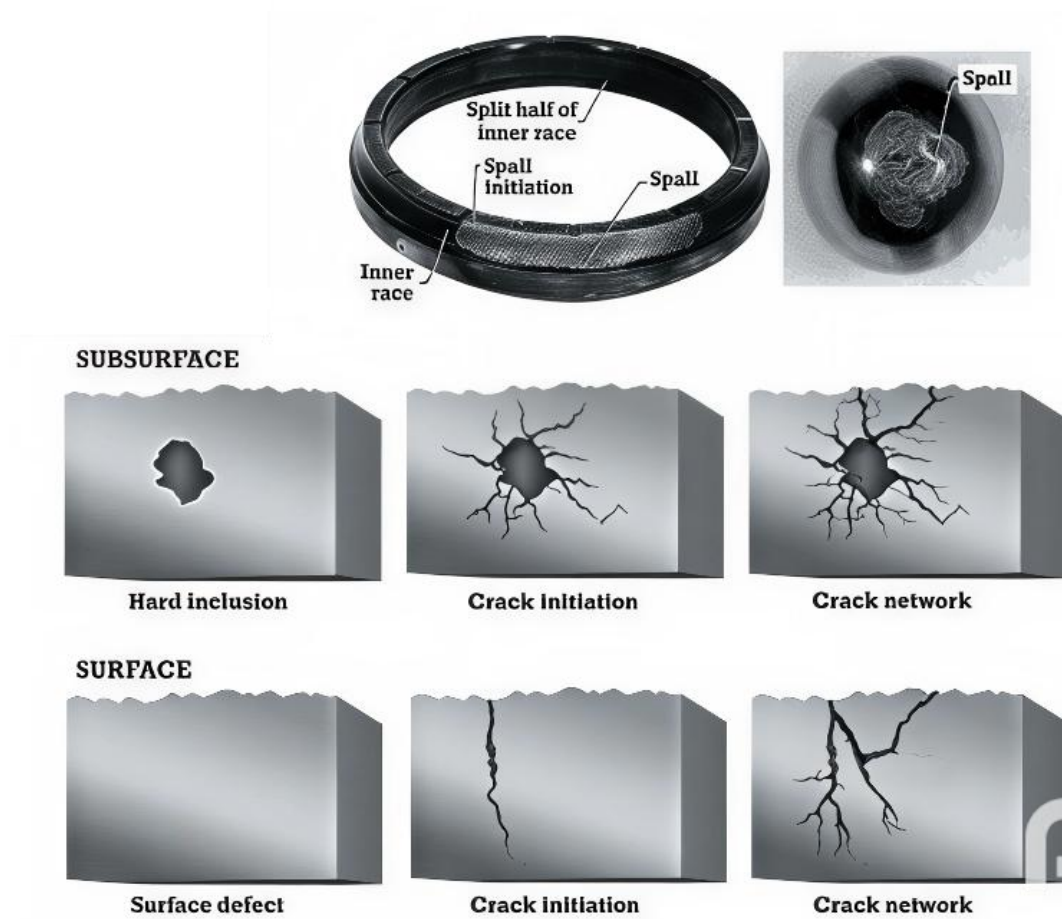


Figure 1.8 Subsurface-initiated spall at a hard inclusion (top) and Surface-initiated crack network from a surface defect [12]

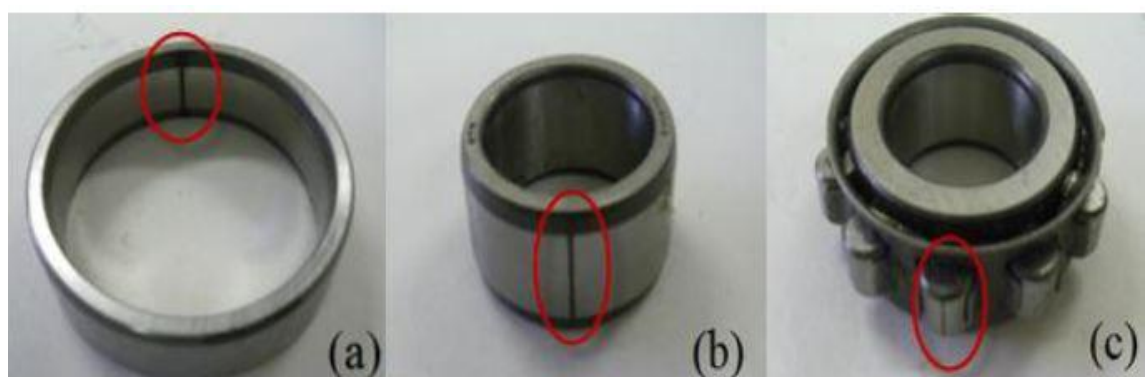


Figure 1.9 Localised bearing defects: (a) outer-race defect, (b) inner-race defect, and (c) roller element defect [12]

1.4.2 Distributed Defects

Distributed defects include surface roughness, waviness, misaligned races and off-size rolling elements. The main causes of distributed defects are manufacturing errors, abrasive wear, and improper installation. In distributed defects, the contact force between rolling elements and raceways varies, which results in vibration. Vibration response due to distributed defects is mainly used for the quality inspection and condition monitoring of bearings [8, 11].

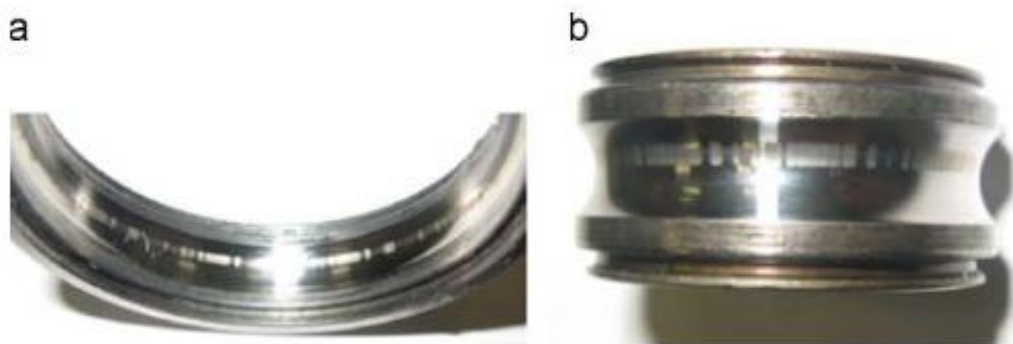


Figure 1.10 Images of naturally born distributed faults (a) Outer and (b) Inner race [12]

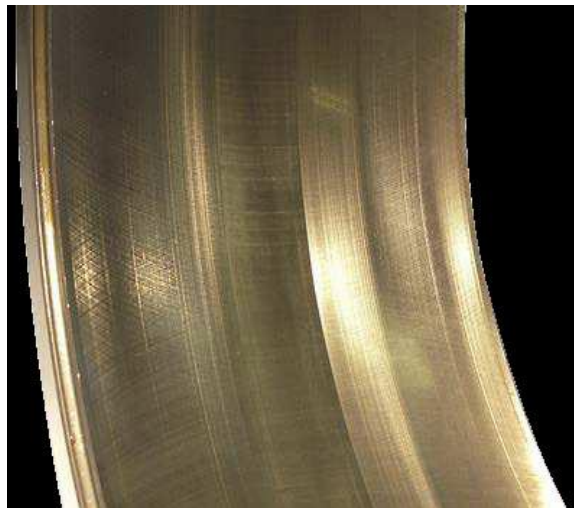


Figure 1.11 Abrased outer ring raceway of spherical roller bearing [13]

1.4.3 Defect in Bearing Elements

Defects may exist in several components, including surface roughness of the inner or outer race, waviness, misalignment of races, and improper sizing of rolling parts.

Other notable problems include cracks, corrosion pitting, and brinelling on the rolling surfaces. Bearing issues are divided into five types based on the defects in these components, as outlined below:

- a) Inner race fault
- b) Outer race fault
- c) Cage fault
- d) Roller or ball fault
- e) Multiple fault

Degradation will manifest in one of four forms: damage to the outer race, known as BPFO (ball pass frequency outer); damage to the inner race, known as BPFI (ball pass frequency inner); damage to the rolling elements, known as BSF (ball or roller spin frequency); or damage to the bearing cage, known as FTF (fundamental train frequency). Each imperfection will produce a distinct frequency, contingent upon the geometry and velocity of the bearing. Characteristic defect frequencies of the bearing can be computed and referenced from the source, as follows [14]:

$$BPFO = \frac{nf_r}{2} \left\{ 1 - \frac{d}{D} \cos\phi \right\} \quad (1.1)$$

$$BPFI = \frac{nf_r}{2} \left\{ 1 + \frac{d}{D} \cos\phi \right\} \quad (1.2)$$

$$FTF = \frac{f_r}{2} \left\{ 1 - \frac{d}{D} \cos\phi \right\} \quad (1.3)$$

$$BSF(RSF) = \frac{D}{2d} \left\{ 1 - \left(\frac{d}{D} \cos\phi \right)^2 \right\} \quad (1.4)$$

Where f_r is the shaft speed, n is the number of rolling elements, and ϕ is the angle of the load from the radial plane, d and D are the ball (rolling element) and pitch diameters. Note that the ball spin frequency is the frequency with which the fault strikes the same race (inner or outer).

The components of rolling contact bearings – i.e. inner raceway, outer raceway, rolling elements, and cage – interact through a combination of rolling and sliding to produce complex vibration signatures. The vibration level depends on the impact energy, the

point at which vibration is measured and the bearing construction. The various sources of vibrations are as follows [9]:

- a) Geometrical Imperfection
- b) Surface Roughness
- c) Waviness
- d) Raceway Defect
- e) Rolling Element Defect
- f) Variable Compliance

1.5 Maintenance Strategies

The maintenance strategy for rotary machines is essential for guaranteeing their dependable and effective performance. Various methodologies are employed, considering the significance of the machine, the conditions under which it operates, and the associated costs. These are primarily classified into three types –

- a) Corrective maintenance,
- b) Preventive maintenance and
- c) Predictive maintenance (or Condition-based maintenance CBM)

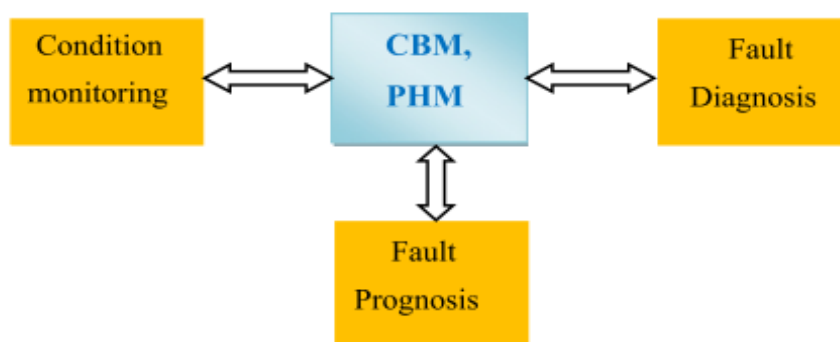


Figure 1.12 Components of condition-based maintenance [15]

Corrective maintenance involves the process of repairing or replacing components following a failure event. The objective is to return the machine to its functional state by addressing the identified issue. This method is typically employed when setbacks do not significantly impact operations or safety. Although it may appear straightforward and economical at first, excessive reliance on it in essential machinery

can result in unexpected outages, increased repair expenses, and possible harm to adjacent systems. Preventive maintenance is scheduled and entails regular servicing to prevent unforeseen failures. Predictive maintenance utilises real-time data, such as vibration, temperature, and noise, to evaluate machine health and schedule maintenance only when necessary, thereby minimising unnecessary downtime.

CBM employs sensors to gather information regarding the components during their operational phase. In this case, sensors provide the benefit of collecting data in real-time during the production process, without causing any interruptions to the workflow. Over time, the collected data are analysed and contrasted to forecast potential failures. In certain instances, this analysis is conducted solely when there is a noticeable decline in machine performance, thereby increasing the risk of breakdown. Condition-Based Monitoring (CBM) is a methodology that primarily employs sensors to assess the condition of various components. This procedure is conducted repeatedly at various intervals to ascertain the impact of time on the component. The primary advantage of this procedure is that it can be conducted while the components are operational, thereby eliminating the necessity for removal for maintenance purposes. Consequently, it will not impact any production schedules and offers information with a high degree of accuracy. The data collected from the sensors can be subjected to further analysis to extract information regarding malfunctions, defects, lifespan, and operational conditions.

As Industry 4.0 progresses, AI-driven maintenance is being increasingly used, utilising data analytics and machine learning for enhanced defect prediction and optimisation. Choosing the appropriate method prolongs machine longevity, reduces expenses, and guarantees operational safety.

1.6 Machine Health Monitoring Techniques

Techniques for monitoring machine health are crucial for evaluating the state of machines in real-time and identifying faults early to avert unforeseen failures. These techniques facilitate maintenance decisions that are informed by the actual condition of the equipment, rather than depending exclusively on time-based schedules. A variety of machine condition monitoring techniques, such as [9, 14, 16]

- a) Acoustic Emission (AE)
- b) Thermography
- c) Oil Debris (OD)
- d) Vibration Analysis (VR)

1.6.1 Acoustic Emission

Acoustic emission (AE) monitoring detects high-frequency stress waves generated during the deformation of materials, crack propagation, or various structural changes. The emissions generally occur within the frequency range of 100 kHz to 1 MHz, produced as a mechanical component experiences the growth and enlargement of a crack. The high-frequency acoustic waves transmit crucial insights regarding the internal state of the material. In AE analysis, the solid-borne acoustic signal is measured, and its statistical features are extracted to evaluate the health state of the system. This method proves to be highly efficient in identifying faults in bearings and gears, as well as cracks in shafts and turbine blades, and defects in reciprocating machinery. In contrast to vibration analysis, acoustic emission can identify micro-level defects at an early stage, rendering it a highly sensitive and valuable instrument for condition monitoring. Nonetheless, it necessitates advanced sensors and a high level of expertise for accurate signal interpretation and effective noise discrimination.

1.6.2 Thermography

Thermography employs infrared cameras or sensors to assess the surface temperatures of machinery while it is in operation. Unusual temperature trends frequently suggest mechanical complications, including overheating bearings, misaligned components, friction from inadequate lubrication, or electrical concerns such as overloading and loose connections. This technique involves monitoring the temperature of the components to identify any abnormalities within the mechanical system. In numerous mechanical systems, the surface temperature fluctuates within the infrared spectrum (0.7 to 100 microns wave band), which is assessed using a thermal imaging camera. Each machine operates within a specific normal temperature range, which can increase due to excessive friction and wear. This can occur from insufficient lubrication, excessive load, or stresses caused by improper loading, faults, or misalignment. The

thermal images allow for the identification of high-temperature regions, emphasising components that are functioning abnormally and necessitating further examination for possible faults. This method, which is both non-contact and non-invasive, is perfectly suited for examining live systems without the need for shutdowns, thereby facilitating prompt maintenance decisions.

1.6.3 Oil Debris

The analysis of oil serves as an effective method for assessing the internal state of mechanical systems that utilise lubricants for lubrication or cooling functions. As time progresses, wear particles produced by components like bearings, gears, chains, and cylinder-piston assemblies contaminate the oil, leading to changes in its physical and chemical properties. Analysing a contaminated lubricant sample can yield valuable insights into the internal health of the machine. The measurement of viscosity serves as a crucial method for assessing the composition of oil and identifying the presence of foreign or wear particles. Additional essential indicators encompass water content, oxidation, acidity, pour point, and flash point, which are vital for evaluating degradation and contamination levels. The analysis of oil, both physical and chemical, offers crucial early indicators of possible issues, facilitating predictive maintenance and minimising the likelihood of severe failures. This method is economical and non-invasive, rendering it particularly appropriate for regular condition assessment.

1.6.4 Vibration Analysis

Vibration monitoring is one of CBM's well-known methods. It addresses abnormal vibration, and if it occurs, this method can identify the machine or component failure based on the vibration pattern. However, one should be aware of natural frequency and vibration before implementing vibration monitoring. So that anomalous vibrations can be measured, and predictions can be made once the natural vibrational situation is known. In general, more vibrations are produced by worn parts. Every spinning component of the machine experiences fundamental vibration because of its revolution. The vibration-based parameter's value rises as the bearing deformation over time does. An increase in the overall vibration level indicates that the machine's condition worsens. The bearing components' misalignment or other defects could be

the source of this elevated vibration level. The main components of vibration diagnostics include feature extraction from the signal and the comparison of the values of the healthy bearing with the defective bearing.

Two fundamental techniques are used in every instance of vibration monitoring: frequency-based vibration data and time-based vibration data. In addition to time-frequency-based vibration, CBM data has recently gained much recognition. Amplitude is a variable in this case; if it is represented on a frequency scale, it is frequency domain analysis; if it is suppressed on a time scale, it is time-domain analysis.

All rotating machines produce vibrations during operation due to their dynamic characteristics, which result in fluctuating stiffness or compliance under specific working conditions. The vibration characteristics are modified by the emergence of defects in the machine, which can be quantified using an appropriate sensor. Based on the frequency of the vibration signal (attributable to flaws), an appropriate vibration parameter (displacement, velocity, or acceleration) is chosen for measurement. For bearings, the vibration signal occurs in the high-frequency range; therefore, accelerometers are typically utilised to capture the vibration acceleration. Various signal processing techniques in both time and frequency domains are employed on the acquired data to improve fault-related signal attributes and eliminate unwanted noise or disruptions, hence facilitating accurate conclusions.

Various instruments exist for detecting the vibration of a body, each operating on distinct principles, such as electrical strain gauges, linear variable differential transformers, piezoelectric devices, and electrodynamic transducers. Vibration transducers are offered in several varieties according to the measured parameter: proximity probes for vibration displacement, velocity pickups for velocity measurement, and accelerometers for acceleration measurement. The accelerometer has a wider dynamic measuring range (often 1- 20 kHz) and is optimally utilised in most industrial applications.

The piezoelectric accelerometer presents numerous advantages, including compactness, durability, high sensitivity, and excellent frequency response [9]. It

utilises the piezoelectric property, whereby electric charges are generated in a material (piezoelectric crystal/ceramic) during deformation due to applied pressure (force/stress). The generated charge is quantified and amplified, ultimately utilised to assess the magnitude of force, stress, or pressure according to the calibration.

An accelerometer produces a continuous voltage signal captured by the data acquisition (DAQ) device at a designated sampling rate. The DAQ transforms the continuous signal from the accelerometer into a digital signal, with the quantity of data points and the degree of digitisation dictated by the sampling frequency and the resolution of the DAQ unit. In addition to digitisation, the latest DAQ cards feature an integrated signal conditioning unit for signal filtering and amplification.

1.7 Vibration Signal Processing and Data Analysis

Signal processing techniques are created to extract accurate information from signals. The precision of signal processing primarily relies on two factors: the quality of the signals and the methodology employed in their processing. In bearings, rotation generates impulse data, which are measured in relation to frequency and referred to as characteristic frequencies. Established methodologies exist for calculating diverse frequencies, and juxtaposing readings with outputs from alternative approaches yields conclusive results on predictions [9, 17].

Upon accessing the data in the computer, several signal processing techniques, such as filtering, linearisation, amplification, noise reduction, and feature enhancement, are utilised to extract pertinent information on the fault from the signal. The signal can be analysed in several domains (time, frequency, or a combination of time-frequency) to identify fault-related properties. Trend analysis is often conducted in the time domain, where the signal's strength serves as an indicator of fault onset and failure. Time domain statistics, such as Root Mean Square (RMS), mean value, peak value, Standard Deviation (SD)/variance, kurtosis, and skewness, are frequently used as fault parameters. The focus in the frequency spectrum is on identifying the peaks associated with bearing fault pass frequencies and their harmonics. The fault pass frequencies for various malfunctioning components are mentioned in section 1.4.3.

The fault pass frequency value is contingent upon the specific component (inner or outer ring, cage, or rolling element) that has incurred a defect (spall), and its existence in the spectrum indicates the defective component within the bearing. The bearing is deemed damaged if the spectrum includes fault frequencies and associated harmonics. To ascertain the defect's severity, alternative methodologies, typically utilising time-frequency frames, are employed. The strategy for bearing replacement and maintenance is implemented.

Recently, the development of systems capable of human-like cognition has become prevalent. However, a distinction exists between human cognition and machine behaviour, as humans comprehend patterns within data, but machines merely recognise them. Humans typically create mental patterns via brain networks and store information through the biological sensors present in the body. Artificial neural networks function similarly to the human brain; they utilise algorithms to train data, identify patterns, and evaluate data against established patterns.

An intelligent information-based fault detection system, capable of self-learning and automatic updating, represents the forthcoming trend in the research of mechanical component failures. Signal processing techniques and the extraction of appropriate features are highly sensitive for identifying specific types of faults. Information-rich signals, such as vibrations, noise, and various physical, electrical, and material properties, are particularly valuable when analysed correctly. Extracting explicit information from extensive data presents a significant challenge in signal processing. Consequently, various strategies such as time domain, frequency domain, and combined time-frequency domain analysis have been developed, each with its respective advantages and limitations [18].

Various techniques are commonly employed in bearing fault detection, including ANN, KNN, SVM, and MLR. The fundamental process in AI methodologies commences with data acquisition. The model's accuracy is significantly contingent upon the data available. Increased training data enhances the model's accuracy. Upon the conclusion of the data collection phase, the subsequent duty is feature selection. Following selecting features using various methods, the data training process

commences. The final trained model is evaluated using unfamiliar data to assess its accuracy.

Recently, the application of data mining techniques has become increasingly sought after alongside signal processing, since substantial data necessitates appropriate data processing. Methods encompass data normalisation, data preparation, data selection, and data processing; determining the appropriate method according to specific requirements is a significant challenge for researchers.

1.8 Structure of the Thesis

This thesis comprises eight systematically organised chapters that comprehensively justify the research work.

Chapter 1 introduces rolling element bearings with a focus on tapered roller bearings. It briefly describes different types of defects in rolling element bearings and commonly available techniques for diagnosing the bearing defects. It also provides a basic understanding of bearing dynamics and the motivation for the present research work.

Chapter 2 presents an overview of extensive research carried out in the field of rolling element bearings. An in-depth exploration of the existing literature has been undertaken, focusing on the study of bearing dynamics. Based on the available research, this chapter identified the research gaps and further discussed the objectives that underpin the current study.

Chapter 3 addresses the first research objective, which focuses on designing and developing an experimental setup for TRB. The framework is constructed to support both damping characterization and bearing fault diagnostics under defined loading circumstances.

Chapter 4 covers the damping analysis of four antifriction bearings within a controlled experimental framework. Both free decay and frequency response function (FRF) methods are utilised to assess the damping characteristics. The objective is to analyse the damping characteristics among different bearing types and their respective

operating conditions. The findings from this analysis enhance our comprehension of vibration attenuation in rotating machinery.

Chapter 5 covers the second objective, involving the vibration analysis of healthy TRB. An experimental study was carried out to assess the impact of various process parameters on the root mean square (RMS) value of vibration signals and the equivalent continuous sound level (Leq) produced during operation.

Chapter 6 is dedicated to the third objective, which examines the vibration analysis of a faulty TRB. Bearings exhibiting artificially induced defects, including inner race faults, outer race faults, and roller element damage, were subjected to controlled testing to analyse their dynamic behaviour. The vibration signatures were captured and examined through unique characteristics linked to each fault type.

Chapter 7 contributes to the fourth objective, focusing on developing an automated fault diagnosis framework for TRB. Leveraging experimental data gathered from diverse fault conditions, the framework combines signal processing techniques with supervised learning algorithms to facilitate automated condition monitoring. It includes details on an automated fault classification approach, proposed using supervised Machine Learning algorithms and a selected combination of statistical feature vectors.

Chapter 8 presents the conclusions derived from the present work, followed by a list of possible future directions related to this work. The results of the damping analysis, fault detection experiments, and the diagnostic framework based on machine learning are emphasised. The study also addresses the industrial implications, highlighting how dependable bearing diagnostics can improve machine safety, lower maintenance expenses, and support sustainable engineering initiatives.

Chapter 2 Literature Review

This Chapter presents an overview of extensive research carried out in the field of rolling element bearings. An in-depth exploration of the existing literature has been undertaken, focusing on the study of bearing dynamics and methodologies for evaluating tapered roller bearings' behaviour. Based on the available research, this chapter identified the research gaps and further discussed the objectives that underpin the current study.

2.1 Introduction

Current trends in driveline design emphasise super-critical, high-speed, lightweight, and extremely reliable systems, employing multi-objective functions to optimise strength and fatigue life while reducing weight and cost. Machinery supported by bearings and linked via couplings is an essential component of all rotating machinery. The optimal performance of these machines is significantly influenced by the seamless and silent operation of the bearings and the extent of misalignment at the coupling site. A functioning machine produces vibrations. These vibrations possess a specific inherent frequency, and any faults or damage to machine components alters these vibrations. The sensors can capture machine vibrations, facilitating fault detection. Diverse methodologies are employed to identify accurate bearing problems, encompassing measurements such as acoustic and vibration analysis, temperature assessment, and wear evaluation. The study indicates that the time-domain characteristics, including kurtosis, root mean square (RMS), crest factor, and probability density, demonstrate that kurtosis is the most useful feature in vibration and acoustic measurement. The frequency domain assists in identifying the location of problems. Two more methodologies, namely sound pressure analysis and sound intensity analysis, are sometimes overlooked; however, their results are not encouraging [19].

The examination of various parameters in the time-frequency domain revealed that kurtosis consistently demonstrates superior performance in parameter selection, as

noted in the literature. Additionally, a novel parameter, the product of kurtosis and RMS, has also yielded significant results in certain research studies. However, only a limited number of scholars have embraced this novel measure [20]. Sections 2.2 provide a concise overview of the damping study of the rotor bearing system. Subsequently, Section 2.2 presents a literature overview concerning the investigation of damping of antifriction bearings. Section 2.3 provides the overview on fault analysis of bearings. Section 2.4 provides a succinct overview of studies on automated fault diagnosis employing machine learning approaches. The conclusions derived from the literature review are presented, together with the research objectives of the current study.

2.2 Literature Survey on the Damping of the Rotor Bearing System

Understanding natural frequency or system damping is crucial before delving into specific fault types. Damping is crucial in rotor-bearing systems, impacting stability, vibration, and performance. Damping parameters provide insights into system behaviour, allowing for precise modeling and analysis [21]. Damping greatly impacts the dynamic behaviour of the rotor bearing system. Gregory et al. [22] emphasised the importance of damping in dynamic loading and the necessity for more study into damping mechanisms in mechanical transmission systems. Damping is used to investigate nonlinearities in mechanical systems. Damping stabilizes rotating parts and prevents instabilities at high speeds. This is especially crucial for aircraft, automotive, and industrial machinery.

Hu and Zhou [23] examined the nonlinear QZS (Quasi-zero-stiffness) vibration isolation system with hysteretic damping to address the constraints of linear damping under fluctuating excitations. The Duffing-Ueda model and harmonic balance approach were employed to investigate and validate main and secondary reactions through simulations and tests. Nonlinear damping guaranteed constrained responses and enhanced isolation efficacy. Key metrics—effective isolation frequency and maximum transmissibility—were established to assess performance. The findings underscore the impact of subharmonic responses and offer design recommendations for enhancing isolation performance.

Furthermore, Brodzinski and Stone [24] observed that rolling element bearings significantly diminished damping in the spindle system. Their experiments indicated that the connection between the outer ring and the housing was the principal source of damping due to the low joint stiffness, allowing relative movement between the two sections and facilitating energy dissipation.

Tiwari and Vyas [25] developed a technique to assess nonlinear stiffness parameters of rolling element bearings in rotor systems by utilizing random vibration signals recorded at the bearing caps. Utilizing the Fokker-Planck equation for system modeling and implementing a curve fitting algorithm, the method derives stiffness parameters independently of excitation force data. The methodology is exhibited on a test rig and corroborated with a pre-existing analytical model.

Tasker and Chopra [26] proposed a wavelet-based approach for estimating nonlinear damping in rotor-bearing systems. Employing the Krylov–Bogoliubov approach, approximate solutions are obtained, and the envelope of free vibration signals is examined to discern damping nonlinearities. Two damping models—coupled and uncoupled—are analysed, and experimental validation substantiates the method's efficacy.

Chen et. al. [27] proposed a frequency-domain approach to estimate the mass, stiffness, and damping matrices of a structural model. The damping matrix is discerned independently by converting complex modes to normal modes, while least squares derive the mass and stiffness matrices. Simulations illustrate the method's precision and resilience to measurement noise.

Béliveau [28] established a comprehensive Bayesian framework for identifying damping, stiffness, and mass characteristics utilizing modal data. A modified Newton-Raphson approach enhances estimates by utilizing natural frequencies, damping coefficients, mode shapes, and phase angles. The methodology is illustrated utilizing actual data from a nine-story steel structure.

A novel approach for estimating structural damping was devised utilizing the established complex frequency response function matrix [29]. The proposed approach

applies to simpler constructions within the anticipated frequency range. However, outside the examined range, the identified Frequency Response Functions (FRFs) do not align with the experimental FRFs. Damping is generally determined in engineering through the half-power bandwidth method, necessitating the analysis of the frequency response curve derived from various vibration tests (such as forced vibration field tests and ambient vibration testing methods), all of which are predicated on the frequency response of a single degree of freedom (SDOF) system [30]. Wang [31] formulated two precise equations for the half-power bandwidth method for displacement and acceleration frequency response functions. The conventional half-power bandwidth method is sufficiently precise for practical scenarios where the damping ratio is below 0.1. Staszewski [32], Ta et al. [33], and Chandra et al. [34] employed wavelet transforms for the detection of non-linear damping. Stiffness and damping characteristics are determined using experimental modal analysis tests [35]. Dietl [36] examined the impact of bearing damping on the dynamic response of multi-body systems, especially when the bearing clearance is minimal. They performed theoretical and experimental investigations to quantify the damping characteristics of rolling bearings. Furthermore, they developed an analytical model to forecast the bearing damping coefficient, which was corroborated by experimental results. The bearing attenuation coefficient escalated with both bearing load and rotating speed, as established by the experiment. Furthermore, they found that the bearing clearance affected the damping coefficient, with reduced clearances leading to increased damping coefficients.

Damping is crucial for the maximum performance and longevity of antifriction bearings, and its significance varies based on specific applications and operational conditions. Additionally, it may manage vibrations, diminish noise, prolong bearing lifespan, guarantee stability in high-speed applications, withstand shock loads, enhance precision in instruments, and control temperatures. High-velocity machinery necessitates meticulous control and stability to avert complications such as shaft misalignment and imbalance. Suryawanshi et al. [37] devised a method to identify angular misalignment faults in rotating machinery. Engineers must evaluate these parameters while developing and selecting bearings for specific applications to

enhance the overall performance and reliability of the machinery. Bearing types, including ball and roller, exhibit inherent damping characteristics that may vary according to design and material composition. Choosing the appropriate bearing type for the specific application is critically important.

2.3 Literature Survey on Rotor Bearing Fault Detection and Diagnosis

In addition to damping analysis, problem diagnostics in bearings is essential for maintaining the reliability and performance of rotating machinery. Bearings are prone to numerous problems, including spalling, pitting, wear, and misalignment, which may result in heightened vibration, noise, and eventual system failure if not identified promptly. Detecting these defects necessitates a thorough investigation of the vibration or acoustic signals produced during operation, frequently employing sophisticated signal processing methods such as envelope detection, wavelet transforms, or machine learning algorithms. Precise defect identification not only improves maintenance plans but also prolongs machinery lifespan and averts expensive unanticipated downtimes. Consequently, the integration of problem diagnostics with damping analyses yields a more thorough comprehension of bearing integrity and system dynamics. Since the 1980s, numerous research on condition monitoring have been conducted, although only a limited number have been adopted in industrial sectors. Bearings account for the majority of the maintenance budget in any industry utilizing rotating machinery. Rotating machines are acknowledged as vital and widely utilized apparatus throughout several industries, including power generation, automotive, aerospace, and processing sectors. Rolling element bearings are identified as the primary cause of machine failure throughout diverse rotating equipment applications, from portable devices to heavy-duty industries. Bearings seldom fail independently; but, in practical applications, unexpected and premature failures are common due to overloading, improper installation, inadequate lubrication, and unsuitable operating conditions [38, 39].

Cao et al. [40] have provided a detailed review of all the major mechanical models of rotor-bearing systems. They are categorised into five major types: lumped parameter, quasi-static, quasi-dynamic, dynamic, and finite element method-based models.

Further, for bearings with localised defects, a brief review of the mathematical models carried out by Shah and Patel [41] provides a quick insight into the subject.

McFadden and Smith [42] were the first to model the vibration response of the bearing with single point defect on inner race (IR) in the form of defect impulses, repeating at characteristic defect frequencies. This model was next extended by McFadden and Smith [43] to the bearings with multiple point defects on the inner race.

Tandon and Choudhary [44] proposed a model to determine the defect frequencies and their amplitudes due to localised defects on outer race (OR), inner race (IR) and single rolling elements under the action of radial and axial load. The defects were modelled as finite-width pulses of different shapes, and the effect of each shape was studied.

Lorza et al. [45] generated a three-dimensional finite element (FE) model according to the real materials' properties, geometry and friction coefficients of all parts that make up the double-row TRB. The maximum load capacity of the TRB was achieved when the radial load obtained was a maximum, while the stress ratios of the two contacts in the outer raceway of the TRB were close to 25%.

Harsha [46] investigated the nonlinear dynamic behaviour due to cage run-out and the number of balls in a rotating system supported by rolling element bearings. The nonlinear response of a perfectly rigid balanced rotor due to self-excited vibration in a ball bearing with a small cage run-out was studied.

Niu et al. [47] proposed a novel method for accurately calculating ball passing frequency (BPFs) based on a complete dynamic model of rolling ball bearings with localised surface defects. Localised surface defects were modelled accurately with consideration of the finite size of the ball, the additional clearance due to material absence, and changes in contact force directions. Two experiments were presented to validate the proposed method.

Mishra et al. [48] found that the conventional diagnosis method to diagnose faults in the rolling element bearing was not applicable for a rotor-bearing system when the rotor operates at low/slow speed, bearings with no fault, fault in the outer race, inner

race, and ball only, and a bearing with combination fault (outer and inner raceway fault with ball fault). This paper used a novel diagnosis scheme based on envelope analysis and wavelet de-noising with sigmoid function-based thresholding to extract the fault-related symptoms from noisy vibration signatures of defective ball bearings operating at slow speed.

Antonia and Randall [49] demonstrated that spectral kurtosis (SK) provides a robust way of detecting incipient faults even in strong masking noise compared to classical kurtosis analysis. SK is a detection tool that precisely identifies which frequency band(s) the fault shows the best contrast from background noise. It also gives the concept of a program which displays the SK as a function of frequency and spectral resolution.

Nataraj and Harsha [50] conducted a theoretical investigation to observe the effect of cage run-out on the vibration characteristics of the ball-bearing system. The results were presented as fast Fourier transformations and Poincare maps. The highest peaks in the vibrations due to cage run-out were at a frequency of the number of balls times the cage speed.

Khanam et al. [51] described an approach based on the principles of engineering mechanics to obtain a time function of the impact force, which was used to simulate the response of the bearing housing. Experiments conducted on deep groove ball bearings for different defect sizes and speeds showed an acceptable correlation with the theoretical simulation.

Yang et al. [52] discussed the mechanical behaviour of double-row tapered roller bearings in current work by extending the mathematical model of three degrees of freedom. Demonstrated the effects of external loads, axial pre-deformation, bearing rotating speed, and angular misalignment on double-row tapered roller bearing characteristics.

Tapered roller bearings (TRBs) are extensively utilized in various industrial applications because of their capacity to effectively manage both radial and axial stresses. Their unique design facilitates enhanced weight distribution and endurance,

rendering them essential components in the heavy industrial, automotive, and aerospace sectors. Despite their importance, the distinct characteristics and failure processes of TRBs are not as thoroughly examined as those of other types of bearings, such as ball bearings or cylindrical roller bearings. Minor localized defects in the inner race, outer race, and rolling elements of bearing components lead to machine malfunctions, often culminating in catastrophic failure. Metal-on-metal contact induces a series of impacts as a rolling component continuously traverses a defect, leading to system vibration. A prominent peak in the frequency domain signal associated with the fault frequency differentiates these events [53]. Sensors are affixed to machines for identification, diagnosis, and prognosis. To attain this goal, it is essential to establish an efficient bearing condition monitoring program that allows for condition-based maintenance rather than schedule-based maintenance, hence enabling prompt remedial measures [54]. Nonetheless, initial fault impulses are often feeble and readily obscured by background noise and interference from other vibration sources, leading to misdiagnosis or undetected issues. To address this issue, much research was conducted, resulting in several effective methods for extracting early defect characteristics from noise and interference [55]. Critical tasks necessary for accomplishing this objective encompass fault identification and diagnosis, defect severity assessment, and prognosis. Typically, the execution of these obligations is facilitated by employing a dependable monitoring system for the bearing's condition. This system comprises sensors, data acquisition, feature extraction, pattern recognition, and forecasting. The sensor response signals are analyzed in the time domain, frequency domain [56], and time-frequency domain (Wavelet transform and Hilbert transform) [57–59]. In recent years, sophisticated signal processing techniques, including wavelets, envelopes, fuzzy logic methods, data-driven approaches, Hilbert-Huang Transform (HHT), Modal Energy Distribution (MED), and spectral kurtosis, have been developed for vibration signals. In addition to the aforementioned applications, the CWT was utilized to assess the instantaneous rotational speed of rotary machines and to extract random vibrations from observed signals to acquire pertinent information on bearing conditions [60]. Signals are analyzed for feature extraction using statistical metrics including RMS (root mean square), kurtosis, peak level, and FFT. RMS is often utilized for correlating bearing

and raw vibration acceleration in signal analysis [61]. Advanced signal processing techniques, including artificial neural networks (ANNs) [62–68], support vector machines (SVM) [69–72], hidden Markov models (HMM) [62], model-based analysis [73], vibro-acoustic data fusion [74], fuzzy logic classifiers [75–77], genetic algorithms in conjunction with ANN [78], wavelet transform, and various soft computing methods, are utilized to extract fault features from vibration signals.

Table 2.1 provides an overview of the chosen research studies. The efficacy of research is assessed through the mathematical analysis of experimental data, resulting in a substantial conclusion regarding the findings. The dynamic reactions of a rotor-bearing system are forecasted utilizing a comprehensive multifactorial design in the present research.

The application of full factorial is beneficial for the development, improvement, and optimization of many processes [79]. Gunerkar et al. [80] examined the impact of localized defects of differing sizes on bearing vibrations, utilizing RMS as the response measure for the process. Patil et al. [81] employed RSM analysis for the condition monitoring of ball bearings and utilized kurtosis as a signal processing technique to examine the effects of load, motion, and defects on vibration. Kankar et al. [82] employed the RSM technique to detect defects in the damaged rolling bearing. Experimental results validated the mathematical model's capacity to forecast faults at their characteristic defect frequencies and harmonics. RSM was established to predict the dynamic response of a rotor-bearing system. Goyal et al. [83] proposed Response Surface Methodology (RSM) to ascertain the appropriate placement strategy for non-contact sensors to achieve efficient condition monitoring of rotating machine components.

Table 2.1 Literature review

Authors	Bearing type	Experimenta l/Modelling	Input parameters			Vibration Feature extract	Response parameters	Technique
			Load	RPM	Fault			
Patil et al. (2010) [84]	Deep groove ball bearing	Experimental			IR, OR, Ball	Time domain	Kurtosis	RSM, ANOVA
Harsha et al. (2011) [85]	Ball bearing	Experimental		1000 and 5000 RPM	IR, OR, Ball with spall	FFT	RMS	RSM, ANOVA
Kumar et al. (2013) [86]	TRB	Experimental	20 and 40 N	1050, 2050 and 3080 RPM	OR (0.5776, 1.1820, 1.7266, 1.9614 mm defect width)	Time domain	CWT, Time–frequency analysis,	Symlet wavelet, Image processing
Hemmati et al. (2015) [87]	TRB on pillow block	Experimental	100 and 200 N	300, 600 and 1100 RPM	OR	Acoustic Emission signal	Acoustic Emission, RMS, kurtosis, crest factor	DOE, Plackett–Burman method
Hongrui et al. (2016) [88]	Rolling element bearing-	Experimental		460, 530, 515 RPM	Slightly rub in the outer race	Time domain,	Empirical Wavelet Transform in	-

	cylindrical roller bearing					Frequency domain	Vibration signal analysis	
Fabio et al. (2017)[89]	Deep groove ball bearing	Experimental	590 and 1180 N	3000 RPM	OR	FFT		DOE, ANOVA
Liu et al. (2017) [90]	TRB	Experimental and Analytical	120 N	1800 RPM	OR, IR	FFT		The non-Hertzian line contact stiffness
Mishra et al. (2017) [91]	Ball bearings	Experimental	50 N	60 RPM	OR, IR	Time domain, Frequency domain	RMS	Envelope analysis and Wavelet de-noising with sigmoid function
He et al. (2018) [92]	CWRU bearing	CWRU bearing data set			OR, Roller	Time domain, Time-frequency domain		multi-scale SR spectrogram

Khadersab et al. (2018) [93]	Rolling element bearing- ball bearing	Experimental		900 RPM	OR fault 0.5mm through EDM	Time domain	Vibration analysis, FFT, IFFT and Spectrogram	
Yi et al. (2018) [94]	Railway axle bearings (Double row TRB)	Experimental	19600 N	581 RPM	OR, Cage, Roller and Coupling	Time domain, Time-frequency domain	Intrinsic mode functions of the vibration signals	Ensemble empirical mode decomposition
Jalan et al. (2019) [95]	Rolling element bearing-Self aligned ball bearing	Experimental	0 and 50 N	1500 and 3000 RPM	OR, IR and Cage fault (CF)	Time domain		ANN and KNN
Jalan et al. (2019) [96]	Self-aligned ball bearing	Experimental	50 N	700 and 1700 RPM	IR, OR, CF	Time domain	Max, Min, SD, Kurtosis, Skewness, RMS, Variance, Median, Peak2rms	KNN

Goyal et al. (2019) [83]	Self-aligned ball bearing	Experimental		1200, 1600, 2000 RPM	OR		FFT amplitude, RMS	RSM, ANOVA
Anil and Rajesh (2019) [97]	TRB	Experimental		2049 RPM	Roller	Time domain	Kurtosis, Impulse factor	Ensemble empirical mode decomposition, Inverse filtering
Li et al. (2021) [98]	CWRU bearing	CWRU bearing data set, Analytical	0,736, 1471, 2207 N		OR, IR, Ball	Time domain		PSO, MOMEDA
Tong et al. (2022) [99]	Deep groove ball bearing	Experimental and Analytical	5000 N, 7000 N	300, 900 RPM	OR, IR, ball	vibration time-domain signal		MSMFIF method, MKACNN network
Wu et al. (2022) [100]	Angular contact ball bearing	Experimental and Analytical	400 N	10000, 20000, 30000 RPM	OR	Time domain and FFT	MAE, SD, Root mean square error	New compound displacement excitation function

2.4 Automated Fault Detection using Machine Learning Techniques

The utilization of Machine Learning (ML) methodologies is progressively prevalent for automated condition monitoring jobs in contemporary businesses, owing to its straightforward implementation and comparatively acceptable accuracy [101]. This entails a series of processes commencing with data collecting, followed by signal processing and subsequent fault categorization. Fundamental machine learning techniques encompass Decision Tree (DT), Support Vector Machines (SVM), Naïve Bayes, Neural Network, Random Forest (RF), k-Nearest Neighbor (k-NN), Artificial Neural Networks (ANN), Deep Belief Network (DBN), Hidden Markov Model, and Convolutional Neural Network (CNN). Extensive study in this domain has led to the development of many algorithms, whose applications in bearing fault diagnosis have been extensively documented. Utilizing a machine learning technique enables not only the detection of faults in a component but also, through an effective classification scheme, the identification of the location and severity of the defect. The premise of supervised machine learning models involves training an algorithm to recognize various class labels based on a set of input features, thereafter assigning a label to the defect features of healthy data according to its previous learning. Consequently, the feature vector significantly influences the precision and efficacy of the acquired model. In numerous earlier and certain contemporary machine learning models, fundamental statistics of the signal in either the time or frequency domain, or both, were employed for the training and testing of supervised algorithms, or to aid in informative mode selection in various unsupervised learning algorithms [102–107].

Extensive research has been conducted on the diagnostics of bearings and rotating machinery defects. Numerous models [108–112], signal-based methods [113], and data-driven methods [114] have been proposed in the literature. Model-based methods are employed to detect faults by constructing accurate mathematical bearings models and comparing the resulting output values with the actual values. A nonlinear dynamic model for rolling bearings effectively simulated individual and compound faults [115]. Traditional fault detection techniques in signal processing mostly use the manual extraction of fault-related information from signals to accurately identify bearing faults. The accuracy of diagnosis can be improved by using a method called group-

based K-singular value decomposition denoising to extract aspects of bearing faults [116]. However, these strategies heavily depend on the understanding of advanced signal processing.

Fault diagnosis (FD) aims to identify the status of a specific component and determine whether maintenance is necessary. There are two approaches to FD: model-based and data-driven. According to [117], the model-based method involves extensive prior knowledge and can be challenging to create reliable diagnosis models for complicated machines. Data-driven models are more popular for generating intelligent techniques. This approach efficiently processes machinery signals and reliably diagnoses findings with minimal prior expertise. The research given in [118] compares two shallow machine learning (ML) models for Failure Identification (FI): support vector regression (SVR) and relevance vector machine (RVM). RVM outperformed the SVR algorithm for FI based on probabilistic discoveries employing random kernel functions. According to [119], individually treating feature selection and parameter tuning can limit SVR predictions' accuracy. The author later proposed two bearing-fault techniques for FI and FD based on an RVM of vibration signals, referencing the previous study, using two relevant models as an observer and classifier. In [120], the stator current is monitored using motor current signature analysis (MCSA) and frequency spectrum subtraction with wavelet transforms to remove dominating components. Spectral subtraction can be performed using DWT, WPD, or SWT techniques [121, 122].

Machine learning methods are more practical than signal-based solutions for defect diagnosis. Multiple research investigations offer a robust theoretical basis for justifying the utilisation of machine learning in defect diagnoses. The properties that machine learning (ML) can extract from data are more objective compared to signal-based approaches. Furthermore, when selecting defect diagnosis approaches, the primary consideration is the effectiveness of machine learning models. Researchers employ several machine-learning techniques to enhance the precision of bearing fault diagnostics. Examples of extensively utilised models include the HMM [123], ANN [124], and SVM [125]. ML is proposed as a method to enhance the accuracy of defect

diagnosis due to the significance of feature extraction when combined with feature ranking. The results may be affected by the findings, as feature extraction, feature reduction, and classification represent the three main processes in conventional techniques for recognising defect types in rolling bearings. A strategy employed in machine learning to improve the accuracy of models is feature ranking. It also enhances the ability of algorithms to predict outcomes by emphasising the most important features and eliminating the redundant and inconsequential ones. Previous research used pre-processing, dimensionality reduction, and feature selection (Chi-square, Gain ratio, ReliefF, and Principal Component Analysis) to diagnose bearing faults accurately. Additionally, they assessed the accuracy of SVM and ANN models in classifying defects [126].

One-way ANOVA and Kruskal-Wallis test feature ranking algorithms have been used in several applications, including text sorting, cancer prediction, e-mail spam sorting, microarray data classification, face identification, and tumour classification [127]. While there are limited studies on using Ow-A and KW technique for bearing fault diagnosis [128]. Ow-A offers the advantage of not requiring an same number observations in each group. The design arrangement and statistical analysis are simple. The Kruskal-Wallis test differs from other parametric tests because it does not assume normality or variance homogeneity. The Kruskal-Wallis test has higher reliability compared to other parametric tests.

2.5 Research Gaps Based on Literature Review

Although many investigations have been conducted in the field of bearing fault diagnosis, there remain several key research gaps:

- Thorough research is available on rolling element bearings, but very limited literature is reported on experimental work on tapered roller bearings.
- Various researchers concentrate on vibration analysis of single defects in ball and roller bearings, but very limited research is available on compound fault analysis. Also, the effect of multifaults in tapered roller bearings on vibration behaviours is limited.

- Various models have been developed for ball bearings through the computational framework in the past, but few of them have focused on tapered roller bearings.
- It might be contended that minimal research has been conducted within the signal processing field about the necessity and characteristics of these problem categories. However, the application of advanced soft computing approaches in auto fault diagnosis for the detection of bearing faults, without disrupting the operation of specific tapered bearings, is notably absent in the comprehensive review of rolling element bearing fault diagnosis. There exists sufficient information on ball bearings that can support tapered bearings, but can also serve as complete replacements.
- In the past two decades, a review of pertinent research indicates that the optimization of parameters and their use in AI techniques for the development of a system capable of autonomously detecting bearing faults remains incomplete. This research presents a data mining strategy, complemented by advanced signal processing methods, which are currently lacking in the domain of tapered bearing problem identification.
- AI methodologies, mostly reliant on the available data and the parameters provided, can also be optimized. The optimization of these based on the information has not been extensively examined and is also addressed in the current study.

2.6 Objectives of this Research

The present research aims to propose validated solutions to overcome these research gaps, with the four main objectives, as outlined below:

- Design and development of an experimental framework for a tapered roller bearing system.
- To study the vibration behaviour of a healthy tapered roller bearing at different operating load and speed.
- To study the vibration behaviour of a faulty tapered roller bearing.
- To develop a computational framework for a tapered roller-bearing system.

Chapter 3 Design and Development of an Experimental Framework for a Tapered Roller Bearing System

This chapter highlights the design and fabrication of the test rig. This pertains to the initial research objective, which encompasses the design and construction of an experimental apparatus for tapered roller bearings (TRB) under defined loading circumstances.

3.1 Introduction

A systematic design methodology was employed to create a specialized test apparatus for bearing defect diagnostics, during which critical system components were identified according to the specifications, and an initial system layout was devised. The power demand was established based on the greatest radial load to be exerted during testing. Consequently, standard components for a compatible power transmission system were determined utilizing the manufacturer's catalog. The appropriate support bearings were acquired based on the reaction forces exerted on the shaft during heavy load application. The anti-vibration rubber mounts were ultimately chosen based on their damping characteristics and specified dimensions. Upon finalisation of the shaft dimensions, static and dynamic analyses were conducted utilising impact testing to evaluate its performance under specified conditions and to ascertain its safety against various modes, resonance, and vibrational instability. This test rig is equipped with an integrated data acquisition system and display system. The developed test rig facilitates the execution of a diverse array of experiments while ensuring minimal assembly time and optimal adaptability. The next section will elucidate the intricate details of the components involved in the experimental test rigs.

3.2 Experimental Test Rig

The creation of a test rig is a crucial component of any investigative activity. Validating the simulation and analytical results with experimental data is crucial. Numerous studies [129–133] have led to the development of test rigs for the validation

of simulation and analytical results. This could directly help our society in terms of money or time.

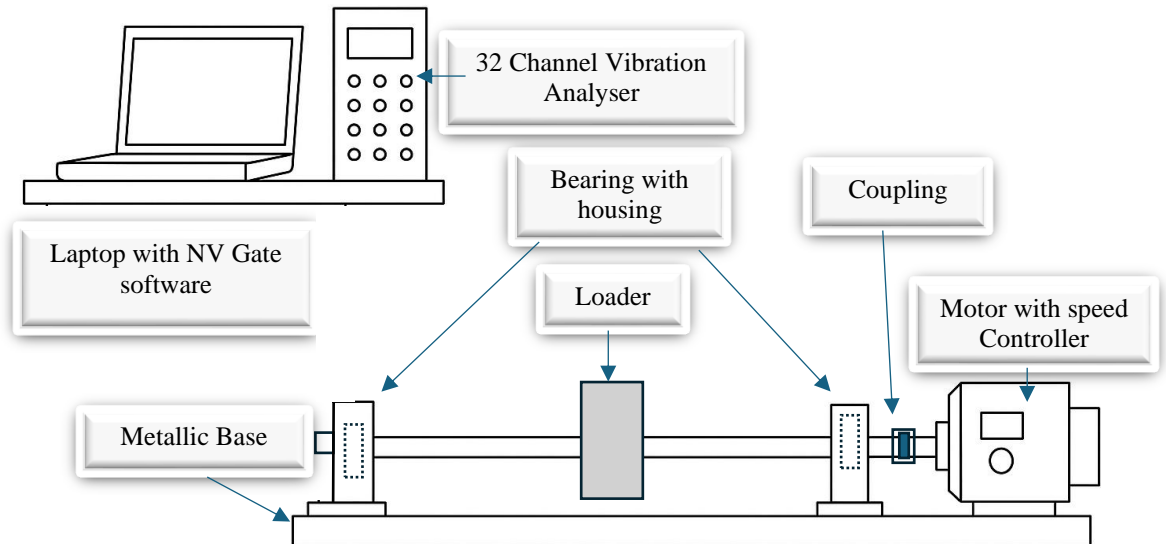


Figure 3.1 Line diagram of test rig

3.2.1 Tapered Roller Bearing System and its Metallic Structure

The base platform serves as a critical component within any rotor system. Given that the rotor shaft operates at an exceptionally high speed of 6000 rpm, it is essential to utilise a robust base plate as the foundation for mounting all components. The base plate consists of mild steel. The rotor system is composed of a direct current motor, bearings, coupling, and fasteners. All components are meticulously assembled and affixed to this sturdy mechanical frame, as illustrated in Fig. 3.1 and its dimension in Table 3.1. The design of the structure ensures adequate rigidity and sufficient strength.

Table 3.1 Shaft details

Shaft Material	Mild steel
Effective Length (Bearing to bearing)	800 mm
Total length	900 mm
Diameter of the shaft	30 mm
Density	7850 kg/m ³

3.2.2 D.C. Motor and Speed Controller

A variable speed D.C motor is employed to rotate the shaft at different speeds during the dynamic analysis of a bearing. The motor is affixed to the rotor located at the extreme right of the frame using fasteners and washers. Figure 3.2 illustrates a D.C. motor utilised in the experimental test rig with the speed controller that regulates the rotor's speed.



Figure 3.2 DC Motor with speed controller

3.2.3 Flexible Coupling

A flexible coupling serves to connect the D.C. motor shaft with the specimen rotor shaft. The specimen shaft and motor shaft exhibit both lateral and angular misalignment under dynamic conditions. These couplings mitigate the impact of misalignment.



Figure 3.3 Flexible coupling [134]

Dissipative coupling is another term for these. Neoprene rubber is subjected to compression and is press-fitted between the two flanges, resulting in a coupling that exhibits significant flexibility and durability. Figure 3.3 illustrates the flexible coupling utilised in the experimental test rig.

3.2.4 Signal Acquisition and Display System

Accurate measurement and appropriate conditioning of signal data are crucial for the successful execution of the experiment. OR36/OR38 is engineered to support a high channel count capacity while maintaining the integrity of the analyser geographies. An OROS36® vibration analyser with 32 channels and a frequency range of 20 kHz is used to collect and analyse the accelerometer's response. They provide both time-domain and FFT data. This analyser has real-time capabilities for simultaneously handling channels like FFT and 1/3 octave analysis. The OR36 and OR38 hardware feature blue LCD screen controls that enable the operation of the analyser, including functions to run or stop it, as well as adjust the fan speed, among other settings.

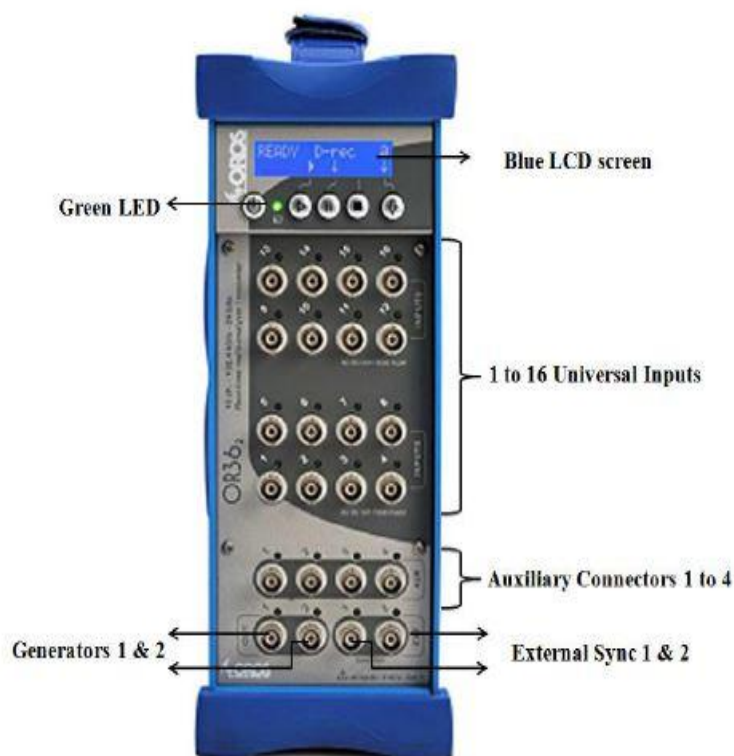


Figure 3.4 Front panel of Oros

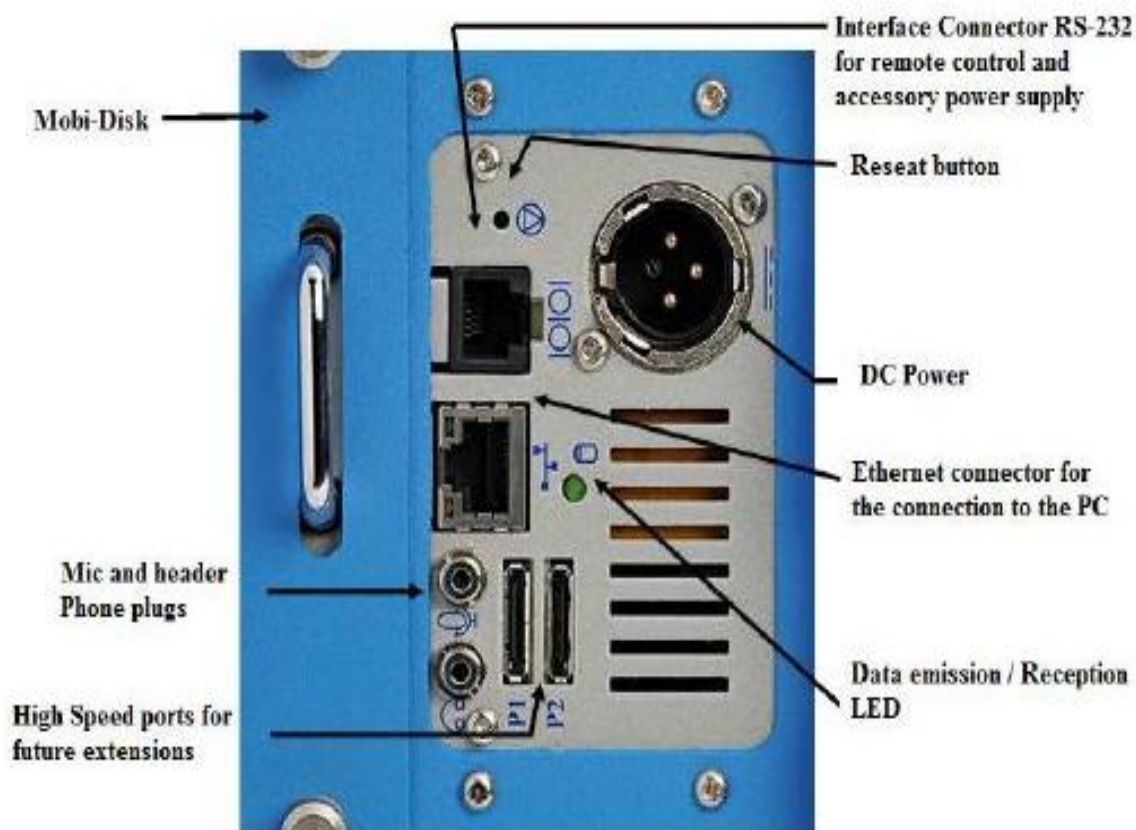


Figure 3.5 Back panel of Oros

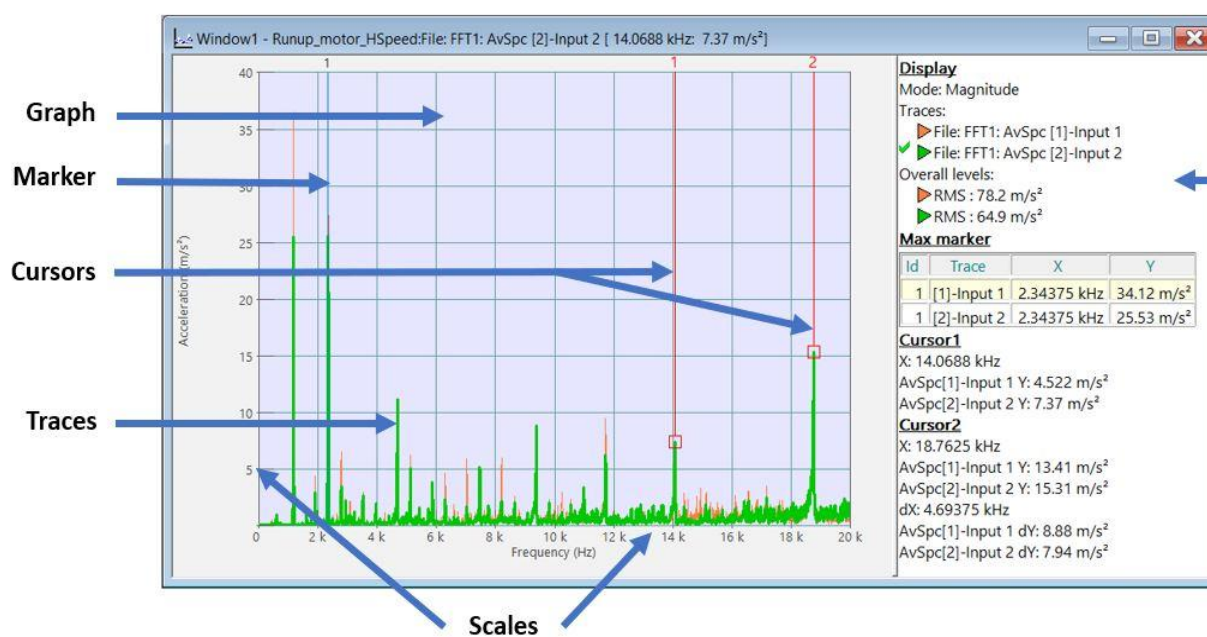


Figure 3.6 Display of signal

The selection of universal input usage is determined by NVGate® software throughout the analyzer's operations. NVGate® software offers an extensive array of tools designed for the acquisition, recording, and analysis of noise and vibration data. The universal inputs collect both dynamic and parametric input through a single connector. Each input connector features a green LED to signify that the input is active, while a red LED indicates an overload condition for the input. Figure 3.4 illustrates the front panel of the OR36. The back panel of the OR36 is illustrated in Fig. 3.5. The back panel includes several components such as the Ethernet connector, data emission/reception LED, connection for PC/OR36, auxiliary DB9 connector, interface connector, and DC power connector.

Personal computers and laptops can be effectively utilised for online display and for storing experimental data for subsequent analysis. Figure 3.6 illustrates the laptop screen displaying the signal reception facilitated by NVGate® software and OR36. The next section will outline the specifics of the experimental configuration used for measuring damping and bearing faults.

3.3 Experimental Arrangement for Impact Testing or Damping Analysis

Experiments are carried out on a customised rotor bearing test rig as shown in Fig. 3.7. The assembly consists of a robust shaft supported by two rolling element bearings with rigid housing. Four different antifriction bearings have been tested with external and internal diameters of 62 mm and 30 mm, respectively, as shown in Fig. 3.8. The bearing's detailed specifications are summarised in Table 3.2. An external DC motor drives the shaft through a flexible Lovejoy coupling. The test rig rotor is impacted by a hammer i.e., plastic/Vinyl tip with no extender hammer configuration (Model: - PCB-086C03) with a sensitivity of 2.25 m(V)/(N) and a range of ± 2224 N pk.

The experiment also aims to observe the damping properties of the bearing based on the amplitude of the FFT plot in dynamic conditions. The bearing is radially loaded with 20, 30 and 50 N, respectively. Two Isotron accelerometers are mounted on the top of the bearing housing with a sensitivity of 100.6 mV/g (10.26 mV/m/s²) and 95.09 mV/g (9.697 mV/m/s²) at 100.0 Hz. These ICP accelerometers record the signals on

the bearing housing at varying speeds from 1000 rpm to 3000 rpm with an interval of 200 rpm at different loading conditions.

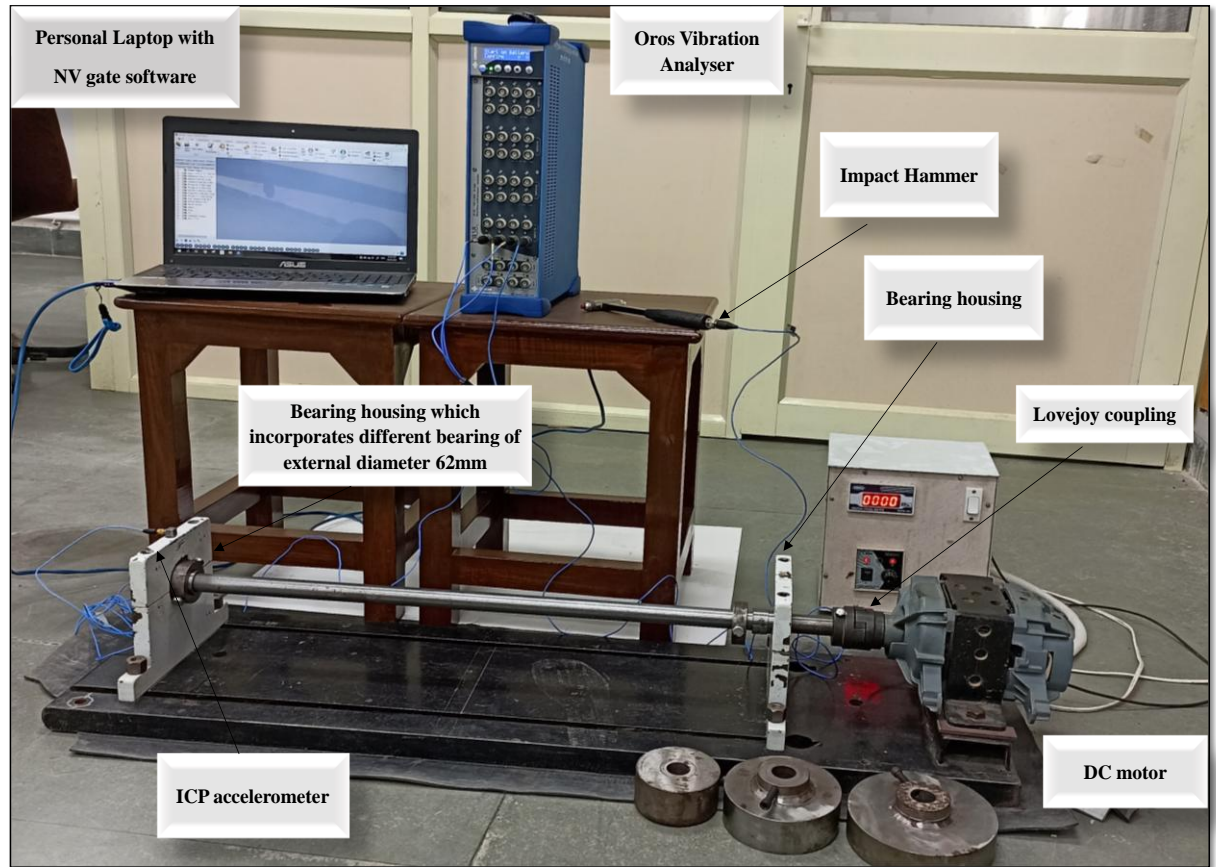


Figure 3.7 Experimental test rig for damping analysis

Table 3.2 Antifriction bearing's specification

Bearing No.	Bore diameter (mm)	No. of roller	Contact angle
Tapered SKF 30206	30	17	14.03°
Cylindrical NJ 2206 ECP	30	13	0°
Spherical 22206 E	30	15	12.83°
Self-Aligned 2206 ETN9	30	11	13.46°

The input parameters are frequency range (0-20 kHz), triggering (threshold: 10 N, and start delay: -20ms), Weighting windows (force: force and acceleration: response), Sampling rate (25.6kS/s), FFT average (domain: spectral, size: 3), FFT analysis

(range: 2kHz, resolution: 1.25 Hz) and number of spectral lines 1601 are selected. This choice was made to ensure accurate and high-resolution data capture during the experiments.



(a) Tapered roller bearing



(b) Cylindrical roller bearing



(c) Spherical roller bearing



(d) Self-aligned bearing

Figure 3.8 Different rolling element or antifriction bearings

3.4 Experimental Arrangement for Bearing Analysis

The accurate prediction of bearing operating conditions and defect patterns before reaching the failure threshold is a critical concern in several industries. This is essential for improving safety, dependability and optimising the utilisation of current assets. The vibration signatures associated with the normal functioning of bearings, which serve as foundational data, can subsequently be compared to the signatures acquired

under outer race (OR), inner race (IR) and roller defect conditions. This section describes the experiment's apparatus and data collection system.

3.4.1 Test Rig

A test rig for conducting an experiment, as shown in Fig. 3.9, is used to replicate real-world rotor bearing system operation. The components of the rotor bearing system are $\frac{1}{2}$ HP motor, flexible lovejoy coupling, TRBs, speed controller and loaders. The support near the end of the motor is the drive end (DE), and the other is the non-drive end (NDE).

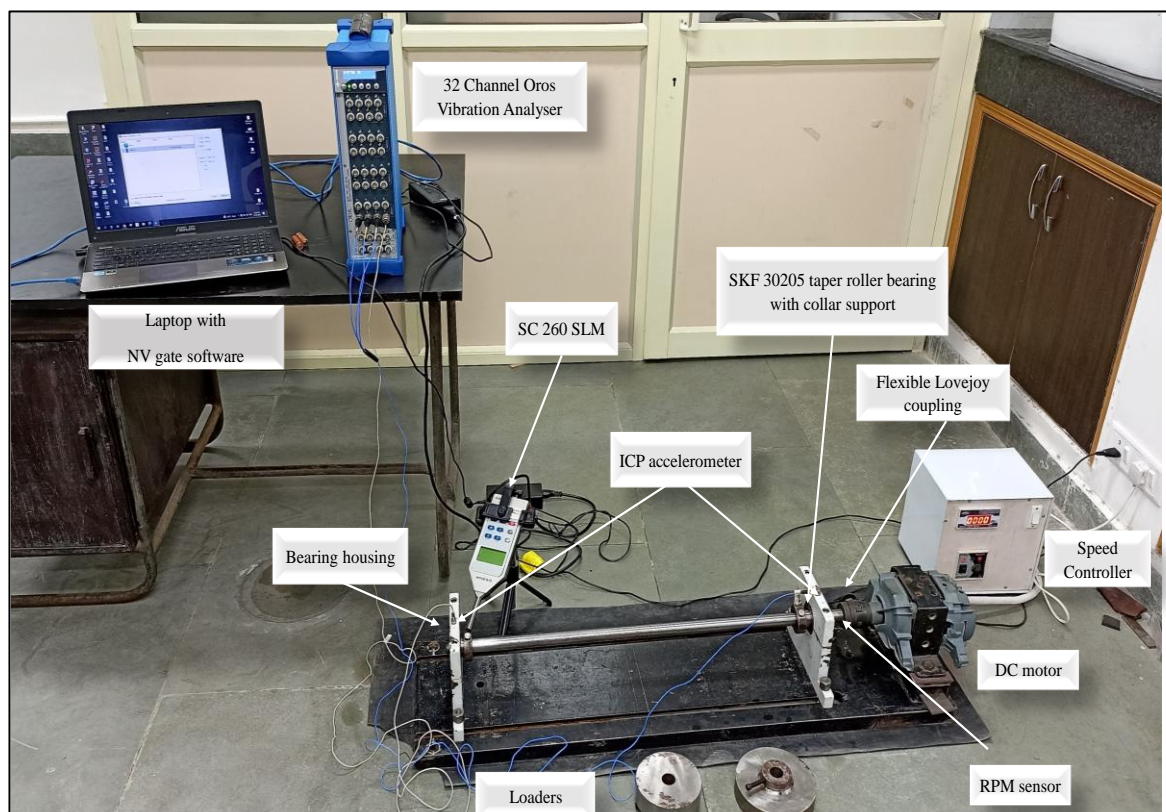


Figure 3.9 Experimental test rig for bearing analysis

A healthy bearing, shown in Fig. 3.10(c), is placed at the DE, and prefabricated defective bearings are installed at the NDE. Different predefined defective bearings shown in Fig. 3.10(e), such as OR, IR and roller defect, are used for the experiment. A mass of 2, 3 and 5 kg is also placed to impart the radial load of 20, 30 and 50 N, which is mounted externally to the shaft as a disk. The rotor is made up of a driving shaft that is supported by bearings in two places. The test rig was capable of balancing

and diagnosing machine defects, which is particularly useful as an experimental research instrument. An accelerometer is attached to the NDE to measure the vibration signal. At the coupling, the RPM is also measured.

3.4.2 Sound Level Meter

Figure 3.10(a) depicts the CESVA SC 260 sound level metre used to measure the sound pressure level (SPL). The SC260 is a very user-friendly class 2 embedded sound level metre. Sound level metres are evaluated based on international standards (IEC 60942: 2017): Class 1 refers to a precision grade that has a tolerance of 0.5 dB and is suitable for both laboratory and field use. On the other hand, Class 2 refers to a general-purpose grade with a tolerance of 1.0 dB specifically designed for field use. The SC260 features a versatile class 2 filter that can function as both a sound level metre (SLM) and a real-time spectrum analyzer. It supports 1/1 or 1/3 octave bands for precise analysis.

3.4.3 Bearings Under Study

The modular design of the experimental apparatus facilitates the removal and replacement of the bearing. The dimensions of the rolling element bearings used in this study are listed in Table 3.3. Since the majority of bearing vibrations are periodic movements, it is simple to derive vibration characteristics from the frequency domain using the powerful and well-known FFT method. Numerous publications [135–137], have examined the frequency characteristics of rolling bearing vibration. Rolling bearings typically consist of two concentric rings, known as the inner raceway and outer raceway, and a set of rolling elements that run in their axis shown in Fig. 3.10(d). Rolling element standard configurations include the ball, cylindrical roller, tapered roller, needle roller, and symmetrical and asymmetrical barrel roller [135]. Typically, the rolling elements in a bearing are positioned in a cage that provides uniform spacing and blocks mutual contact. A shaft with a 30 mm diameter is sustained by these bearings mounted on an adjusted pedestal.

3.4.4 Defects Creation in Test Bearings

The rectangular slits used as artificial faults in the bearings induced by EDM (electro-discharge machining) have dimensions of 1.5 mm wide and 1 mm deep over the entire

length of OR, IR and Roller shown in Fig. 3.10(d&e). In the case of the outer race defect, the flaw was introduced on the loaded zone of the raceway centred @6:00, ensuring repeated contact with the rollers during rotation. This placement was chosen because it is the most critical region where vibration responses are most pronounced and comparable to real-world failure scenarios. The specified dimensions are large enough to be consistently observed by the experiment's sensors. Smaller defects may provide signals that are difficult to identify from background noise. The dimensions correlate with those employed in earlier bearing defect detection investigations, ensuring that the results are comparable.



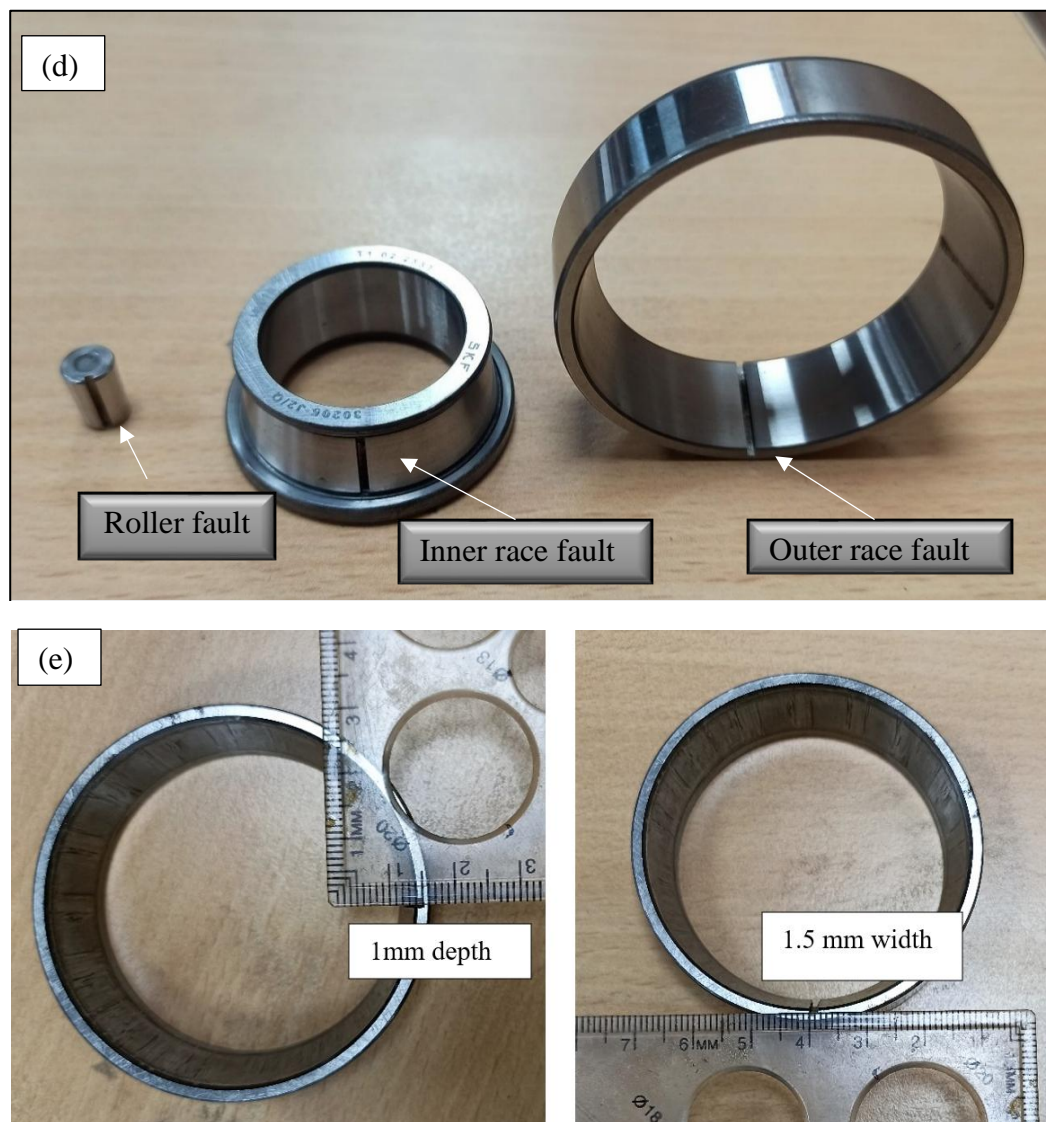


Figure 3.10 (a) Sound level meter (b) CAD model of TRB (c) Healthy TRB (d) Prefabricated faults in different parts of TRB (e) Dimensions of faults

Table 3.3 Tapered roller bearing specifications

Parameters	Descriptions
Type	SKF 30206
Contact angle	14.03 degree
Pitch diameter	38.32 mm
No. of rolling elements	17
Rolling element diameter	6.79 mm
No. of rows	1

A rectangular slit creates a consistent and easily repeatable damage shape, allowing for controlled experimentation and ensuring repeatability of results. While actual bearing damages might vary in shape, rectangular slits are a simplified illustration of typical damage types like spalls and cracks.

Additionally, in rolling element bearing there are a series of rolling elements which are moving on wavy surface with surface roughness. So, this is the origin of vibration in even new bearing. On top of it, so, to reduce this vibration manufacturer put a layer of lubricant to remove the surface asperities. But what happens in the process of operation, bearings are subjected to high temperature because of the process requirements or because of friction. So, this lubricant will get baked and then they will form hard carbon residues which will be on the surface of this waves. So, when the rolling element comes and moves on the surface it is going to get an impulse excitation and sometimes this hard surface or the hard residues may even scrape the surface, and they will generate pits of this nature.

3.5 Summary of the Chapter

This chapter primarily concentrates on the design and development of a detailed experimental framework for rotor bearing systems. The framework is designed to facilitate the characterisation of damping and the diagnosis of bearing faults in a controlled laboratory environment. This chapter consists of two primary sections. The initial segment emphasises the setup and tools utilised in the test rig designed for damping evaluation. The work details the configuration established to assess system damping characteristics across different operational scenarios, emphasising sensor positioning, excitation methods, and data collection techniques. The second section provides a detailed examination of the test rig designed for the analysis of bearing faults. This encompasses the incorporation of accelerometers and categorise prevalent bearing defects, including outer race, inner race, and rolling element faults.

This chapter establishes a solid groundwork for experimental enquiries by outlining the rig's flexibility, the selection of components, and the instrumentation approach to guarantee precise and consistent outcomes in studies related to damping and fault diagnosis.

Chapter 4 Damping Analysis of Anti-friction Bearings

This chapter describes the damping analysis conducted on four distinct antifriction bearings within a controlled experimental framework. Both free decay and frequency response function (FRF) methods are utilised to assess the damping characteristics. The objective is to analyse the damping characteristics among different bearing types and their respective operating conditions. The findings from this analysis enhance our comprehension of vibration attenuation in rotating machinery.

4.1 Introduction

The damping behaviour of a system necessitates a comprehensive assessment of both static and dynamic properties of different antifriction bearings. The static analysis aims to ascertain load distribution and deformation under steady-state conditions, guaranteeing that the rig can endure the anticipated forces without structural failure. This work is essential for choosing suitable bearing designs capable of enduring diverse loads and enhancing overall system longevity. Dynamic analysis assesses various antifriction bearings' vibration, resonance, and stability under varied speeds and loads. This factor is crucial for forecasting the system's behaviour in actual operational conditions, reducing undesirable vibrations and improving accuracy in defect identification. The amalgamation of static and dynamic analyses guarantees that the experimental framework is resilient and can yield consistent and reproducible data for examining bearing performance.

The importance of damping in rotor-bearing systems is well recognised and directly affects system stability, vibration levels, and overall system performance. Damping parameters provide valuable system behaviour insight and enable accurate modelling and analysis [21].

As shown in Fig. 4.1, damping plays a vital role in various engineering applications, where it helps in reducing vibrations, controlling oscillations, and enhancing system stability. Damping aids in stabilizing the rotating elements, preventing instabilities that can arise at high speeds. This is particularly important in applications such as

aerospace, automotive, and industrial machinery. The literature that has come before us sheds light on the effect of bearing on natural frequency and modes of rotor bearing systems in various settings. The present work effectively connects theoretical models with real-world bearing performance by emphasising experimental investigation for enhancing the damping characteristics, align with the demands and conditions of practical applications. Comprehending the damping characteristics of bearings is essential for creating dependable and effective systems, especially in situations where damping significantly influences stability and performance. The findings have potential applications in bearing system design and optimisation for rotating machines. However, to the author's best knowledge, the calculation of damping ratios of bearings has not been extensively studied.

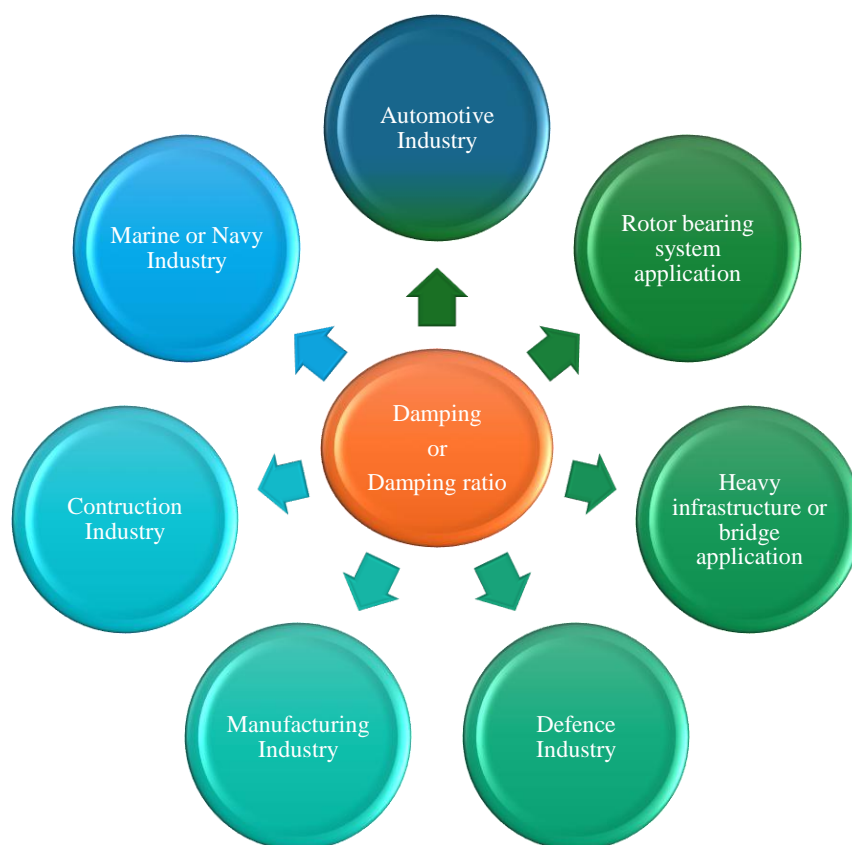


Figure 4.1 Areas of damping application

This research work aims to identify the best-suited antifriction bearing for rotor-bearing systems. Therefore, this paper experimentally compared the damping ratio of four different antifriction bearings under different operating conditions. Since the test

bearings used in this study were pre-lubricated with either grease or oil as supplied by the manufacturer and hence, lubrication was present during testing. The free decay and FRF methods have been employed to find the damping ratio of bearings. The damping behaviour of antifriction bearings highlights the importance of understanding the sources and magnitude of damping in these critical machine components. By understanding bearing damping, one can improve the performance and reliability of various mechanical systems.

4.2 Damping Identification Methods

The damping ratio is a dimensionless measure, and it is the process of dissipating energy to prevent vibratory motions such as mechanical oscillations, noise, and vibrations. It can be expressed by several metrics, including specific damping capacity, loss factor, Q-factor, and damping ratio [138].

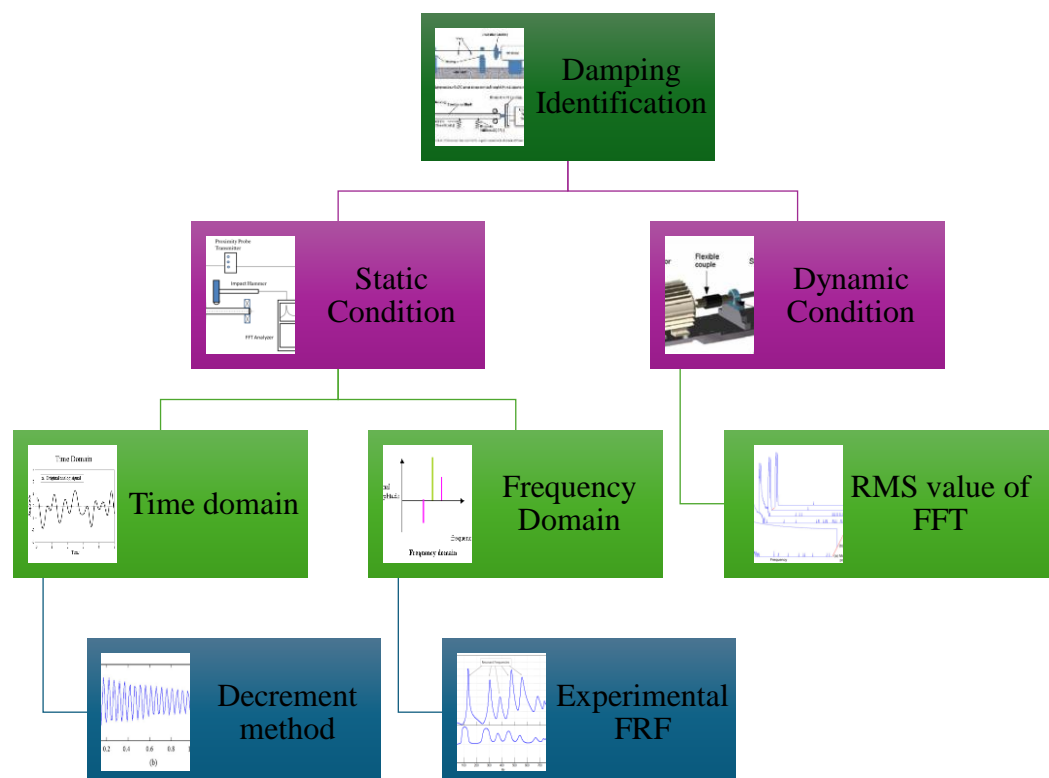


Figure 4.2 Methods for experimental identification of damping

To develop accurate structural damping matrices, some scholars have researched damping identification for various systems, such as rotor systems, mistuned blisks, and

monopile foundations. The damping parameters in rotor-bearing systems can be determined using several experimental methods shown in Fig. 4.2.

4.2.1 Static Condition

In this section, we will talk about the "classic" method of determining the damping of a rolling bearing in static conditions. The vibration damping can be calculated using a time-domain or frequency-domain approach.

4.2.1.1 Logarithmic Decrement Method

The rate of decay of free vibrations in a system is measured using the Logarithmic Decrement approach. The time-domain response of an energised system exhibits a decreasing amplitude of subsequent peaks as it is allowed to vibrate freely. The rate at which this decay takes place reveals information about the damping properties of the system [139]. The logarithmic decrement method involves measuring the amplitude of vibration over multiple cycles by using equation (4.1) [140].

$$\delta = \frac{1}{n} * \ln \frac{A_i}{A_{i+n}} \quad (4.1)$$

$$\xi = \frac{\delta}{\sqrt{4\pi^2 + \delta^2}} \quad (4.2)$$

where ξ - damping ratio,

δ - logarithmic decrement

n - number of cycles,

A_i - amplitude of the i^{th} cycle, and

A_{i+n} is the amplitude of the $(i+n)^{th}$ cycle.

In a system with slower damping, a lower Logarithmic Decrement value suggests slower vibration decay, whereas a larger value denotes a faster decay. It is a frequently employed method for determining the damping ratio of a system by using equation (4.2). The damping ratio is a vital metric that describes the ability of a system to disperse energy while undergoing vibrations. It is crucial to comprehending the dynamic characteristics of structures and enhancing their efficiency.

4.2.1.2 Half-power Bandwidth

A concept used in frequency analysis and signal processing to measure a frequency band width is called the half-power bandwidth. It is frequently used in vibration analysis, especially when working with Frequency Response Functions (FRFs) or signals in the frequency domain, to describe the width of resonance peaks or modes. An FRF's resonance peaks show the system's reaction at its natural frequencies. Resonance peaks manifest themselves in the FRF when a system is excited close to its natural frequency. There is a noticeable rise in amplitude at these peaks. Identifying the frequency spots where the amplitude decreases to 0.707 times the peak amplitude defines the half-power bandwidth. It is common to refer to these positions as the half-power points. In real-world vibration analysis, the frequency points at the reduced amplitude are identified and the FRF is measured to estimate the half-power bandwidth empirically by equation (4.3) [140, 141].

$$\xi = \frac{\omega_2 - \omega_1}{2\omega_n} = \frac{\Delta\omega}{2\omega_n} \quad (4.3)$$

where ξ - Damping ratio, $\Delta\omega$ - Bandwidth

ω_1 and ω_2 – Minimum and maximum frequencies at half-power amplitude

$$\frac{Y_{max}}{\sqrt{2}}$$

ω_n – First Natural frequency.

The Fourier Transform establishes a strong relationship between the FRF and a system's impulse response. The impulse response's Fourier Transform is known as the FRF. To determine a structure's inherent frequencies, damping ratios, and mode shapes, modal analysis makes extensive use of FRFs. Coherence is the proportion of the FRF's output that can be attributed to each input, measured as a function of frequency. It may serve as a gauge of the FRF's overall strength. It tests the FRF's repeatability or performance when the same measurement is repeated. During the impact test, one of the most important things to remember is that the impact should happen in the same place and direction for each average. The impact occurring in the same direction and place ensures a consistent and repeatable excitation of the system.

This consistency is essential for obtaining reliable and comparable frequency response measurements.

The first mode is often the primary mode of interest in many practical engineering applications. Understanding the damping characteristics in the primary mode is crucial as it can have a significant impact on the overall dynamic behaviour and stability of the system [142]. In many mechanical systems, the first mode represents the dominant response to excitations. By concentrating on the first mode, our study aimed to provide focused insights into the critical mode that most directly influences system performance and reliability. In this research, author focused on calculating damping in the first mode, each of which contributes to the specific goals and scope of this study.

4.2.2 Dynamic Condition

In the context of a rotor-bearing system, damping is crucial in determining the system's dynamic behaviour and stability. Damping is efficient at preventing resonance, which happens when the stimulation frequency matches the system's natural frequency. Resonance can cause enormous vibrations, which might cause harm. Damping helps in shifting or broadening natural frequencies, reducing the risk of resonance. It affects the critical speeds of the rotor-bearing system [143]. It can potentially change the form and size of the response curve around critical speeds. In a rotor-bearing system, the bearings themselves contribute to damping. Compared to fluid film bearings, antifriction bearings, for example, have reduced inherent damping. The bearing type and design can influence the total damping properties.

In order to verify the reliability of the data obtained under static conditions, another approach is used in which the rotor is subjected to regulated external forces or excitations in the forced excitation technique. The obtained time domain signal raw data are executed in MATLAB for giving response parameters in terms of RMS (root mean square) for vibration in both DE and NDE. The RMS value of the raw signal provides a measure of the overall magnitude or amplitude of the vibrations. It does not directly provide information about damping characteristics. Here, the authors tried to match the trend with the static condition results over the entire range of speed with different loading conditions. It has a significant impact on the RMS (Root Mean

Square) value of vibration data. The RMS value is a measure of the magnitude of vibration signals and is commonly used to quantify the overall energy content of a signal. It reflects the effective amplitude of the vibration signal, taking into account this decay. The RMS value of the amplitude of the FFT response as given by equation (4.4) [144, 145].

$$Y_{RMS} = \sqrt{\frac{1}{N} \sum_i y_i^2} \quad (4.4)$$

where y_i – Raw time signal,

N – No. of samples

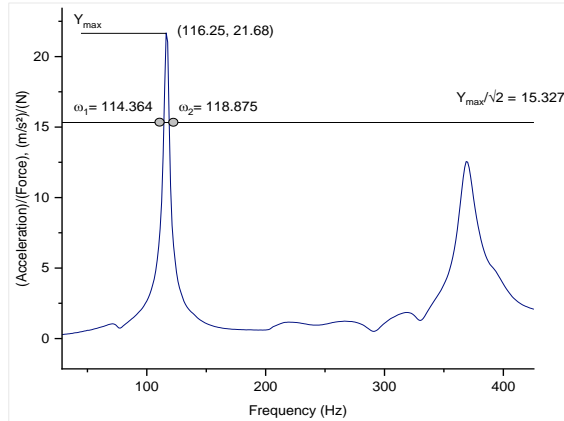
4.3 Results and Discussion

The experimental test rig as shown in Fig. 3.8, is used to analyse the damping behaviour of various antifriction bearings. Damping of antifriction bearings is observed in two different scenarios. The first is a static condition, where an impact hammer hits the shaft in the middle, and an accelerometer is placed on the bearing housing at DE and NDE. The decision to use the hammer to hit the middle of the shaft in the radial direction is made to simulate realistic loading conditions that the system may encounter during operation. By impacting the middle of the shaft, we aim to capture vibrations and responses at DE and NDE that are representative of typical dynamic scenarios in practical applications. The second is a dynamic condition in which the rotor rotates at different speeds between 1000 RPM and 3000 RPM.

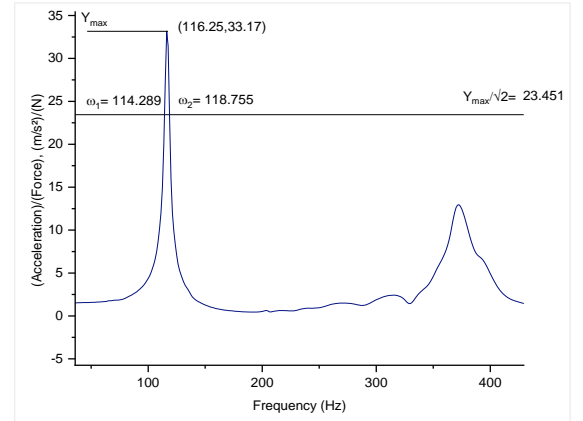
4.3.1 Static Condition

Frequency response functions and coherence are measured for tapered, cylindrical, spherical and self-aligned bearings during the impact hammer test at DE and NDE. When the impact test is conducted, the position of the input impact has a vital effect on the FRF results, which can be seen in the coherence response function. All bearing's input and output spectra are coherent, dropping at antinodes. The experiments are deemed replicable due to the high coherence between the input and output spectra, except at the antinodes. The high sampling rate provides a high resolution of the frequency spectrum. However, the half-power bandwidth method is originally derived

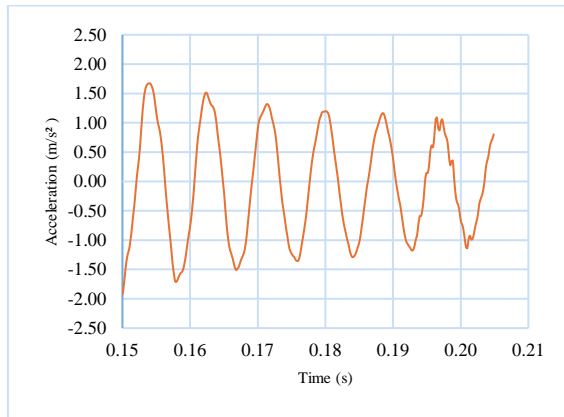
from the frequency response of a single-DOF system and is also widely used for estimating damping in multi-DOF systems. The resonance peaks width indicates modal damping, and the vibration analyser software analyses the input and output amplitude signals. The frequency response functions (FRFs) are generated using the acquired input and output signals.



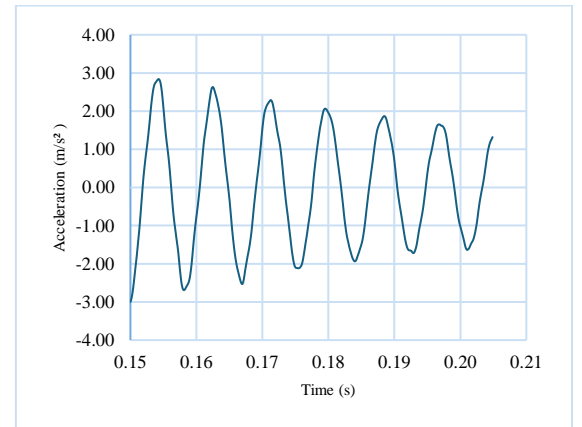
(a) FRF at DE



(b) FRF at NDE



(c) Free decay/ logarithmic decrement graph at DE



(d) Free decay/logarithmic decrement graph at NDE

Figure 4.3 Zoomed view of cylindrical bearing graphs for damping calculation

The half-power bandwidth method is employed to estimate the frequency domain damping ratio. Firstly, the resonant frequency (ω_n) and the maximum amplitude (Y_{max}) at resonance are identified in the frequency spectrum. The half-power points are established when the amplitude is $Y_{max}/\sqrt{2}$, and the corresponding frequencies on either side of the resonant frequencies, ω_1 and ω_2 , are also identified as illustrated in Fig. 4.3

(a)-(b) at both DE and NDE. The frequency range between these two points is greater at the lower amplitudes of the excitation frequency range. To calculate the half-power bandwidth, divide the frequency difference between the two half-power points by the mode's fundamental frequency. Finally, the damping ratio is computed using the half-power bandwidth expression given in equation (4.3) for cylindrical bearings. Similarly, the experimental damping ratio is then analysed using equation (4.3) for experimentally obtained FRF curves for various bearings. The calculated values of damping coefficients for all four bearings are shown in Table 4.1 for both DE and NDE.

Table 4.1 Damping coefficients of different bearings

	Experimental FRF				Free Decay Method	
	DE		NDE		DE	NDE
Bearing type	ω_n (Hz)	ξ (Damping)	ω_n (Hz)	ξ (Damping)	ξ (Damping)	ξ (Damping)
Tapered	90	0.02200	90	0.02202	0.02077	0.02149
Cylindrical	116.25	0.01920	116.25	0.01920	0.01747	0.01768
Spherical	110	0.01506	110	0.01537	0.01630	0.01658
Self-aligned	103.75	0.01321	103.75	0.01351	0.01132	0.01181

A free decay graph depicts the time-dependent behaviour of a damped system as shown in Fig. 4.3 (c)-(d) at both DE and NDE. Typically, it shows the amplitude or displacement of the system across successive peaks at an equilibrium position. The damping ratio quantifies the quantity of system damping. It is determined using the logarithmic decrement method, which compares the amplitudes of two peaks. In Fig. 4.3 (c)-(d), the amplitudes of the first and fourth peaks are used for damping calculations for cylindrical bearings at DE and NDE. Similarly, the experimental damping ratio is then analysed using equation (4.2) for experimentally obtained free decay curves for various bearings. The damping coefficients calculated for all four bearings are displayed in Table 4.1 for both DE and NDE. The FRF experiment

essentially measures the system's response to an input force across a range of frequencies, whereas, the free decay method, analyses the natural decay of the system's vibrations after an initial impulsive excitation. It is beneficial to validate damping values obtained from both methods and compare the results. This can help ensure consistency and reliability in the measurements. If the results align closely, it adds confidence to the accuracy of the chosen method.

Figures 4.4-4.7 (a)-(b) show the FRF curves of tapered roller, cylindrical roller, spherical roller and self-aligned bearings, respectively at both DE and NDE. It has been observed that the natural frequency of the rotor bearing system in the case of tapered roller bearings at DE and NDE is found to be 90 Hz each as shown in Fig. 4.4 (a)-(b). Peak amplitudes decrease when the damping ratio increases, which shows that the system's reaction is attenuated more quickly. Conversely, larger peak amplitudes and lower damping ratios indicate a less damped or more resonant response. Narrower bandwidths also attenuate vibrations more tightly around the resonant frequency, which indicates a higher damping ratio. The response is influenced by a broader range of frequencies when the damping ratio is low [143]. In Fig. 4.4 (a)-(b), peak amplitudes in FRF are different, but their bandwidths are tuned to achieve the same damping ratio at DE and NDE, i.e., 0.02200. Similarly, for all other bearings shown in Figs. 4.5-4.7 (a)-(b), the natural frequency at both DE and NDE is exactly same (116.25 Hz for cylindrical bearings, 110 Hz for spherical bearings and 103.75 Hz for self-aligned bearings) with some minor changes in peak amplitude and bandwidth which results in the same damping ratio in both DE and NDE. The experimental damping ratios of bearings from the FRF plot are found to be 0.01920, 0.01506 and 0.01321 at DE and 0.01920, 0.01537 and 0.01351 at NDE for cylindrical bearings, spherical bearings and self-aligned bearings respectively.

Figures 4.4-4.7 (c)-(d) show the coherence graphs corresponding to the FRF curve for tapered roller, cylindrical roller, spherical roller and self-aligned bearings at both DE and NDE. In all the graphs, the value of coherence is almost 95-100% except at antinodes which shows that the amplitude and phase of the FRF are very stable from one test to the next [146, 147].

Figures 4.4-4.7 (e)-(f) show the free decay curves of tapered roller, cylindrical roller, spherical roller and self-aligned bearings at both DE and NDE. The damping ratio affects the rate at which the amplitude or displacement diminishes with time. The damping ratio of the tapered bearing at DE is 0.02077 and at NDE is 0.02149. As shown in Fig. 4.4 (e)-(f), the variation in decay characteristics at the DE and NDE may suggest differences in damping and stiffness. It also aids in the identification of any imbalances, misalignments, mechanical looseness, or bearing-related problems that may be causing the observed discrepancies in decay patterns [148]. Similarly, for all other bearings, the experimental damping ratio from the free decay plot is found to be 0.01747, 0.01630 and 0.01132 at DE and 0.01768, 0.01658 and 0.01181 at NDE for cylindrical bearings, spherical bearings and self-aligned bearings respectively.

Figure 4.8 (a)-(b) show all bearings combined free decay graph to better visualise the settling time at DE and NDE. Furthermore, there is a significant difference in the settling time of the different bearings. It has been observed that the tapered roller bearing has the highest vibration amplitude of 2.85 m/s^2 , followed by the self-aligned bearing (2.09 m/s^2), cylindrical roller bearing (1.53 m/s^2), spherical roller bearing (0.74 m/s^2) at DE. The tapered roller bearing has the same settling time as cylindrical and spherical bearings. It has a high decay rate, which means a higher damping ratio. For self-aligned bearings, the settling time is much longer than other bearings, which indicates that self-aligned has a lower decay rate, which means a lower damping ratio.

For an underdamped single mode, the free response is

$$x(t) = Ae^{-\xi\omega t} \sin(\omega_d t), \quad \omega_d = \omega_n \sqrt{1 - \xi^2} \quad (4.5)$$

The visible envelope $e^{-\xi\omega t}$ is set by modal damping ratio ξ of the whole rotor bearing housing system. Changing the bearing changes both the equivalent damping and stiffness, so the decay rate change. Differences in ξ arise primarily from lubricant film shear/traction and rolling-sliding kinematics, which depend on bearing geometry and preload. In tapered roller bearings, the rolling element slides slightly along its length due to geometry mismatch (slide-roll ratio). This produces extra damping, so vibrations decay faster. Cylindrical rollers are nearly pure rolling in the central band and sliding at ends only which results in moderate damping. Self-aligning bearings

have more clearance and can adjust to misalignment which means less load concentration, so less damping. These mechanisms also shift the effective stiffness and natural frequency, explaining small differences in oscillation frequency. Resonance peaks shift in frequency because each bearing alters the equivalent system stiffness as shown in Fig. 4.9 (a)-(b).

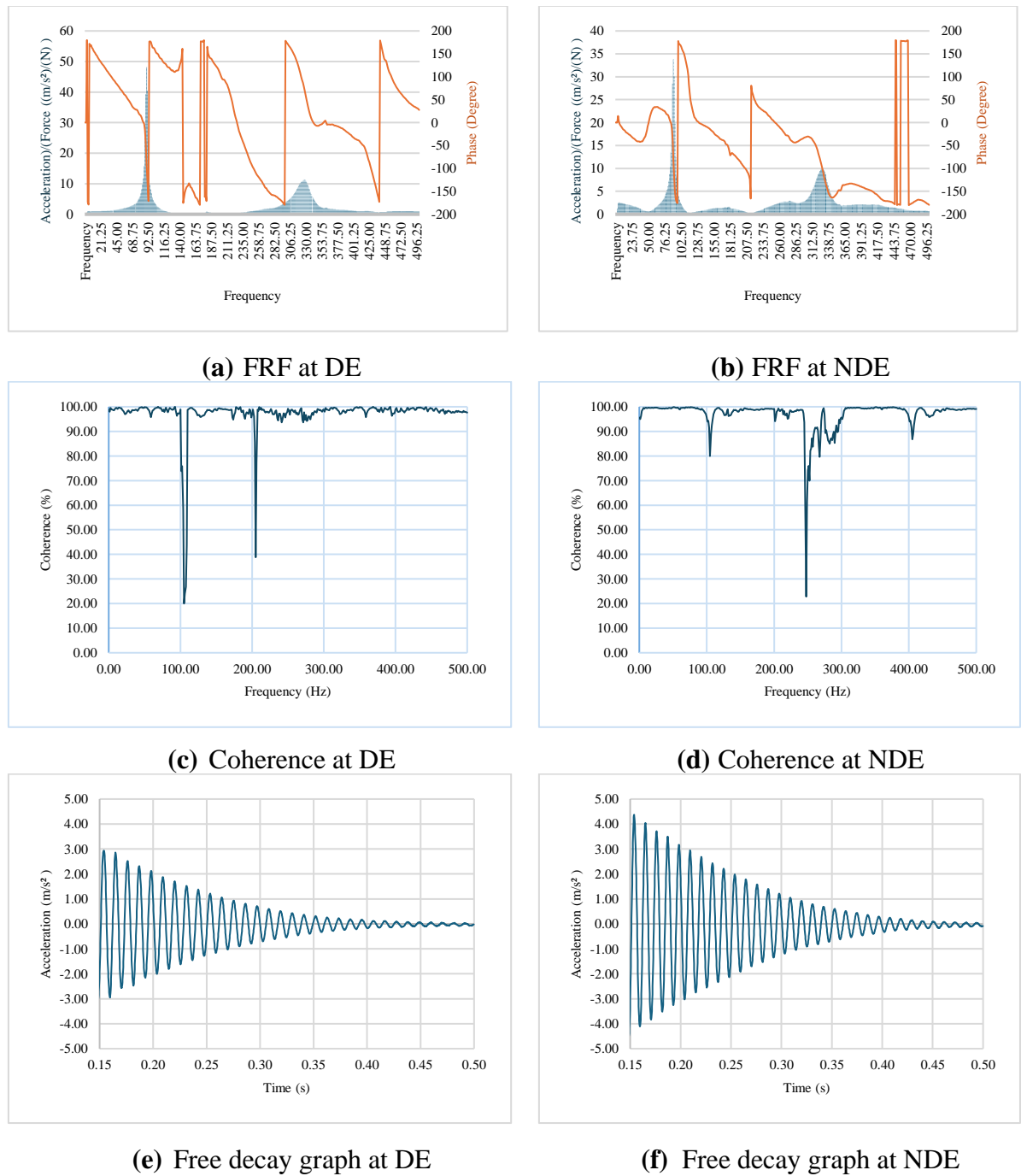
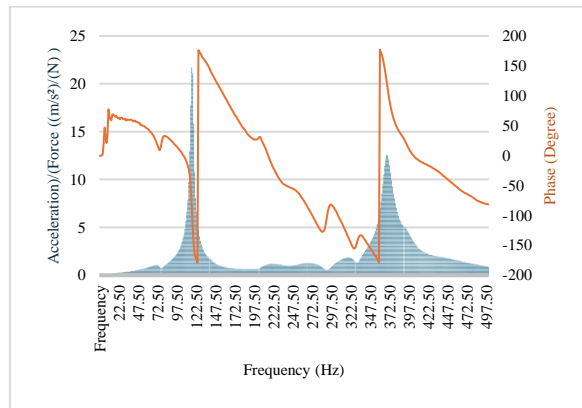
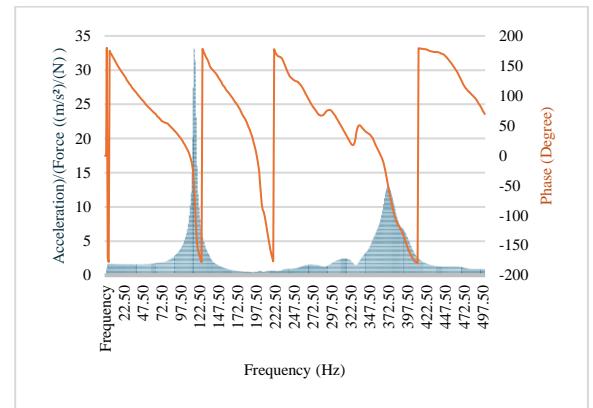


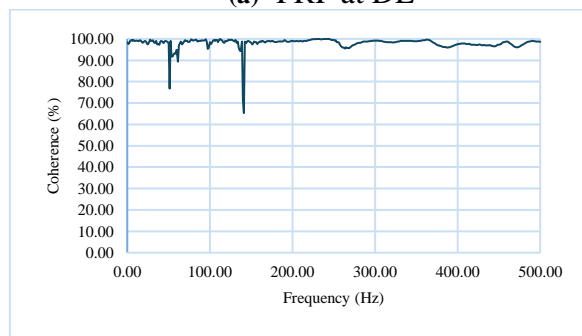
Figure 4.4 Tapered roller bearing



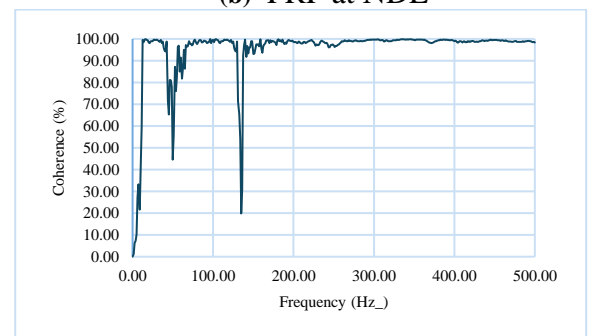
(a) FRF at DE



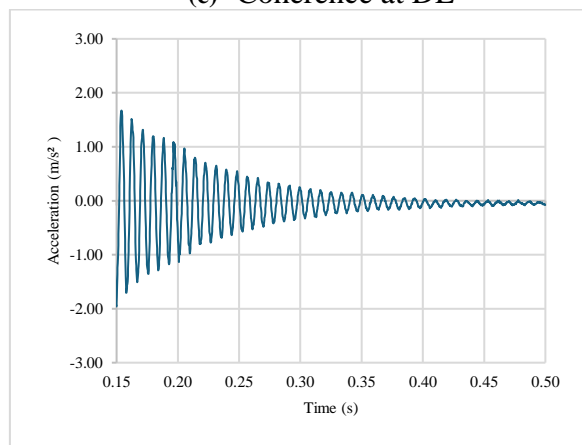
(b) FRF at NDE



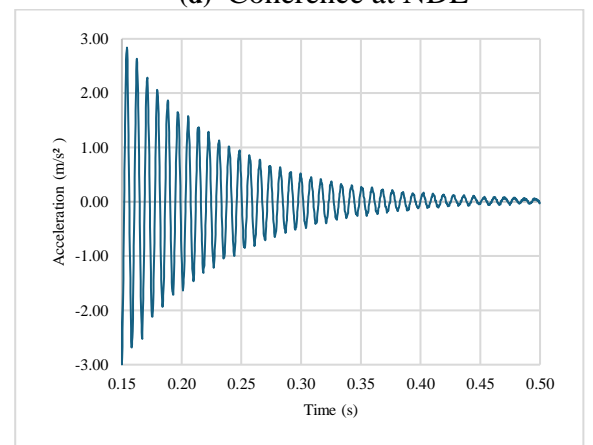
(c) Coherence at DE



(d) Coherence at NDE

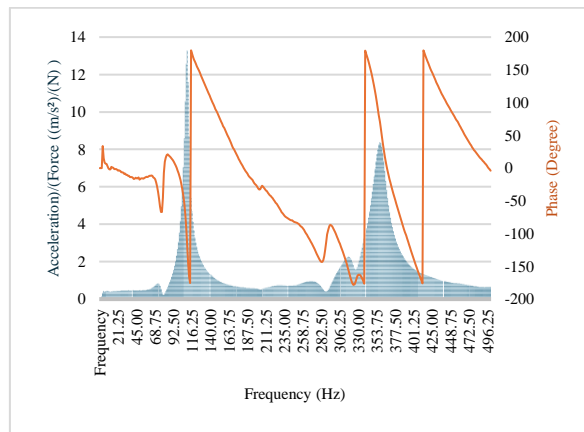


(e) Free decay graph at DE

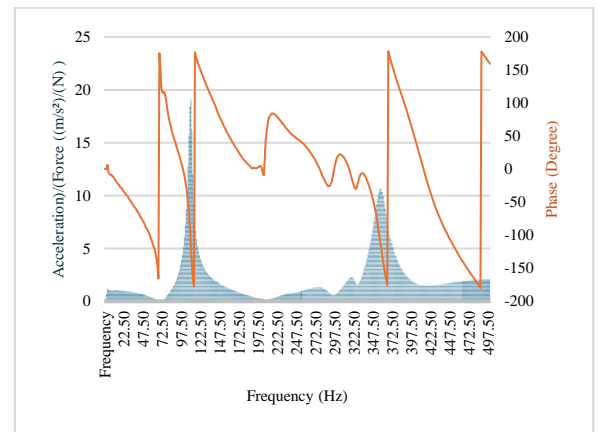


(f) Free decay graph at NDE

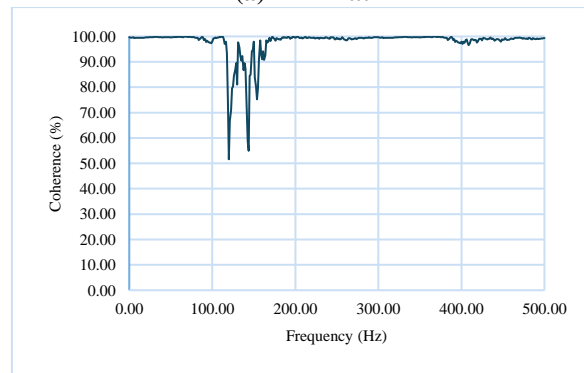
Figure 4.5 Cylindrical roller bearing



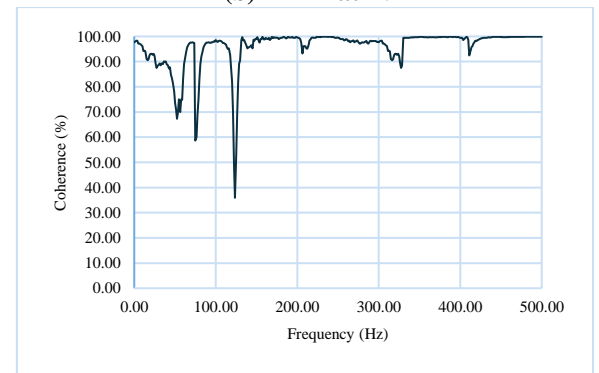
(a) FRF at DE



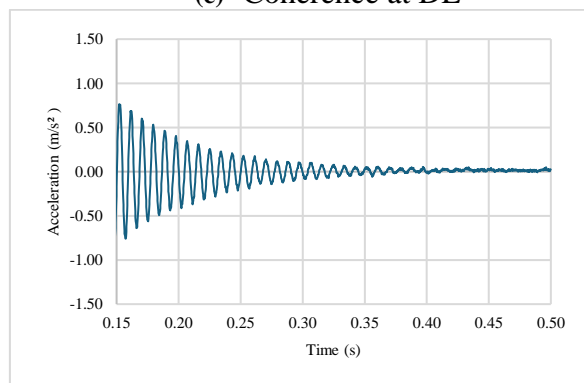
(b) FRF at NDE



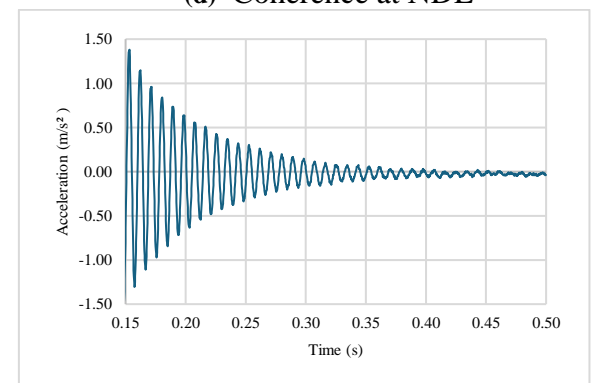
(c) Coherence at DE



(d) Coherence at NDE

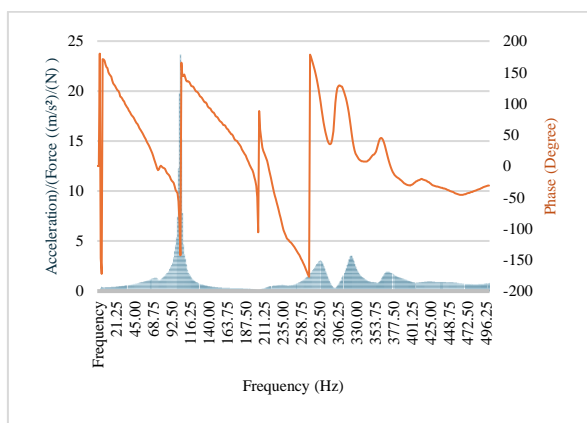


(e) Free decay graph at DE

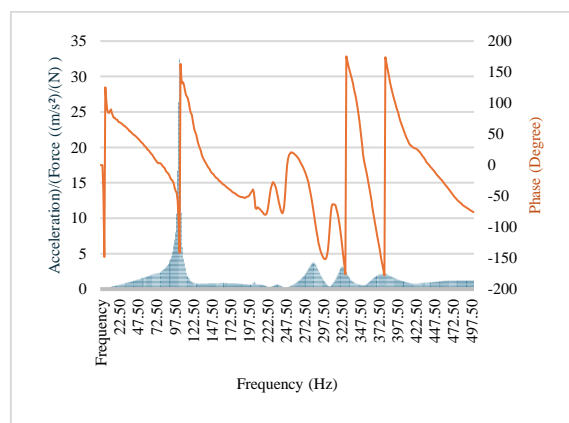


(f) Free decay graph at NDE

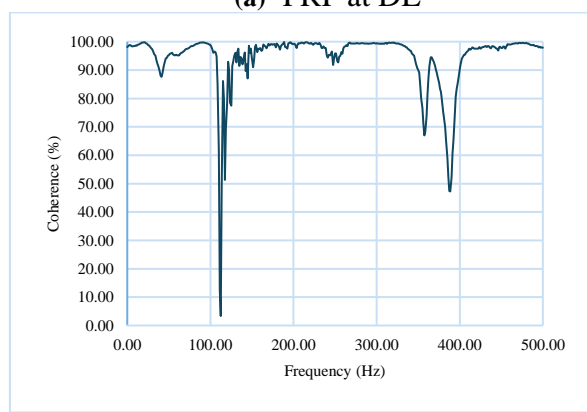
Figure 4.6 Spherical roller bearing



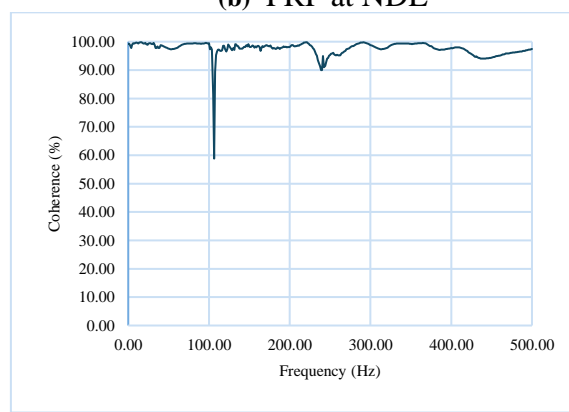
(a) FRF at DE



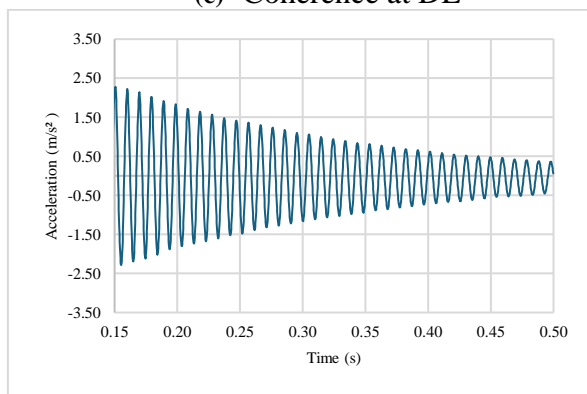
(b) FRF at NDE



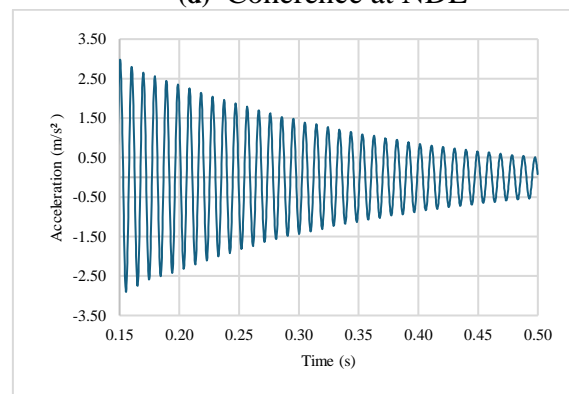
(c) Coherence at DE



(d) Coherence at NDE

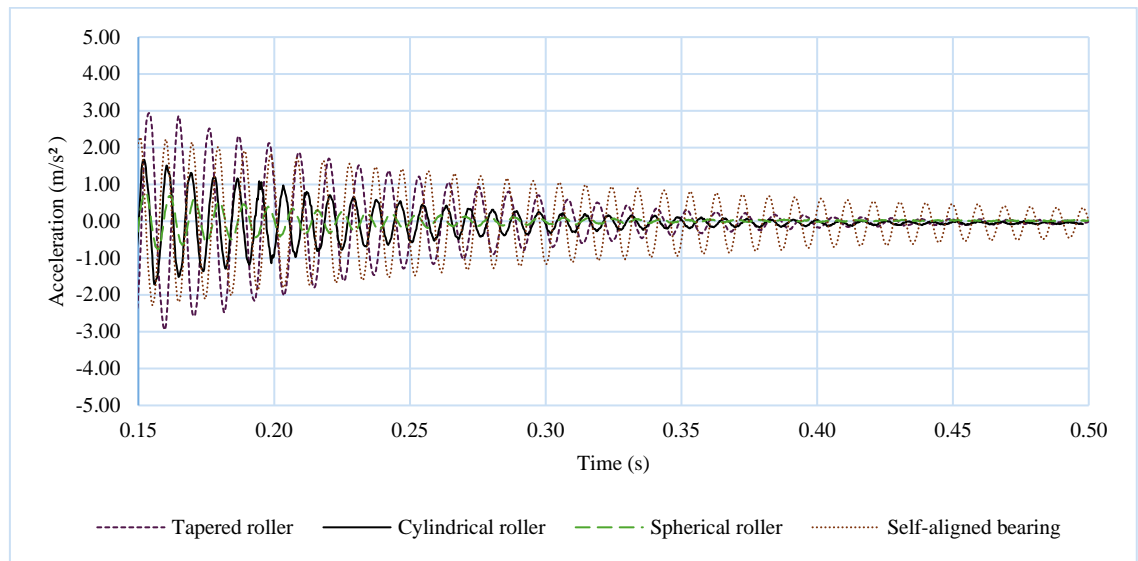


(e) Free decay graph at DE

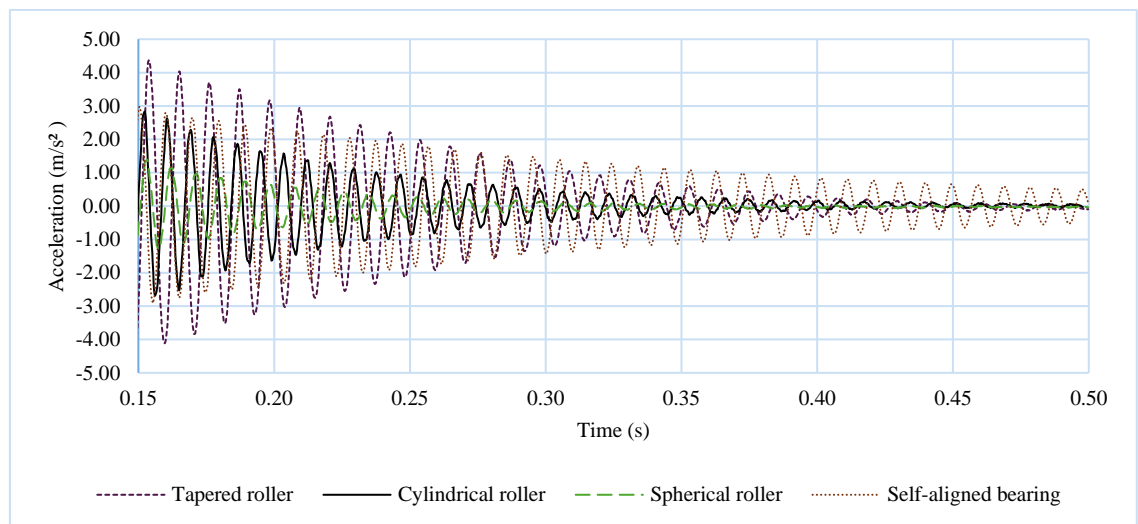


(f) Free decay graph at NDE

Figure 4.7 Self-aligned bearing



(a) Free decay at DE

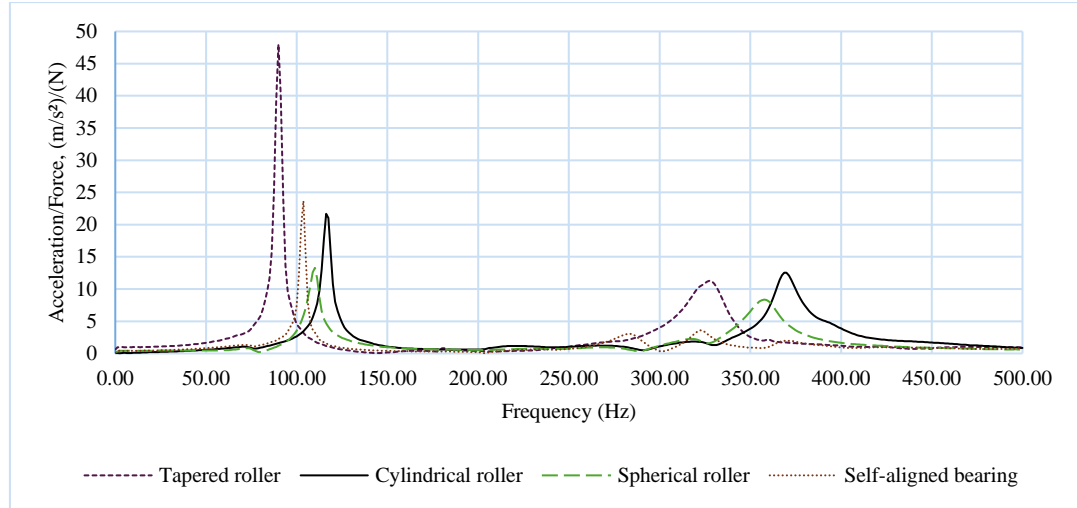


(b) Free decay at NDE

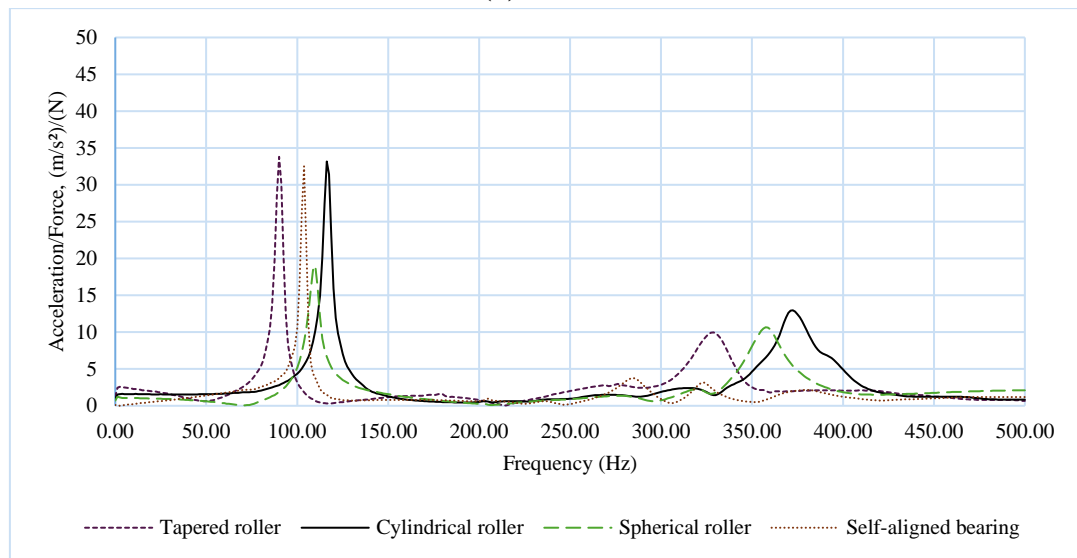
Figure 4.8 Combined free decay graph for all bearings

Figure 4.9 (a)-(b) shows the combined FRFs amplitude graph of all the bearings for improved visualisation at DE and NDE. It has been observed that the tapered bearing has a lower natural frequency of 90 Hz at both the DE and NDE. The damping ratio affects the natural frequency as well. The damping ratio ranges from 0 to 1 and is defined as the ratio of actual damping to critical damping. A higher damping ratio reduces the natural frequency more than a lower damping ratio [149]. As the damping

ratio approaches 1, the natural frequency approaches zero, denoting a system dampened to its critical level.



(a) FRF at DE



(b) FRF at NDE

Figure 4.9 Combined FRFs for all bearings

4.3.2 Dynamic Condition

Dynamic performance is the most essential analysis for a rotor-bearing system in its application. The antifriction bearings are loaded with different radial loads and the experimental frequency spectra have been obtained for four different types of bearings. However, the effect of the damping behaviour of different types of rolling element bearings is also examined with the help of the RMS value of acceleration.

Table 4.2. RMS (m/s^2) value of the acceleration of tapered roller bearing

RPM LOAD	1000	1200	1400	1600	1800	2000	2200	2400	2600	2800	3000
No load	0.42	0.58	0.59	0.76	2.72	1.39	1.62	1.78	1.55	1.96	1.91
2kg	0.48	0.56	0.82	1.70	1.50	1.52	1.64	1.74	2.01	2.19	2.75
3kg	0.71	0.84	1.32	1.63	1.98	1.68	1.80	2.17	2.97	3.54	3.59
5kg	0.39	0.57	0.78	0.93	1.05	1.12	1.39	1.41	1.91	2.15	2.02

Table 4.3. RMS (m/s^2) value of the acceleration of cylindrical roller bearing

RPM LOAD	1000	1200	1400	1600	1800	2000	2200	2400	2600	2800	3000
No load	1.12	1.31	1.59	1.91	2.55	2.83	3.01	3.27	3.81	4.84	5.08
2kg	1.19	1.33	1.76	1.82	2.23	2.65	3.03	3.47	3.99	4.30	4.49
3kg	0.92	1.33	1.67	1.80	2.37	2.47	2.74	3.42	3.74	4.07	4.27
5kg	0.87	1.34	1.49	1.81	2.09	2.64	3.01	3.44	3.95	4.19	4.18

Table 4.4. RMS (m/s^2) value of the acceleration of spherical roller bearing

RPM LOAD	1000	1200	1400	1600	1800	2000	2200	2400	2600	2800	3000
No load	2.14	2.33	2.82	3.07	6.68	5.14	4.79	5.95	6.15	5.56	6.12
2kg	1.44	1.85	2.54	3.40	3.69	4.54	5.81	7.11	7.49	8.57	10.48
3kg	1.83	2.10	2.76	2.82	3.10	4.19	3.83	4.64	4.52	5.38	7.59
5kg	1.75	2.30	2.42	2.74	3.29	4.16	3.54	3.88	5.16	5.18	5.67

Table 4.5. RMS (m/s^2) value of the acceleration of self-aligned bearing

RPM LOAD	1000	1200	1400	1600	1800	2000	2200	2400	2600	2800	3000
No load	2.93	4.21	5.61	8.23	9.38	10.17	11.11	13.09	19.39	20.28	20.51
2kg	2.80	4.16	5.23	6.30	8.01	10.81	11.71	13.82	15.15	16.07	20.05
3kg	2.87	4.98	6.35	7.52	9.02	10.35	12.65	14.68	16.65	19.84	19.84
5kg	3.12	3.91	4.40	5.10	5.77	6.17	7.94	10.06	11.32	12.77	14.24

The RMS values for different loading conditions (No load, 2kg, 3 kg and 5 kg radial load) at different speeds between 1000-3000 rpm are tabulated in Tables 4.2-4.5. The graphs between the measured RMS value of amplitude for bearings (tapered, cylindrical, spherical and self-aligned bearings) vs speed are shown in Fig. 4.10.

Figure 4.10 (a) shows the relationship between the RMS value of acceleration and speed under no load conditions. An interesting result has been observed that the RMS value increases as the speed increases for all the bearings [150, 151]. At the same time, the RMS value of the tapered bearing is lower across all the speed ranges, which shows that the tapered bearing damps more vibration among all the bearings. The root mean square (RMS) value is a metric that quantifies the energy level of a signal by measuring the magnitude of its vibration signals. It measures the amplitude of the vibration signal, considering its decay. A lower RMS value corresponds to a reduced amplitude of vibration, indicating a higher damping ratio.

Furthermore, the self-aligned bearing has a higher RMS value for all the speed ranges, showing the self-aligned bearing damps less vibration. Similarly, it has been observed that RMS acceleration values are low in tapered bearings at almost all shaft rotational speeds for other loading conditions of 2kg, 3kg and 5kg as shown in Fig. 12 (b)-(d). The tapered roller bearings' geometric design can potentially decrease contact stresses and vibrations. Tapered roller bearings are specifically engineered to accommodate both radial and axial loads, and their tapered shape enables effective distribution of the load. This design feature can facilitate a more seamless rolling interaction between the rolling components and the raceways, leading to reduced levels of vibration.

The trend of these experimental results is compared with the half-power bandwidth and logarithmic decrement methods to check the results correctness. The results are good in agreement with each other, proving the experiment's correctness and robustness.

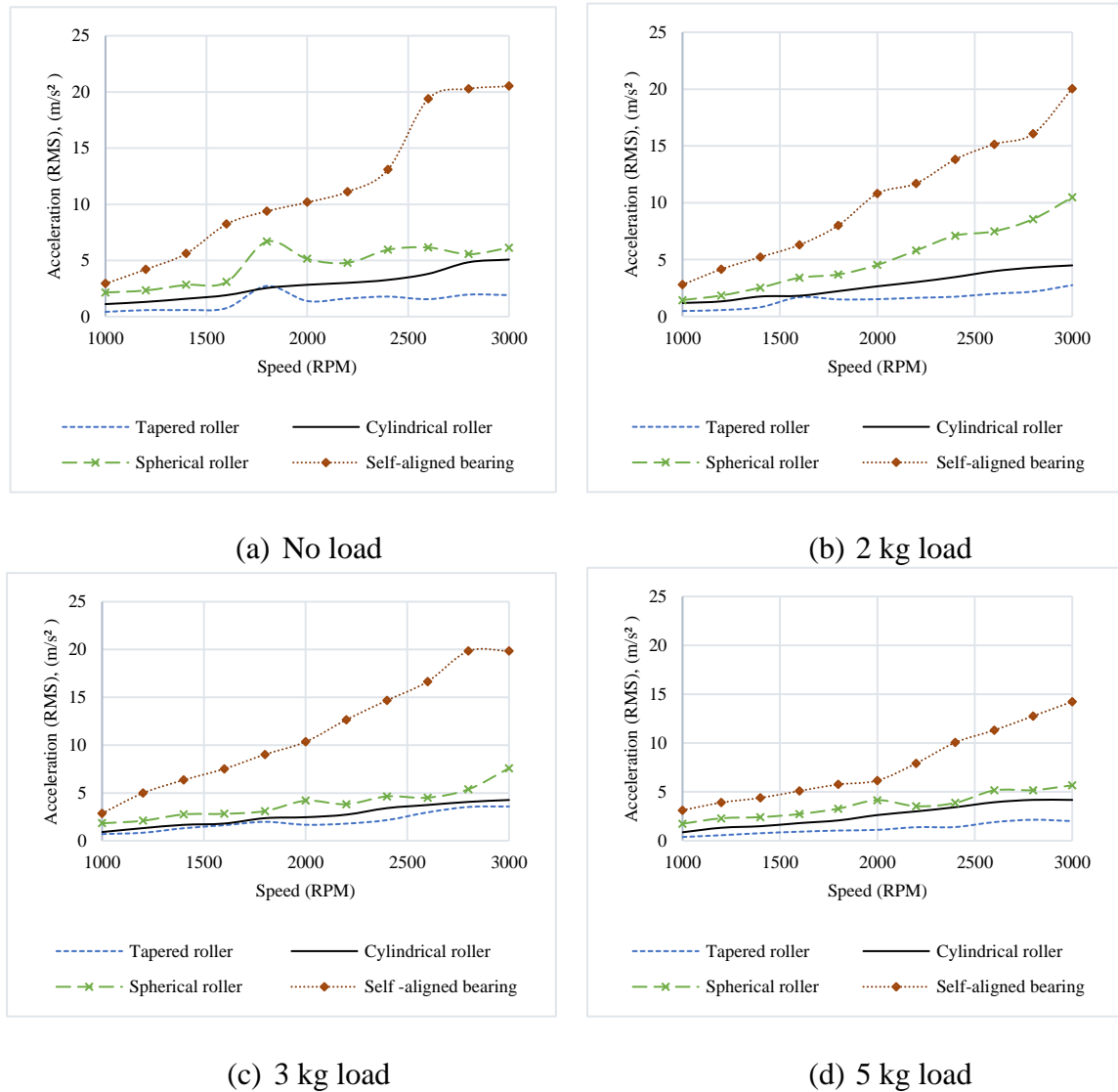


Figure 4.10 RMS value of acceleration at a different speed under different loading conditions

4.4 Summary of the Chapter

This chapter provided an in-depth analysis of damping in four antifriction bearings. The damping ratios were determined through two distinct approaches—free decay and

frequency response function (FRF)—while under static conditions. To corroborate and reinforce the findings from the static analysis, dynamic tests were performed by applying forced vibration to the bearings at different speeds. The analysis of outcomes from both static and dynamic methods revealed consistent patterns, enhancing the credibility of the experimental techniques and providing important insights into the damping characteristics of various bearing types. The experimental work observes the following significant findings:

- The natural frequency and damping ratios are different for each antifriction bearing, which shows that different bearing designs exhibit different vibration characteristics.
- The damping ratios derived from the frequency response function and free decay methods appear to be consistent between DE and NDE for each type of bearing. The results from these two methods align well with one another.
- The tapered roller bearing exhibits a significant decay rate, indicating a higher damping ratio, in comparison to cylindrical, spherical, and self-aligned bearings. Experimental findings prove that ball bearings exhibit lower damping compared to roller bearings. The explanation could lie in their smaller contact area and low internal friction.
- The trend of dynamic analysis results supports the half-power bandwidth and logarithmic decrement method results. Both experimental techniques validate each other by showing similar findings. For all bearings, vibration amplitude rises as rotor speed or frequency increases. RMS, on the other hand, increases with load until it reaches a maximum and then declines.
- Sometimes, systems may not be fully explained by a single approach because many things can affect them. So, using multiple methods to characterise the damping behaviour of structural dynamics precisely is advantageous.
- Due to the simplicity of the proposed implementation, the present approach may have future applications. It is believed that the comprehensive nature of our experimental setup and analysis can serve as a foundation for future

research in the field of bearing dynamics. Researchers can build upon our methodologies and findings to delve deeper into the complexities of damping behaviour in diverse bearing types and operating conditions, whereby deriving the various universal results.

Chapter 5 Vibration Behaviour of Healthy Tapered Roller Bearing at Different Operating Load and Speed

This chapter examines the vibration and noise characteristics of a healthy tapered roller bearing (TRB) across different operational conditions. An experimental study was carried out to assess the impact of various process parameters on the root mean square (RMS) value of vibration signals and the equivalent continuous sound level (L_{eq}) produced during operation.

5.1 Introduction

The vibrational characteristics of tapered roller bearings (TRBs) under various operational and loading conditions are essential for comprehending their dynamic performance and overall reliability. Vibration and acoustic investigations have been performed on healthy TRBs to establish a baseline for comparison. These analyses assist in explaining the intrinsic vibration signatures of healthy bearings, which provide reference data for detecting variations in subsequent defect identification investigations.

Researchers have developed various machine fault detection systems and achieved great success in early detection by continuous monitoring and analysing vibration signals [152–154]. Vibration is a mechanical phenomenon reflecting the running condition and fault statistics. It is widely used in the detection of bearing faults. Some statistical techniques based on root mean square, kurtosis, and so on have been used for condition monitoring in previous studies [155, 156]. The Fourier transform has been used to connect the time and frequency domains [157]. When dealing with stationary signals, the FFT is the most commonly used signal processing technique [158]. However, it has various drawbacks, one being the loss of temporal information during frequency domain transformation. It is impossible to tell when an event occurred by looking at the FFT of a signal. This disadvantage is not significant in the case of a stationary signal [159] However, it is known that its accuracy declines when time-varying frequencies are present. As previously stated, frequency will be the

primary factor in predicting faults. Many references have been provided which revolve around the accuracy of estimating the signal frequency. Sensor response signals are analysed in time, frequency, and time-frequency domains [154]. The effectiveness of research is marked by mathematical analysis of experiment data, which provides a meaningful inference of the same. RSM is valuable for the process development, enhancement, and optimisation [79]. RSM is used to investigate the role of localised defects of different sizes in bearing vibration as the process response [160]. Using kurtosis as a signal processing technique for condition monitoring of ball bearings, RSM investigates the influence of load, speed, and defect on bearing vibration [81]. RSM technique to diagnose defects on a faulty rolling bearing [82]. The experimental data confirmed the mathematical model's capacity to anticipate fault frequencies and harmonics. They developed RSM to predict the dynamic response of a rotor-bearing system. RSM was suggested by [83] to determine the ideal placement strategy for sensors that do not require physical contact to ensure effective monitoring of rotating machine parts. The essence of practical research is theoretical predictions supported by experimental data. The effectiveness of studies is substantially enhanced, and insightful conclusions can be drawn from the data collected when statistical methods are properly applied. The experiment's design and data analysis are the two main focuses of each scientific investigation. To experiment well, you need to know the important things that affect the results. Designing experiments helps find the important factors that explain a change in a process. DOE also helps people to figure out how the things that affect the system work together [161]. Experiments can be planned using approaches such as the response surface method (RSM), the factorial design, or the Taguchi method. Most of the researchers used the ball bearing and cylindrical roller bearing to obtain the optimal condition of bearing vibration through different optimisation techniques. But few of them considered tapered bearing for the analyses.

The author has found that in addition to vibration analyses, the noise data is an important parameter and its effect on bearing response should also be investigated. This study examines the application of the Taguchi technique on the time domain values of the bearing noise and vibration signal to analyse the influence of load and RPM on tapered bearing performance. For statistical analysis, time domain indices

such as Leq for noise and RMS, crest factor, and kurtosis are typically employed for vibration. The RMS and Leq of the signal have been selected as the response or output parameters in this investigation. Kurtosis is regarded as a useful criterion for measuring bearing defects. The DOE approach is used to create experiments. Experiments were conducted using SKF 30206 tapered roller. Mathematical relations and models have been established to assess input factors' effect on response variables.

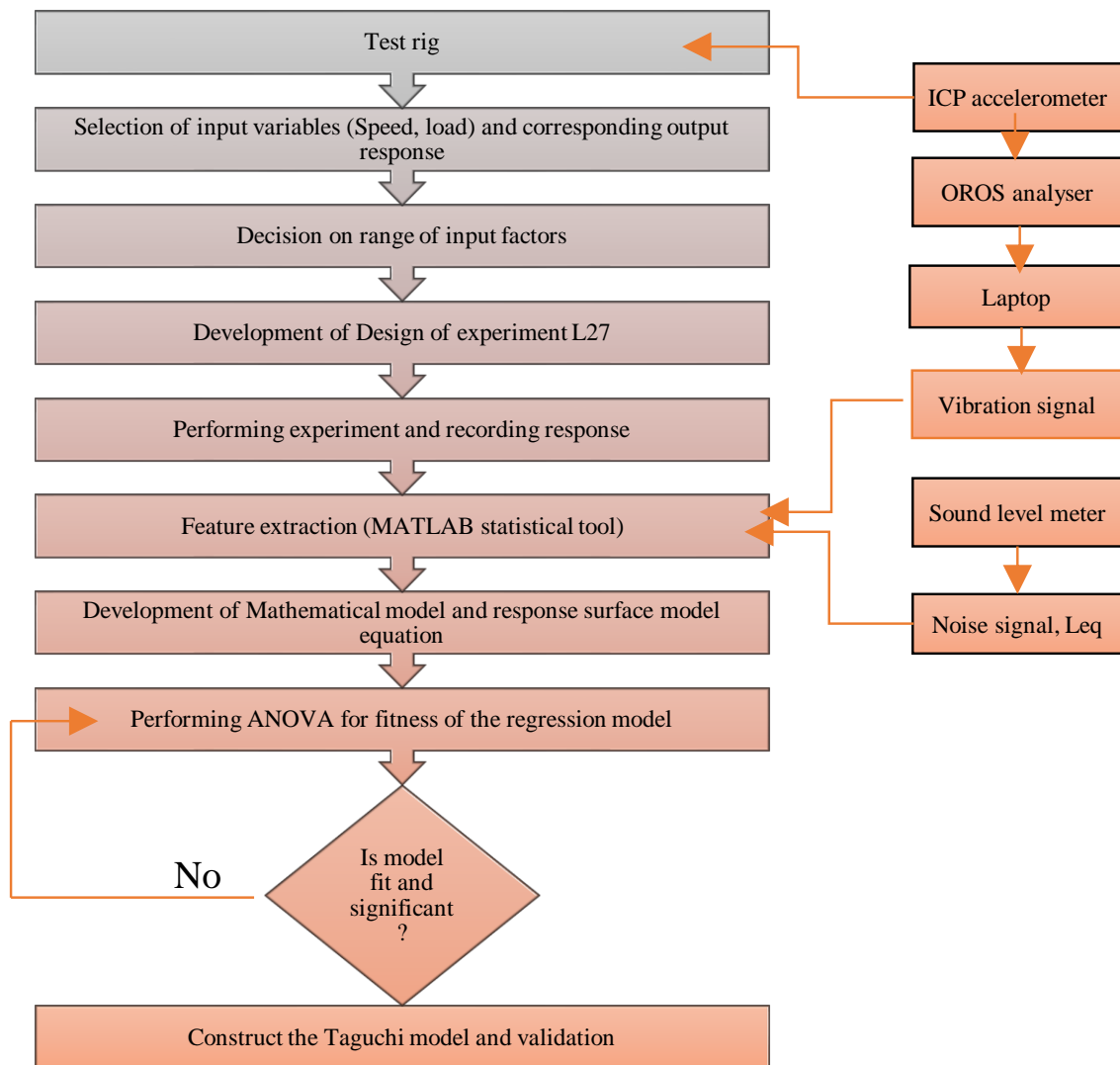


Figure 5.1 Flowchart of the proposed methodology

5.2 Design of Experiment using the Taguchi Technique

In the present study, the Taguchi approach is used to design the experiment, and the importance of parameters is investigated. ANOVA is a statistical method for

determining the impact of process parameters on experiments. The F-test determines the extent to which the parameters contribute to the process's response. The significance of factors and their interactions is indicated in the analysis of variance table by $\text{prob} < 0.05$ (for 95% confidence interval, CI). Three-level full factorial design is a way to set up an experiment by putting each of the factors at three stages: low, medium, and high. These levels are encoded in computer code (1, 2, 3), and two factors are considered for the study. The process of the whole Taguchi is shown in Fig. 5.1. DOE has been established for three levels with two variables (speed and load). As shown in Table 5.1, all factors are evaluated as (L-1, L- 2, L-3) for the low, medium and high, and high levels, respectively. The experimental runs have been carried out as per experimental design L27 (3^2) to obtain vibration responses in terms of RMS and Leq values at drive and non-drive ends, as shown in Table 5.2. RMS values are calculated using the accelerometer's time domain signal for acceleration.

Table 5.1 Input parameters and their level

Input parameters	Load (N)	RPM
Symbol	A	B
L- 1	20	1000
L- 2	30	1500
L- 3	50	2000

In the Taguchi method, the response for each observation is shown in Table 5.3 as a signal-to-noise (S/N) ratio. The "smaller is better" principle is used in this evaluation, so the RMS and Leq values must be small. The process response and the control factors are used to determine the signal-to-noise ratio. Also, an analysis of variance has been conducted to determine which governing feature was statistically important so that the optimal combo of the controlling factors, called the "optimal combination," could be predicted [162, 163]. The Taguchi method gives the S/N ratio (smaller is better) as follows [164]:

$$(S/N)_{SB} = -10 \log \left(\frac{1}{n} \sum y_i^2 \right) \quad (5.1)$$

Where n= number of replications.

Table 5.3 provides average factor characteristics for each level. The S/N ratio response combines the repetitions and the effects of noise stages into one coherent piece of information.

Table 5.2 I/P (uncoded form) and O/P (or response) parameters as per DOE and experiment results

Exp. No	I/P parameters		O/P or response parameter			
	A	B	RMS (DE) m/s ²	RMS (NDE) m/s ²	Leq (DE) dB	Leq (NDE) dB
1	1	1	28.65	3.1	96.4	95.6
2	1	1	27.84	2.78	96.2	95.1
3	1	1	28.79	3.27	96.5	95.8
4	1	2	55.52	9.15	101.5	99.7
5	1	2	54.72	9.93	101.1	99.6
6	1	2	58.29	9.89	101.2	99.7
7	1	3	73.36	13.79	103.7	101.9
8	1	3	79.66	13.72	103.9	101.9
9	1	3	77.87	14.22	103.7	102.1
10	2	1	60.09	7.29	95.6	94.5
11	2	1	52.95	6.00	95.2	94.3
12	2	1	51.97	6.55	95.2	94.6
13	2	2	64.66	8.26	102.2	99.6
14	2	2	72.36	8.54	103.3	99.7
15	2	2	68.81	8.59	102.5	99.6
16	2	3	75.3	12.52	104.1	102.4
17	2	3	74.95	12.81	103.9	102.5
18	2	3	82.82	13.22	104.4	102.3
19	3	1	37.44	6.36	92.8	92.5
20	3	1	39.42	6.08	92.9	92.1

21	3	1	35.85	7.64	92.1	92.9
22	3	2	60.38	12.5	99.2	98.4
23	3	2	53.83	12.17	98.9	98.3
24	3	2	62.93	12.2	99.4	98.3
25	3	3	66.32	12.84	101.1	98.9
26	3	3	76.8	15.74	102	99.1
27	3	3	79.6	16.3	102.2	99.3

Table 5.3 Signal-to-noise ratio for RMS DE, RMS NDE, Leq DE and Leq NDE

Exp. No	S/N ratio RMS (DE)	S/N ratio RMS (NDE)	S/N ratio Leq (DE)	S/N ratio Leq (NDE)
1	-29.0755	-9.70522	-39.6785	-39.6001
2	-34.9943	-19.7025	-40.1093	-39.971
3	-37.7308	-22.8676	-40.3212	-40.1692
4	-34.8265	-16.4384	-39.5849	-39.5056
5	-36.7369	-18.5521	-40.2287	-39.9681
6	-37.8168	-22.1802	-40.3518	-40.206

Table 5.4 Response table for signal-to-noise ratio

Response	Level	Load	RPM
RMS DE (smaller is better)	Delta Rank	2.53 2	5.86 1
RMS NDE (smaller is better)	Delta Rank	3.21 2	8.63 1
Leq DE (smaller is better)	Delta Rank	0.25 2	0.74 1
Leq NDE (smaller is better)	Delta Rank	0.21 2	0.62 1

5.3 Results and Discussion

5.3.1 Effect of Process Parameters on Leq

To achieve the lower Leq at both drive and non-drive ends is always desirable, smaller the better option is selected. Leq's signal-to-noise ratio is determined by Equation (5.1).

For our study, we have considered L27 orthogonal array design, that is, 3^2 factorial designs with three times replication. Each of the 9 experiments is performed thrice. In this, 27 experimental combination runs have 26 degrees of freedom (DOF). Each main effect (ME) has 1 DOF. Thus 2 DOF out of 26 are utilised to analyse A and B. For analysing the statistical significance of factors, an additional 24 DOF are now available. These are used in ANOVA. It may be necessary to get an adequate degree of freedom, sample size, and sensitivity in case of small effects. A larger number of replications will provide more degrees of freedom for error term and improve the precision and power of the experiment.

The linear polynomial mean of squares (MS) and a sum of squares (SS) were determined, and ANOVA was used to test for "probability>F" (≤ 0.05) with a 95 percent confidence interval (CI) at the 5% level of significance. For the model of Leq at DE and NDE, the F-values are 107.97 and 135.22, as shown in Tables 6 and 7 entails its significance. p-values less than 0.05 indicate significant model terms in the ANOVA table. Two model terms are important here: A and B. In contrast, model terms are deemed insignificant when p-values are greater than 0.05.

The involvement of each input process parameter is shown in Tables 5.5 and 5.6. The RPM shows the maximum delta value and is graded 1, i.e., RPM is the utmost momentous factor for Leq followed load, as shown in Table 5.4 [87]. Analysis of variance results for Leq also suggests that the RPM has the prime role of about 80.43 and 80.9% for DE and NDE, respectively, as shown in Tables 5.5 and 5.6. The influence of different parameters, like RPM and load on Leq, are shown in Figs. 5.2(a) and 5.3(a). The Leq is directly related to speed, and it always goes up as the speed goes up. However, Leq increases with load up to a maximum value and then decreases. This is because the equipment's natural frequency matches the excitation frequency, producing high noise, and the resonance noise becomes less after passing. Figs. 5.2(b)

and 5.3(b) show the main effect plot of the signal-to-noise ratio for Leq. This graph determines the input process variables values that decrease Leq. The minimum Leq is achieved at level 3 for load and level 1 for speed. The best value across various parameters for minimising Leq is A3B1. The linear dependency among the value of governing factors (Load and Speed) and Leq is obtained. Using predetermined values for the load, speed, and ANOVA to predict Leq, a linear regression model is built, which is shown below. The created model offers a linear relationship between parameters and the unknown quantity.

$$Leq (DE) = 90.17 - 0.954 A + 0.008456 B \quad (5.2)$$

$$Leq (NDE) = 90.48 - 0.842 A + 0.007000 B \quad (5.3)$$

At A3B1 Leq (DE) = 93.856 and Leq (NDE) = 93.271

Equations (2) and (3), which is used to make a model for predicting Leq, worked well because the points on the normal probability graph in Figs. 5.4 and 5.5 showed an approximate linear pattern with a normal distribution that broke apart only slightly [165, 166]. Figures 5.4 and 5.5 also show that the RVFV graph displays a random pattern, indicating that residual variance is nearly constant. The RVOP demonstrate that the obtained data can be used to determine the non-random error. Also, the FVRP shows no outliers, which proves that the data were more diverse. But the bar chart is negatively skewed, indicating that the initial observations are much more crucial to the overall results [167].

Table 5.5 ANOVA effect for S/N Ratios of Leq (DE)

Parameters	DoF	Sum of squares	Mean of squares	F-value	p-value*	% Contribution
Model	2	359.956	179.978	107.89	0.000	
LOAD	1	38.222	38.222	22.91	0.000	9.5
RPM	1	321.734	321.734	192.87	0.000	80.43
Error	24	40.036	1.668			
Lack-of-Fit	6	37.802	6.300	50.78	0.000	
Pure Error	18	2.233	0.124			
Total	26	399.992				

Note: A p -value of 0.000 (commonly shown as 0.000 in software outputs, but technically indicating $p < 0.001$) holds significant importance and relevance in statistical analysis. The value is not zero; instead, it indicates that the p -value is exceedingly small—beyond the accurate display capabilities of the software [168]

In Fig. 5.10 the Pareto chart shows the absolute values of the standardised effects, from the biggest effect to the smallest effect. A reference line is also drawn on the chart to show which effects are statistically important. The significance level (represented by alpha) determines the location of the statistical significance reference line. Figures 5.10(a) and (b) show a Pareto chart. Bars that cross the reference line are statistically important. In this Pareto chart, the bars showing factors A and B cross the 2.06-point reference line. With the current model terms, there is a 0.05 chance that these factors are important.

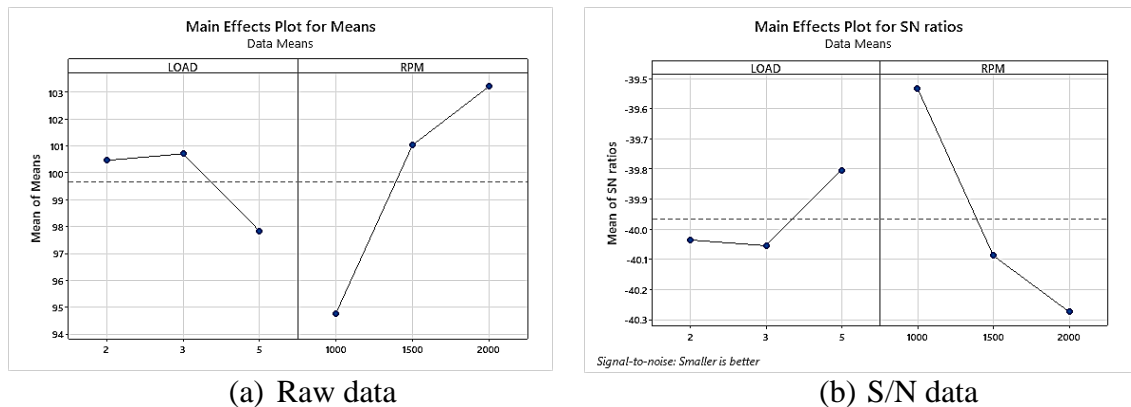


Figure 5.2 Effect of process parameter on Leq DE

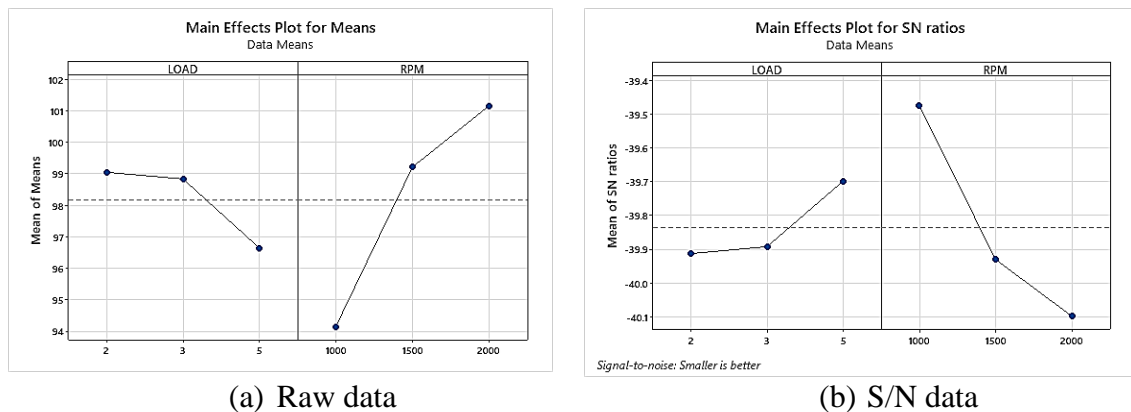


Figure 5.3 Effect of process parameter on Leq NDE

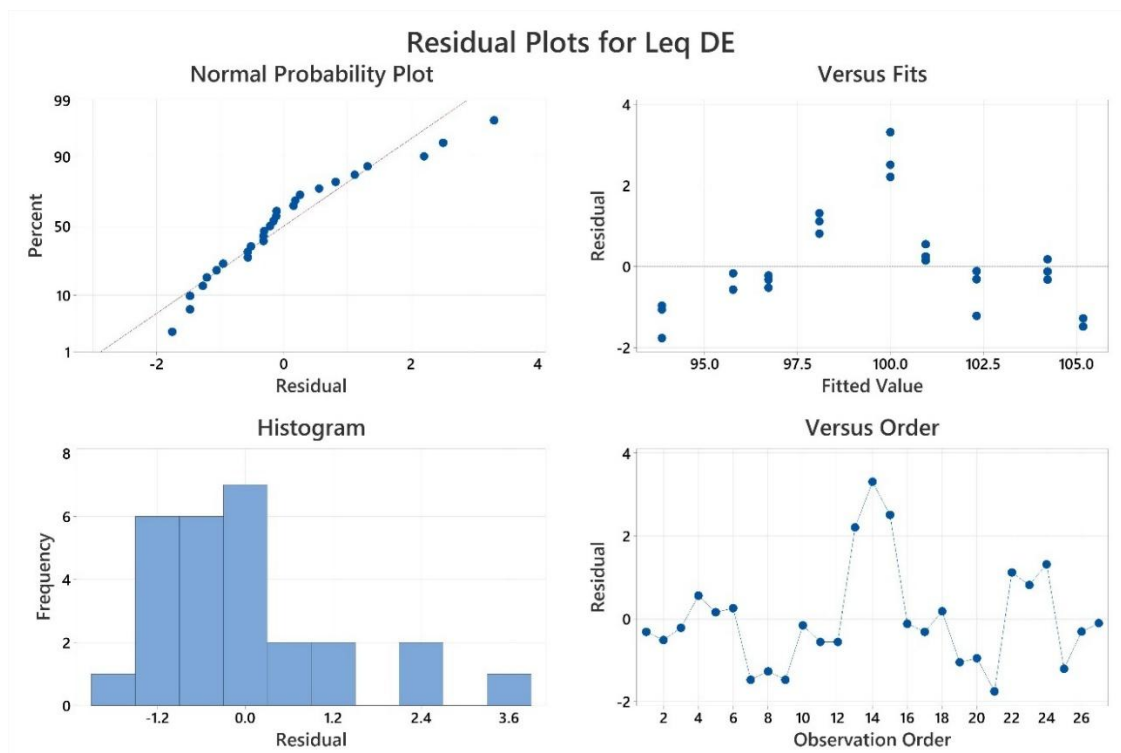


Figure 5.4 Residual plot of Leq DE

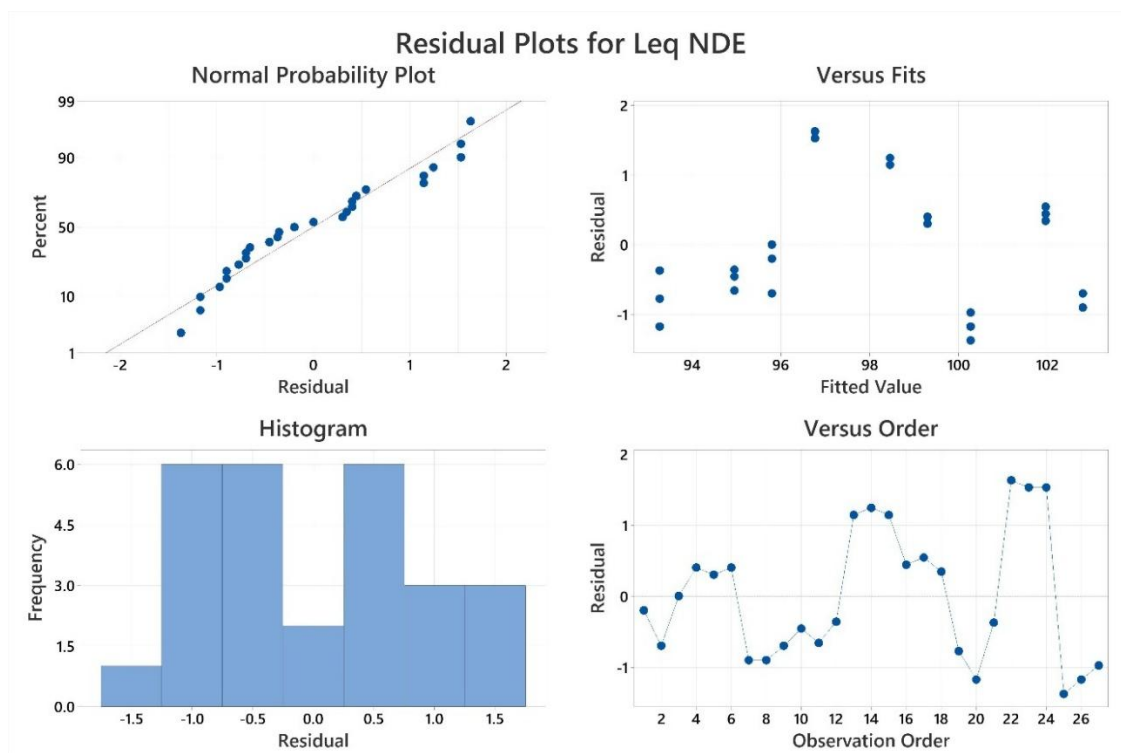


Figure 5.5 Residual plot of Leq NDE

Table 5.6 ANOVA effect for S/N Ratios of Leq (NDE)

Parameters	DoF	Sum of squares	Mean of squares	F-value	p-value*	% Contribution
Model	2	250.281	125.140	135.22	0.000	
LOAD	1	29.781	29.781	32.18	0.000	10.9
RPM	1	220.500	220.500	238.26	0.000	80.9
Error	24	22.211	0.925			
Lack-of-Fit	6	21.438	3.573	83.16	0.000	
Pure Error	18	0.773	0.043			
Total	26	272.492				

5.3.2 Effect of Process Parameters on RMS

Achieving the lower RMS value at both DE and NDE is always desirable, so smaller the better option have opted. The signal-to-noise ratio for RMS DE is designed by Equation (5.1).

For the model of RMS at DE and NDE, the F-values are 40.97 and 112.82 in Tables 5.7 and 5.8 shows that it is significant. In the analysis of variance table, significant model terms are specified with p-values < 0.05. In the RMS DE case, term A is significant, and term B is insignificant. But in the RMS NDE case, both terms are significant. Participation of numerous input parameters is shown in Tables 5.7 and 5.8. The RPM shows the maximum delta value and is graded 1, i.e., the RPM is the utmost important parameter for RMS, followed by the load [83] [87], as expressed in Table 5.4. Analysis of variance results for RMS also confirms that the RPM has a major role of about 77.33 and 82.7%, as shown in Tables 5.7 and 5.8. The influence of different parameters, like RPM and load on RMS, are shown in Figs. 5.7(a) and 5.8(a). The RMS is proportionate to speed and increases with an increase in speed. However, RMS increases with load up to a maximum value and then decreases [83]. This is because the equipment's natural frequency matches the excitation frequency, which produces high vibration, and the resonance vibration becomes less after passing. Figs. 5.7(b) and 5.8(b) display the RMS's main effect plot of the signal-to-noise ratio. This plot is used to find the values of the I/P process parameters that will minimise RMS. The minimum

RMS reaches level 1 for load and level 1 for speed. The linear relationship between the values of the controlling factors (Load and Speed) and RMS is discovered. The linear regression equation is derived using Minitab software from established load and speed values. To predict RMS, the following linear regression model is obtained. The developed model provides a linear relationship between parameters and the unknown quantity. The model developed for RMS prediction, represented by Equations (4 & 5), was acceptable. The points on the normal probability graph shown in Figs. 5.6 and 5.9 follow a roughly linear pattern with a normal distribution and a small disintegration. Figures 5.6 and 5.9 also show that the RVFV graph demonstrates a random pattern, which shows that residuals have an almost constant variance. The RVOP shows that the collected data can be used to find an error that is not random. Also, because no outliers were found, the plot of frequency versus residual confirms that the data vary more finely [167].

$$RMS (DE) = 4.82 + 0.16 A + 0.03596 B \quad (5.4)$$

$$RMS (NDE) = -5.65 + 0.841 A + 0.008454 B \quad (5.5)$$

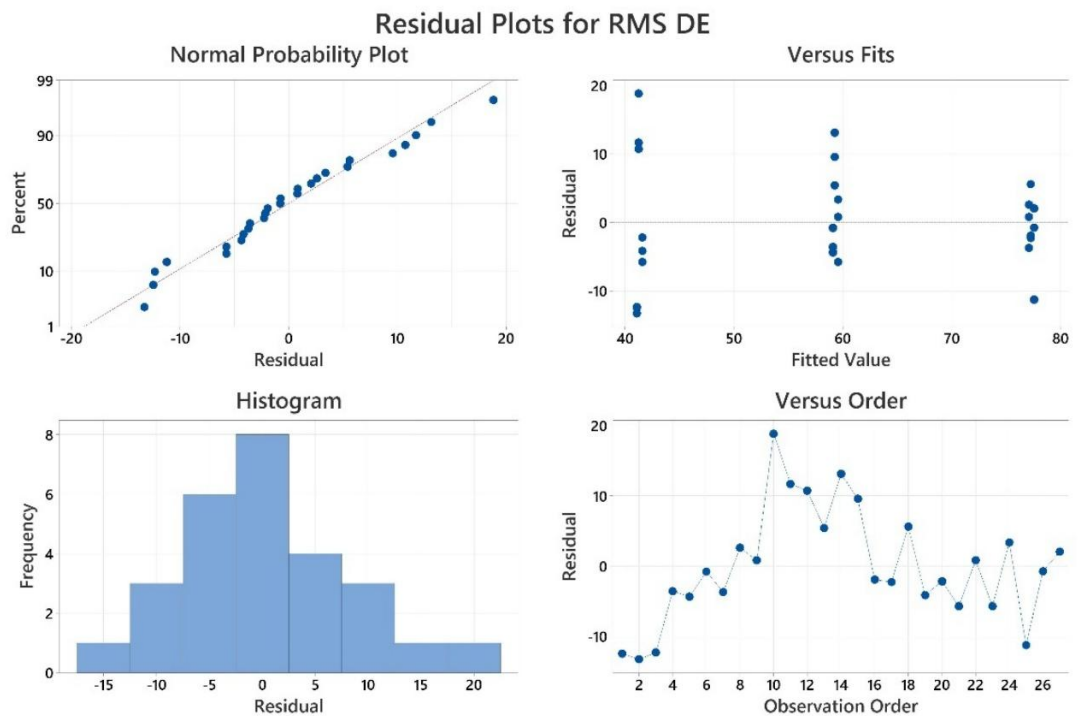
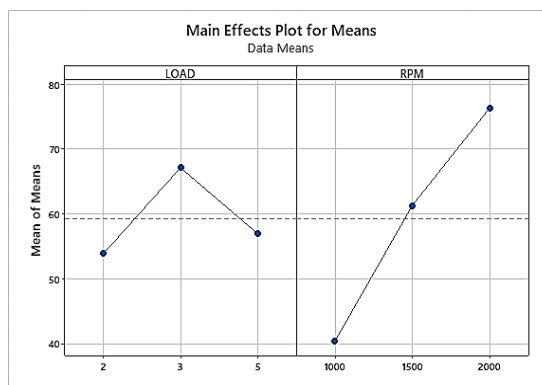


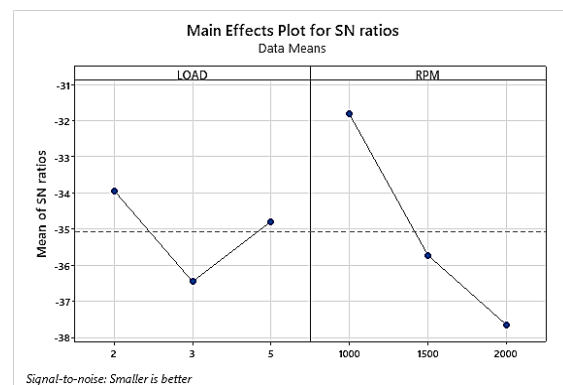
Figure 5.6 Residual plot for RMS DE

Table 5.7 ANOVA effect for S/N Ratios for RMS DE

Parameters	DoF	Sum of squares	Mean of squares	F-value	p-value	% Contribution
Model	2	5821.56	2910.78	40.97	0.000	
LOAD	1	1.07	1.07	0.02	0.903	0.014
RPM	1	5820.49	5820.49	81.92	0.000	77.33
Error	24	1705.18	71.05			
Lack-of-Fit	6	1419.55	236.59	14.91	0.000	
Pure Error	18	285.64	15.87			
Total	26	7526.74				

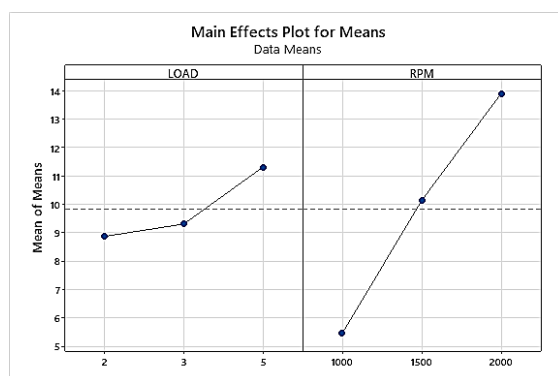


(a) Raw data

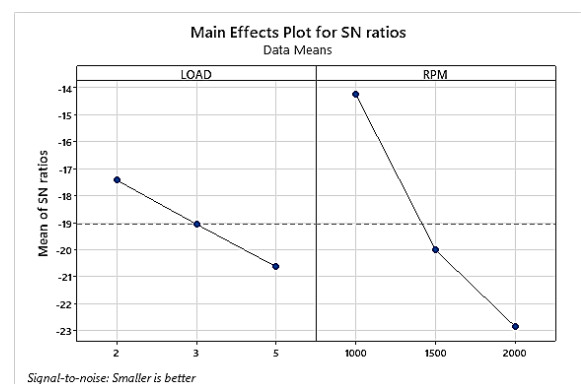


(b) S/N data

Figure 5.7 Effect of process parameter on RMS DE



(a) Raw data



(b) S/N data

Figure 5.8 Effect of process parameter on RMS NDE

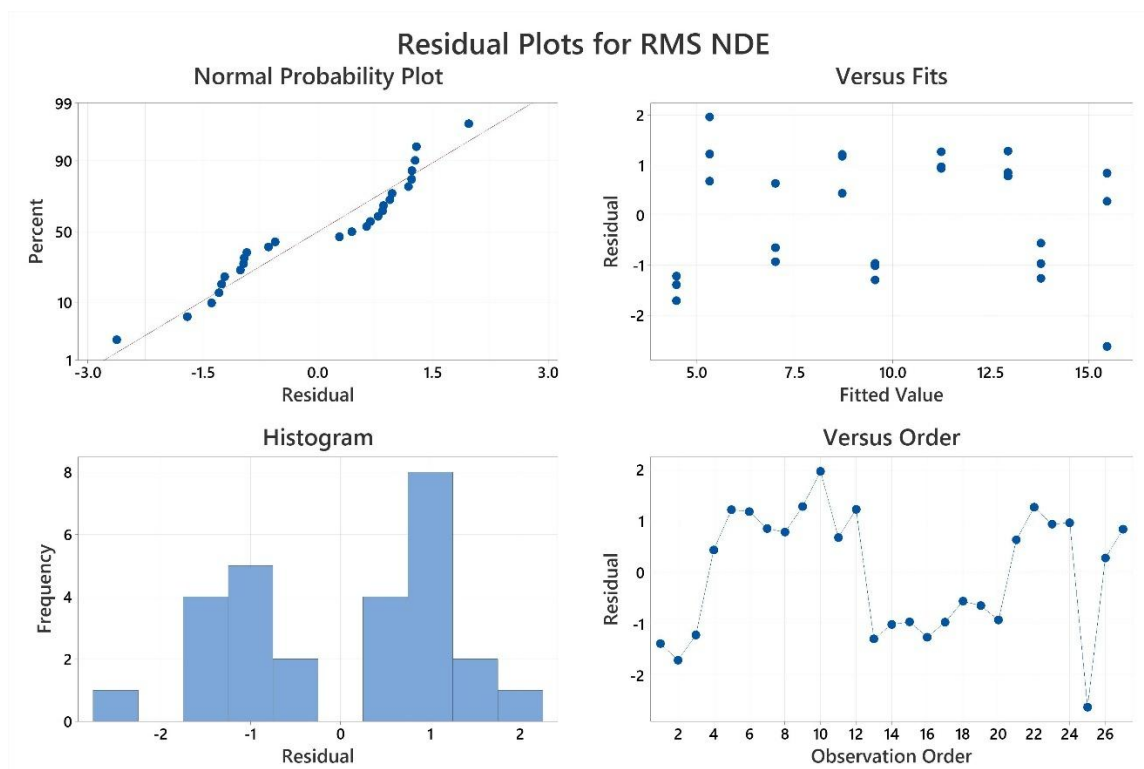


Figure 5.9 Residual plot for RMS NDE

Table 5.8 ANOVA effect for S/N Ratios for RMS NDE

Parameter	DoF	Sum of squares	Mean of squares	F-value	p-value	% Contribution
Model	2	351.30	175.652	112.82	0.000	
LOAD	1	29.70	29.705	19.08	0.000	7.6
RPM	1	321.60	321.599	206.56	0.000	82.7
Error	24	37.37	1.557			
Lack-of-Fit	6	27.22	4.537	8.05	0.000	
Pure Error	18	10.15	0.564			
Total	26	388.67				

On the Pareto chart in Figs. 5.10(c) and (d), bars that cross the reference line are statistically significant. For RMS NDE, the bars representing factors A and B cross the reference line at 2.06, but only factor B crosses in RMS DE. These factors are statistically significant at 0.05 with the current model terms.

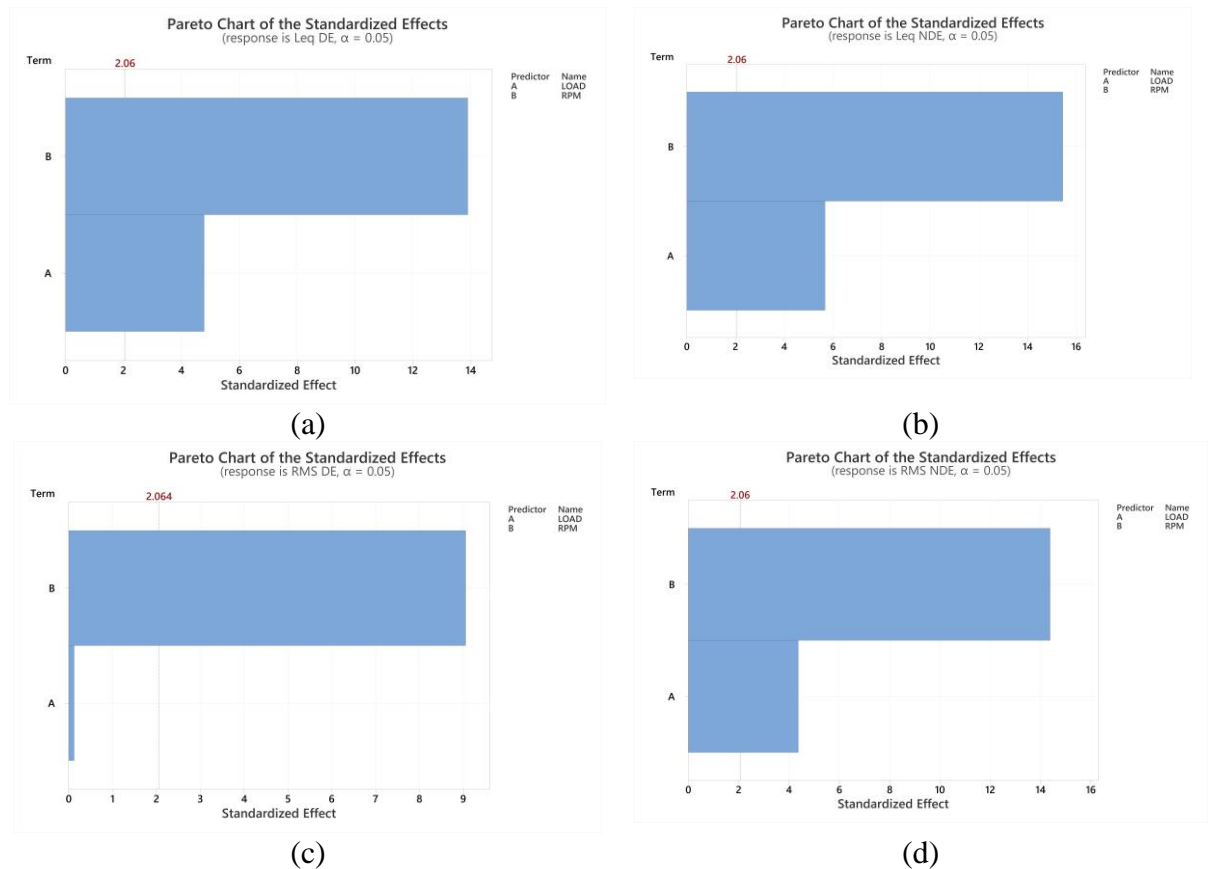
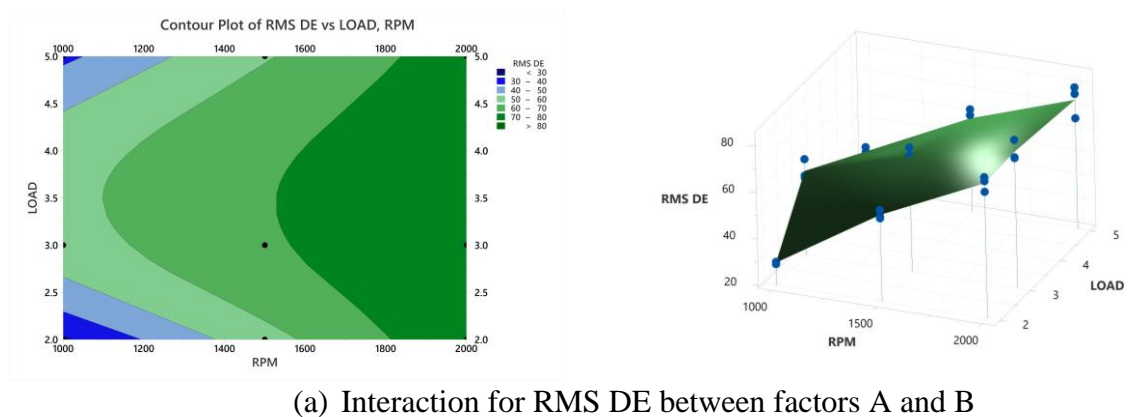
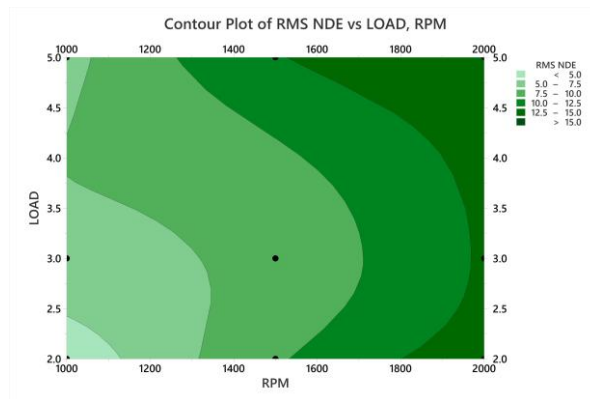


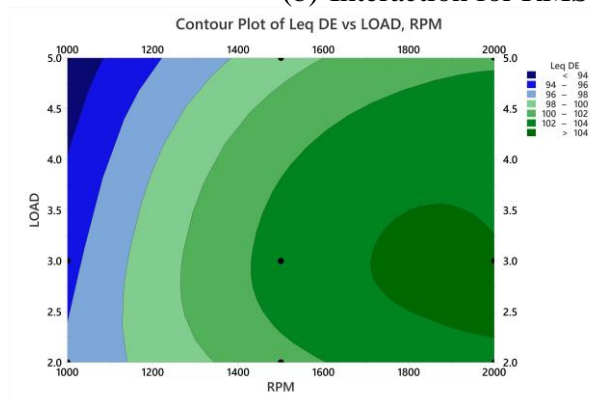
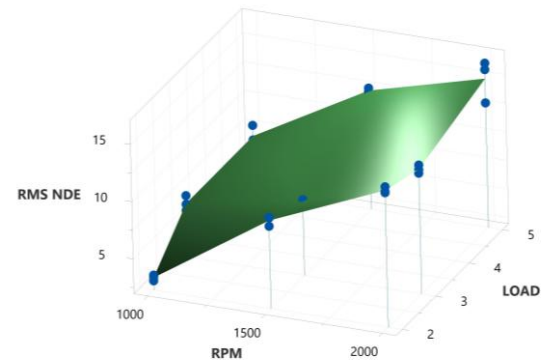
Figure 5.10 Pareto chart



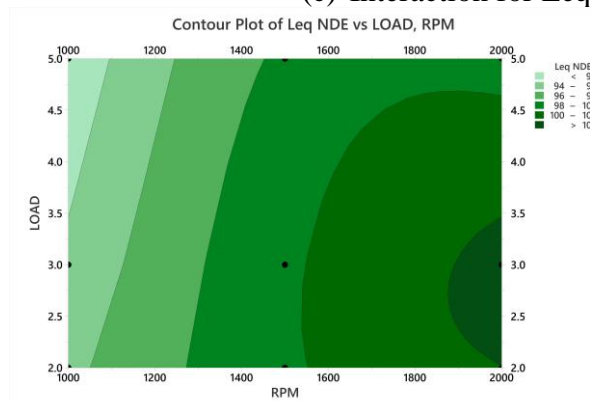
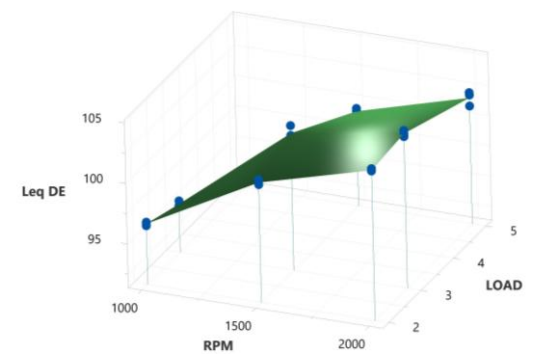
(a) Interaction for RMS DE between factors A and B



(b) Interaction for RMS NDE between factors A and B



(c) Interaction for Leq DE between factors A and B



(d) Interaction for Leq NDE between factors A and B

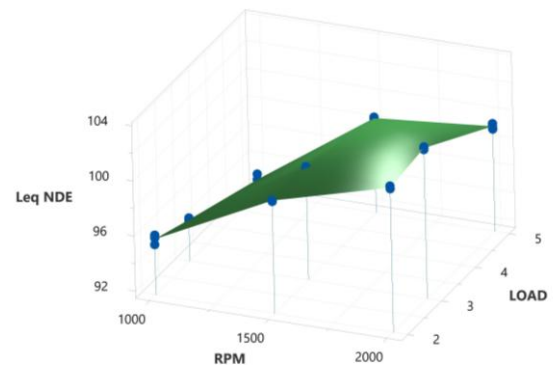


Figure 5.11 Contour and Surface plot of interaction

5.3.3 Contour and Response Surface Plot

The contour plot is a two-dimensional (2D) representation of the responses plotted against combinations of process parameters. A response surface plot is a 3-D representation of the behaviour of responses as a function of various process parameters. The interaction effect between speed and load on 3D surface plots can

provide a clearer concept of the response surface than contour plots for vibration (RMS) and Noise (Leq) in both drive and non-drive ends.

Examining Figs. 5.11(a) for the interaction between RPM and load for RMS DE, the vibration amplitude increases at high speed significantly for all loads. Still, around 1600-1700 rpm, its amplitude increases and then decreases with the load. Figure 5.11(a) also identifies dark blue regions with smaller z-values (RMS DE). The contour levels reveal a low value in the vicinity of 1000 rpm & 2 kg weight and 1000 rpm & 5 kg weight. RMS DE scores in this region range from 30-40. Examining Fig. 5.11(b), for interaction between speed and load for RMS NDE shows a similar response regarding RMS value ranges as in RMS DE. The vibration response contour plot in DE and NDE shows analogous but varying amplitude [80]. Speed primarily increases dynamic excitation frequency and energy, causing higher RMS and Leq at both DE and NDE. Curved contour lines are observed as a result of the linear regression equation. Figure 5.11(c) illustrates a contour plot for noise (Leq DE) in the vertical (Z) direction. The higher noise amplitude can be observed near the speed range of 1800-2000 rpm under the loading range condition of 2.5-3.5 kg. The interaction between load and speed for Leq NDE is plotted in Fig. 5.11(d). The noise responses in DE and NDE look the same on the contour plot, but the magnitudes differ.

Table 5.9 Kurtosis value at different RPM and different loading conditions

RPM	Kurtosis (DE)			Kurtosis (NDE)		
	2kg	3kg	5kg	2kg	3kg	5kg
1000	2.55	2.76	1.34	1.95	1.89	2.32
1500	0.37	0.88	1.15	1.33	2.02	1.59
2000	0.05	1.39	1.50	0.42	1.05	1.31

5.4 Summary of the Chapter

In the present experimental work on tapered roller bearing, a 3-level complete factorial design and Taguchi are employed to determine the influence of input factors on vibration RMS and noise Leq. Kurtosis is regarded as a useful criterion for measuring bearing defects, but the bearing is healthy in this case, and all values are within the

range, i.e., less than 3, as shown in Table 5.9. As input variables, speed and bearing load are analysed for variations due to individual and interaction effects between input parameters. The number of experiments is determined using the Taguchi method, and subsequent experiments involve measuring noise and vibration responses in DE and NDE. Experiments are repeated three times to prevent noise and error. The ANOVA technique also confirms the obtained results. The MEPPM (mean effect plot for means) is used to investigate the consequence of input process parameters on RMS and Leq responses, whereas the signal-to-noise plots aid in determining the optimum level and values of process parameters. The ANOVA evaluates the vibration response for the model's applicability and fits the statistical data to the linear regression equation. The contour plot is also used to determine the influence of speed and load change levels on the vibration response. The experimental work yielded the following significant findings.

- The analysis of variance indicates that speed is the most significant factor influencing vibration RMS and noise Leq. Taguchi's method validates that the RMS and Leq values of the tapered bearing increase as speed rises. It has been found that RMS and Leq initially rise with an increase in load before subsequently declining.
- The objective of the current study is to minimise RMS and Leq. In the Taguchi technique, S/N plots are used to determine the optimal process parameters to achieve the best response. The optimal level of process parameters for RMS is A1B1, and for Leq is A3B1.
- The response surface in RMS at DE and NDE exhibits comparable characteristics, although at varying magnitudes. Leq exhibits comparable characteristics for DE and NDE, albeit at a different magnitude.
- Due to the simplicity of the proposed implementation, the current method may give practical, effective applications for bearing condition monitoring and other complex machine studies in the future.

Chapter 6 Vibration Behaviour of Faulty Tapered Roller-Bearing

This chapter examines how different fault conditions affect the vibration response of tapered roller bearings (TRBs). Bearings exhibiting artificially induced defects, including inner race faults, outer race faults, and roller element damage, were subjected to controlled testing to analyse their dynamic behaviour. The vibration signatures were captured and examined through unique characteristics linked to each fault type. This study presents an experimental framework and diagnostic methodology that establish a systematic approach for detecting faults, crucial for condition monitoring in rotating machinery.

6.1 Introduction

Investigating the faults of tapered roller bearings (TRB) and their influence on vibration behaviour is crucial for timely fault diagnosis and effective predictive maintenance strategies. Vibration and acoustic analyses have been conducted on defective TRBs to explore these effects, facilitating a comparative evaluation with healthy bearings. The analyses conducted facilitate the identification of distinct fault signatures and provide insights into the impact of various defects on the overall dynamic response of the bearing system. Bearings typically fail on their own; however, in real-world applications, unexpected and early failures are common due to factors such as overloading, improper installation, inadequate lubrication, and unsuitable operating conditions [38].

Most researchers work on TRB for lubrication, contact behaviour [169, 170] and misalignment [171, 172]. Very few of them considered the faults in all components. The primary objective of this study is to determine the impact of faults on TRB components on their stability and the resulting dynamic reactions within the rotary system. Artificial defects on the roller, races, and compound location are introduced to facilitate a more comprehensive examination of faults. This aspect is not considered by Patil et al. and Kankar et al. in their study. Gunerkar et al. employed the L8 method

for analysis, which yielded a linear relationship between the parameters under investigation. However, the current work examines three factors at varying levels (64 experiments) and establishes a quadratic relationship between them.

This approach enhances the analysis of faults and nonlinearity prediction. The author has discovered that, alongside vibration assessments, considering noise data is also important for the investigation to understand its impact on bearing response. Statistical analysis commonly utilises time domain indices such as Leq for noise and RMS, crest factor, skewness and kurtosis for vibration. In this investigation, the RMS (calculated from time domain data and commonly used to quantify the amplitude of vibrations), kurtosis (calculated from time domain data and is often regarded as an accurate measure for evaluating the presence of bearing problems) and Leq (equivalent continuous sound level measured from the SLM and is often used in noise assessments) have been chosen as output response. The DOE methodology is used to design experiments. SKF 30206 TRBs are utilised in experiments. Mathematical relations and models have been developed to assess the effect of input factors on response variables.

6.2 Experimental Methodology

The methodology utilised to analyse TRB in this study is shown in Fig. 6.1. Factorial designs are used for modelling and analysis of issues when multiple factors affect the response of interest. The factorial design is commonly employed for process improvement, development, and optimisation. The primary effect of a factor is defined as the variation in the response that can be attributed to a change in the amount of that particular component, while keeping the other factors constant. Interaction dependence exists between variables when the behaviour of one factor influences the effect of another. Once the significant factors influencing the response have been identified, the factorial design is essential when it is believed that the relationship between the factor and dependent variable must be investigated throughout the experimental region, not just at the borders. This is accomplished by correlating the k active variables using the following form of a second-degree polynomial expression (6.1):

$$Y = b_o + \sum_{i=1}^k b_i x_i + \sum_{i=1}^k b_{ii} x_i^2 + \sum_{i=1}^{k-1} \sum_{j=i+1}^k b_{ij} x_i x_j + \epsilon \quad (6.1)$$

where x_i represents the variable with which we wish to correlate Y , and where Y represents the dependent variable. The symbols b_0 , b_i , and b_{ij} are constants, ϵ = error observed in the response.

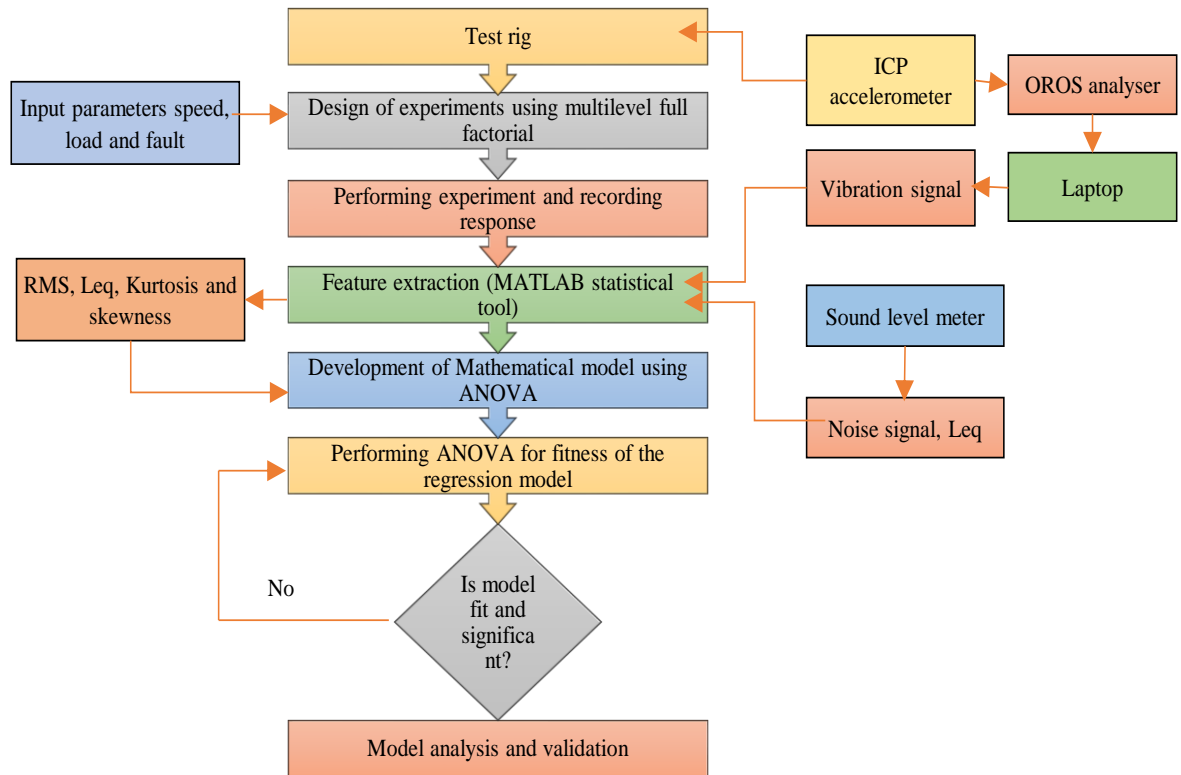


Figure 6.1 Flowchart of the proposed methodology

A polynomial regression is used to fit the trial values to the above equation. Normal statistics can then be used to check how well the fit is. The factorial designs are classified into 2-level factorial design, 2-level split-plot, Plackett-Burman design and general full factorial design. The present work uses the general full factorial design.

In analysing the effect of defective TRBs on vibration responses, General multifactorial design has been used to identify the behaviour of the rotor bearing system against different types of faults fabricated in TRBs with a number of replicates one. A total of 64 trials were conducted using a full factorial analysis of three factors, namely speed (A), load (B), and defect (C). Experiments are conducted using healthy and defective bearings at four input parameter levels. The vibration signatures are acquired in NDE at a sampling rate of 25.6 kHz and 60 k data points are collected for all cases, and each experiment is repeated three times to derive the average value.

During the removal and installation of a bearing, precautions are taken. Table 6.1 outlines the parameters and their levels in uncoded form. RMS, Leq and Kurtosis are considered as response parameters.

Root Mean Square (RMS): RMS measures the overall energy content of the vibration signal, which is useful for determining the bearing's general condition and health. Higher RMS values may indicate increasing vibration levels frequently linked to bearing failures. RMS can be determined from time domain data using equation 6.2 as [173]:

$$Y_{rms} = \sqrt{\frac{1}{N} [\sum_{i=1}^N (y_i)^2]} \quad (6.2)$$

where y represents the actual time signal, N is the number of samples, and i is the sample index.

Leq (Equivalent Continuous Sound Level): Leq measures the steady sound level over a given duration with the same energy as the varying sound levels. Leq measures acoustic energy over time, providing information about noise characteristics and their impact on bearing performance. Leq is measured directly from SLM and it can also be determined using equation 6.3 as [174]:

$$Leq = 10 \log_{10} \left(\frac{1}{T} \int_0^T \left(\frac{P_t}{P_o} \right)^2 dt \right) \quad (6.3)$$

where T is total monitoring time, P is the sound pressure or acoustic, and P_o is the reference pressure level $2 \times 10^{-5} Pa$.

Kurtosis: Kurtosis is a statistical indicator that indicates whether a signal's distribution is peaked or flat. Kurtosis is used in vibration analysis to detect impulsive occurrences or variations from normal behaviour that may indicate bearing failures or defects. High kurtosis values may suggest the presence of impulsive events, which are common in bearing defects like spalls or cracks. Kurtosis can be determined from time domain data using Equation 6.4 as [84]:

$$Kurtosis = \frac{M_4}{M_2^2} = \frac{\frac{1}{N} \sum_1^N [x(n) - \bar{x}]^4}{\left[\frac{1}{N} \sum_1^N [x(n) - \bar{x}]^2 \right]^2} = \frac{\frac{1}{N} \sum_1^N [x(n) - \bar{x}]^4}{\sigma^4} \quad (6.4)$$

Where M_4 is the fourth-order statistic moment, M_2 is the second-order statistic moment, $x(n)$ is the signal's amplitude for the n samples, and \bar{x} is the mean value of the amplitudes.

RMS and Leq assess overall vibration levels, while kurtosis provides extra information about the nature of the vibration signal, which is useful for diagnosing early-stage defects. The combination of RMS, Leq, and kurtosis enables a comprehensive and complex study of the vibration signals. Each metric provides distinct information that, when combined, creates a comprehensive picture of the bearing's condition.

Table 6.1 Input parameters and levels for experimental design

Input parameters	Speed (RPM)	Load (N)	Defect type
Symbols	A	B	C
L1	1000	0	Healthy
L2	1600	20 (2kg)	OR
L3	2200	30 (3kg)	IR
L4	2800	50 (5kg)	Roller

During operation, bearings with local defects generate high-frequency vibration amplitudes modulated by pulse force [175]. As the vibration signal comprises data regarding the periodic impulse and intensity of each impulse, the defect fault characteristic factors that are derived from the signal must accurately represent the fault pattern and operational condition. Signals are processed utilising MATLAB's available tools.

Using full factorial, models are derived from data collected by an ICP accelerometer along the NDE. F-value and Analysis of variance (ANOVA) analysis are conducted to determine whether the obtained models are productive or not. The design matrix of RMS, Leq and kurtosis for healthy and defective bearings is shown in Table 6.2. The table comprises the input parameters (speed, load, and defect type) and the corresponding output responses (RMS, Leq, and Kurtosis). The energy of the vibration signal can be enhanced by increasing the speed, which facilitates the identification of

defects. Energy in the vibration signal can also be increased by loading, which can potentially affect the wear and tear on the bearings, thereby influencing defect detection. Distinct vibration patterns can be generated by various forms of defects (Outer Race, Inner Race, Roller), which can be captured and analyzed using RMS, Leq, and Kurtosis. The results are investigated using ANOVA, and the obtained values are optimised using Minitab software.

Table 6.2 Experimental design matrix

Run	Input parameters			Output response		
	Speed (A) (RPM)	Load (B) (N)	Defect (C)	RMS (m/s ²)	Leq (dB)	Kurtosis
1	2200	0	Healthy	16.513	85	1.101
2	2200	0	OR	179.714	86	6.535
3	2800	0	OR	191.967	85	7.134
4	1000	30	IR	4.823	87	3.451
5	2200	50	OR	1.132	86	3.126
6	1600	50	Roller	10.694	85	3.124
7	1600	20	IR	41.629	86	6.526
8	1000	30	Healthy	7.043	85	1.969
9	1600	0	IR	12.103	86	3.589
10	2200	20	IR	43.640	85	3.068
11	1600	20	Healthy	17.371	85	1.579
12	1600	30	IR	18.141	88	7.212
13	2200	30	Healthy	18.273	87	1.368
14	1600	0	Healthy	7.492	84	1.699
15	2800	50	OR	1.132	87	3.173
16	1600	30	OR	20.883	87	3.594
17	1000	0	Healthy	4.124	85	1.991
18	2800	30	OR	66.181	88	3.391
19	2200	20	OR	21.925	86	3.198
20	2800	30	Roller	47.697	88	3.867
21	2200	30	Roller	22.341	88	5.335
22	1600	0	Roller	27.924	87	3.709
23	1000	20	Roller	5.919	85	6.437
24	1000	50	OR	1.134	85	3.503
25	2800	20	OR	46.712	86	9.669
26	2200	30	IR	45.248	88	20.243

27	2800	20	Healthy	22.491	86	1.158
28	2800	50	Roller	22.020	86	3.462
29	1600	50	OR	1.134	86	3.593
30	1600	50	IR	10.838	84	3.821
31	2200	0	IR	19.780	87	4.251
32	2800	50	Healthy	23.718	85	2.107
33	1000	20	IR	5.582	85	4.826
34	2200	50	Healthy	13.842	86	0.688
35	1000	20	OR	7.295	86	5.523
36	1600	30	Roller	19.131	87	7.959
37	1000	50	Healthy	3.755	83	1.648
38	1000	50	IR	4.736	83	3.875
39	1600	30	Healthy	21.318	87	1.763
40	1000	20	Healthy	4.838	86	2.556
41	1000	0	IR	8.234	86	3.122
42	1600	20	Roller	15.092	86	14.827
43	2800	30	Healthy	38.772	87	1.253
44	2800	20	IR	26.745	86	3.490
45	1000	0	OR	8.195	85	4.175
46	2800	50	IR	17.303	85	3.253
47	1600	0	OR	100.692	85	5.187
48	2200	20	Healthy	16.733	86	2.158
49	1000	0	Roller	5.991	86	3.918
50	2200	30	OR	68.011	87	3.066
51	2200	50	IR	13.716	84	3.820
52	2800	0	IR	20.027	86	5.745
53	2800	0	Healthy	20.819	86	0.998
54	1000	50	Roller	5.876	85	3.944
55	2800	0	Roller	20.749	88	5.489
56	2200	20	Roller	17.469	87	3.821
57	2800	30	IR	22.755	87	3.024
58	1000	30	OR	9.132	86	3.726
59	1600	20	OR	13.687	87	3.060
60	2200	50	Roller	14.601	84	3.620
61	1000	30	Roller	8.755	86	3.394
62	2200	0	Roller	18.713	87	7.241
63	2800	20	Roller	27.826	87	3.301
64	1600	50	Healthy	9.058	85	1.064

Table 6.3 Regression values of response parameters

Response	Standard deviation	R²	Adjusted R²	PRESS	Predicted R²
RMS	0.0472410	97.46%	94.07%	0.3385	85.71%
Leq	0.667247	87.03%	69.73%	67.5413	27.10%
Kurtosis	0.105367	86.10%	67.57%	1.6842	21.92%

6.3 Results and Discussion

A mathematical model has been established to analyse the experimental data and response parameters via multilevel full factorial design. The ANOVA statistical test is employed to identify the significant terms in the model with a confidence level of 95%. The regression study of response parameters for different bearing circumstances with standard deviation, adjusted R², and predicted R² values has been depicted in Table 6.3.

This study incorporates a multilayer full factorial design. There are 63 degrees of freedom (DOF) in 64 experimental combination runs. Each main effect (ME) has three degrees of freedom (DOF). As a result, 9 DOF out of 63 are used to assess A, B and C. Each interaction effect (IE) has three degrees of freedom (DOF). An additional 27 DOF are now accessible for examining the statistical significance of variables. These are employed in ANOVA. In the case of small effects, it may be necessary to obtain an acceptable degree of freedom, sample size, and sensitivity. The accuracy and power of the experiment will be enhanced by increasing the number of replications, which will increase the number of degrees of freedom for the error term. Minitab, a statistical software, is utilised to examine the response parameter RMS obtained from experiments. An analysis of variance (ANOVA) is performed to compute the mean square and sum square of second-order polynomials. The significance of the polynomials is evaluated by assessing the "prob>F" value with a 95% confidence interval (CI) at a 5% level of significance. The relevant polynomials are used to generate the response surface and develop the second-order regression equation.

6.3.1 Effect of Process Parameters on RMS

To determine the significance of the F probability value for various bearing conditions, an ANOVA for the quadratic multi-response model is performed; the resulting residual data for RMS are presented in Table 6.4. The F-probability value of the model, which is less than 0.05, is satisfactory for bearing conditions. As a result, it is advised that the model is regarded as significant. Separate models are built for both healthy and defective bearings (OR, IR and roller faults) to determine the impact of input parameters on response variables. The regression model is adjusted to account for the adequacy of the response data. The Box-Cox plot is useful for determining the best power transformation. For the best model fit, the $\lambda=0$ transformation is used in this model at the 95% confidence interval. The regression equation in the uncoded factor is as follows:

Fault type

$$\textbf{Healthy: } \ln(RMS) = 0.548 + 0.001026 A + 0.125 B - 0.000058 A*B \quad (6.5)$$

$$\textbf{OR: } \ln(RMS) = 2.517 + 0.001112 A - 0.670 B - 0.000058 A*B \quad (6.6)$$

$$\textbf{IR: } \ln(RMS) = 1.242 + 0.000879 A + 0.044 B - 0.000058 A*B \quad (6.7)$$

$$\textbf{Roller: } \ln(RMS) = 1.169 + 0.000880 A + 0.068 B - 0.000058 A*B \quad (6.8)$$

The results of the regression analysis conducted on the root mean square (RMS) values of the vibration data for various bearing conditions demonstrate that the impact of speed, load, and fault type on the dependent variable is statistically significant. Table 6.4 also reveals that the interaction effect between the load and fault only has significant contributions, as evidenced by the p-value being less than 0.05. The model's F-value of 28.74 indicates its relevance, with a 0.05% chance. Significant model terms with P-values less than 0.05 are specified in the ANOVA table. A, B, C and BC model terms are significant in this scenario. However, values greater than 0.05 reveal insignificant model terms. With insignificant terms, the reduction of the model improves the present model. Table 6.3 displays the model's fit statistics. R^2 is 97.46% indicating that the data is well fitted to the regression model. The predicted R^2 implies that healthy data is likely to explain 85.71% of the variation in the complete model. PRESS (prediction error sum of squares) is a cross-validation statistic that measures

statistical model prediction power. This is prevalent in regression analysis. Lower PRESS levels indicate higher predicting performance. The PRESS statistic measures how well the model predicts new data points that are not used in the model training. The PRESS value of 0.3385 shows that the model is likely to be an accurate prediction.

Table 6.4 Model significance of RMS using ANOVA

Source	DoF	Sum of squares	% Contribution	Adj. Sum of squares	Mean of squares	F value	p value
Model	36	2.30907	97.46%	2.30907	0.064141	28.74	0.000
Linear	9	1.17519	49.60%	1.17519	0.130577	58.51	0.000
Speed (A)	3	0.43294	18.27%	0.43294	0.144313	64.66	0.000
Load (B)	3	0.59833	25.25%	0.59833	0.199444	89.37	0.000
Fault (C)	3	0.14392	6.07%	0.14392	0.047974	21.50	0.000
2-Way Interactions	27	1.13388	47.86%	1.13388	0.041995	18.82	0.000
Speed*Load	9	0.00752	0.32%	0.00752	0.000836	0.37	0.937
Speed*Fault	9	0.01534	0.65%	0.01534	0.001704	0.76	0.650
Load*Fault	9	1.11101	46.89%	1.11101	0.123446	55.31	0.000
Error	27	0.06026	2.54%	0.06026	0.002232		
Total	63	2.36932	100.00%				

The main effect plot shown in Fig. 6.2 depicts the effect of several factors on RMS, such as speed, load, and fault type. The RMS value, which measures the overall vibration level, rises with the speed of rotation. This is expected since higher speeds cause more vibrations in mechanical systems. The trend indicates a substantial positive link between speed and RMS. The RMS value varies with load. Raising the load reduces the RMS value, but subsequent increases result in greater RMS values, followed by a decrease at the highest load level. This nonlinear relationship suggests

that the effect of load on vibration is more complex and may be influenced by other factors, such as equipment's inherent frequency aligning with the stimulation frequency or structural vibration added, which causes high vibration and reduces resonance vibration after passing [151]. Different fault kinds have distinct effects on the RMS value. Bearings with outer race defects have the highest RMS values, suggesting severe vibrations. Inner race faults produce lower RMS values than outer race faults but greater than healthy and roller situations. Bearings with roller faults have the lowest RMS values among all fault states, indicating less severe vibrations. This emphasizes the role of fault type in determining vibration characteristics.

The minimum RMS is achieved at level 1 for speed, level 4 for load and level 1 for fault. A1B4C1 is the ideal value across all parameters to minimise RMS. At A1B4C1, $\text{RMS}=3.755 \text{ m/s}^2$. Equations (6.5-6.8), which are used to create a model for forecasting RMS, performed well since the points on the normal probability graph in Fig. 6.3 displayed an approximate linear pattern with a normal distribution and only slight disintegration at the extremities, which implies that there may be minor deviations from the norm. Figure 6.3 also indicates that the RVFV (Residual vs Fit value) graph has a random pattern, indicating that residuals have a nearly constant variance or the data points appear to be evenly distributed at the top and bottom of the line. The RVOP (Residual Vs order plot) demonstrates that the collected data can be used to identify a non-random error. The RVOP also shows that residuals bounce about the zero line at random. This behaviour often indicates the absence of serial correlation. The graphs reveal a random distribution with no visible trend, indicating that the model fits and meets the regression assumptions. Furthermore, because no outliers are discovered, the frequency versus residual plot demonstrates that the data change more finely. The histogram further emphasises the assumption of normality by displaying a bell-shaped curve. Furthermore, the verses order plot is valuable for detecting patterns over time, such as shifts or drifts. The residuals are arbitrarily distributed around zero without any discernible pattern, suggesting that there is no significant time-based trend or autocorrelation in the residuals. These findings indicate that the regression model adequately accommodates the data and that the model assumptions are satisfactorily fulfilled. Nevertheless, it is important to consider minor deviations from normality.

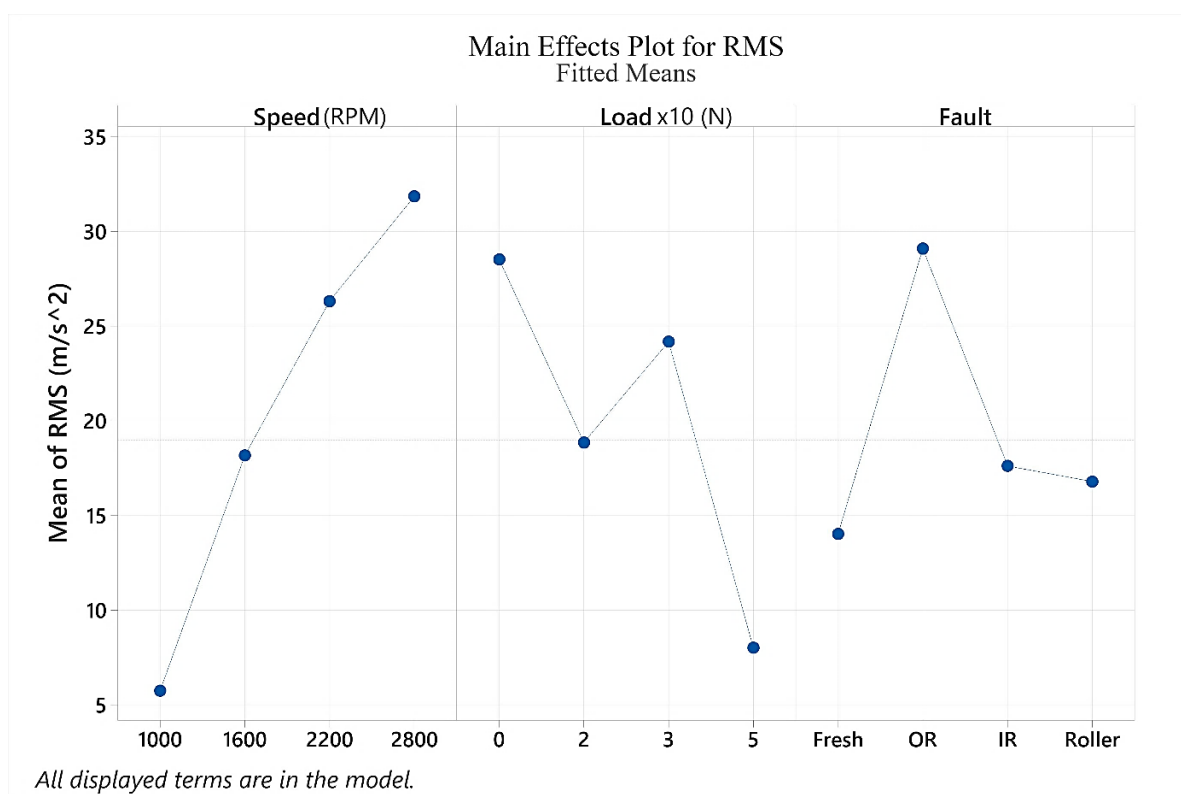


Figure 6.2 Effect of process parameters on RMS

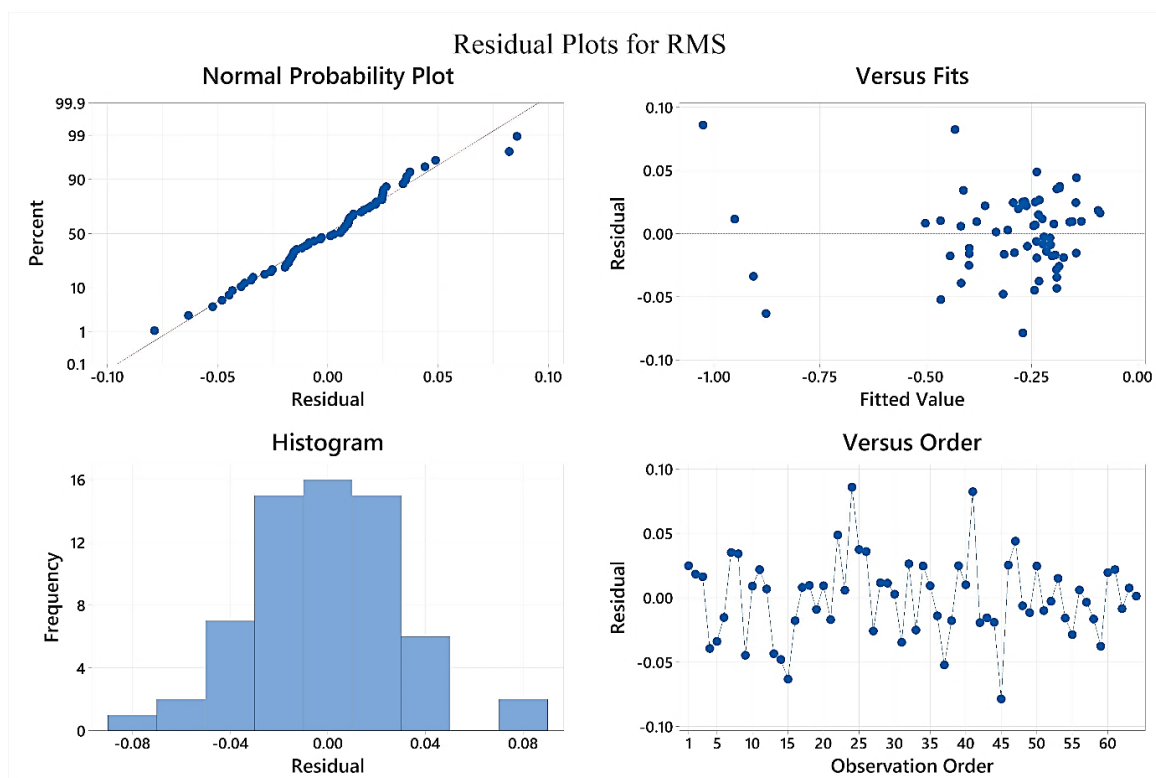


Figure 6.3 Residual plot for RMS

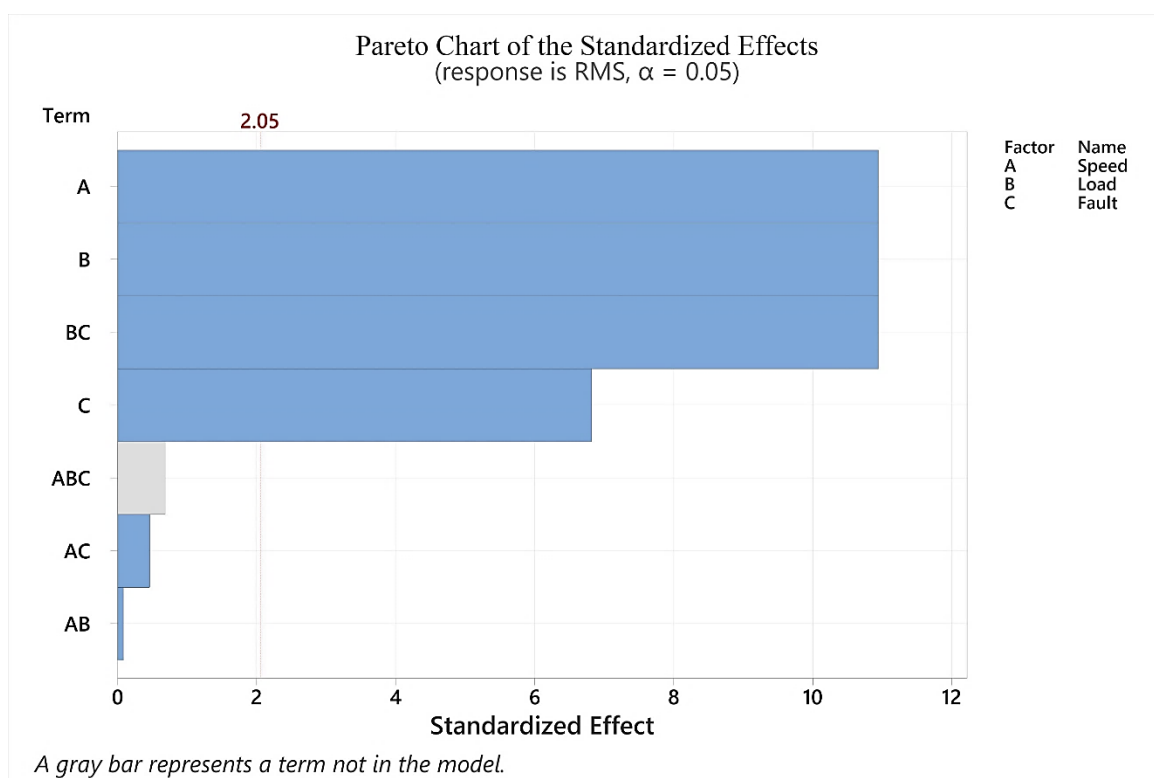


Figure 6.4 Pareto chart for RMS

In Fig. 6.4, the absolute values of the standardised effects are displayed on the Pareto chart from the largest to the smallest. A reference line is added to the chart to illustrate statistically significant effects. The significance level (expressed by alpha) determines the statistical significance reference line. The bars representing factors A, B, BC, and C cross the reference line at the 2.05-point mark in this Pareto chart. With the existing model terms, there is a 0.05 % chance that these factors are significant. Analysis of variance results for RMS also suggests that the A, B, C and BC are significant.

6.3.2 Effect of Process Parameters on Leq

An ANOVA for the quadratic multi-response model is done to establish the significance of the F probability value for various bearing states. The resulting residual data for Leq are provided in Table 6.5. The model's F-probability value, which is less than 0.05, is adequate for bearing situations and considered significant. To examine the influence of input parameters on response variables, distinct models are constructed for both healthy and faulty bearings. Adjustments are made to the regression model and the Box-Cox plot can be used to find the optimal power

transformation. The $\lambda=8$ transformation is applied in this model at 95 % CI for the best model fit. The uncoded factor's regression equation is as follows:

Fault type

$$\textbf{Healthy: } (Leq^{\lambda-1})/(\lambda \times g^{\lambda-1}) = 9.49 + 0.000474 A - 0.183 B + 0.000092 A*B \quad (6.9)$$

$$\textbf{OR: } (Leq^{\lambda-1})/(\lambda \times g^{\lambda-1}) = 9.98 + 0.000292 A + 0.000 B + 0.000092 A*B \quad (6.10)$$

$$\textbf{IR: } (Leq^{\lambda-1})/(\lambda \times g^{\lambda-1}) = 11.17 + 0.000203 A - 0.533 B + 0.000092 A*B \quad (6.11)$$

$$\textbf{Roller: } (Leq^{\lambda-1})/(\lambda \times g^{\lambda-1}) = 10.71 + 0.000743 A - 0.521 B + 0.000092 A*B \quad (6.12)$$

$(\lambda = 8, g = 85.9288 \text{ is the geometric mean of } Leq)$

Table 6.5 Model significance of Leq using ANOVA

Source	DoF	Sum of squares	% Contribution	Adj. Sum of squares	Mean of squares	F value	p value
Model	36	80.630	87.03%	80.630	2.2397	5.03	0.000
Linear	9	59.220	63.92%	59.220	6.5800	14.78	0.000
Speed (A)	3	13.439	14.51%	13.439	4.4797	10.06	0.000
Load (B)	3	38.586	41.65%	38.586	12.8621	28.89	0.000
Fault (C)	3	7.195	7.77%	7.195	2.3983	5.39	0.005
2-Way Interactions	27	21.409	23.11%	21.409	0.7929	1.78	0.070
Speed*Load	9	3.300	3.56%	3.300	0.3667	0.82	0.600
Speed*Fault	9	2.770	2.99%	2.770	0.3078	0.69	0.711
Load*Fault	9	15.339	16.56%	15.339	1.7043	3.83	0.003
Error	27	12.021	12.97%	12.021	0.4452		
Total	63	92.650	100.00%				

The regression analysis results on the Leq values for various bearing circumstances show that the influence of speed, load, and fault type on the dependent variable is statistically significant. Table 6.5 further shows that the interaction effect between the load and the fault has only effects, as demonstrated by a p-value less than 0.05. With a 0.05% chance, the model's F-value of 5.03 confirms its relevance. The ANOVA table includes important model terms with p-values less than 0.05. The model terms A, B, C, and BC are important in this case. The reduction of the model with insignificant terms enhances the current model. The model's fit statistics are shown in Table 6.3, R^2 of 87.03% indicates that the data fits the regression model effectively. According to the predicted R^2 , new data will likely explain 27.10% of the variation in the overall model. PRESS statistics indicate how well the model predicts new data. The PRESS value of 67.5413 indicates that the model will likely be correct. Figure 6.5 demonstrates the effect of various parameters on Leq, including speed, load, and fault type. The Leq is proportional to speed and rises as it increases. Leq, on the other hand, rises with load until it reaches a peak and then falls [151]. This is due to the equipment's inherent frequency matching the excitation frequency, resulting in loud noise and the resonating noise becoming less after passing. Roller fault has the greatest impact on Leq value, followed by OR, IR and healthy bearing.

At level 1 for speed, level 4 for load, and level 1 for fault, the minimum Leq is reached. A1B4C1 is the best number for minimising Leq across all parameters, i.e. Leq = 83 dB at A1B4C1. The model for predicting RMS is effectively constructed using equations (6.9–6.12), as evidenced by the data points depicted on the normal probability graph in Fig. 6.6, which showed a mostly straight pattern with a normal distribution and only a little disintegration. The RVFV graph in Fig. 6.6 also shows a random pattern and is evenly distributed at the top and bottom of the line, meaning that residuals have a constant variance. The RVOP indicates that information can be utilised to identify a non-random error. The plots also show a random distribution with no noticeable trend, which indicates that the model fits and meets the regression assumptions. In addition, the frequency versus residual plot shows that the data change more finely because no outliers are found.

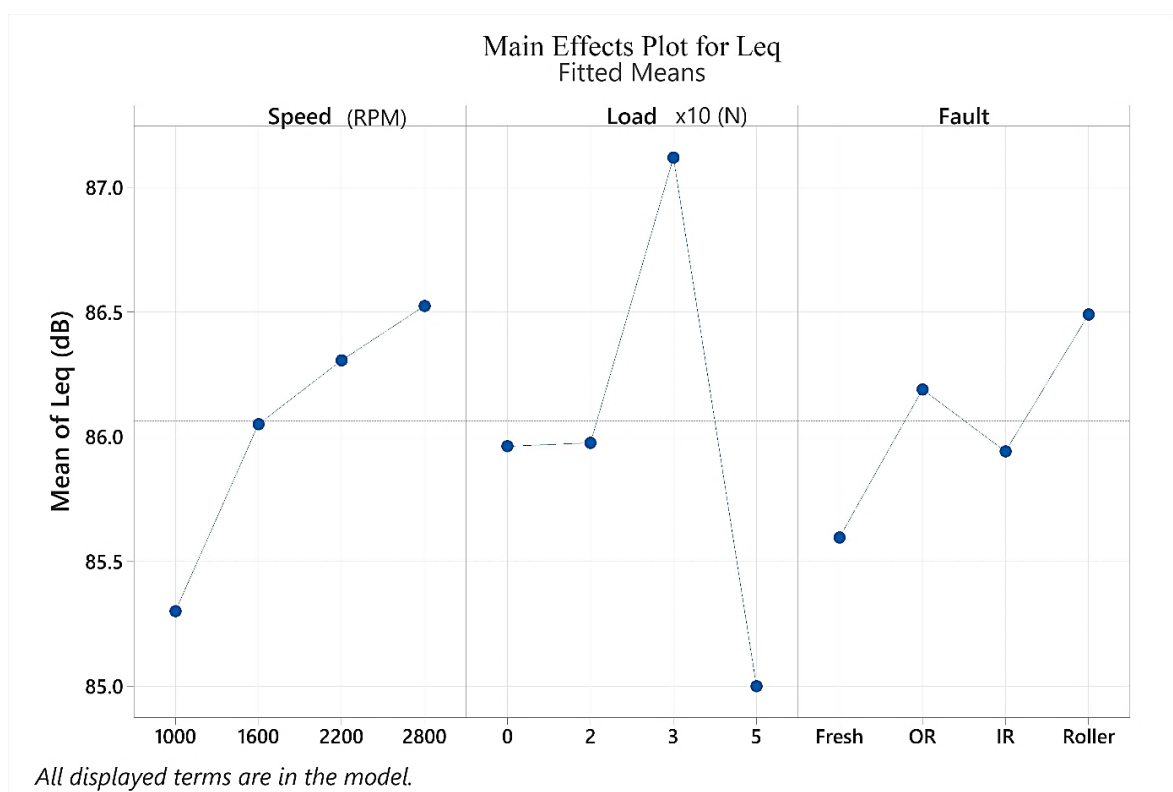


Figure 6.5 Effect of process parameter on Leq

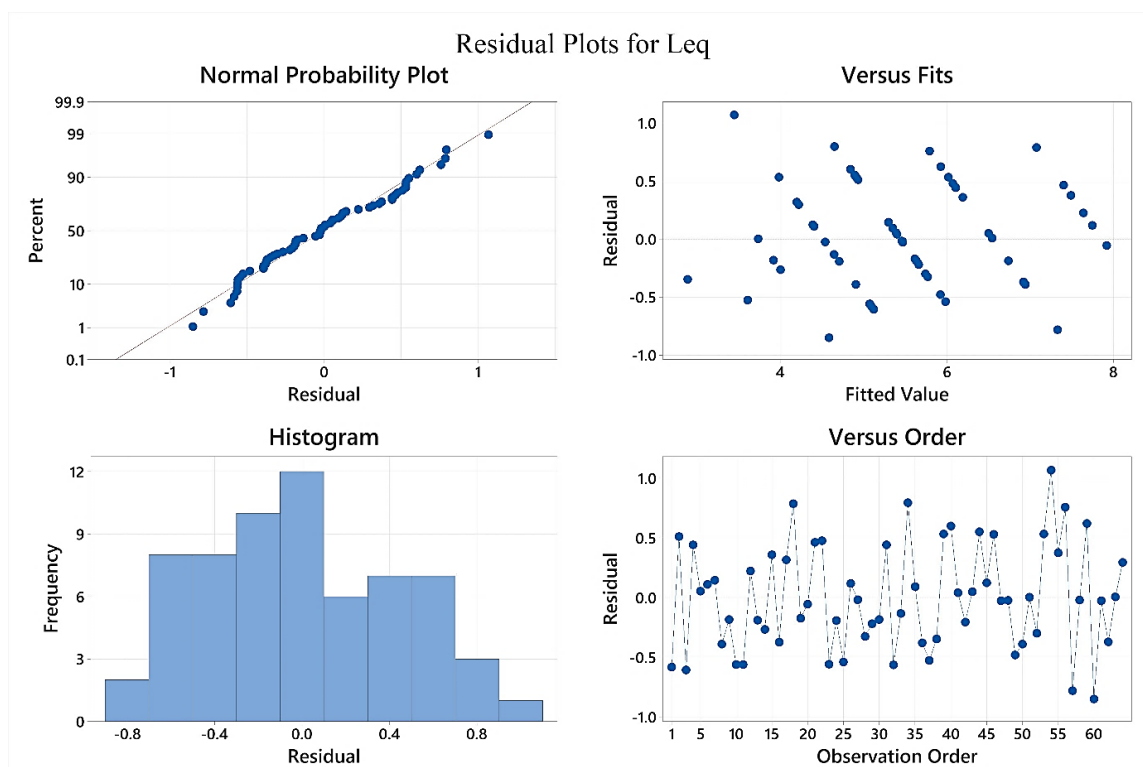


Figure 6.6 Residual plot for Leq

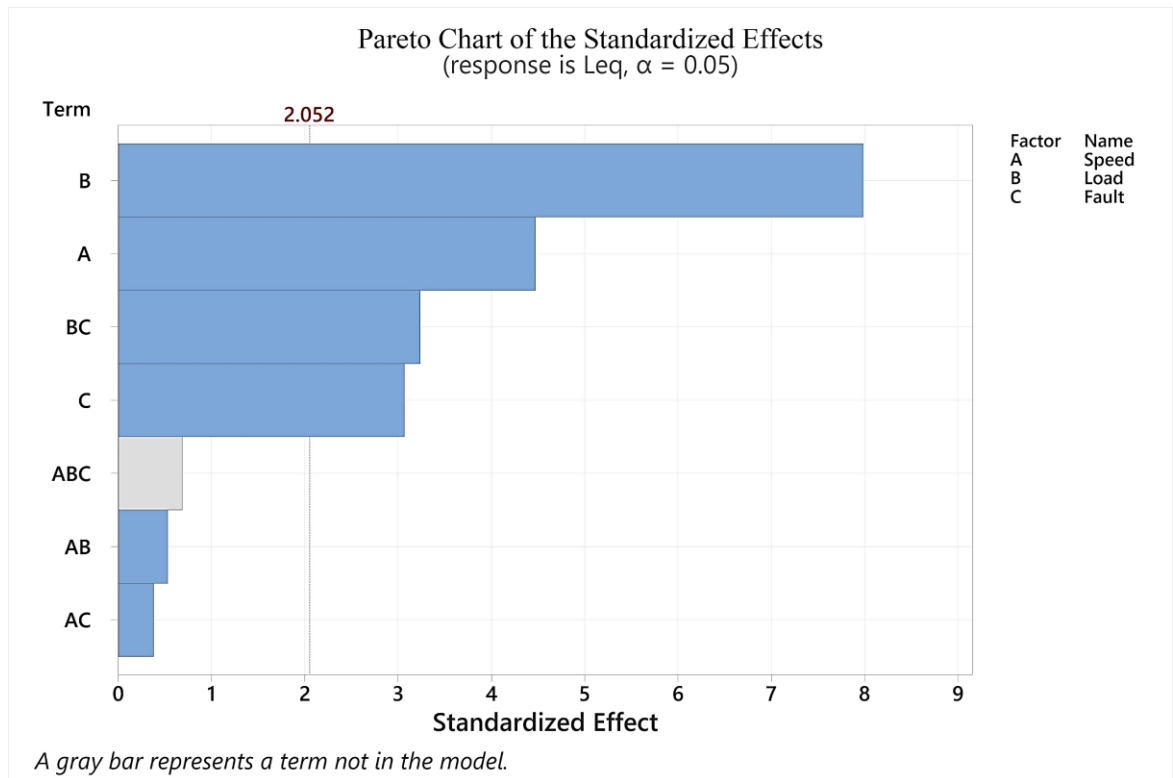


Figure 6.7 Pareto chart for Leq

The Pareto chart in Fig. 6.7 shows which factors are statistically important. It shows the absolute magnitude of the impacts, allowing for the identification of significant effects. However, it does not provide information on the direction of these effects, whether they result in an increase or decrease in the response. The significance level, which is written as alpha, sets the statistical significance reference line. The bars in this Pareto chart show that factors B, A, BC, and C all cross the 2.052-point line. Based on the analysis of the variance of Leq, the same factors A, B, C, and BC are significant.

6.3.3 Effect of Process Parameters on Kurtosis

The residual data for kurtosis obtained by conducting an analysis of variance for the quadratic multi-response model to determine the significance of the F probability value for different bearing conditions are presented in Table 6.6. The model's F-probability value, which is less than 0.05, is adequate for bearing conditions. Consequently, it is advisable to regard the model as statistically significant. To examine the influence of input parameters on response variables, distinct models for healthy and defective

bearings are developed. The regression model is modified, and the plot is utilised to determine the most effective power transformation. The $\lambda = -0.5$ transformation is implemented at the 95% CI to achieve the most optimal model fit in this model. The following is the regression equation for the uncoded factor:

Fault type

$$\text{Healthy: } -Kurtosis^{-0.5} = -0.6186 - 0.000097 A - 0.0073 B - 0.000002 A*B \quad (6.13)$$

$$\text{OR: } -Kurtosis^{-0.5} = -0.4784 + 0.000026 A - 0.0218 B - 0.000002 A*B \quad (6.14)$$

$$\text{IR: } -Kurtosis^{-0.5} = -0.4883 + 0.000005 A + 0.0027 B - 0.000002 A*B \quad (6.15)$$

$$\text{Roller: } -Kurtosis^{-0.5} = -0.4111 - 0.000010 A - 0.0114 B - 0.000002 A*B \quad (6.16)$$

Table 6.6 Model significance of kurtosis using ANOVA

Source	DoF	Sum of squares	% Contribution	Adj. Sum of squares	Mean of squares	F value	p value
Model	36	1.85717	86.10%	1.85717	0.051588	4.65	0.000
Linear	9	1.57023	72.80%	1.57023	0.174470	15.72	0.000
Speed (A)	3	0.02149	1.00%	0.02149	0.007163	0.65	0.593
Load (B)	3	0.07679	3.56%	0.07679	0.025598	2.31	0.099
Fault (C)	3	1.47195	68.24%	1.47195	0.490650	44.19	0.000
2-Way Interactions	27	0.28694	13.30%	0.28694	0.010627	0.96	0.545
Speed*Load	9	0.09469	4.39%	0.09469	0.010521	0.95	0.502
Speed*Fault	9	0.13095	6.07%	0.13095	0.014550	1.31	0.277
Load*Fault	9	0.06130	2.84%	0.06130	0.006811	0.61	0.775
Error	27	0.29976	13.90%	0.29976	0.011102		
Total	63	2.15693	100.00%				

A regression analysis conducted on the kurtosis values under different bearing conditions reveals that only defect type has a statistically significant effect on the dependent variable. A p-value below 0.05 further demonstrates in Table 6.6 that the fault has only effects. With a 0.05% probability, the relevance of the model is confirmed by its F-value of 4.65. The present model is improved through the elimination of insignificant variables. Table 6.3 presents the statistics of the model's fit. The R^2 value of 86.10% suggests that the data fits the regression model well. The predicted R^2 indicates that including new data is probable to account for 21.92% of the variability observed in the overall model. PRESS statistics indicate the model's ability to forecast new data. Based on the PRESS value of 1.6842, it can be concluded that the model is probably accurate.

Figure 6.8 demonstrates the effect of various parameters on kurtosis, including speed, load, and fault type. The influence of speed and load on kurtosis is less at higher speeds [84] the p-value greater than 0.05 for speed, load and all interaction effects are insignificant. The minimal kurtosis is reached at level 4 for speed, level 4 for load, and level 1 for fault. A4B4C1 is the optimal value for kurtosis when considering a variety of factors. The kurtosis value is 0.688 at A4B4C1. The points on the normal probability graph in Fig. 6.9 show an approximate linear pattern with a normal distribution with minor disintegration. Equations (6.13-6.16), which are used to develop a model for forecasting kurtosis, worked well. Additionally, Fig. 6.9 shows a random pattern on the RVFV graph, which suggests that the variance of residuals is almost constant. A non-random error can be found using the gathered data, as shown by the RVOP. Moreover, the frequency versus residual plot shows that the data vary more finely because no outliers are found. The Pareto chart in Fig. 6.10 shows the standardised absolute values ranked from largest to smallest. The bars in this Pareto chart show only factor C crosses the 2.05 reference line. There is a 0.05 chance that this factor only matters with the present model terms. The results of the kurtosis value in the analysis of variance also indicate that only factor C, i.e., fault condition, affect the kurtosis value.

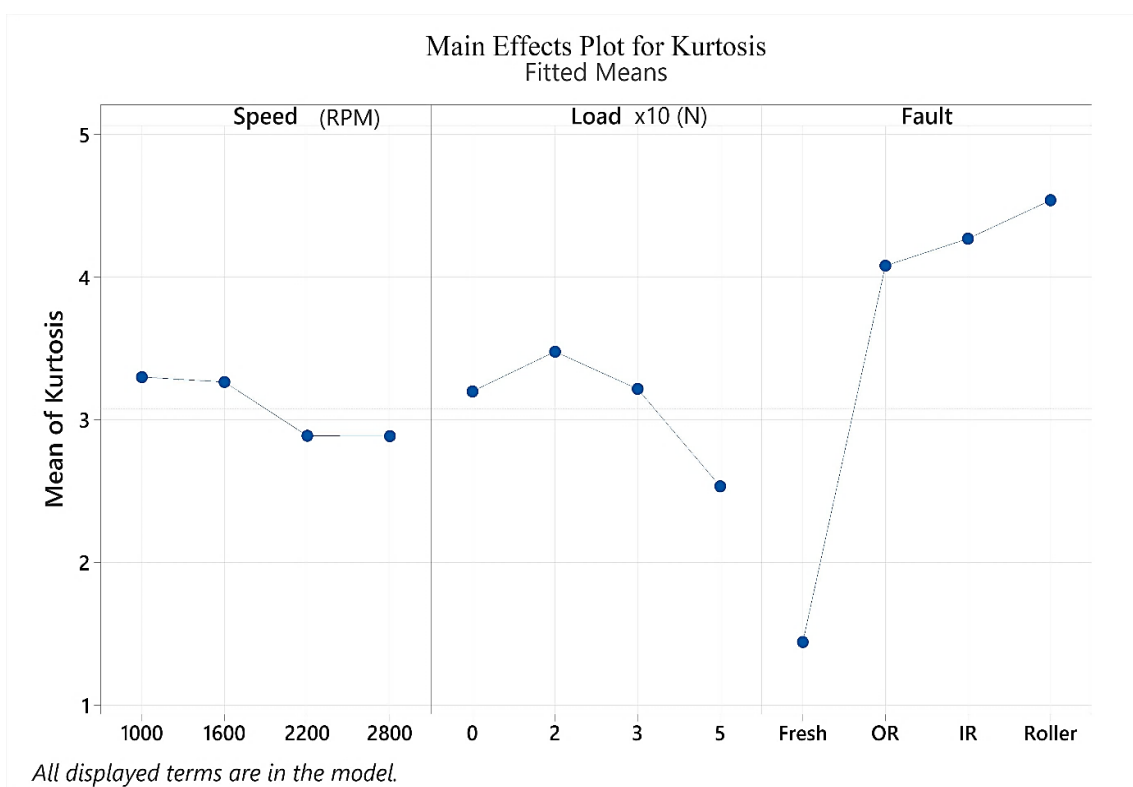


Figure 6.8 Effect of process parameters in kurtosis

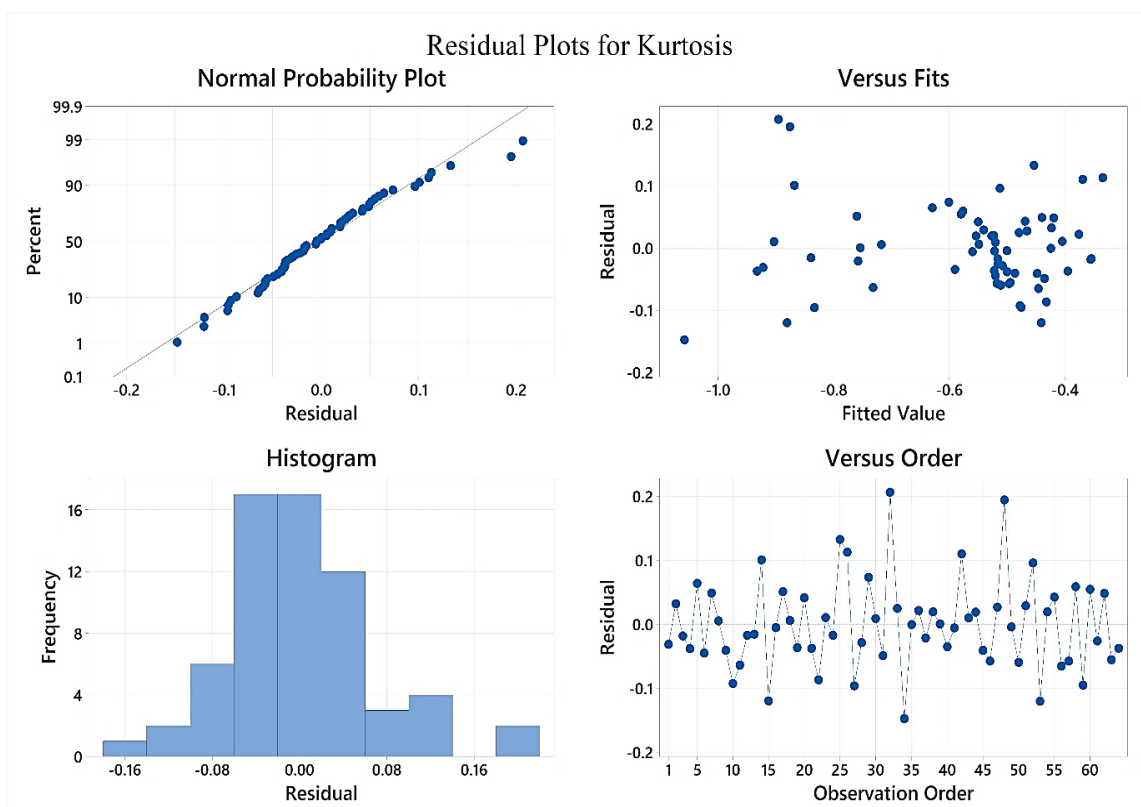


Figure 6.9 Residual plot for kurtosis

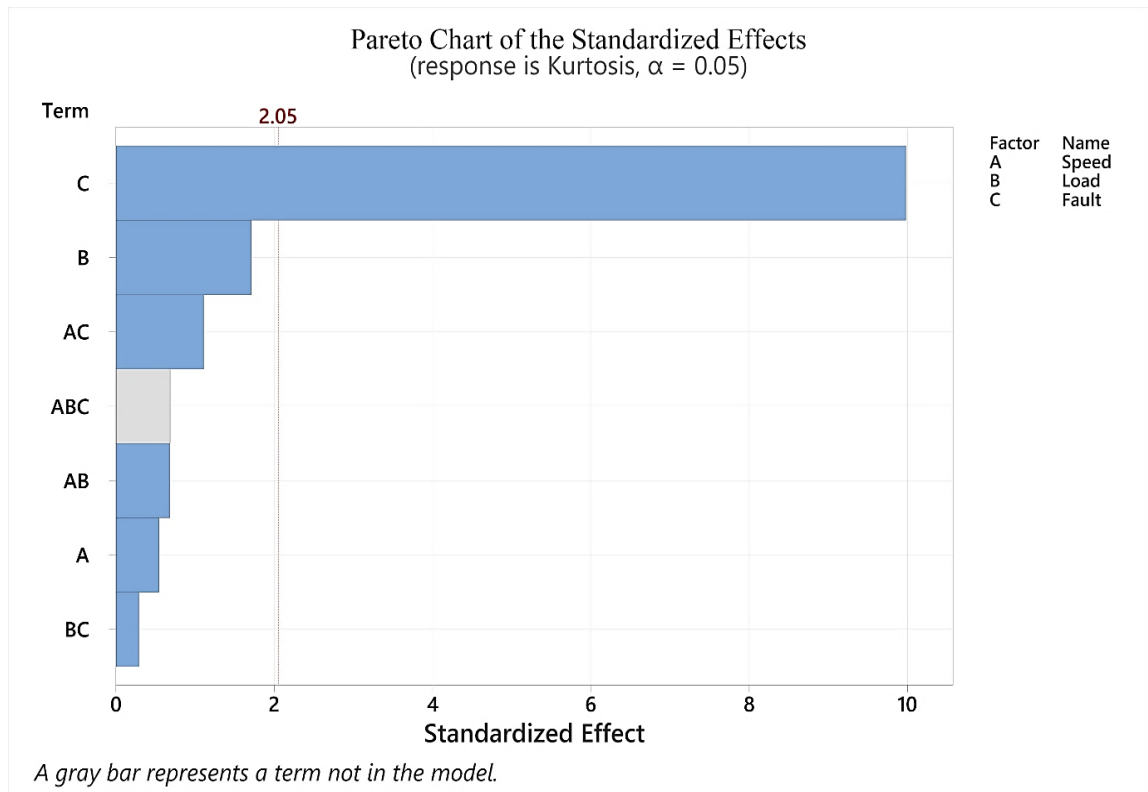


Figure 6.10 Pareto chart for kurtosis

6.3.4 Response Surface Plot

A response surface plot is a three-dimensional visual representation depicting the relationship between responses and process factors. The interaction effect between the speed (RPM) and load (N) on three-dimensional surface plots can enhance the comprehension and visualisation of the fundamental concept. Response surface plots are more advantageous than contour plots when analysing vibration levels, specifically the RMS (m/s^2) values. Furthermore, the level of noise (Leq in dB) and kurtosis are also observed in non-drive ends.

The 3-D surface plots of the interaction between speed and load on the RMS vibration response for healthy, OR, IR, and roller defects are depicted in Fig. 6.11. The response surface analysis of the bearing illustrates the impact of speed and load condition on the bearing over the speed range of 1000 RPM to 2800 RPM, as shown in Fig. 6.11. The vibration amplitude increases at high speed significantly for all bearing condition. Under loading conditions of 28 N at 2600 RPM, the greatest vibration amplitude of 25 m/s^2 is observed for a healthy bearing. When subjected to loads ranging from no load

to 25 N, the vibration response of a bearing exhibits only a slight variation as the speed increases. However, the vibration response drops as the load increases from 30 N to 50 N. Without faults, vibration mainly arises from surface roughness, manufacturing waviness, and imbalance. The effect of an OR defect in bearing components on the vibration response of the system under similar speed and loading conditions is illustrated in Fig. 6.11(b). When load is set to 30 N at 2200 RPM, the maximum amplitude of vibration is observed to be 102 m/s^2 . The OR defect influences the RMS value of acceleration more significantly, followed by IR, roller and healthy bearing. The outer-race defect is fixed in the loaded arc, so every roller produces a strong, repeatable impact. Higher load increases impact force, while higher speed increases frequency and intensity of these impacts. The inner-race defect rotates with the shaft, meaning it only enters the load zone part of the time. Similar interaction effects are observed in Figs. 6.11(c)-(d) for IR and roller fault as of healthy bearing but with different magnitude.

The interaction between speed and load on the noise response, L_{eq} for healthy, OR, IR, and roller defects are depicted in Fig. 6.12. There is a trend of increased sound in response to speed. However, the response surface behaviour with increasing loading situations is substantially higher than with increasing speed. This indicates that given a constant speed state, the noise level declines as the load on the bearing rises. The interaction effect between speed and load for all bearing conditions has a similar effect on L_{eq} as on RMS value vibration. The maximum amplitude of noise i.e., 88 dB, is observed at 30 N and 2600 RPM for roller defect and for OR, which is 87.5 dB at 30 N and 2400 RPM, followed by IR and healthy bearing. The minimum noise is noticed at low speed and high load for all bearing conditions.

Figure 6.13 shows the surface plot of kurtosis for healthy, OR, IR and roller defect conditions. It is observed that the kurtosis value always falls below 3 for healthy bearing, and for defect conditions, it is greater than 3. It is also observed that the kurtosis value is mostly affected by roller fault followed by OR, IR and healthy bearing. The minimum kurtosis is noticed at high speed and high load for healthy bearings. Conversely, minimal kurtosis is observed at low speed and high load for OR

defects. Similarly, minimal kurtosis is observed at low speed and low load for IR defects. Lastly, minimal kurtosis is observed at high speed and high load for roller defects.

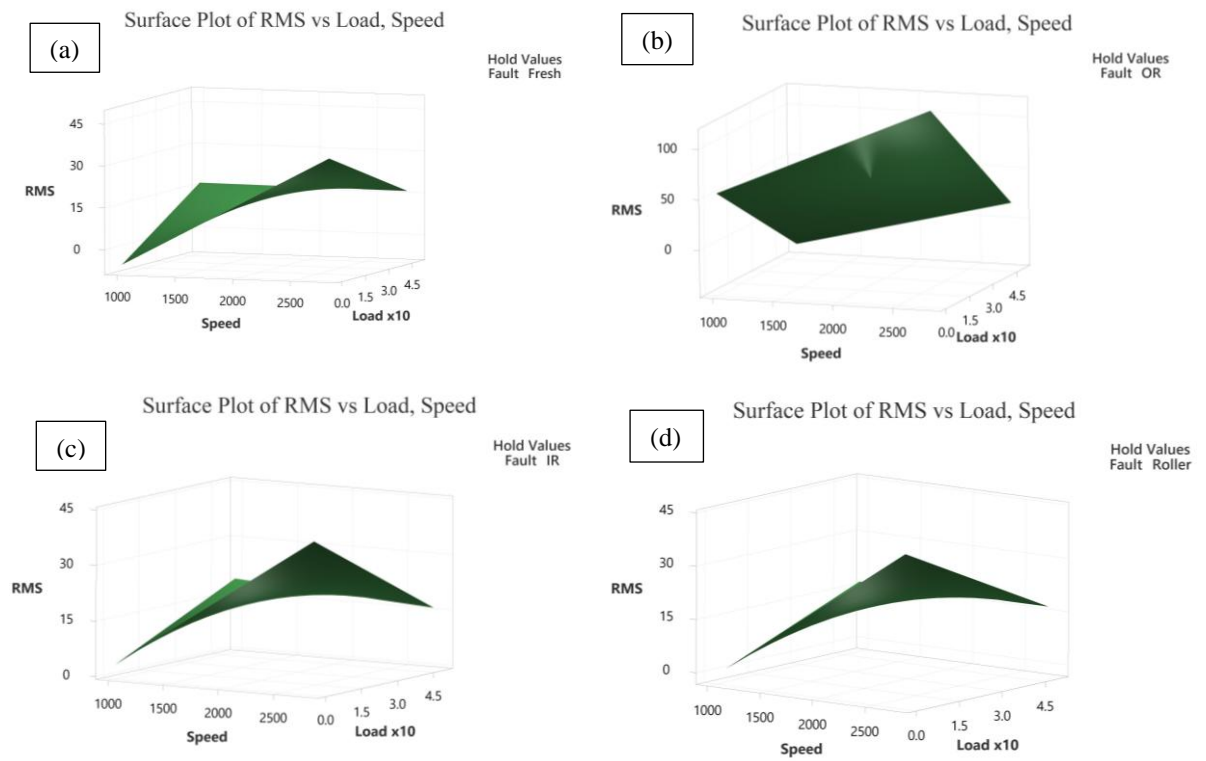
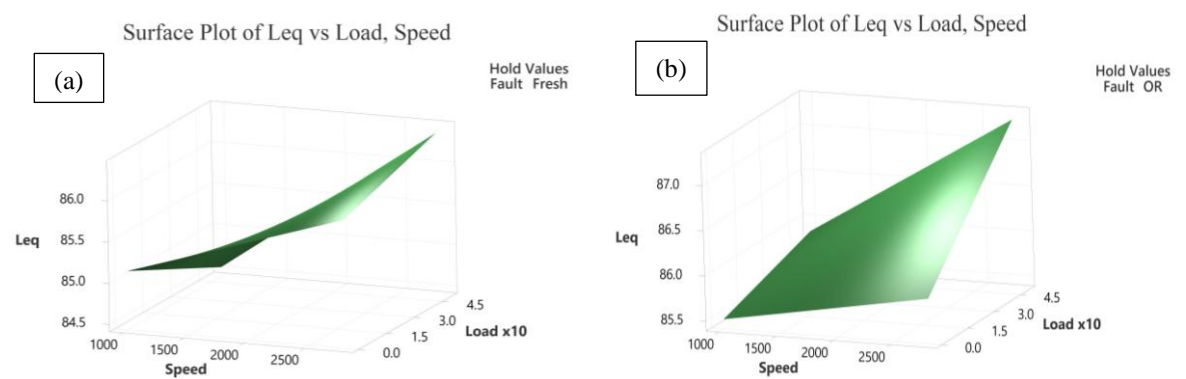


Figure 6.11 Surface plot of interaction for RMS



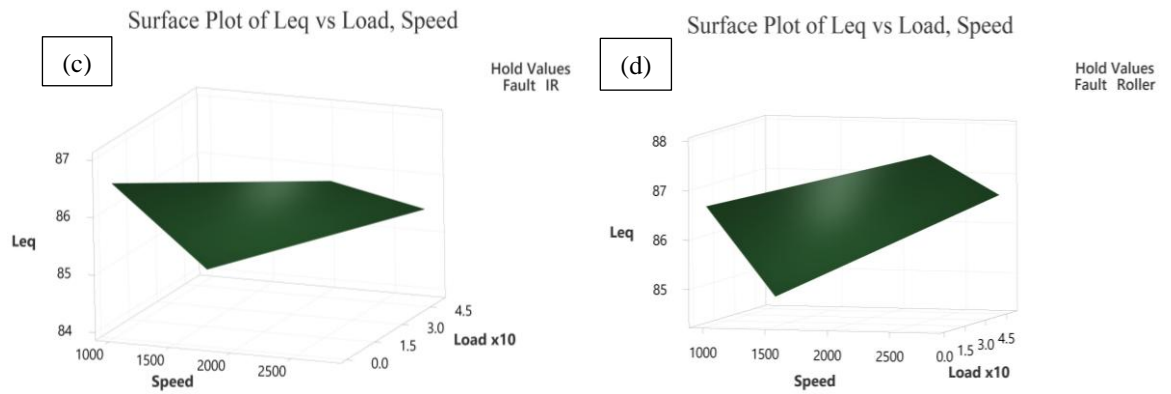


Figure 6.12 Surface plot of interaction for Leq

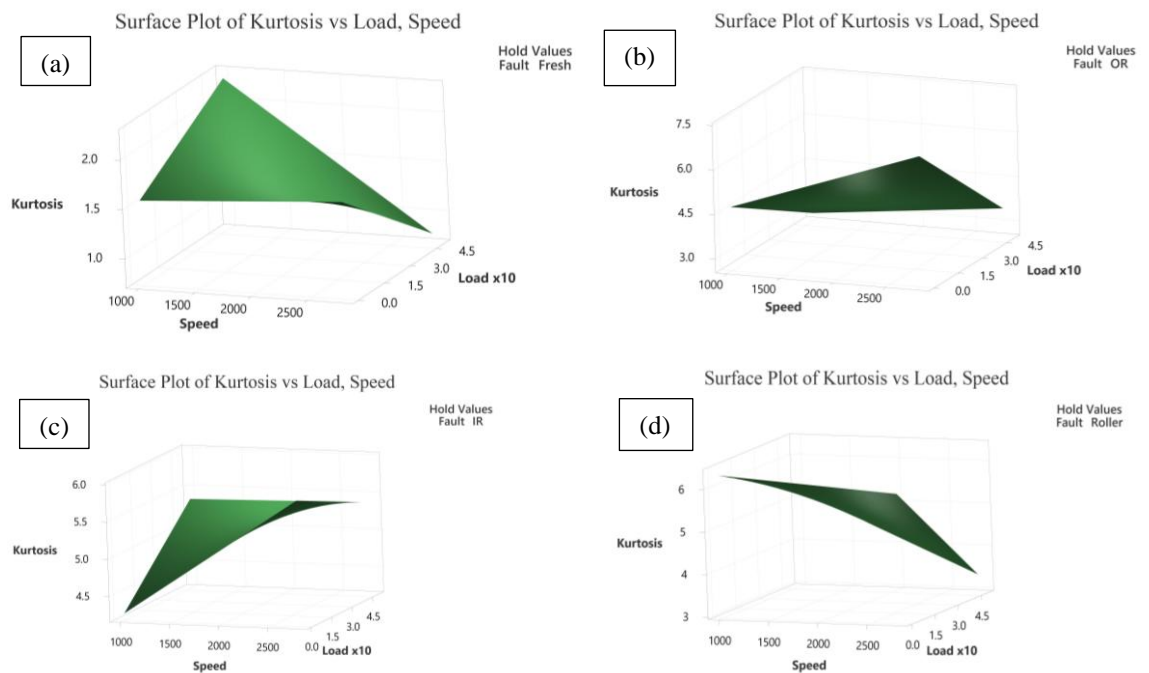


Figure 6.13 Surface plot of interaction for kurtosis

6.4 Summary of the Chapter

This chapter provides a comprehensive experimental analysis of the vibration characteristics of tapered roller bearings (TRBs) across various fault conditions. Faults of the same dimensions were introduced independently on the outer race (OR), inner race (IR), and roller elements, as well as compound faults that combined various defect types. The aim was to assess the distinct impact of each fault type on the vibration response of the bearing system.

The experimental configuration ensured stable loading and rotational velocity, with vibration signals recorded through accelerometers. A full factorial design of experiments was utilised to quantitatively evaluate the influence of fault types and operating parameters. This statistical method facilitated the detection of notable main effects and interaction effects of fault type, load, and speed on critical response parameters like RMS vibration, Leq and kurtosis. The comprehensive factorial analysis yielded significant insights into the interplay between fault severity and operational parameters on bearing behaviour, establishing a solid foundation for condition monitoring and fault diagnosis in TRBs. The following conclusions can be drawn from this study.

- The utilisation of the full factorial method, incorporating the Box-Cox transformation, has demonstrated its efficacy as a successful approach for evaluating the influential elements associated with bearing vibrations.
- The ANOVA results indicate that the interaction between load and fault is the most significant factor influencing vibration RMS, accounting for 46.89%. This is followed by the linear effects of load at 25.25%, speed at 18.27%, and fault at 6.07%.
- The analysis of variance indicates that the interaction of load is the most significant factor influencing noise (Leq), accounting for 41.65% of the contribution.
- The elevation in speed leads to a corresponding rise in the RMS value of vibration. The RMS value is most influenced by OR faults, followed by IR, roller, and healthy bearings.
- The full factorial method provides empirical evidence supporting the positive correlation between speed and the root mean square (RMS) and equivalent sound level (Leq) of the TRB. It has been observed that the root mean square (RMS) and equivalent sound level (Leq) exhibit an initial increase when the load is increased, followed by a subsequent reduction.
- The response of RMS and Leq shows similar features but at different magnitudes.

- A minor variation in the kurtosis value is observed at lower speeds; however, at elevated speeds, the kurtosis metric exhibits considerable stability. The sensitivity of kurtosis to load decreases as well.
- In industrial settings, additional effort is necessary to achieve sound signal results. The initial step is to measure the background noise and verify the decibel level, followed by correction using a noise correction chart.

Chapter 7 Automated Fault Diagnosis for a Tapered Roller-Bearing System using a Machine Learning Approach

This chapter presents an automated framework designed for the detection and classification of faults in tapered roller bearing (TRB) systems through the application of machine learning techniques. Leveraging experimental data gathered from diverse fault conditions, the framework combines signal processing techniques with supervised learning algorithms to facilitate automated condition monitoring. The methodology centres on extracting features from vibration and acoustic signals, followed by the training and validation of models. The strategy focusses on improving the precision of fault detection and facilitating predictive maintenance through the utilisation of data-driven insights. This chapter outlines the development process, covering data preprocessing through to model evaluation, thereby creating a strong pipeline for intelligent TRB health assessment.

7.1 Introduction

In recent decades, the identification of bearing defects has been a prominent research focus [176]. The majority of roller bearing faults are located on the outer race, inner race, or rolling elements, as indicated by previous research [177]. Many methods are employed for data collection to identify the most probable faults that may contribute to failure, such as vibration monitoring, thermal imaging, and oil particle analysis. The extensive study and use of vibration signal analysis as a condition monitoring approach for roller bearings is justified by its effectiveness, cost-effectiveness, and convenience [178]. Various strategies have been developed for feature extraction, including time-domain analysis, frequency-domain analysis, and time-frequency domain analysis.

Vibration analysis is a highly effective method for closely checking the state of bearings. This phenomenon can be attributed to a sequence of periodic and consecutive impulses in machine vibration when a ball is passed through a damaged race. In addition, vibration-based methods offer advantages such as low equipment expenses, simplicity of setup, and the ability to generate detailed data on the affected region,

resulting in more precise outcomes. Comprehending vibration sources and vibration characteristics is crucial for identifying defects. Despite the presence of geometrically flawless bearings, a certain degree of vibration is inevitable, commonly called variable compliance. Vibration is caused by surface roughness, which arises from geometrical imperfections resulting from the manufacturing process. The extraction of fault features is a crucial stage in defect diagnosis. Signal analysis can be used to check the health of the bearing by analysing the vibration signals that are generated. Classification of a bearing defect can be achieved by assessing the FFT data and analysing the components at the characteristic fault frequencies. These frequencies are clearly defined and are subject to the influence of factors such as the rotational speed, the bearing's design, and the specific location of a defect inside the bearing [8]. Electrical machinery failures can arise from a range of circumstances, which can be categorised as either internal or external based on the origin of the issue. Internal source failures occur due to manufacturing defects and the degradation of materials, whereas external source failures arise from exposure to the working environment, power supply, and load. The categorization of internal and exterior source failures into distinct fault types, such as rotor strikes, dielectric loss, eccentricity and inappropriate installation, can be achieved by using mechanical, electrical, and environmental subcategories [179].

Developing a computational framework for a tapered roller bearing (TRB) system using a machine learning (ML) approach is vital in improving fault diagnosis and predictive maintenance strategies. We have focused on enhancing machine learning classifier performance in bearing fault diagnosis through feature-based ranking. This method ensures that the most relevant features are selected, improving the ML models' classification accuracy and robustness. The study involves extracting key features from vibration signals of both healthy and faulty TRBs. Time-domain and frequency-domain features are computed to capture critical fault signatures. However, not all extracted features contribute equally to the classification process. To address this, feature selection techniques such as mutual information, correlation analysis, and ranking algorithms are employed to identify the most significant features that enhance model performance while reducing computational complexity.

Once the optimal features are selected, various ML classifiers are trained and evaluated to classify different bearing conditions effectively. Integrating feature-based ranking into the computational framework significantly improves the accuracy, precision, and overall reliability of fault detection. This approach optimises the ML model's efficiency and contributes to real-time condition monitoring applications, ensuring early detection of TRB faults and enhancing the reliability of rotating machinery systems.

One-way ANOVA and Kruskal-Wallis test feature ranking algorithms have been used in several applications, including text classification, cancer diagnosis, e-mail spam classification, microarray data classification, face recognition, and tumour classification [180]. While there are limited studies on using One-way ANOVA and the Kruskal-Wallis technique for bearing fault diagnosis. One-way ANOVA offers the advantage of not requiring an equal number of observations in each group. The design arrangement and statistical analysis are straightforward. The Kruskal-Wallis test differs from other parametric tests because it does not assume normality or variance homogeneity. This work examines the impact of two ranking strategies on bearing defect classification using distinct ML classifiers. Classifier performance is measured based on classification accuracy, training time, and prediction speed. The research is based on SKF30206 bearing data from a customised rotor-bearing test rig. Vibration datasets for healthy and damaged bearings with 20 fault classes are analysed. This study's results indicate that the feature ranking process, which assists in identifying certain features of signals in the time and frequency domains, significantly influences the effectiveness of machine learning classifiers.

7.2 Machine Learning Approaches

Machine learning techniques have greatly improved the field of fault identification and prognosis in bearing systems. These techniques allow for extracting significant feature from enormous amounts of data numerous sensors acquire. Smart defect diagnosis approaches often use feature identification to turn input patterns into small-dimensional vectors for better fitting and evaluation [181, 182]. Intelligent fault recognition algorithms use feature vectors as input. In the fault recognition stage, data

from the feature space is translated to machine defects in the defect space. Decision Trees, a supervised learning approach, are widely used classification algorithms [183]. A Decision Tree consists of decision nodes, segment data, and leaf nodes, which generate output. Reference [184] describes utilising the Decision Tree technique to identify bearing defects based on time-domain information.

The Support Vector Machine (SVM) is a strong and adaptable supervised learning technique that can be applied to classification and regression applications [185]. It is best suited for binary classification problems but may also be used for multi-class classification with approaches such as one-vs-one or one-vs-all. SVMs are well-known for their capacity to handle high-dimensional data and their success in situations where the number of dimensions exceeds the number of samples. The Support Vector Machine (SVM) technique aims to identify a hyperplane in an N-dimensional space (where N is the number of features) that effectively separates the data points into various classes. A hyperplane can be written as equation (7.1):

$$w \cdot x - b = 0 \quad (7.1)$$

Here, w is the weight vector, x is the input feature vector, and b is the bias term.

For a given data point x_i , the decision function can be written as equation (7.2):

$$f(x_i) = w \cdot x_i - b \quad (7.2)$$

If $f(x_i) > 0$, the data point is classified as one class (let's say positive class).

If $f(x_i) < 0$, it is classified as the other class (negative class).

The margin can be defined in equation (7.3):

$$Margin = \frac{2}{\|w\|} \quad (7.3)$$

Here, $\|w\|$ is the Euclidean norm of the weight vector w .

The SVM aims to maximize the margin, which can be formulated as an optimization problem:

$$\min_{w,b} \frac{1}{2} \|w\|^2$$

Subjected to:

$$y_i(w \cdot x_i - b) \geq 1, \forall_i$$

Here, y_i is the class label of the data point x_i , which can be either +1 or -1.

This problem can be transformed into a dual problem using Lagrange multipliers in equation (7.4):

$$\max_{\alpha} \sum_{i=1}^n \alpha_i - \frac{1}{2} \sum_{i=1}^n \sum_{j=1}^n \alpha_i \alpha_j y_i y_j x_i \cdot x_j \quad (7.4)$$

Subject to

$$\sum_{i=1}^n \alpha_i y_i = 0, \quad \alpha_i \geq 0, \quad \forall i$$

Here, α_i are the Lagrange multipliers.

The data points corresponding to $\alpha_i > 0$ are called support vectors. These data points lie on the margin and are critical for defining the hyperplane.

Kernel trick is a method that enables Support Vector Machines (SVM) to function in a higher-dimensional space without explicitly calculating the coordinates of the data in that region. Typical kernels consist of linear, polynomial and Gaussian/radial basis functions (Fine, Medium and Coarse Gaussian) in equation (7.5)-(7.7).

$$\text{Linear kernel } K(x_i, y_j) = x_i \cdot y_j \quad (7.5)$$

$$\text{Polynomial kernel } K(x_i, y_j) = (x_i \cdot y_j + 1)^d, \text{ where } d \text{ is degree.} \quad (7.6)$$

Radial basis function (RBF) kernel/Gaussian kernel

$$K(x_i, y_j) = \exp\left(-\frac{\|x_i - y_j\|^2}{2\sigma^2}\right) \quad (7.7)$$

Based on statistical learning frameworks, support vector machines (SVM) are among the most dependable prediction methods. Given a set of training examples, each designated as belonging to one of two categories, an SVM training algorithm generates a model that assigns new examples to one of the two categories, making it a non-probabilistic binary linear classifier.

The goal is to identify which class will get a new data point once some existing data points have been assigned to one of the two classes. In SVM, a data point is seen as a p -dimensional vector (a list of p numbers), and the question is whether such points can

be divided using a $(p - 1)$ -dimensional hyperplane. A maximum-margin hyperplane is the hyperplane that maximises the distance between itself and the closest data points of distinct classes in a linear classification scenario, where data is separated by hyperplanes. If this hyperplane exists, it is regarded as the optimal separating hyperplane and functions as a maximum-margin classifier. The optimal hyperplane can be determined by looking at the hyperplane that shows the largest margin, or separation, between the two classes. The classes are not divided by the hyperplane H_1 , as Fig. 7.1 illustrates. There is a small but significant advantage to the hyperplane H_2 . The hyperplane H_3 divides them as much as feasible with maximum success. A study on SVMs for identifying bearing defects found that they outperformed neural networks by up to 20% [186]. Several studies have used SVM as a defect classifier [187, 188].

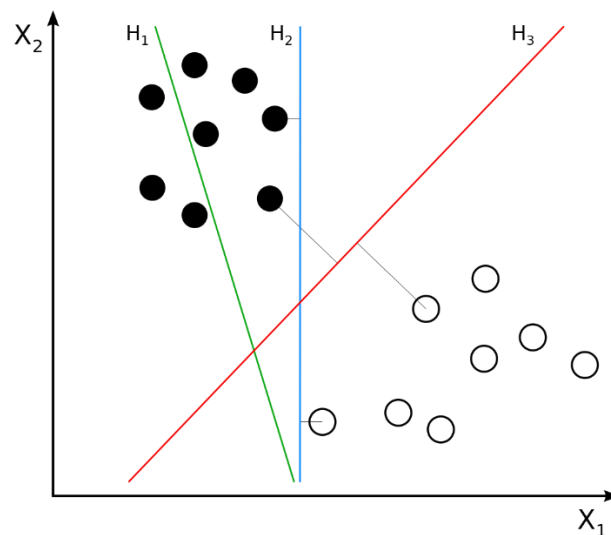


Figure 7.1 Two sets of data points are divided by distinct hyperplanes in SVM [189]

7.3 Hyperparameter Tuning for Machine Learning Models

A hyperparameter is a variable whose value controls an ML model's learning process. Hyperparameter optimization, sometimes referred to as hyperparameter tuning, is the process of determining an optimal collection of hyperparameters for a learning algorithm [190]. Hyperparameter tuning is an essential phase in developing machine learning models. Before the model is trained, hyperparameters are established to regulate the learning process. The model's performance can be substantially enhanced

by appropriately tuning these hyperparameters. Grid, random and Bayesian optimization are the three methods utilized for hyperparameter setting.

The traditional approach to hyperparameter optimization has been grid search or parameter sweep, a thorough search of a manually selected subset of the hyperparameter space of a learning system. A performance metric, often determined via cross-validation on the training set [191] or assessment on a hold-out validation set, is required to direct a grid search algorithm. Machine learner's parameter space may include real-valued or unbounded value spaces, grid search may need to establish limits and discretise some parameters manually.

Random search is used in random search instead of a comprehensive listing of every possible combination. This can be readily extended to continuous and mixed spaces, as well as previously discussed discrete environment. Grid search cannot match the performance of a machine learning method when just a small number of hyperparameters affect its result. In this case, the optimization problem is said to have low intrinsic dimensionality [192]. Random Search is embarrassingly parallel since it defines the distribution from which to sample and permits the inclusion of previous knowledge. Despite its simplicity, random search remains an essential benchmark for assessing the performance of novel hyperparameter optimization methods.

For noisy black-box functions, a general optimization method is Bayesian optimization. The relationship between hyperparameter values and the established goal, as determined by a validation set, is crucial for optimising hyperparameters to create a probabilistic model of the function. Bayesian optimization iteratively evaluates a plausible hyperparameter configuration based on the current model. Then, it updates it to gather observations that tell as much as possible about this function, particularly the optimum location. It attempts to achieve a balance between exploitation and exploration. In real-world applications, Bayesian optimization has been shown [193] to yield better results in fewer evaluations than grid search and random search because of its ability to forecast the quality of experiments before they are undertaken. This study involved the application of Bayesian optimisation alongside cross-validation to fine-tune hyperparameters for Support Vector Machine (SVM)

classifiers. This approach offers a more efficient and intelligent solution for hyperparameter tuning compared to alternative methods, particularly in high-dimensional search spaces.

7.4 Feature Ranking Techniques

Raw signals allow several aspects to be retrieved and interpreted meaningfully. Still, not every component is equally crucial for a given objective. Thus, optimal feature selection is crucial in defect diagnosis and severity estimate. Feature ranking methods aim to rank the features depending on physical spacing and information. The current work investigates their influence on the performance of machine learning models by following two feature ranking approaches [194].

7.4.1 One-way ANOVA

One-way ANOVA (Analysis of Variance) is a statistical approach for determining whether there are statistically significant variations in the means of three or more independent (unrelated) groups. It is used in feature ranking to identify properties that differ significantly across distinct groups (classes). The null hypothesis is that all means of the feature across all groups are equal. $H_o : \mu_1 = \mu_2 = \mu_3 = \dots = \mu_k$. Alternative Hypothesis (H_a) is at least one group mean is different. Total Sum of Squares (SS_T) measures the total variation in the data in equation (7.8).

$$SS_T = \sum_{i=1}^n (X_i - \bar{X})^2 \quad (7.8)$$

where N is the total number of observations, X_i is each observation, and \bar{X} is the overall mean.

The between-Group Sum of Squares (SS_B) measures the variation due to group interaction in equation (9).

$$SS_B = \sum_{j=1}^k n_j (\bar{X}_j - \bar{X})^2 \quad (7.9)$$

where k is the number of groups, n_j is the number of observations in group j , \bar{X}_j is the mean of group j , and \bar{X} is the overall mean.

The average of the sums of squares in equation (10).

$$MS_B = \frac{SS_B}{k-1} \text{ and } MS_W = \frac{SS_W}{N-k} \quad (7.10)$$

where MS_B is the mean square between groups and MS_W is the mean square within groups.

The ratio of MS_B to MS_W is called the *F-statistic*. In light of the null hypothesis, it adheres to the *F-distribution*. To ascertain whether the null hypothesis may be rejected, compare the computed *F-statistic* to the crucial value in the *F-distribution* table or utilise the *p-value*. Reject the null hypothesis if the *p-value* is less than the selected significance level (e.g., $\alpha=0.05$).

7.4.2 Kruskal-Wallis test

A non-parametric technique for determining if samples come from the same distribution is the Kruskal-Wallis test. It is applied when the ANOVA's normality and equal variances assumptions are not satisfied. The null hypothesis (H_o) is that the distributions of the feature across all groups are equal. The alternative Hypothesis (H_a) is that at least one group distribution differs. Combine all the group observations and rank them from smallest to largest, giving average ranks for ties. Test Statistics (H) in equation (7.11)

$$H = \frac{12}{N(N+1)} \sum_{j=1}^k \frac{R_j^2}{n_j} - 3(N+1) \quad (7.11)$$

where N is the total number of observations across all groups, k is the number of groups, n_j is the number of observations in group j , and R_j is the sum of ranks for group j . To reject the null hypothesis, compare the generated *H statistic* to the critical value from the chi-square distribution table with $k-1$ degrees of freedom. Alternatively, use the *p-value*. If the *p-value* falls below the chosen significance level (e.g., $\alpha=0.05$), reject the null hypothesis.

The Kruskal-Wallis test assumes that all observations are independent of each other and that all tests originate from populations with the similar continuous distribution, excluding any possible variations in locations due to group effects. The classic One-way ANOVA replaces the weaker initial assumption with a stronger one, namely that the populations have normal distributions.

7.5 Experimental Methodology

The experimental methodology for this study has been split into two sections. The first section, labelled Experimental Setup and Data Description, describes and classifies the data and apparatus utilised throughout the experiment. The second half focuses on Data Ensembles for Fault Classification and feature ranking. Figure 7.2 depicts the approach used to analyse taper roller bearings in this study.

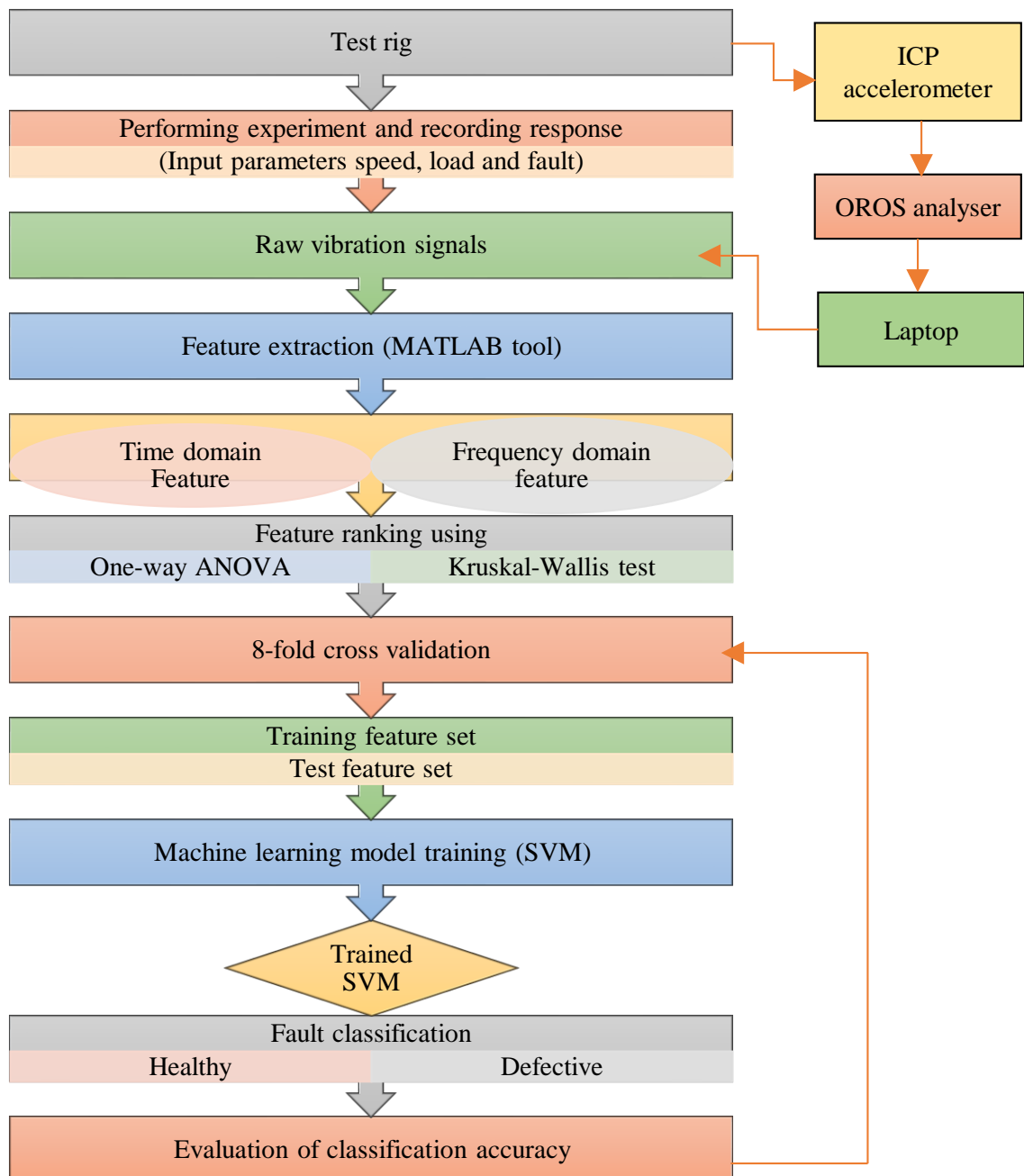


Figure 7.2 Methodology flowchart

7.6 Data set for Fault Classification

The data from the above test rig is utilised to evaluate the proposed methodology. Vibration measurements are acquired with the accelerometer on the housing of NDE. SKF 30206 bearings are employed for both DE and NDE. Wire EDM is used to induce a 1.5 mm wide and 1 mm deep OR, IR, and roller defect for defective bearing signals.

Table 7.1 Description of tapered bearing dataset chosen for fault diagnosis

Bearing Position	Shaft Speed (RPM)	Load (N)	Condition of bearing	Fault code	Size of sample	No of samples
Non-Drive End	1000	0	Healthy	1	2560	800 (40x20)
	1000	50	Healthy	2		
	2000	0	Healthy	3		
	2000	50	Healthy	4		
	1000	0	Outer race fault	5		
	1000	50	Outer race fault	6		
	2000	0	Outer race fault	7		
	2000	50	Outer race fault	8		
	1000	0	Inner race fault	9		
	1000	50	Inner race fault	10		
	2000	0	Inner race fault	11		
	2000	50	Inner race fault	12		
	1000	0	Roller fault	13		
	1000	50	Roller fault	14		
	2000	0	Roller fault	15		
	2000	50	Roller fault	16		
	1000	0	Compound fault	17		
	1000	50	Compound fault	18		
	2000	0	Compound fault	19		
	2000	50	Compound fault	20		

Vibration signals are recorded at 25.6 kHz, under motor speeds of 1000 and 2000 RPM, and used load operating conditions, denoted as no-load condition and 50 N radial load, which is mounted externally to the shaft of the disk. The present analysis considers the bearing defects classes as outlined in Table 7.1. Twenty fault classifications have been assigned using numeric codes ranging from 1 to 20 based on speed and load. A total of 40 data subsets or samples created from 102400 data points, each subset consisting of 2560 data points, are extracted from each defect category for data preparation. This yields an ensemble of 800 entities.

The approach utilized in this research consists of a series of sequential procedures executed within the MATLAB environment. An ensemble of raw data comprising healthy bearing, inner, outer, roller and compound defects is prepared in the initial stage. In the subsequent phase, the time domain and frequency domain characteristics of the ensemble of data are extracted. Supervised feature ranking techniques are implemented to rank the extracted features. The Kruskal-Wallis test and one-way ANOVA are the two methods utilized.

7.7 Results and Discussion

To diagnose rolling element bearings, signals' frequency-domain and statistical time-domain characteristics can be employed to differentiate between healthy and defective states. As bearing health declines, a specific signal's peak frequency or amplitude may fluctuate. Skewness and Kurtosis are examples of specific higher-order signal properties that can be employed to accomplish the objective. With these characteristics, it is possible to establish threshold values that differentiate between healthy and problematic operations. Additionally, rapid fluctuations in the associated values may suggest that the bearing condition has changed.

MATLAB was employed to conduct the analysis. Initially, a data ensemble consisting of various defect classes is established. The efficacy of machine learning methods in grouping the datasets is assessed using the fault features. The ML classifiers are trained, and their performance is evaluated using a variety of performance metrics, including Accuracy, Training Time, and Prediction Speed after the features are ranked using two distinct methodologies to identify effective condition indicators.

Table 7.2 Time-domain and frequency-domain features used for fault classification

Time domain features	peak value, shape factor, clearance factor, crest factor, impulse factor, standard deviation, skewness, kurtosis, SNR, SINAD, mean and root mean squares (RMS).
Frequency domain features	Peak amplitude, peak frequency and band power.

7.7.1 Raw data

The defect categories listed in Table 7.1 are illustrated in Fig. 7.3, which displays normalised vibration data ensemble measurements. These are denoted by fault codes 1–20 and are represented by varying colours in the diagram. Figure 7.4 illustrates power spectral density (PSD) that highlights dominant frequency components for each fault case. For nearly all fault cases, a significant peak is observed in 5500–7000 Hz frequency range. This may be linked to the natural frequencies of the bearing structure or resonance zones that are induced by faults.

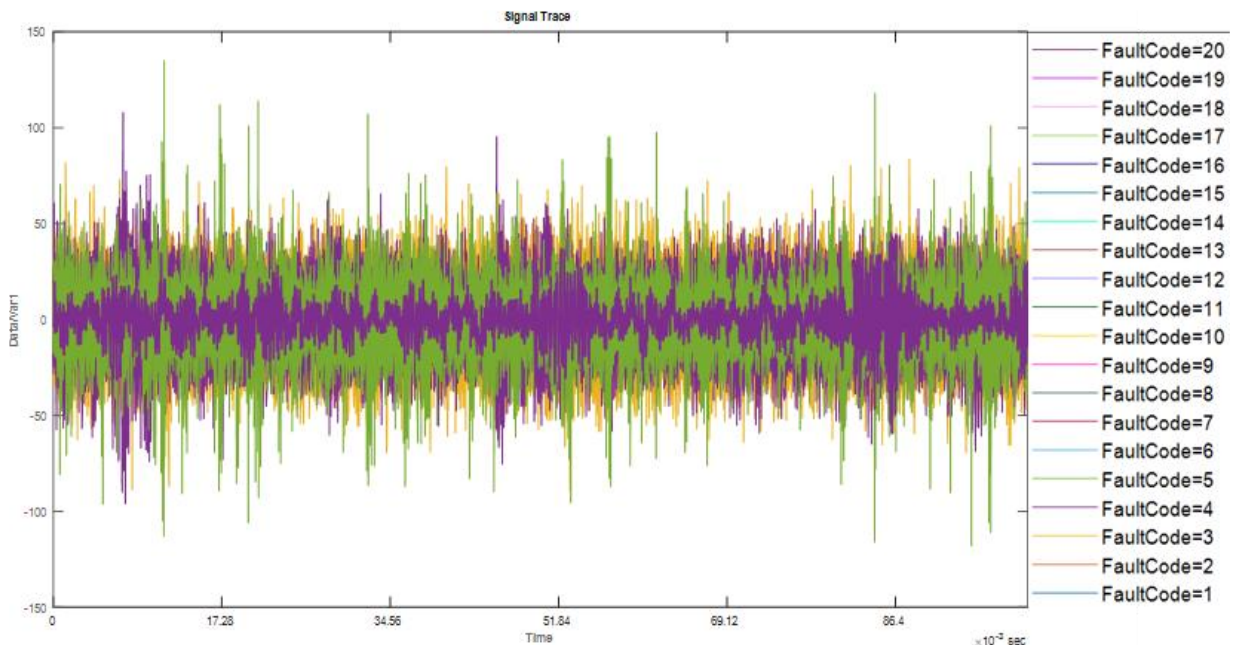


Figure 7.3 Collective vibration raw data of 20 faults from test bearing

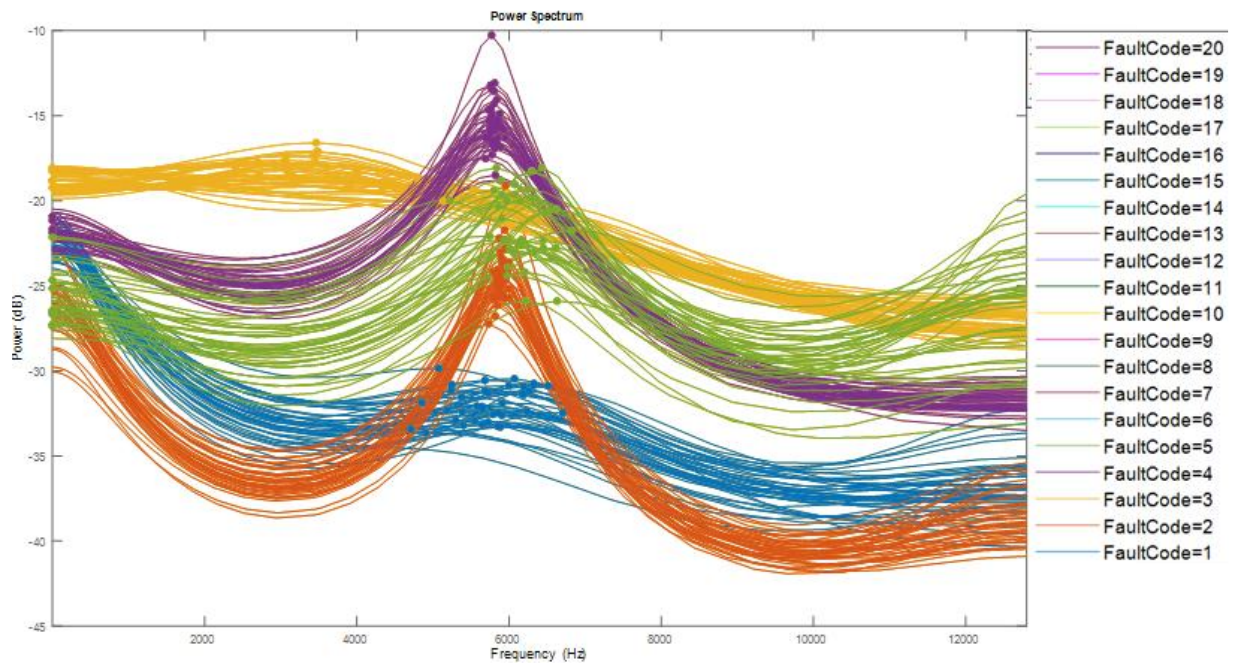


Figure 7.4 Collective Power Spectrum density data of 20 faults from test bearing

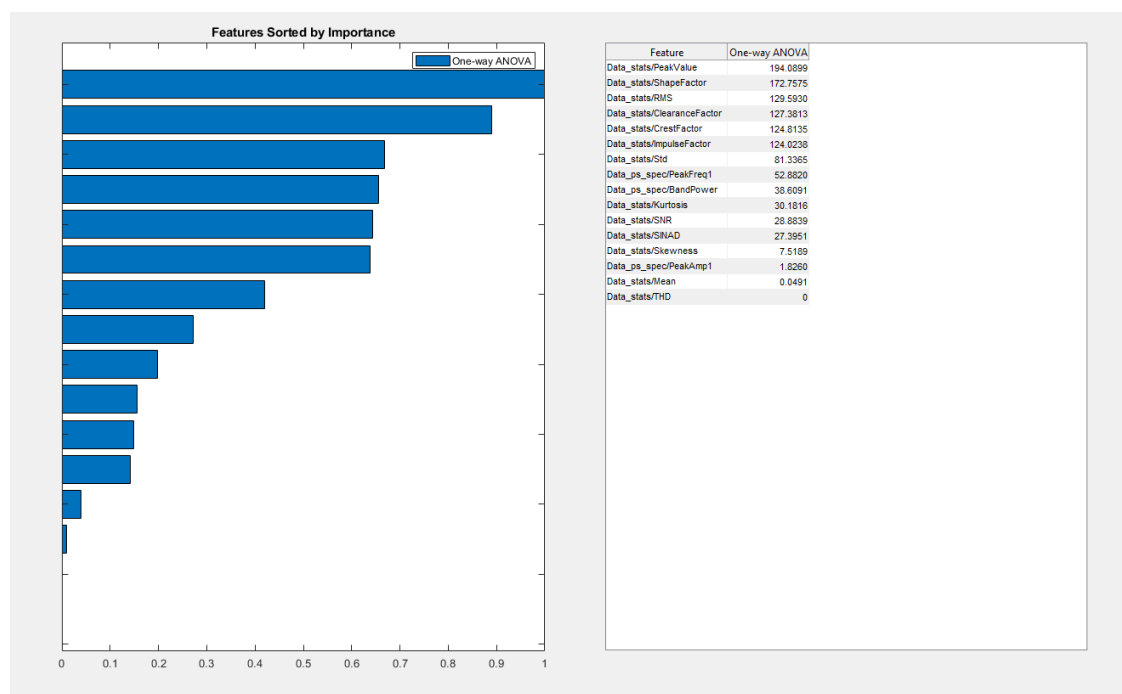
7.7.2 Feature Ranking

Features are gauges that can serve as indicators of bearing conditions. The following are time domain features: peak value, shape factor, clearance factor, crest factor, impulse factor, standard deviation, skewness, kurtosis, SNR, SINAD, mean and root mean squares (RMS). Frequency domain features include peak amplitude, peak frequency and band power. Sixteen features were extracted from the vibration signal depicted in Table 7.2 for this investigation. MATLAB was employed to calculate all 16 features from each bearing dataset. This led to a feature matrix that measured 800 by 16. Features are ranked using Ow-A and KW tests after they have been extracted. The relative ranking of the features is illustrated in Table 7.3. Feature classification is demonstrated in Fig. 7.5, which is based on normalised scores.

Table 7.3 Features ranked by Ow-A and KW Test

Ow-A Test		KW Test	
Features	Rank	Features	Rank
Peak value	1	RMS	1

Shape factor	2	<i>Band power</i>	2
RMS	3	Standard deviation	3
Clearance factor	4	Peak value	4
Crest factor	5	<i>Peak amplitude</i>	5
Impulse factor	6	Shape factor	6
Standard deviation	7	Clearance factor	7
<i>Peak frequency</i>	8	Impulse factor	8
<i>Band power</i>	9	Crest factor	9
Kurtosis	10	Kurtosis	10
SNR	11	<i>Peak frequency</i>	11
SINAD	12	SNR	12
Skewness	13	SINAD	13
<i>Peak amplitude</i>	14	Skewness	14
Mean	15	Mean	15
THD	16	THD	16



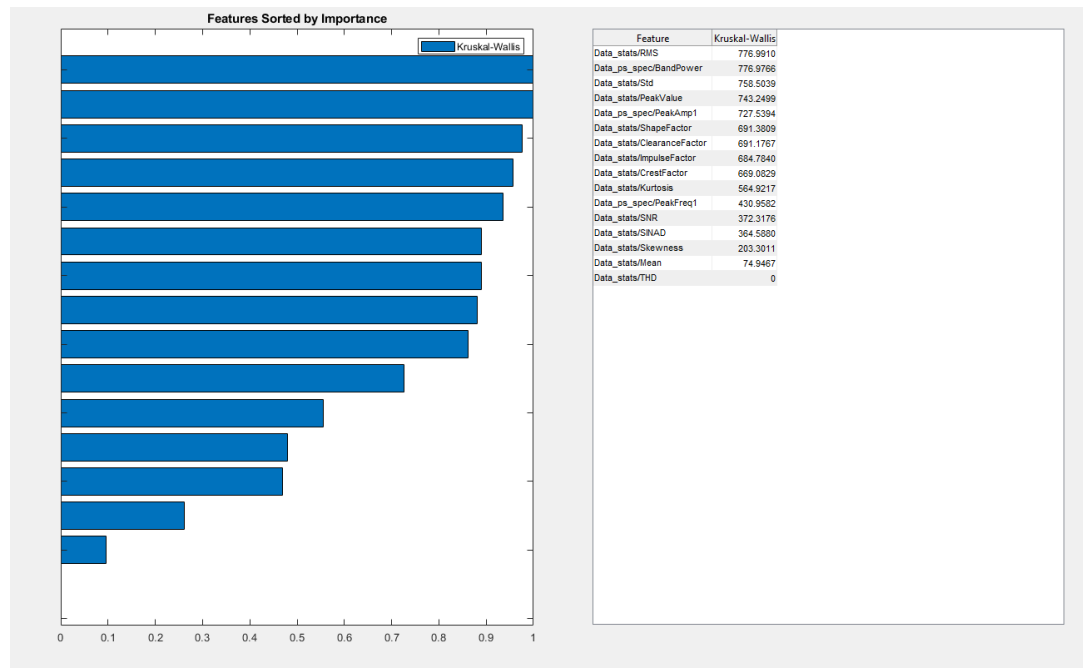


Figure 7.5 Normalized results of OWA and KW test for test bearing data

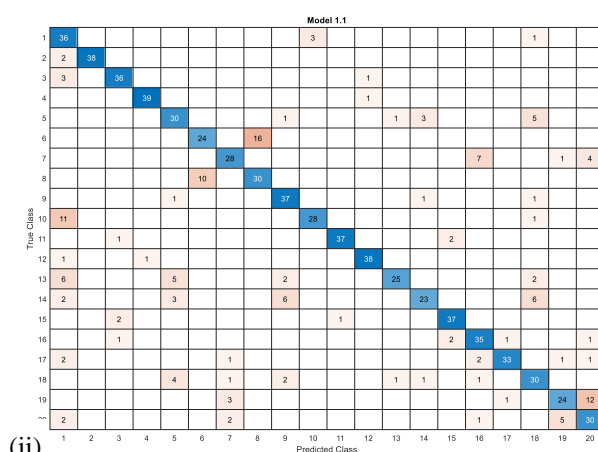
7.7.3 Feature Selection and Model Training

Initially, all features are selected for training machine learning classifiers, disregarding their ranking. To evaluate the impact of feature ranking compared to non-ranking on classifier performance, two groups, including the top five and top ten feature, are chosen based on their ranking scores. Numerous comparable investigations in the domain have employed top-N feature subsets (commonly $N = 5, 10, 15$) to evaluate the effectiveness of feature importance and the impact of dimensionality reduction. This convention was adhered to in order to maintain consistency and ensure comparability. The system is intentionally kept simple and controlled, with a focus on slit-type faults, which represent the initial phase of defect development in bearings. The experimental conditions were carefully maintained to minimize external disturbances, and the use of early-stage, localized damage makes the system less susceptible to noise interference. As a result, the extracted features remain stable and largely unaffected by environmental noise in our case.

An identical analysis is conducted on SVM classifiers with different kernels. The classifier outcomes are presented as a scatter plot (SP) and a confusion matrix (CM).

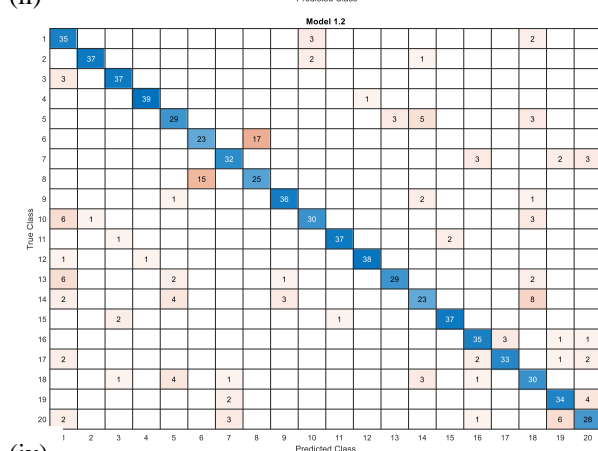
A SP actively analyses data from several fault categories and selects the most prominent characteristics. The SP illustrates both the training data and the misclassified instances. The confusion matrix is employed to evaluate the performance of a classifier in each class and to pinpoint the areas in which the classifier is failed. Columns denote predicted classes, whereas rows indicate true classes. In the cross-validation procedure, predictions generated from data not utilised for training are employed to construct a confusion matrix. The diagonal cells, indicating instances where the true and predicted classes match, demonstrate that the classifier functioned as planned and accurately identified true class observations. The present study used the k -fold cross-validation method for training the ML models. This technique partitions a dataset into k equally sized folds randomly. The model is subsequently trained on the remaining $k-1$ folds after designating one-fold as the holdout set. The model is evaluated using the observations that were excluded in the fold. The procedure is executed k times, utilising a distinct set as the holdout set on each occasion. The 800 data samples undergo an 8-fold cross-validation technique. The provided data is partitioned into several folds or subsets, with one designated as a validation set while the other folds are utilised for model training. This procedure is performed multiple times, employing a distinct fold as the validation set. The outcomes of each validation phase are averaged to yield a more dependable assessment of the model's performance. Cross-validation is a crucial phase in the machine learning process that guarantees the selected model for deployment is resilient and applicable to new data.

Figures 7.6-7.10 present scatter plots and confusion matrices for the Support Vector Machine (SVM) classifiers with different kernels. The classifiers were trained to utilise all features without feature ranking, the top five features ranked by the OwA and KW tests, and the top ten features in both the OwA and KW tests. The feature clearance factor is graphed against the feature peak value across all classifiers to evaluate the results. The system attains superior accuracy, necessitates reduced training duration, and generates swifter predictions. Table 7.4 encapsulates the quantitative data about classification accuracy, speed and training duration for all feature selection methodologies.



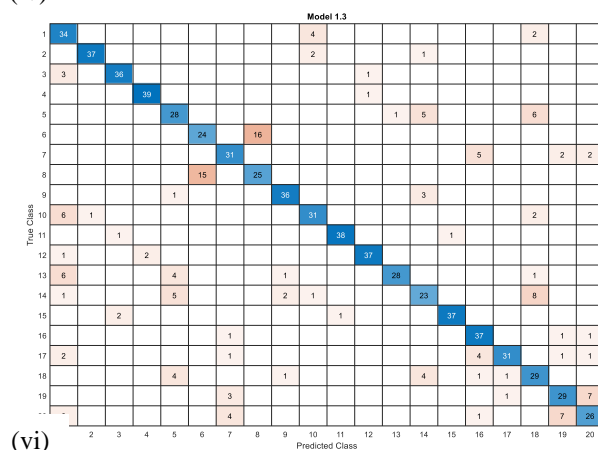
(i)

(ii)



(iii)

(iv)



(v)

(vi)

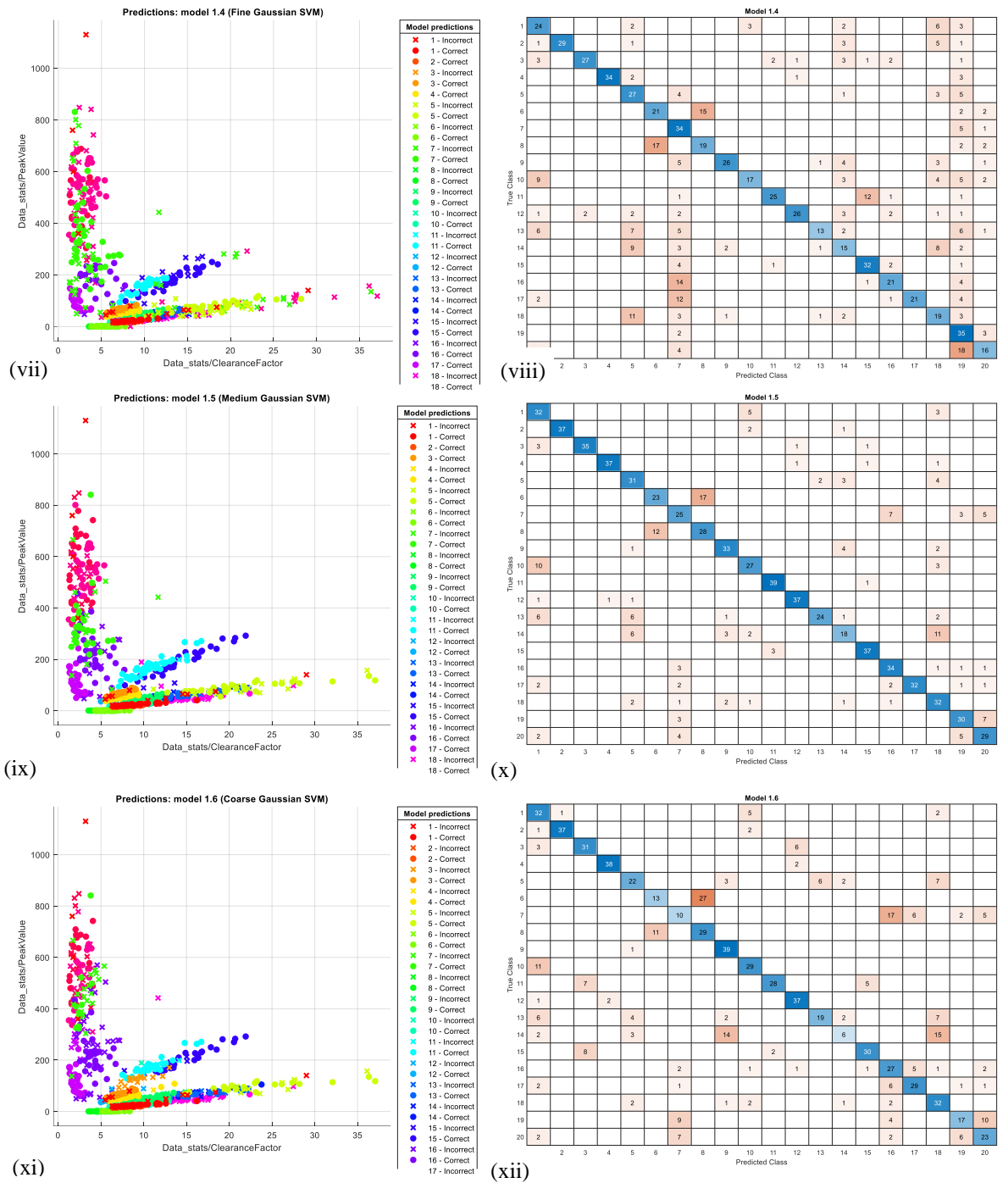
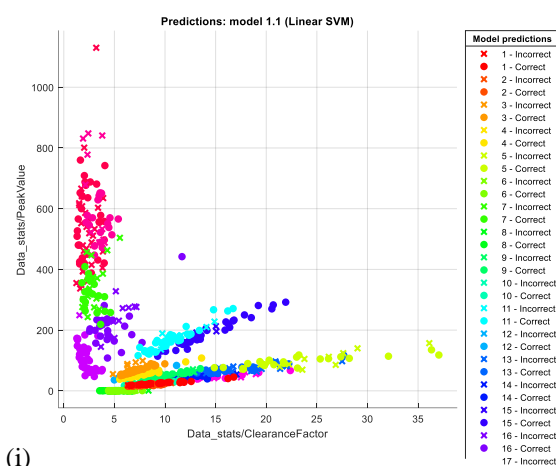
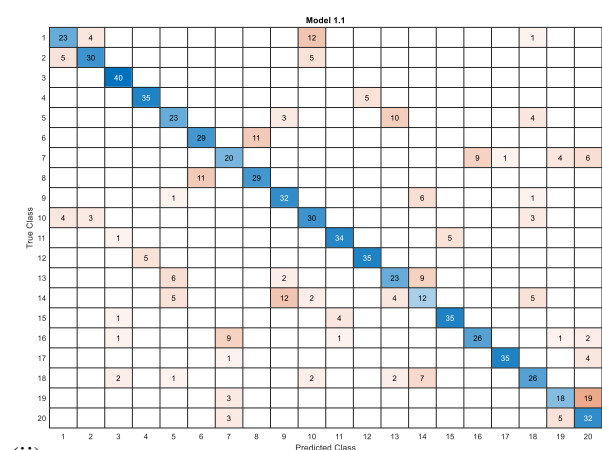


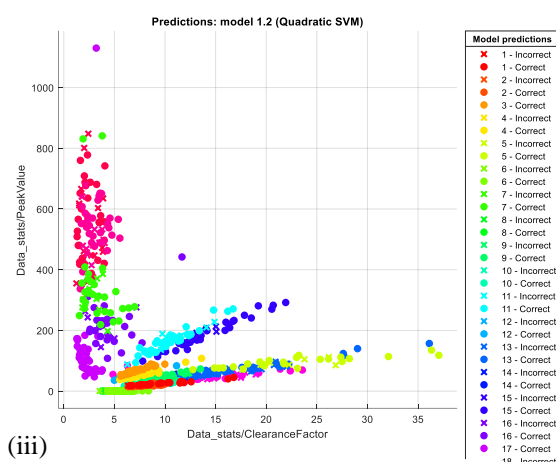
Figure 7.6 Fault classification by SVM model for all features without ranking (i) SP linear kernel (ii) CM for linear kernel (iii) SP quadratic kernel (iv) CM quadratic kernel (v) SP for cubic kernel (vi) CM for cubic kernel (vii) SP for fine kernel (viii) CM for fine kernel (ix) SP for medium kernel (x) CM for medium kernel (xi) SP for coarse kernel (xii) CP for coarse kernel



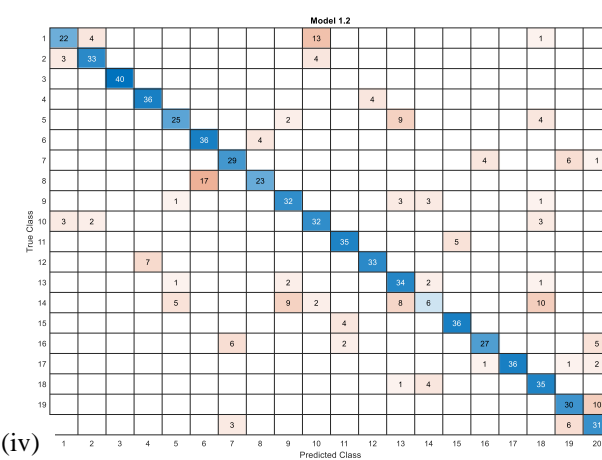
(i)



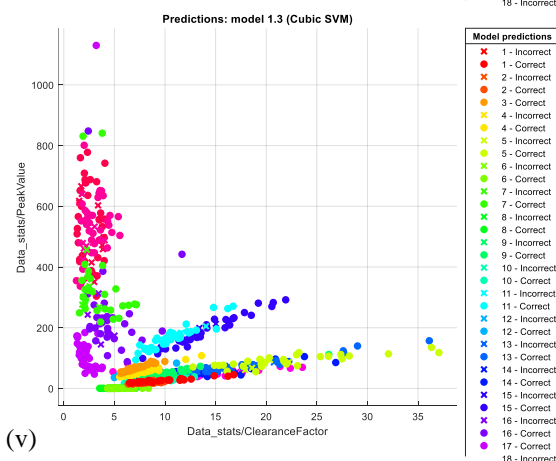
(ii)



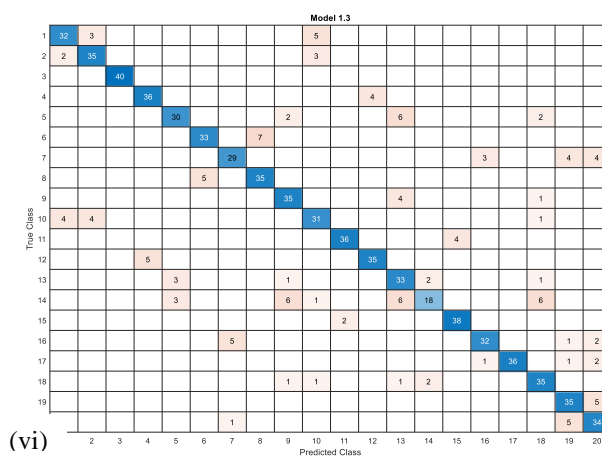
(iii)



(iv)



(v)



(vi)

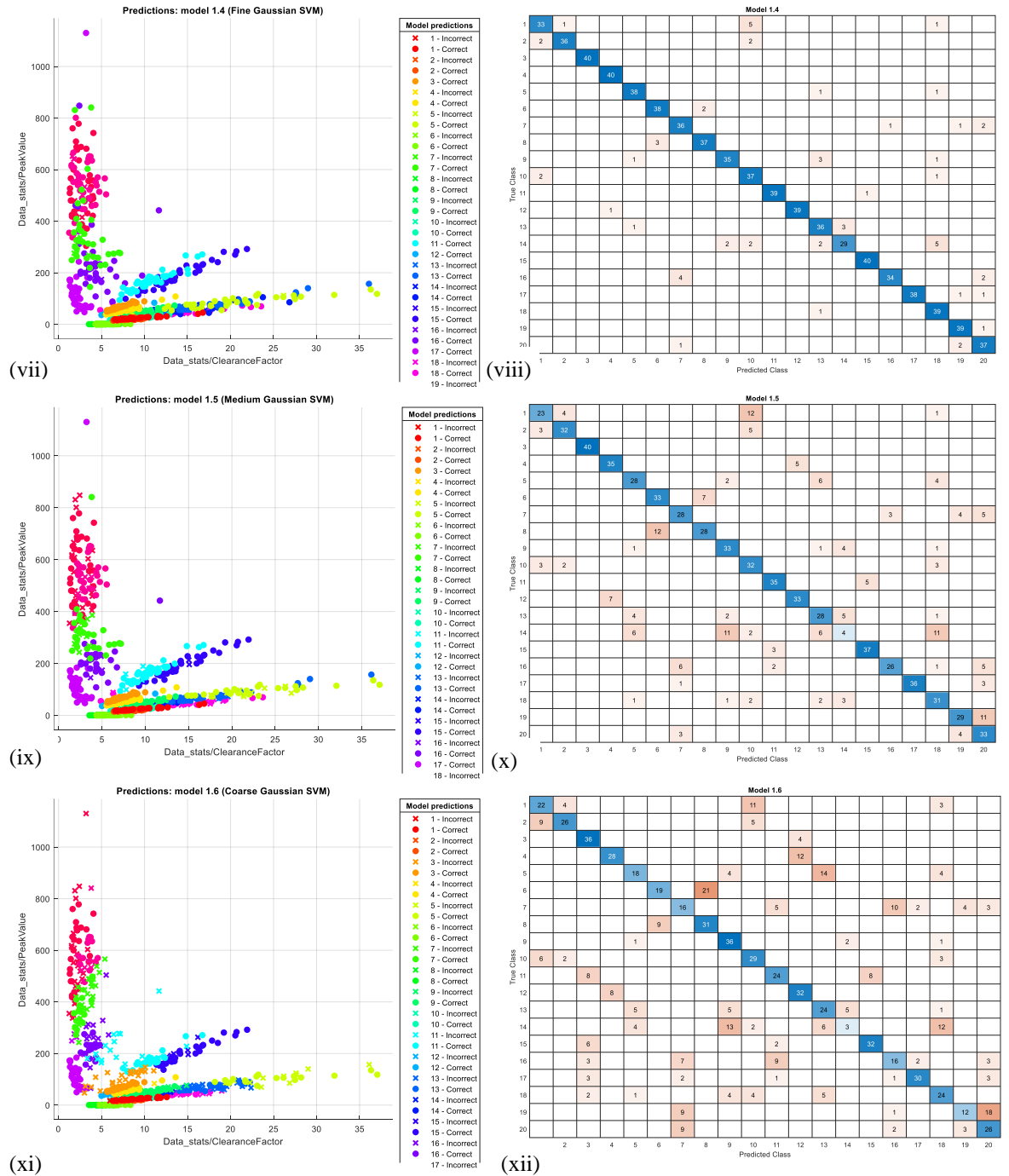
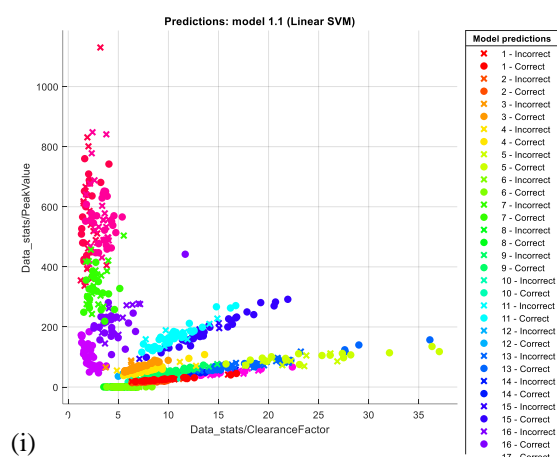
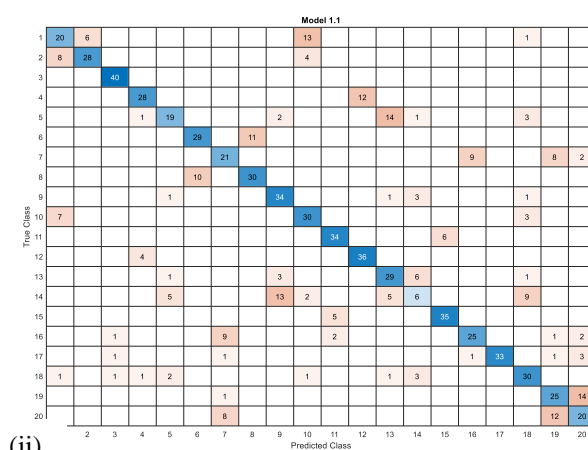


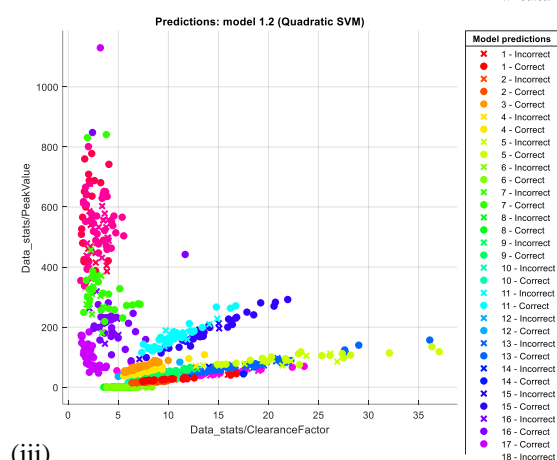
Figure 7.7 Fault classification by SVM model for top five features of OwA test (i) SP linear kernel (ii) CM for linear kernel (iii) SP quadratic kernel (iv) CM quadratic kernel (v) SP for cubic kernel (vi) CM for cubic kernel (vii) SP for fine kernel (viii) CM for fine kernel (ix) SP for medium kernel (x) CM for medium kernel (xi) SP for coarse kernel (xii) CP for coarse kernel



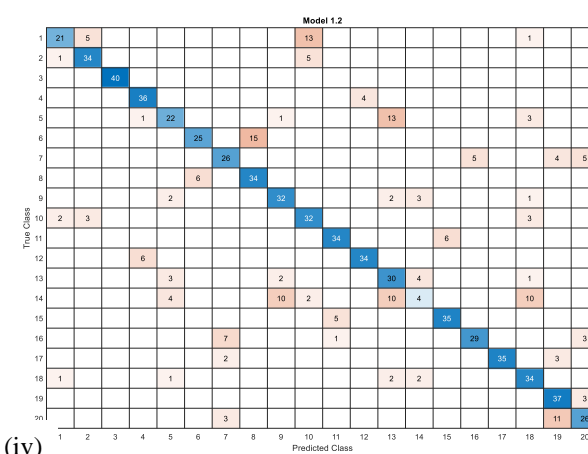
(i)



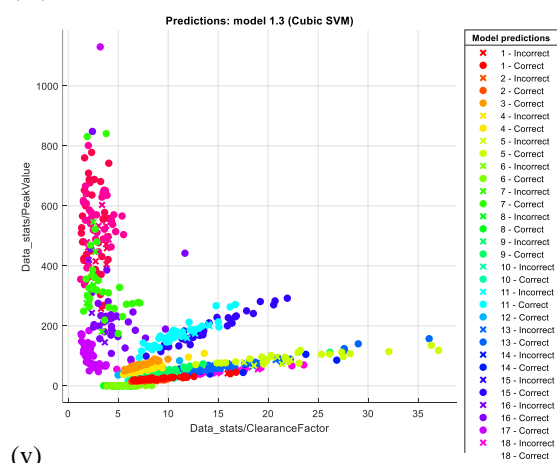
(ii)



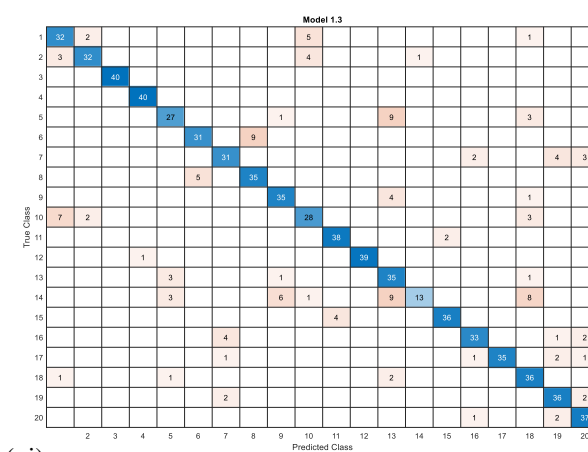
(iii)



(iv)



(v)



(vi)

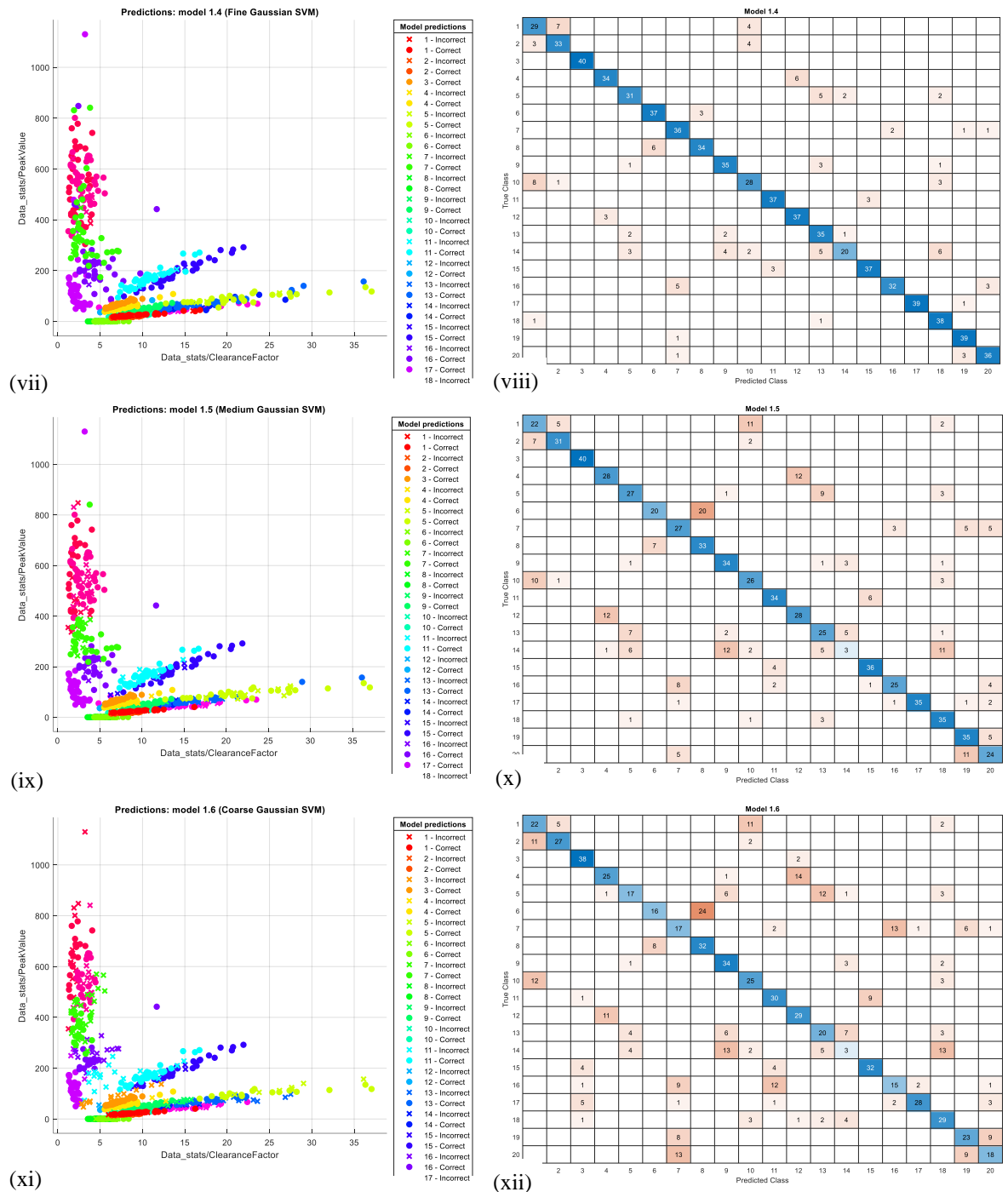
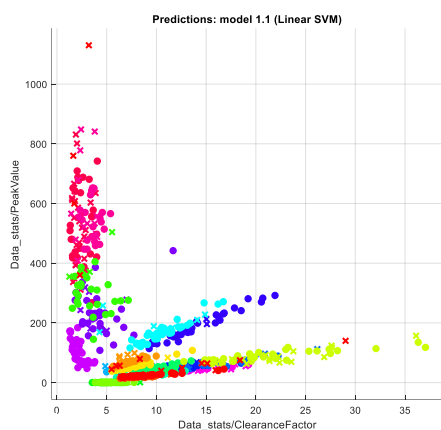
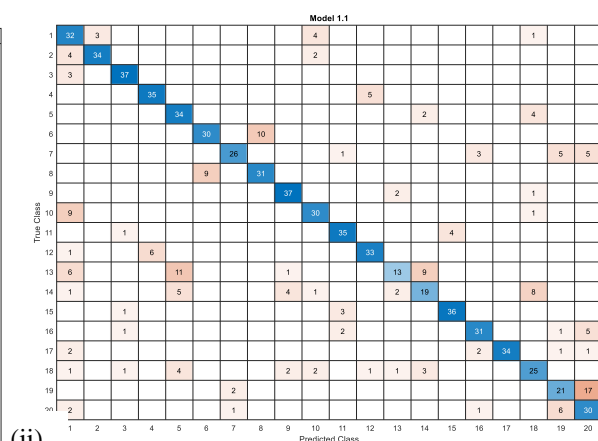
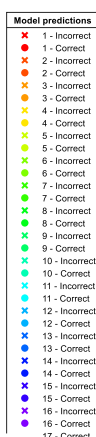


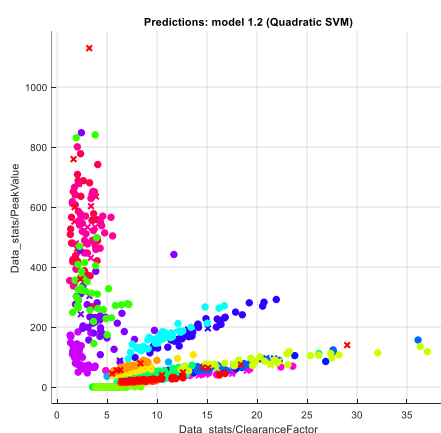
Figure 7.8 Fault classification by SVM model for top five features of KW test (i) SP linear kernel (ii) CM for linear kernel (iii) SP quadratic kernel (iv) CM quadratic kernel (v) SP for cubic kernel (vi) CM for cubic kernel (vii) SP for fine kernel (viii) CM for fine kernel (ix) SP for medium kernel (x) CM for medium kernel (xi) SP for coarse kernel (xii) CP for coarse kernel



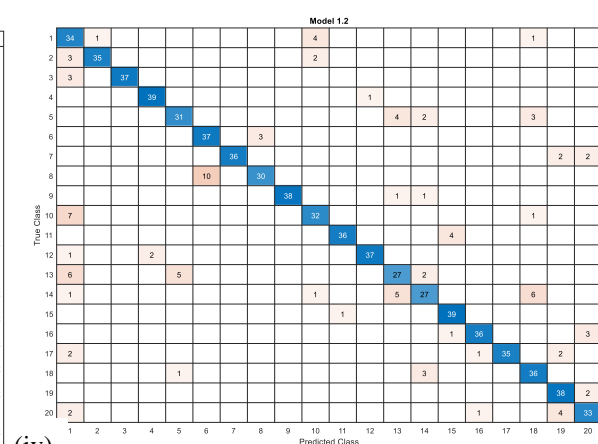
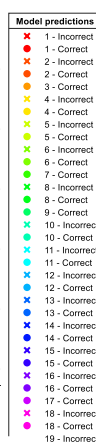
(i)



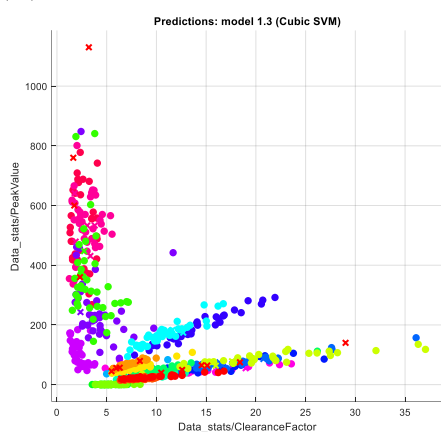
(ii)



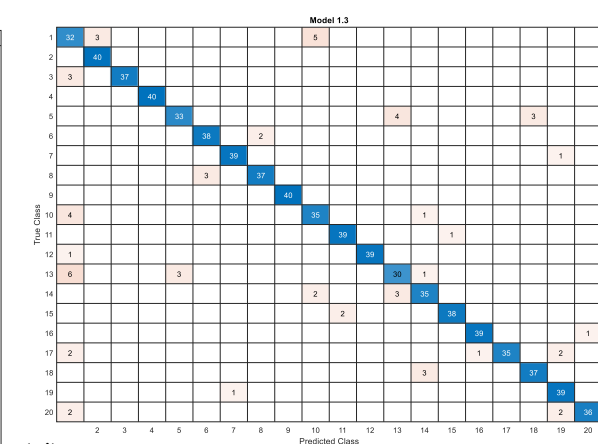
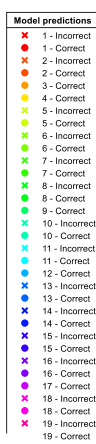
(iii)



(iv)



(v)



(vi)

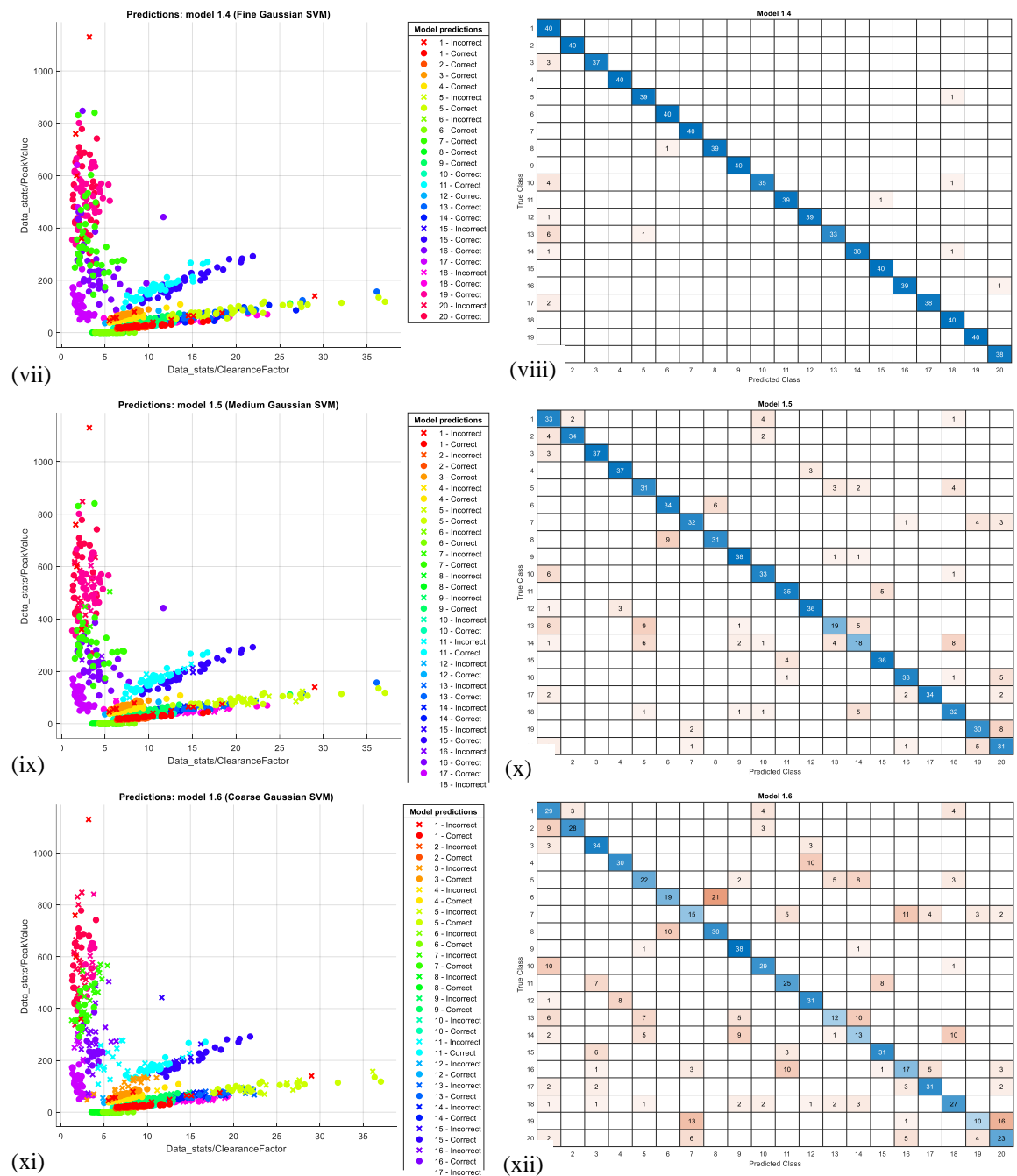
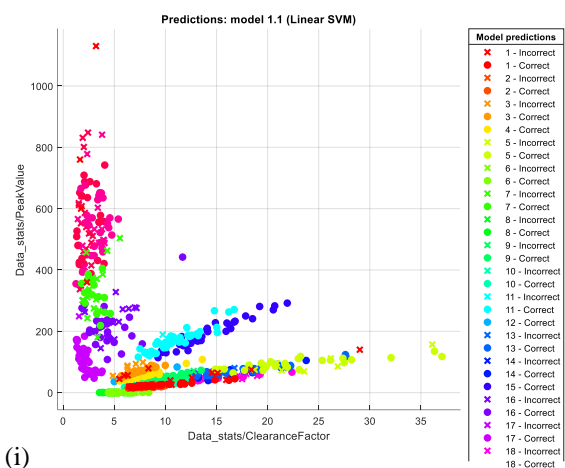
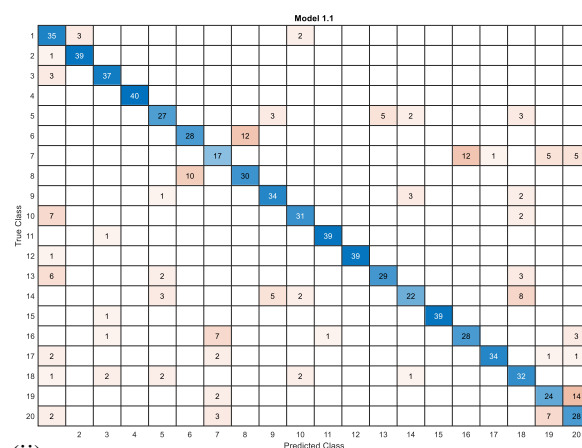


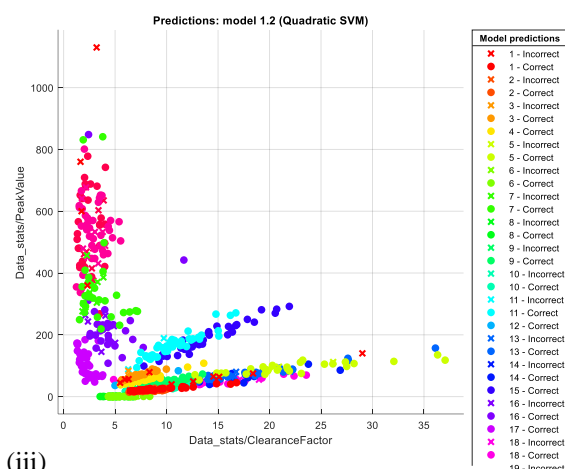
Figure 7.9 Fault classification by SVM model for top 10 features of OWA test (i) SP linear kernel (ii) CM for linear kernel (iii) SP quadratic kernel (iv) CM quadratic kernel (v) SP for cubic kernel (vi) CM for cubic kernel (vii) SP for fine kernel (viii) CM for fine kernel (ix) SP for medium kernel (x) CM for medium kernel (xi) SP for coarse kernel (xii) CP for coarse kernel



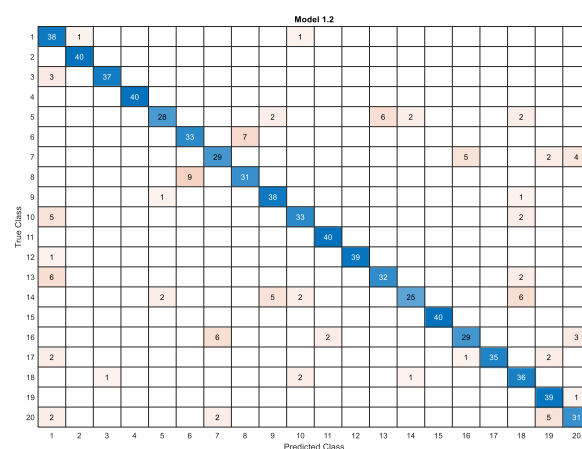
(i)



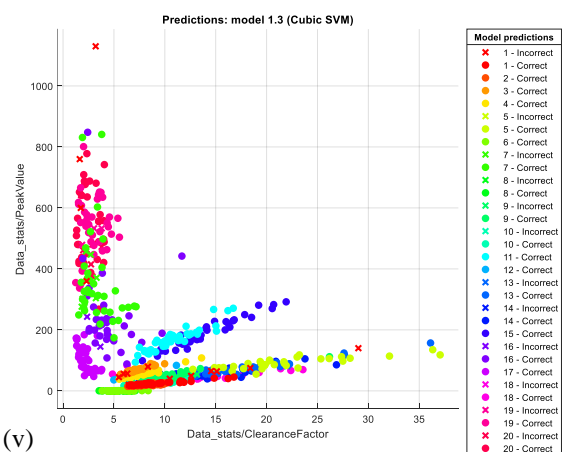
(ii)



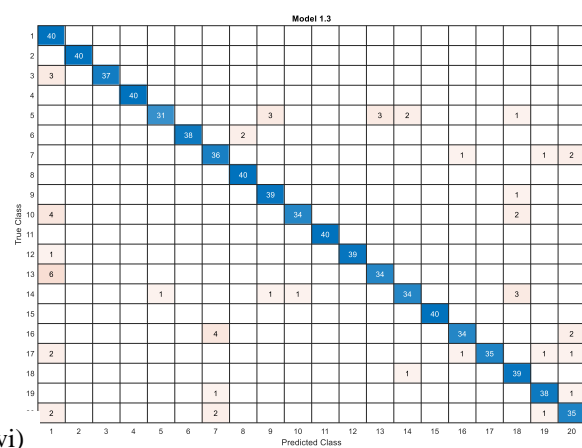
(iii)



(iv)



(v)



(vi)

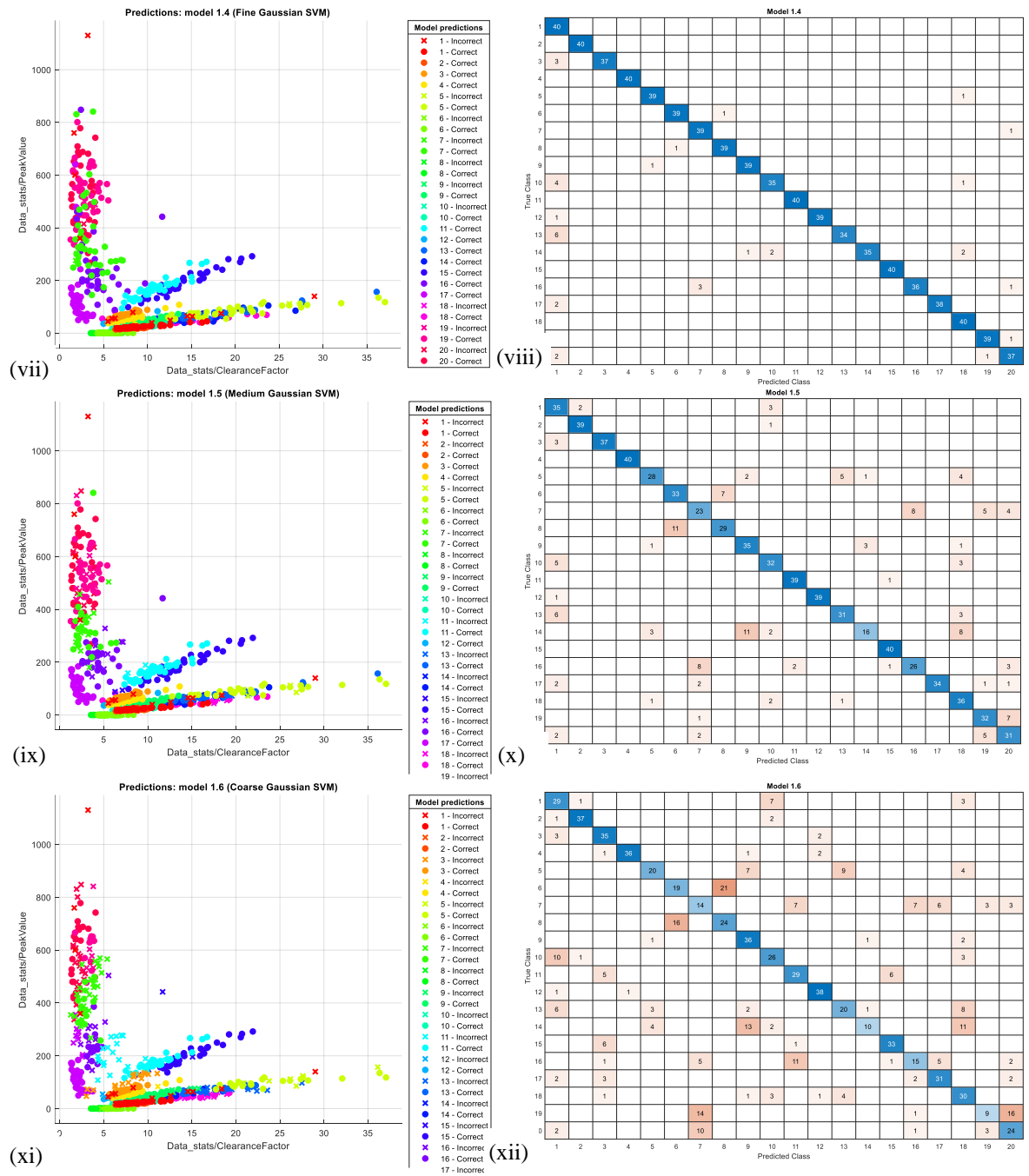


Figure 7.10 Fault classification by SVM model for top 10 features of KW test (i) SP linear kernel (ii) CM for linear kernel (iii) SP quadratic kernel (iv) CM quadratic kernel (v) SP for cubic kernel (vi) CM for cubic kernel (vii) SP for fine kernel (viii) CM for fine kernel (ix) SP for medium kernel (x) CM for medium kernel (xi) SP for coarse kernel (xii) CP for coarse kernel

Table 7.4 Performance metrics of ML models with and without using feature ranking for test data

Performance Metrics	ML Model	Without features ranking (All Features)	With features ranking			
			One-way ANOVA		Kruskal-Wallis test	
			Top 5 features	Top 10 features	Top 5 features	Top 10 features
Classification Accuracy (%)	Linear	69.8	70.9	75.4	69.0	79.0
	Quadratic	80.9	76.4	86.6	75.0	86.6
	Cubic	79.5	83.5	92.2	83.6	92.9
	Fine	60.1	92.5	96.8	85.9	97.6
	Medium	77.5	75.5	80.5	71.0	81.9
	Coarse	56.0	60.5	61.8	60.0	64.4
Training Time (sec)	Linear	8.80	1.47	1.45	1.80	1.26
	Quadratic	7.91	1.19	1.14	1.59	1.04
	Cubic	8.20	1.61	1.24	2.01	1.23
	Fine	8.04	1.20	1.36	1.29	1.35
	Medium	7.89	1.16	1.29	1.23	1.22
	Coarse	8.38	1.29	1.21	1.36	1.20
Prediction Speed (Obs/Sec)	Linear	2300	14000	13000	12000	9200
	Quadratic	1900	10000	10000	9700	10000
	Cubic	1800	11000	10000	10000	10000
	Fine	1800	9200	8600	9200	8800
	Medium	1800	10000	9700	9900	9400
	Coarse	1800	9900	9200	8600	9200

For the SVM classifier fine kernel with five feature selection options: all features (no ranking), top five features ranked by the Ow-A test, top five features ranked by the KW test, top ten features ranked by the Ow-A, top ten features ranked by the KW test, The classification accuracies that were attained are, in order, 60.1%, 92.5.5%, 85.9%, 96.8%, and 97.6%. The SVM model enhances maximum classification accuracy using the top 10 characteristics identified by the Kruskal–Wallis test. The top 10 features of the KW test outperform Ow-A well due to its high classification accuracy and reduced training time for all kernels.

The comparative efficacy of machine learning models employing various feature selection methodologies is illustrated through Classification Accuracy (CA), Training Time (TT), and Prediction Speed (PS) in Figs. 7.11, 7.12, and 7.13, utilising bar charts. The principal criterion for selecting the optimal model or feature selection method is CA. TT and PS also contribute to identifying the best model when accuracy values are comparable.

Figure 7.11 demonstrates that the Classification Accuracy reaches its peak for all SVM kernels for top 10 features, ranked by the KW test. However, an exception exists in the case of the Quadratic kernel. The maximum accuracy is 86.6%, which remains consistent whether evaluating the top 10 features from the KW test, utilising the top 10 features ranked by Ow-A and incorporating all features to train the classifier. Consequently, accuracy alone is inadequate as a criterion for the SVM to determine the optimal feature selection strategy. Consequently, TT is utilised to evaluate the outcomes. The training durations for the classifier are 1.04 s, 1.14 s, and 7.19 s in the three situations, as illustrated in Fig. 7.12. Again, KW test enhance the efficiency of classifier training, suggesting that this method is ideal for the quadratic kernel.

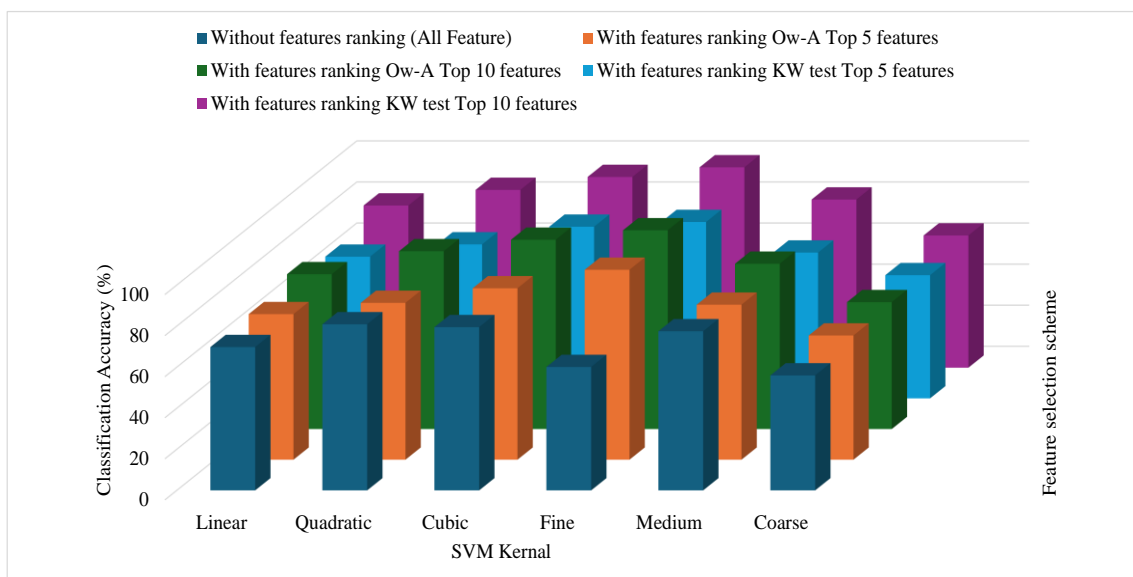


Figure 7.11 Influence of feature ranking on classification accuracy of SVM models with different kernels

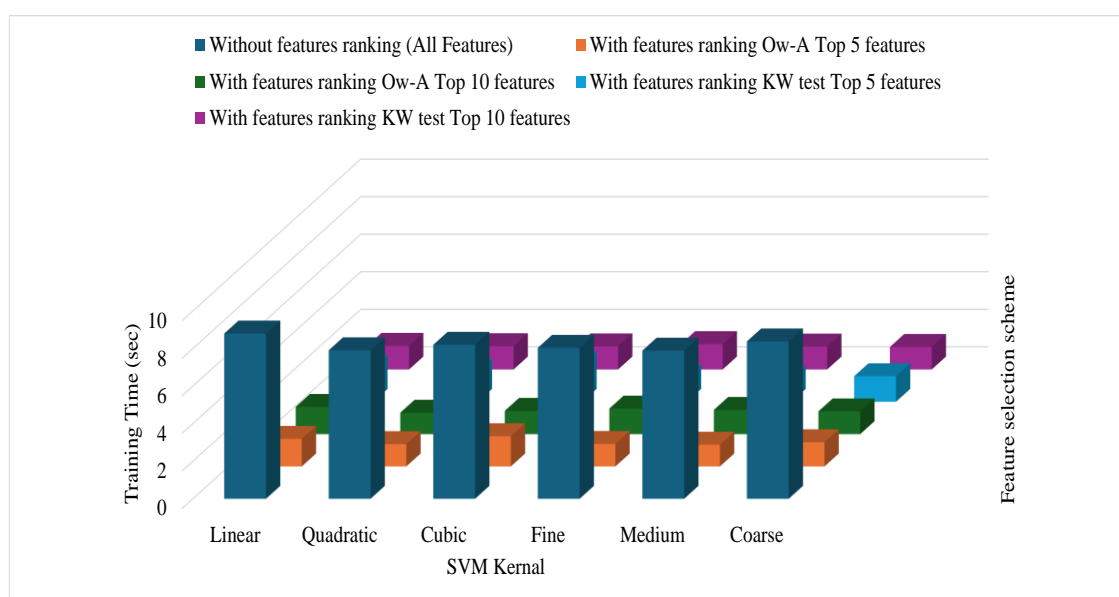


Figure 7.12 Influence of feature ranking on training time of SVM models with different kernels

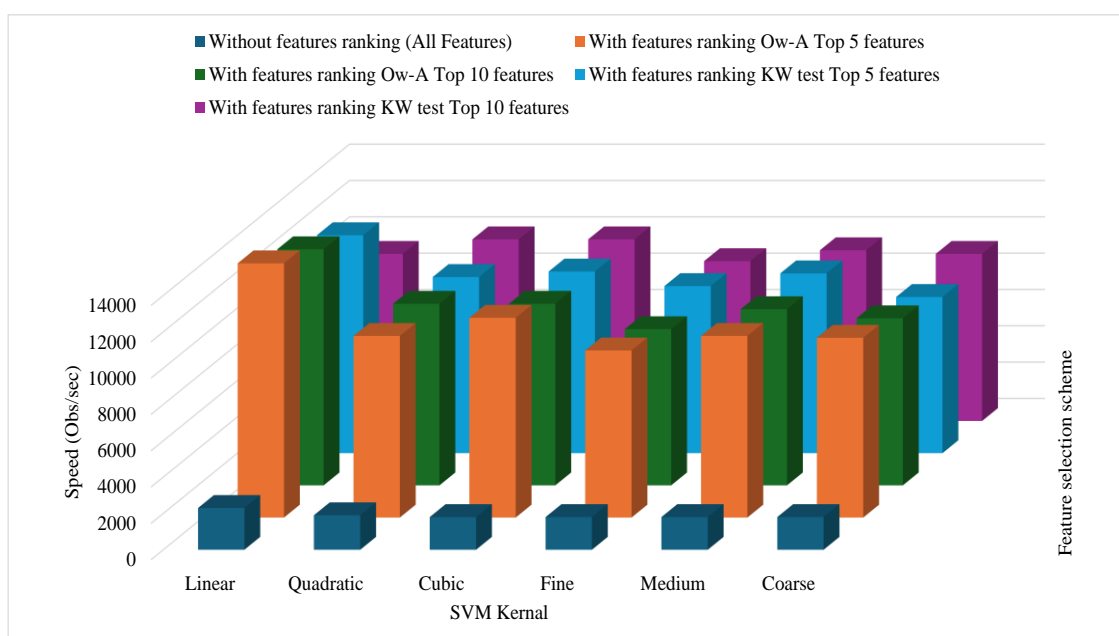


Figure 7.13 Influence of feature ranking on speed of SVM models with different kernels

Figure 7.13 illustrates the PS of the classifiers measured in observations per second. A comparison of prediction speed is emphasised to reinforce the results of the quadratic classifier. The respective numbers for the previously mentioned examples are 10,000 Obs/Sec, 10,000 Obs/Sec, and 1900 Obs/Sec. Although the top 10 features of both

OwA and KW tests are identical, the maximum values support the top 10 feature selection methodology of the KW test, in conjunction with Classification Accuracy and Training Time.

7.8 Summary of the Chapter

This study aims to examine the impact of feature ranking by Ow-A and the KW test on the training of several machine learning models for the classification of bearing defects utilising test datasets. These methods are extensively employed in applications including text sorting, cancer prediction and many more; Yet the existing literature on fault diagnosis of rolling element bearings rarely recognises their significance. The solutions presented in the literature exhibited specific limitations; therefore, evaluating the proposed procedures to ascertain their efficacy in the specified domain compared to those previously utilised was essential. This constitutes the principal contribution of the present study. SVM classifiers utilising different kernels are first trained on the complete set of features (without any feature ranking), and subsequently, training is conducted with the top five and top ten features chosen through both ranking methodologies. A thorough assessment of model performance is performed, focussing on Classification Accuracy, Training Time, and Prediction Speed, both with and without feature ranking.

The highest accuracy in defect classification is attained using the best 10 features ranked by the Kruskal–Wallis test across all classifiers. The accuracies achieved are 79.0%, 86.6%, 92.9%, 97.6%, 81.9%, and 64.4% for linear, quadratic, cubic, fine, medium, and coarse models, respectively, using the test dataset. The Kruskal–Wallis test surpasses the One-way ANOVA. Nonetheless, there exists a singular exception concerning the SVM quadratic kernel. Upon assessing the top 10 characteristics of the KW test and identifying the top 10 features as determined by Ow-A, the maximum accuracy achieved is consistently 86.6% in both instances. The minimum Training Time of 1.04 s for the top 10 features identified by the KW test indicates that this scheme is optimal for the quadratic kernel, indicating that out of all the models examined, this feature selection approach yields the best results.

Chapter 8 Conclusions, Future Scope and Implications

This concluding chapter encapsulates the essential findings and contributions of the study centred on the experimental and computational examination of tapered roller bearing (TRB) systems. The results of the damping analysis, fault detection experiments, and the diagnostic framework based on machine learning are emphasised. This chapter delineates prospective avenues for further investigation. The study also addresses the industrial implications, highlighting how dependable bearing diagnostics can improve machine safety, lower maintenance expenses, and support sustainable engineering initiatives.

8.1 Contributions of the Work

The summary of the thesis as follows

This experimental framework that has been meticulously crafted to enable the exploration of rotor bearing systems across a range of operating and fault conditions. The test rig was designed with versatility in mind, allowing for various types of analyses, such as damping behaviour and fault diagnostics. Essential elements including the shaft, bearing housing, drive motor, loading mechanisms, and data acquisition systems were meticulously chosen and assembled to guarantee dependable performance and consistent measurements. Distinct configurations were examined for damping tests and fault analysis to guarantee that each goal could be achieved without sacrificing precision.

The damping analysis of four antifriction bearings has uncovered significant variations in their capacity to dissipate vibrational energy. This study discusses the effect of damping for tapered, cylindrical, spherical and self-aligned bearings. Experimental damping ratios are obtained using FRF measurements and a free decay curve under static conditions, and dynamic testing further confirmed these findings at operational speeds and found that tapered roller bearing performs better in terms of damping.

A detailed vibration and noise analysis of a healthy tapered roller bearing (TRB) employing the Taguchi method. The experimental study aimed to assess the impact of

critical process parameters—namely load, speed, and lubrication condition—on the root mean square (RMS) vibration values and equivalent continuous noise level (Leq). The Taguchi design of experiments was utilised to effectively identify the impact of each parameter and their optimal combination with a reduced number of trials.

The effects of different fault types—outer race, inner race, roller element, and compound faults—on the vibration characteristics of tapered roller bearings (TRBs) are also examined. Identical dimensions of controlled faults were introduced into the bearings, and vibration signals were recorded under consistent operating conditions to ensure comparability. A comprehensive factorial analysis was conducted to methodically assess the impact of fault types and operational parameters, including load and speed. The statistical analysis revealed that the type of fault is the primary factor influencing the vibration response, with interaction effects related to load and speed following closely behind.

Finally, the creation of an automated framework aimed at detecting and classifying faults in tapered roller bearing (TRB) systems through the application of machine learning techniques are outlined. The data on vibration gathered from experimental tests underwent preprocessing, and pertinent statistical and time, frequency-domain features were extracted to create the input dataset. A variety of supervised learning algorithms were developed and assessed to categorise bearing conditions, such as healthy, outer race fault, inner race fault, roller defect, and compound faults. The findings indicate that the integration of machine learning with efficient signal processing and feature engineering offers a strong and scalable method for diagnosing bearing faults intelligently. The proposed framework establishes a foundation for the implementation of real-time condition monitoring systems and aligns with the overarching objective of predictive maintenance in rotating machinery.

8.2 Conclusions

The conclusions of the present research work:

- The damping ratios obtained from FRF and free decay methods seem relatively consistent across DE and NDE for each bearing type. These two methods are in good agreement with each other.
- Tapered roller bearing has a high decay rate, which means a higher damping ratio, followed by cylindrical, spherical and self-aligned bearings. Experimental findings also show that ball bearings have less damping than roller bearings. The reason may be their smaller contact surface and reduced internal friction.
- Based on the analysis of variance, it has been seen that speed is the most significant factor affecting vibration RMS and noise Leq. Taguchi's method confirms that the RMS and Leq of the tapered bearing rise with an increase in speed. It is discovered that RMS and Leq initially increase with an increase in load and then decrease.
- Response surface in RMS at DE and NDE shows similar features but in a different magnitude. Leq also shows similar characteristics for DE and NDE but in a different magnitude.
- Based on the ANOVA, it has been observed that the interaction of load and fault is the most significant factor affecting vibration RMS which contributes 46.89% followed by the linear effect of load (25.25%), speed (18.27%) and fault (6.07%).
- Based on the analysis of variance, it has been seen that the interaction of load is the most significant factor affecting noise (Leq) which contributes 41.65%.
- For RMS value, the increase in speed results in an increase in RMS value of vibration. Also, RMS value is mostly affected by OR fault followed by IR, Roller and healthy bearing.
- In the context of Leq noise measurements, it has been shown that a rise in speed leads to a corresponding increase in noise levels. Also, Leq value is mostly affected by Roller fault followed by OR, IR and healthy bearing.

- A slight fluctuation in the kurtosis value is seen at lower speeds; however, at higher speeds, the kurtosis metric remains quite stable. Kurtosis also becomes less sensitive to load.
- The Kruskal–Wallis test surpasses the One-way ANOVA and achieve higher accuracy in all cases.
- The SVM employing fine kernel classifiers has the highest classification accuracy of 97.6% when trained with the top 10 characteristics identified by the Kruskal–Wallis test.
- As an extension, the current approach will be compared with deep learning-based methods such as CNNs and autoencoders to evaluate trade-offs in accuracy, interpretability, and computational cost.

8.3 Future Scope of Work

- In real-world applications, bearings often experience multiple types of damage simultaneously, which can lead to more complex failure behaviour. Experiments that combine multiple damages on a single element to study their cumulative effects on bearing performance. Second is the fault of varying dimensions in the same element.
- The performance of the proposed feature set for automated fault classification can further be examined with natural spalls of more variability.
- The correlation between rotation speed, temperature variations, lubricant viscosity, and bearing damping has not been worked out. The same may be considered in future research.
- The damping study is based on the first harmonics. So, the approach demonstrated in the present study can be extended to investigate higher modes if desired.

8.4 Implication of Work

The findings of this study are of considerable importance to both society and industry, especially in improving the safety, reliability, and sustainability of machinery and mechanical systems that play a crucial role in everyday life. Tapered roller bearings find extensive application across various sectors, including transportation (such as automotive and railways), heavy machinery, energy systems, and manufacturing industries. Unforeseen bearing failures in these contexts may result in equipment malfunctions, production setbacks, heightened maintenance expenses, and, in certain instances, safety risks.

This work establishes an experimental and computational framework aimed at early fault detection and condition monitoring of tapered roller bearings, contributing to:

Improved Machinery Safety: Identifying faults at an early stage can avert disastrous failures, thus minimising the likelihood of accidents and promoting safer working conditions in both industrial and transportation fields.

Cost-Effective Maintenance: This study's implementation of predictive maintenance strategies can greatly reduce maintenance costs by minimising unplanned downtime and preventing unnecessary part replacements.

Energy Efficiency and Sustainability: Defective bearings frequently result in heightened friction and greater energy usage. Prompt detection and correction of issues enhance the overall performance of machinery, leading to energy conservation and promoting environmental sustainability.

Skill Development and Technological Advancement: This study also encourages the incorporation of cutting-edge technologies like machine learning into conventional mechanical engineering fields, enhancing interdisciplinary understanding and skill development for the future workforce.

REFERENCES

1. Harris TA, Anderson WJ (1967) Rolling Bearing Analysis: Advanced Concepts of Bearing Technology
2. Mufazzal S, Muzakkir SM, Khanam S (2022) Enhancing the Classification Performance of Machine Learning Techniques by Using Hjorth's and Other Statistical Parameters for Precise Tracking of Naturally Evolving Faults in Ball Bearings. *International Journal of Acoustics and Vibrations* 27:138–150. <https://doi.org/10.20855/ijav.2022.27.21847>
3. Bearing Market Size, Share & Growth Analysis Report, 2030. <https://www.grandviewresearch.com/industry-analysis/bearings-market>. Accessed 7 Feb 2025
4. Rail Inquiry 07-114 Derailment caused by a wheel-bearing failure, Huntly, 19 October 2007. Accessed 13 Jun 2025
5. Plane left Leeds Bradford runway due to failed bearing. <https://www.bbc.com/news/articles/cvg0d72n42wo>. Accessed 13 Jun 2025
6. Adams ML (2001) Rotating Machinery Vibration From Analysis To Troubleshooting
7. Kumar R, Singh M (2013) Outer race defect width measurement in taper roller bearing using discrete wavelet transform of vibration signal. *Measurement (Lond)* 46:537–545. <https://doi.org/10.1016/j.measurement.2012.08.012>
8. Harris TA, Kotzalas MN (2006) Rolling Bearing Analysis: Essential Concepts of Bearing Technology
9. Randall RB (2013) Vibration-based condition monitoring
10. Isermann R (2006) Fault-Diagnosis Systems
11. Harris TA Rolling Bearing Analysis

12. Dolenc B, Boškoski P, Juričić D (2016) Distributed bearing fault diagnosis based on vibration analysis. *Mech Syst Signal Process* 66–67:521–532. <https://doi.org/10.1016/J.YMSSP.2015.06.007>
13. How to understand ISO 15243 | Evolution. <https://evolution.skf.com/bearing-damage-analysis-iso-15243-is-here-to-help-you/#>. Accessed 13 Jun 2025
14. Randall RB, Antoni J (2011) Rolling element bearing diagnostics-A tutorial. *Mech Syst Signal Process* 25:485–520. <https://doi.org/10.1016/j.ymssp.2010.07.017>
15. Rai A, Upadhyay SH (2016) A review on signal processing techniques utilized in the fault diagnosis of rolling element bearings. *Tribol Int* 96:289–306. <https://doi.org/10.1016/j.triboint.2015.12.037>
16. Mohanty AR (2014) Machinery Condition Monitoring: Principles and Practices. *Machinery Condition Monitoring*. <https://doi.org/10.1201/9781351228626>
17. Rao SS., Griffin Philip (2018) Mechanical vibrations. 1147
18. Kankar PK, Sharma SC, Harsha SP (2011) Fault diagnosis of ball bearings using machine learning methods. *Expert Syst Appl* 38:1876–1886. <https://doi.org/10.1016/J.ESWA.2010.07.119>
19. Tandon N, Choudhury A (1999) A review of vibration and acoustic measurement methods for the detection of defects in rolling element bearings. *Tribol Int* 32:469–480. [https://doi.org/10.1016/S0301-679X\(99\)00077-8](https://doi.org/10.1016/S0301-679X(99)00077-8)
20. Mathew J, Alfredson RJ (1984) The condition monitoring of rolling element bearings using vibration analysis. *Journal of Vibration and Acoustics-transactions of The Asme* 106:447–453. <https://doi.org/10.1115/1.3269216>
21. Li Q, Wang W, Chu F (2019) Damping ratio identification in rotordynamic system with inverse directional Fourier transform, multiple-tests-multiple-outputs and clustering techniques. *Int J Mech Sci* 151:797–807. <https://doi.org/10.1016/J.IJMECSCI.2018.12.020>

22. Gregory RW, Harris SL, R. G. Munro G (1963) Dynamic Behaviour of Spur Gears. *Proceedings of the Institution of Mechanical Engineers* 178:207–218. <https://doi.org/10.1177/002034836317800130>
23. Hu X, Zhou C (2022) Dynamic analysis and experiment of Quasi-zero-stiffness system with nonlinear hysteretic damping. *Nonlinear Dyn* 107:2153–2175. <https://doi.org/10.1007/S11071-021-07136-1/FIGURES/21>
24. Brodzinski R, B. J. Stone. (1985) The Significance of Joints on the Stiffness and Damping of Rolling Element Bearings. *Proceedings of the 3rd International Modal Analysis Conference* 28–31
25. Tiwari R, Vyas NS (1995) Estimation of non-linear stiffness parameters of rolling element bearings from random response of rotor-bearing systems. *J Sound Vib* 187:229–239. <https://doi.org/10.1006/JSVI.1995.0517>
26. Tasker F, Chopra I (2012) Nonlinear damping estimation from rotor stability data using time and frequency domain techniques. *AIAA Journal* 30:1383–1391. <https://doi.org/10.2514/3.11074>
27. Chen SY, Ju MS, Tsuei YG (1996) Estimation of Mass, Stiffness and Damping Matrices from Frequency Response Functions. *J Vib Acoust* 118:78–82. <https://doi.org/10.1115/1.2889638>
28. Béliveau JG (1976) Identification of Viscous Damping in Structures From Modal Information. *J Appl Mech* 43:335–339. <https://doi.org/10.1115/1.3423835>
29. Arora V (2014) Structural damping identification method using normal FRFs. *Int J Solids Struct* 51:133–143. <https://doi.org/10.1016/J.IJSOLSTR.2013.09.017>
30. Naeim F (2007) *Dynamics of Structures—Theory and Applications to Earthquake Engineering*, Third Edition. *Earthquake Spectra* 23:491–492. <https://doi.org/10.1193/1.2720354>

31. Wang I (2011) An analysis of higher order effects in the half power method for calculating damping. *Journal of Applied Mechanics, Transactions ASME* 78:0145011–0145013. <https://doi.org/10.1115/1.4002208/465690>
32. Staszewski WJ (1998) Identification of non-linear systems using multi-scale ridges and skeletons of the wavelet transform. *J Sound Vib* 214:639–658. <https://doi.org/10.1006/JSVI.1998.1616>
33. Ta MN, Lardis J (2006) Identification of weak nonlinearities on damping and stiffness by the continuous wavelet transform. *J Sound Vib* 293:16–37. <https://doi.org/10.1016/J.JSV.2005.09.021>
34. Chandra NH, Sekhar AS (2016) Nonlinear damping identification in rotors using wavelet transform. *Mech Mach Theory* 100:170–183. <https://doi.org/10.1016/J.MECHMACHTHEORY.2016.02.007>
35. Huynh HN, Altintas Y (2022) Multibody dynamic modeling of five-axis machine tool vibrations and controller. *CIRP Annals* 71:325–328. <https://doi.org/10.1016/J.CIRP.2022.04.003>
36. Dietl P, Wensing J, Van Nijen GC (2005) Rolling bearing damping for dynamic analysis of multi-body systems—experimental and theoretical results. *Proceedings of the Institution of Mechanical Engineers, Part K: Journal of Multi-body Dynamics* 214:33–43. <https://doi.org/10.1243/1464419001544124>
37. Suryawanshi GL, Patil SK, Desavale RG, Suryawanshi GL, Patil SK, Desavale RG (2024) Empirical-based DA and ANN to diagnose misalignment in rotor-bearing system. *NTE* 39:776–801. <https://doi.org/10.1080/10589759.2023.2228979>
38. Holm-Hansen BT, Gao RX (2000) Vibration analysis of a sensor-integrated ball bearing. *Journal of Vibration and Acoustics, Transactions of the ASME* 122:384–392. <https://doi.org/10.1115/1.1285943>
39. Gao RX, Yan R, Sheng S, Zhang L (2006) Sensor Placement and Signal Processing for Bearing Condition Monitoring. *Condition Monitoring and*

- Control for Intelligent Manufacturing 167–191. https://doi.org/10.1007/1-84628-269-1_7
40. Cao H, Niu L, Xi S, Chen X (2018) Mechanical model development of rolling bearing-rotor systems: A review. *Mech Syst Signal Process* 102:37–58. <https://doi.org/10.1016/j.ymssp.2017.09.023>
 41. Shah DS, Patel VN (2014) A Review of Dynamic Modeling and Fault Identifications Methods for Rolling Element Bearing. *Procedia Technology* 14:447–456. <https://doi.org/10.1016/j.protcy.2014.08.057>
 42. McFadden PD, Smith JD (1984) Model for the vibration produced by a single point defect in a rolling element bearing. *J Sound Vib* 96:69–82. [https://doi.org/10.1016/0022-460X\(84\)90595-9](https://doi.org/10.1016/0022-460X(84)90595-9)
 43. McFadden PD, Smith JD (1985) The vibration produced by multiple point defects in a rolling element bearing. *J Sound Vib* 98:263–273. [https://doi.org/10.1016/0022-460X\(85\)90390-6](https://doi.org/10.1016/0022-460X(85)90390-6)
 44. Tandon N, Choudhury A (1999) Review of vibration and acoustic measurement methods for the detection of defects in rolling element bearings. *Tribol Int* 32:469–480. [https://doi.org/10.1016/S0301-679X\(99\)00077-8](https://doi.org/10.1016/S0301-679X(99)00077-8)
 45. Lostado-Lorza R, Escribano-Garcia R, Fernandez-Martinez R, Illera-cueva M, Mac Donald BJ (2017) Using the finite element method and data mining techniques as an alternative method to determine the maximum load capacity in tapered roller bearings. *Journal of Applied Logic* 24:4–14. <https://doi.org/10.1016/j.jal.2016.11.009>
 46. Harsha SP (2006) Nonlinear dynamic response of a balanced rotor supported by rolling element bearings due to radial internal clearance effect. *Mech Mach Theory* 41:688–706. <https://doi.org/10.1016/j.mechmachtheory.2005.09.003>
 47. Niu L, Cao H, He Z, Li Y (2015) A systematic study of ball passing frequencies based on dynamic modeling of rolling ball bearings with localized surface defects. *J Sound Vib* 357:207–232. <https://doi.org/10.1016/j.jsv.2015.08.002>

48. Mishra C, Samantaray AK, Chakraborty G (2017) Rolling element bearing fault diagnosis under slow speed operation using wavelet de-noising. *Measurement (Lond)* 103:77–86. <https://doi.org/10.1016/j.measurement.2017.02.033>
49. Antoni J, Randall RB (2006) The spectral kurtosis: Application to the vibratory surveillance and diagnostics of rotating machines. *Mech Syst Signal Process* 20:308–331. <https://doi.org/10.1016/j.ymssp.2004.09.002>
50. Nataraj C, Harsha SP (2008) The effect of bearing cage run-out on the nonlinear dynamics of a rotating shaft. *Commun Nonlinear Sci Numer Simul* 13:822–838. <https://doi.org/10.1016/j.cnsns.2006.07.010>
51. Khanam S, Dutt JK, Tandon N (2015) Impact Force Based Model for Bearing Local Fault Identification. *J Vib Acoust* 137:051002. <https://doi.org/10.1115/1.4029988>
52. Yang L, Xu T, Xu H, Wu Y (2018) Mechanical behavior of double-row tapered roller bearing under combined external loads and angular misalignment. *Int J Mech Sci* 142–143:561–574. <https://doi.org/10.1016/j.ijmecsci.2018.04.056>
53. Tyagi CS (2008) A Comparative Study of SVM Classifiers and Artificial Neural Networks Application for Rolling Element Bearing Fault Diagnosis using Wavelet Transform Preprocessing. 2:904–912
54. Goyal D, Pabla • B S, Dhami • S S, Lachhwani • Kailash Optimization of condition-based maintenance using soft computing. *Neural Comput Appl* 28:. <https://doi.org/10.1007/s00521-016-2377-6>
55. Li B, Li C, Liu J (2023) Incipient detection of bearing fault using impulse feature enhanced weighted sparse representation. *Tribol Int* 184:108467. <https://doi.org/10.1016/J.TRIBOINT.2023.108467>
56. Martin G, Becker FM, Kirchner E (2022) A novel method for diagnosing rolling bearing surface damage by electric impedance analysis. *Tribol Int* 170:107503. <https://doi.org/10.1016/J.TRIBOINT.2022.107503>

57. Rai VK, Mohanty AR (2007) Bearing fault diagnosis using FFT of intrinsic mode functions in Hilbert–Huang transform. *Mech Syst Signal Process* 21:2607–2615. <https://doi.org/10.1016/J.YMSSP.2006.12.004>
58. Shi DF, Wang WJ, Qu LS (2004) Defect Detection for Bearings Using Envelope Spectra of Wavelet Transform. *J Vib Acoust* 126:567–573. <https://doi.org/10.1115/1.1804995>
59. Cao H, Fan F, Zhou K, He Z (2016) Wheel-bearing fault diagnosis of trains using empirical wavelet transform. *Measurement (Lond)* 82:439–449. <https://doi.org/10.1016/j.measurement.2016.01.023>
60. Singh GK, Al Kazzaz SAS (2009) Isolation and identification of dry bearing faults in induction machine using wavelet transform. *Tribol Int* 42:849–861. <https://doi.org/10.1016/J.TRIBOINT.2008.11.008>
61. El-Thalji I, Jantunen E (2015) A summary of fault modelling and predictive health monitoring of rolling element bearings. *Mech Syst Signal Process* 60–61:252–272. <https://doi.org/10.1016/J.YMSSP.2015.02.008>
62. Ocak H, Loparo KA (2005) HMM-Based Fault Detection and Diagnosis Scheme for Rolling Element Bearings. *J Vib Acoust* 127:299–306. <https://doi.org/10.1115/1.1924636>
63. Gunerkar RS, Jalan AK, Belgamwar SU (2019) Fault diagnosis of rolling element bearing based on artificial neural network. *Journal of Mechanical Science and Technology* 2019 33:2 33:505–511. <https://doi.org/10.1007/S12206-019-0103-X>
64. Yu Y, YuDejie, Junsheng C (2006) A roller bearing fault diagnosis method based on EMD energy entropy and ANN. *J Sound Vib* 294:269–277. <https://doi.org/10.1016/J.JSV.2005.11.002>
65. Al-Raheem KF, Roy A, Ramachandran KP, Harrison DK, Grainger S (2008) Application of the Laplace wavelet combined with ANN for rolling bearing fault diagnosis. *Journal of Vibration and Acoustics, Transactions of the ASME* 130:. <https://doi.org/10.1115/1.2948399/438837>

66. Chow MY, Yee SO, Mangum PM (1991) A Neural Network Approach to Real-Time Condition Monitoring of Induction Motors. *IEEE Transactions on Industrial Electronics* 38:448–453. <https://doi.org/10.1109/41.107100>
67. Samanta B, Al-Balushi KR (2003) Artificial neural network based fault diagnostics of rolling element bearings using time-domain features. *Mech Syst Signal Process* 17:317–328. <https://doi.org/10.1006/MSSP.2001.1462>
68. Uhrig RE, Loskiewicz-Buczak A (1993) Monitoring and Diagnosis of Rolling Element Bearings Using Artificial Neural Networks. *IEEE Transactions on Industrial Electronics* 40:209–217. <https://doi.org/10.1109/41.222642>
69. Samanta B, Al-Balushi KR, Al-Araimi SA (2003) Artificial neural networks and support vector machines with genetic algorithm for bearing fault detection. *Eng Appl Artif Intell* 16:657–665. <https://doi.org/10.1016/J.ENGAPPAL.2003.09.006>
70. Sugumaran V, Muralidharan V, Ramachandran KI (2007) Feature selection using Decision Tree and classification through Proximal Support Vector Machine for fault diagnostics of roller bearing. *Mech Syst Signal Process* 21:930–942. <https://doi.org/10.1016/J.YMSSP.2006.05.004>
71. Widodo A, Yang BS (2007) Support vector machine in machine condition monitoring and fault diagnosis. *Mech Syst Signal Process* 21:2560–2574. <https://doi.org/10.1016/J.YMSSP.2006.12.007>
72. Lei Y, He Z, Zi Y, Hu Q (2007) Fault diagnosis of rotating machinery based on multiple ANFIS combination with GAs. *Mech Syst Signal Process* 21:2280–2294. <https://doi.org/10.1016/j.ymssp.2006.11.003>
73. Jalan AK, Mohanty AR (2009) Model based fault diagnosis of a rotor-bearing system for misalignment and unbalance under steady-state condition. *J Sound Vib* 327:604–622. <https://doi.org/10.1016/j.jsv.2009.07.014>
74. Gunerkar RS, Jalan AK (2019) Classification of Ball Bearing Faults Using Vibro-Acoustic Sensor Data Fusion. *Experimental Techniques* 2019 43:543:635–643. <https://doi.org/10.1007/S40799-019-00324-0>

75. Wang WQ, Golnaraghi MF, Ismail F (2004) Prognosis of machine health condition using neuro-fuzzy systems. *Mech Syst Signal Process* 18:813–831. [https://doi.org/10.1016/S0888-3270\(03\)00079-7](https://doi.org/10.1016/S0888-3270(03)00079-7)
76. Lou X, Loparo KA (2004) Bearing fault diagnosis based on wavelet transform and fuzzy inference. *Mech Syst Signal Process* 18:1077–1095. [https://doi.org/10.1016/S0888-3270\(03\)00077-3](https://doi.org/10.1016/S0888-3270(03)00077-3)
77. Zhang L, Xiong G, Liu H, Zou H, Guo W (2010) Bearing fault diagnosis using multi-scale entropy and adaptive neuro-fuzzy inference. *Expert Syst Appl* 37:6077–6085. <https://doi.org/10.1016/J.ESWA.2010.02.118>
78. Chen J, Randall RB (2016) Intelligent diagnosis of bearing knock faults in internal combustion engines using vibration simulation. *Mech Mach Theory* 104:161–176. <https://doi.org/10.1016/J.MECHMACHTHEORY.2016.05.022>
79. Myers, Raymond H., Douglas C. Montgomery and CMA-Cook (2016) *Response surface methodology: process and product optimization using designed experiments*. John Wiley & Sons.
80. Mishra HP, Jalan A (2021) Analysis of faults in rotor-bearing system using three-level full factorial design and response surface methodology. *Noise and Vibration Worldwide* 52:365–376. <https://doi.org/10.1177/09574565211030711>
81. Patil MS, Mathew J, Rajendrakumar PK, Karade S (2010) Experimental studies using response surface methodology for condition monitoring of ball bearings. *J Tribol* 132:1–6. <https://doi.org/10.1115/1.4002520>
82. Kankar PK, Sharma SC, Harsha SP (2011) Fault diagnosis of high speed rolling element bearings due to localized defects using response surface method. *Journal of Dynamic Systems, Measurement and Control, Transactions of the ASME* 133:1–14. <https://doi.org/10.1115/1.4003371>
83. Goyal D, Vanraj, Pabla BS, Dharmi SS (2019) Non-contact sensor placement strategy for condition monitoring of rotating machine-elements. *Engineering*

- Science and Technology, an International Journal 22:489–501. <https://doi.org/10.1016/j.jestch.2018.12.006>
84. Patil MS, Mathew J, Rajendrakumar PK, Karade S (2010) Experimental studies using response surface methodology for condition monitoring of ball bearings. *J Tribol* 132:. <https://doi.org/10.1115/1.4002520/468763>
 85. Kankar PK, Sharma SC, Harsha SP (2011) Fault diagnosis of high speed rolling element bearings due to localized defects using response surface method. *Journal of Dynamic Systems, Measurement and Control, Transactions of the ASME* 133:. <https://doi.org/10.1115/1.4003371/456398>
 86. Kumar R, Singh M (2013) Outer race defect width measurement in taper roller bearing using discrete wavelet transform of vibration signal. *Measurement (Lond)* 46:537–545. <https://doi.org/10.1016/j.measurement.2012.08.012>
 87. Hemmati F, And MA, Gadala1 MS (2015) Optimized statistical parameters of acoustic emission signals for monitoring of rolling element bearings. *Proceedings of the Institution of Mechanical Engineers, Part J: Journal of Engineering Tribology*, 230(8), 897–906 | 10.1177/135065011561961. In: *Proc IMechE Part J: J Engineering Tribology*. Accessed 30 Sep 2022
 88. Cao H, Fan F, Zhou K, He Z (2016) Wheel-bearing fault diagnosis of trains using empirical wavelet transform. *Measurement* 82:439–449. <https://doi.org/10.1016/J.MEASUREMENT.2016.01.023>
 89. Immovilli F, Cocconcelli M (2017) Experimental Investigation of Shaft Radial Load Effect on Bearing Fault Signatures Detection. *IEEE Trans Ind Appl* 53:2721–2729. <https://doi.org/10.1109/TIA.2016.2633236>
 90. Liu J, Shao Y, Qin X (2017) Dynamic simulation for a tapered roller bearing considering a localized surface fault on the rib of the inner race. *Proceedings of the Institution of Mechanical Engineers, Part K: Journal of Multi-body Dynamics* 231:670–683. <https://doi.org/10.1177/1464419317695171>

91. Mishra C, Samantaray AK, Chakraborty G (2017) Rolling element bearing fault diagnosis under slow speed operation using wavelet de-noising. *Measurement* 103:77–86. <https://doi.org/10.1016/J.MEASUREMENT.2017.02.033>
92. He Q, Wu E, Pan Y (2018) Multi-Scale Stochastic Resonance Spectrogram for fault diagnosis of rolling element bearings. *J Sound Vib* 420:174–184. <https://doi.org/10.1016/J.JSV.2018.01.001>
93. Khadersab A, Shivakumar S (2018) Vibration Analysis Techniques for Rotating Machinery and its effect on Bearing Faults. *Procedia Manuf* 20:247–252. <https://doi.org/10.1016/J.PROMFG.2018.02.036>
94. Yi C, Wang D, Fan W, Tsui KL, Lin J (2018) EEMD-Based Steady-State Indexes and Their Applications to Condition Monitoring and Fault Diagnosis of Railway Axle Bearings. *Sensors* 2018, Vol 18, Page 704 18:704. <https://doi.org/10.3390/S18030704>
95. Gunerkar RS, Jalan AK (2019) Classification of Ball Bearing Faults Using Vibro-Acoustic Sensor Data Fusion. *Exp Tech* 43:635–643. <https://doi.org/10.1007/s40799-019-00324-0>
96. Gunerkar RS, Jalan AK, Belgamwar SU (2019) Fault diagnosis of rolling element bearing based on artificial neural network. *Journal of Mechanical Science and Technology* 33:505–511. <https://doi.org/10.1007/s12206-019-0103-x>
97. Kumar A, Kumar R (2013) Adaptive wavelet based signal processing scheme for detecting localized defects in rolling element of taper roller bearing. *Surveillance* 7 1–9
98. Li Y, Cheng G, Liu C (2021) Research on bearing fault diagnosis based on spectrum characteristics under strong noise interference. *Measurement* 169:108509. <https://doi.org/10.1016/J.MEASUREMENT.2020.108509>
99. Hong X, Duan L, Zhang - L, Zeng Y, Liu R, Liu - X, Liu C, Tong J, Zheng J, Pan H, Bao J (2022) Rolling bearing fault diagnosis method based on multi-

- sensor two-stage fusion. *Meas Sci Technol* 33:125105. <https://doi.org/10.1088/1361-6501/AC8894>
100. Wu X, Qin Y, Luo J, Wang S, Chen B (2022) Fault dynamic model of high-speed rolling bearing by a compound displacement excitation function considering the effect of defect roughness. *Mech Mach Theory* 177:. <https://doi.org/10.1016/j.mechmachtheory.2022.105061>
 101. Dias AL, Turcato AC, Sestito GS, Brandao D, Nicoletti R (2021) A cloud-based condition monitoring system for fault detection in rotating machines using PROFINET process data. *Comput Ind* 126:103394. <https://doi.org/10.1016/J.COMPIND.2021.103394>
 102. Yan X, Jia M (2018) A novel optimized SVM classification algorithm with multi-domain feature and its application to fault diagnosis of rolling bearing. *Neurocomputing* 313:47–64. <https://doi.org/10.1016/J.NEUCOM.2018.05.002>
 103. Ben Ali J, Fnaiech N, Saidi L, Chebel-Morello B, Fnaiech F (2015) Application of empirical mode decomposition and artificial neural network for automatic bearing fault diagnosis based on vibration signals. *Applied Acoustics* 89:16–27. <https://doi.org/10.1016/J.APACOUST.2014.08.016>
 104. Shen C, Wang D, Kong F, Tse PW (2013) Fault diagnosis of rotating machinery based on the statistical parameters of wavelet packet paving and a generic support vector regressive classifier. *Measurement* 46:1551–1564. <https://doi.org/10.1016/J.MEASUREMENT.2012.12.011>
 105. Tahir MM, Khan AQ, Iqbal N, Hussain A, Badshah S (2017) Enhancing Fault Classification Accuracy of Ball Bearing Using Central Tendency Based Time Domain Features. *IEEE Access* 5:72–83. <https://doi.org/10.1109/ACCESS.2016.2608505>
 106. Liu J, Xu Z, Zhou L, Nian Y, Shao Y (2019) A statistical feature investigation of the spalling propagation assessment for a ball bearing. *Mech Mach Theory* 131:336–350. <https://doi.org/10.1016/J.MECHMACHTHEORY.2018.10.007>

107. Li C, Sánchez RV, Zurita G, Cerrada M, Cabrera D (2016) Fault Diagnosis for Rotating Machinery Using Vibration Measurement Deep Statistical Feature Learning. *Sensors* 2016, Vol 16, Page 895 16:895. <https://doi.org/10.3390/S16060895>
108. Liu Y, Xue Z, Jia L, Shi T, Ma H (2017) Response Characteristics of Looseness-Rubbing Coupling Fault in Rotor-Sliding Bearing System. *Math Probl Eng* 2017:8742468. <https://doi.org/10.1155/2017/8742468>
109. Ansari AK, Kumar P (2024) Vibration and Acoustics Analyses of Tapered Roller Bearing. *Journal of Vibration Engineering and Technologies* 12:2467–2484. <https://doi.org/10.1007/S42417-023-00991-9/METRICS>
110. Ansari AK, Kumar P (2024) Experimental investigation of the static and dynamic damping behaviour of antifriction bearings. *Nondestructive Testing and Evaluation*. <https://doi.org/10.1080/10589759.2024.2322658>
111. Kumar P, Nigam SP, Kumar N (2014) Vehicular traffic noise modeling using artificial neural network approach. *Transp Res Part C Emerg Technol* 40:111–122. <https://doi.org/10.1016/j.trc.2014.01.006>
112. Kumar P, Hirani H, Agrawal AK (2018) Online condition monitoring of misaligned meshing gears using wear debris and oil quality sensors. *Industrial Lubrication and Tribology* 70:645–655. <https://doi.org/10.1108/ILT-05-2016-0106/FULL/PDF>
113. Li Y, Cheng G, Liu C (2021) Research on bearing fault diagnosis based on spectrum characteristics under strong noise interference. *Measurement* 169:108509. <https://doi.org/10.1016/J.MEASUREMENT.2020.108509>
114. Cen J, Yang Z, Liu X, Xiong J, Chen H (2022) A Review of Data-Driven Machinery Fault Diagnosis Using Machine Learning Algorithms. *Journal of Vibration Engineering and Technologies* 10:2481–2507. <https://doi.org/10.1007/S42417-022-00498-9>

115. Yang Y, Yang W, Jiang D (2018) Simulation and experimental analysis of rolling element bearing fault in rotor-bearing-casing system. *Eng Fail Anal* 92:205–221. <https://doi.org/10.1016/J.ENGFAILANAL.2018.04.053>
116. Zeng M, Zhang W, Chen Z (2019) Group-Based K-SVD Denoising for Bearing Fault Diagnosis. *IEEE Sens J* 19:6335–6343. <https://doi.org/10.1109/JSEN.2019.2910868>
117. Ding Y, Jia M, Miao Q, Cao Y (2022) A novel time–frequency Transformer based on self–attention mechanism and its application in fault diagnosis of rolling bearings. *Mech Syst Signal Process* 168:108616. <https://doi.org/10.1016/J.YMSSP.2021.108616>
118. Zhang S, Zhang S, Wang B, Habetler TG (2020) Deep Learning Algorithms for Bearing Fault Diagnostics - A Comprehensive Review. *IEEE Access* 8:29857–29881. <https://doi.org/10.1109/ACCESS.2020.2972859>
119. Lu C, Wang ZY, Qin WL, Ma J (2017) Fault diagnosis of rotary machinery components using a stacked denoising autoencoder-based health state identification. *Signal Processing* 130:377–388. <https://doi.org/10.1016/J.SIGPRO.2016.07.028>
120. Zhang T, Liu S, Wei Y, Zhang H (2021) A novel feature adaptive extraction method based on deep learning for bearing fault diagnosis. *Measurement* 185:110030. <https://doi.org/10.1016/J.MEASUREMENT.2021.110030>
121. Singh S, Kumar A, Kumar N (2014) Motor Current Signature Analysis for Bearing Fault Detection in Mechanical Systems. *Procedia Materials Science* 6:171–177. <https://doi.org/10.1016/J.MSPRO.2014.07.021>
122. Ali T, #1 D, Abdulhady A, #2 J (2020) Bearing Fault Diagnosis Using Motor Current Signature Analysis and the Artificial Neural Network. 10:
123. Liu T, Chen J, Dong G (2013) Singular spectrum analysis and continuous hidden Markov model for rolling element bearing fault diagnosis. <https://doi.org/10.1177/1077546313496833> 21:1506–1521.

124. Refaat SS, Abu-Rub H, Saad MS, Aboul-Zahab EM, Iqbal A (2013) ANN-based for detection, diagnosis the bearing fault for three phase induction motors using current signal. *Proceedings of the IEEE International Conference on Industrial Technology* 253–258. <https://doi.org/10.1109/ICIT.2013.6505681>
125. Li Y, Wang X, Si S, Huang S (2020) Entropy Based Fault Classification Using the Case Western Reserve University Data: A Benchmark Study. *IEEE Trans Reliab* 69:754–767. <https://doi.org/10.1109/TR.2019.2896240>
126. Sharma A, Amarnath M, Vib PK-IJA, 2018 undefined (2018) Use of feature ranking techniques for defect severity estimation of rolling element bearings. *Int J Acoust Vib* 23:49–56. <https://doi.org/10.20855/ijav.2018.23.11104>
127. Vora S, Yang H (2018) A comprehensive study of eleven feature selection algorithms and their impact on text classification. *Proceedings of Computing Conference* 2017 2018-January:440–449. <https://doi.org/10.1109/SAL.2017.8252136>
128. Ragulskis M, Cao M, Zimroz R, Fakher C, Konieczny Ł, Betta G, Altaf M, Akram T, Attique Khan M, Iqbal M, Munawwar M, Ch I, Hsu C-H (2022) A New Statistical Features Based Approach for Bearing Fault Diagnosis Using Vibration Signals. *Sensors* 2022, Vol 22, Page 2012 22:2012. <https://doi.org/10.3390/S22052012>
129. Ali NJ, García JM (2010) Experimental studies on the dynamic characteristics of rolling element bearings. *Proceedings of the Institution of Mechanical Engineers, Part J: Journal of Engineering Tribology* 224:659–666. <https://doi.org/10.1243/13506501JET698>
130. Mayank T, Gupta PK, Prakash O (2002) Experimental study of a rotor supported by deep groove ball bearing. *International Journal of Rotating machinery* 8:243–258
131. Patil MS, Mathew J, Rajendrakumar PK, Karade S (2010) Experimental studies using response surface methodology for condition monitoring of ball bearings. *J Tribol* 132:. <https://doi.org/10.1115/1.4002520/468763>

132. Li D, Kang YS (2016) Simulation and Experimental Validation of Tapered Roller Bearing Vibration Induced by Geometrical Imperfection on Cup Raceway Desheng. *Proceedings of the ASME* 2014 1–8
133. Lostado R, Martinez RF, Mac Donald BJ (2015) Determination of the contact stresses in double-row tapered roller bearings using the finite element method, experimental analysis and analytical models. *Journal of Mechanical Science and Technology* 29:4645–4656. <https://doi.org/10.1007/s12206-015-1010-4>
134. Lovejoy Couplings Jaw Type 3-Piece Flexible Coupling Bodies, 1-3/4" Body Diameter. <https://www.dultmeier.com/jaw-type-3-piece-flexible-coupling-bodies-1-34-body-diameter>. Accessed 26 May 2025
135. Harris TA (1991) *Introduction to Rolling Bearings*. 1–1086
136. Taylor JJ (1994) *The vibration analysis handbook*. 360
137. Lu S (2021) A Transfer Matrix Method for Nonlinear Vibration Analysis of Rotor-Bearing Systems. *Proceedings of the ASME Design Engineering Technical Conference Part F168436-4:75–83*. <https://doi.org/10.1115/DETC1991-0321>
138. Mevada H, Patel D (2016) Experimental Determination of Structural Damping of Different Materials. *Procedia Eng* 144:110–115. <https://doi.org/10.1016/J.PROENG.2016.05.013>
139. Dynamics and Vibrations: Notes: Forced Vibrations. https://www.brown.edu/Departments/Engineering/Courses/En4/Notes/vibrations_forced/vibrations_forced.htm. Accessed 1 Jun 2023
140. Tweten DJ, Ballard Z, Mann BP (2014) Minimizing error in the logarithmic decrement method through uncertainty propagation. *J Sound Vib* 333:2804–2811. <https://doi.org/10.1016/J.JSV.2014.02.024>
141. Singh B, Nanda BK (2012) Estimation of Damping in Layered Welded Structures with Unequal Thickness. *Shock and Vibration* 19:1463–1475. <https://doi.org/10.3233/SAV-2012-0720>

142. Bilgili D, Budak E, Altintas Y (2022) Multibody dynamic modeling of five-axis machine tools with improved efficiency. *Mech Syst Signal Process* 171:108945. <https://doi.org/10.1016/J.YMSSP.2022.108945>
143. Sun P, Wang D (2021) Comparison of damping parameters based on the half-power bandwidth methods of viscous and hysteretic damping models. *Journal of Vibration and Control* 29:968–979. <https://doi.org/10.1177/10775463211054646>
144. Duchemin M, Berlioz A, Ferraris G (2006) Dynamic behavior and stability of a rotor under base excitation. *Journal of Vibration and Acoustics, Transactions of the ASME* 128:576–585. <https://doi.org/10.1115/1.2202159>
145. Wang X, Liu K, Liu H, He Y (2018) Damping Identification with Acceleration Measurements Based on Sensitivity Enhancement Method. <https://doi.org/10.1155/2018/6476783>
146. Presas A, Valentin D, Egusquiza E, Valero C, Egusquiza M, Bossio M (2017) Accurate Determination of the Frequency Response Function of Submerged and Confined Structures by Using PZT-Patches. *Sensors (Basel)* 17:660. <https://doi.org/10.3390/S17030660>
147. Kazeminasab M (2021) Experimental Investigation on the Dynamics of a dummy Blade and Disk coupled by a dovetail root joint. *Webthesis - Politecnico di Torino*
148. Mogal SP, Lalwani DI (2015) Experimental investigation of unbalance and misalignment in rotor bearing system using order analysis. *Journal of Measurements in Engineering* 3:114–122
149. Cao MS, Sha GG, Gao YF, Ostachowicz W (2017) Structural damage identification using damping: a compendium of uses and features. *Smart Mater Struct* 26:043001. <https://doi.org/10.1088/1361-665X/AA550A>
150. Inman D (2001) DAMPING MODELS. *Encyclopedia of Vibration* 335–342. <https://doi.org/10.1006/RWVB.2001.0060>

151. Ansari AK, Kumar P (2023) Vibration and Acoustics Analyses of Tapered Roller Bearing. *Journal of Vibration Engineering and Technologies* 1–18. <https://doi.org/10.1007/S42417-023-00991-9/METRICS>
152. Feng Z, Zuo MJ (2012) Vibration signal models for fault diagnosis of planetary gearboxes. *J Sound Vib* 331:4919–4939. <https://doi.org/10.1016/j.jsv.2012.05.039>
153. Zhu A, Yang S, Li Q, Yang J, Fu C, Zhang J, Yao D (2019) Research on Prediction of Metro Wheel Wear Based on Integrated Data-Model-Driven Approach. *IEEE Access* 7:178153–178166. <https://doi.org/10.1109/ACCESS.2019.2950391>
154. Cao H, Fan F, Zhou K, He Z (2016) Wheel-bearing fault diagnosis of trains using empirical wavelet transform. *Measurement (Lond)* 82:439–449. <https://doi.org/10.1016/j.measurement.2016.01.023>
155. Mohanty AR (2014) *Machinery Condition Monitoring Principles and Practices*, 1st Editio. CRC Press, Boca Raton
156. Corni I, Symonds N, Wood RJK, Wasenczuk A, Vincent D (2015) Real-time on-board condition monitoring of train axle bearings. *Stephenson Conference Research for Railways 2015* 2015-April:477–489
157. Bergland GD (1969) A guided tour of the fast Fourier Transform. *IEEE Spectr* 6:41–52. <https://doi.org/10.1109/MSPEC.1969.5213896>
158. Rai VK, Mohanty AR (2007) Bearing fault diagnosis using FFT of intrinsic mode functions in Hilbert-Huang transform. *Mech Syst Signal Process* 21:2607–2615. <https://doi.org/10.1016/j.ymssp.2006.12.004>
159. Mehala, Neelam and RDahiya (2008) A comparative study of FFT, STFT and wavelet techniques for induction machine fault diagnostic analysis. *Proceedings of the 7th WSEAS international conference on Computational intelligence, man-machine systems and cybernetics* 203–208
160. Gunerkar R JA and BS (2018) Experimental study of rolling element bearing with localized defect using response surface methodology. *International*

conference on advances and soft computing applications in design and manufacturing

161. Hinkelmann K (2012) Design and Analysis of Experiments. John Wiley & Sons
162. Souza HJC de, Silva MB, B. Moyses C, Alberto FL, Pontes FJ, R. Ferreira U, Duarte RN, Silva CES da (2013) Robust Design and Taguchi Method Application. Design of Experiments - Applications. <https://doi.org/10.5772/56580>
163. Sarkar K, Roy RK (2010) Book Review #3: A Primer on the Taguchi Method A Primer on the Taguchi Method 2nd edition. <https://doi.org/10.13140/RG.2.2.21506.84163>
164. Kumar P, Parkash R (2016) Experimental investigation and optimization of EDM process parameters for machining of aluminum boron carbide (Al-B₄C) composite. Machining Science and Technology 20:330–348. <https://doi.org/10.1080/10910344.2016.1168931>
165. Meadt R (1990) The Non-orthogonal Design of Experiments. J R Statist Soc A 153:151–201
166. Judd CM, McClelland GH, Ryan CS (2017) Data Analysis: A Model Comparison Approach to Regression, ANOVA, and Beyond. <https://doi.org/10.4324/9781315744131>
167. Ahmad S, Singari RM, Mishra RS (2020) Modelling and optimisation of magnetic abrasive finishing process based on a non-orthogonal array with ANN-GA approach. Transactions of the Institute of Metal Finishing 98:186–198. <https://doi.org/10.1080/00202967.2020.1776966>
168. Myers H Raymond MCD& A-CCC (2016) Response Surface Methodology: Process and Product Optimization Using ... -. Wiley Series in Probability And Statistics, 4th ed, John Wiley & Sons Inc, New Jersey 894
169. Chen H, Wang W, Liang H, Zhang H (2023) Elastohydrodynamic lubrication analysis of tapered roller bearing considering effect of free ends. Tribol Int 180:108304. <https://doi.org/10.1016/J.TRIBOINT.2023.108304>

170. Maccioni L, Chernoray VG, Mastrone MN, Bohnert C, Concli F (2022) Study of the impact of aeration on the lubricant behavior in a tapered roller bearing: Innovative numerical modelling and validation via particle image velocimetry. *Tribol Int* 165:107301. <https://doi.org/10.1016/J.TRIBOINT.2021.107301>
171. Tong VC, Hong SW (2017) The effect of angular misalignment on the stiffness characteristics of tapered roller bearings. *Proc Inst Mech Eng C J Mech Eng Sci* 231:712–727. <https://doi.org/10.1177/0954406215621098>
172. Tong VC, Hong SW (2016) The effect of angular misalignment on the running torques of tapered roller bearings. *Tribol Int* 95:76–85. <https://doi.org/10.1016/J.TRIBOINT.2015.11.005>
173. Goyal D, Vanraj, Pabla BS, Dharmi SS (2019) Non-contact sensor placement strategy for condition monitoring of rotating machine-elements. *Engineering Science and Technology, an International Journal* 22:489–501. <https://doi.org/10.1016/J.JESTCH.2018.12.006>
174. Bernard P (1975) *L eq , SEL WHAT? WHY? WHEN? What are L eq and SEL?* Brüel & Kjær
175. Sun Q, Tang Y (2002) Singularity analysis using continuous wavelet transform for bearing fault diagnosis. *Mech Syst Signal Process* 16:1025–1041. <https://doi.org/10.1006/MSSP.2002.1474>
176. Patel S, Shah U, Khatri B, Patel U (2022) Research progress on bearing fault diagnosis with localized defects and distributed defects for rolling element bearings. <https://doi.org/10.1177/09574565221114661>. <https://doi.org/10.1177/09574565221114661>
177. Orhan S, Aktürk N, Çelik V (2006) Vibration monitoring for defect diagnosis of rolling element bearings as a predictive maintenance tool: Comprehensive case studies. *NDT and E International* 39:293–298. <https://doi.org/10.1016/J.NDTEINT.2005.08.008>

178. Susilo DD, Widodo A, Prahasto T, Nizam M (2017) Fault diagnosis of roller bearing using parameter evaluation technique and multi-class support vector machine. AIP Conf Proc
179. Thorsen OV, Dalva M (1995) A Survey of Faults on Induction Motors in Offshore Oil Industry, Petrochemical Industry, Gas Terminals, and Oil Refineries. IEEE Trans Ind Appl 31:1186–1196. <https://doi.org/10.1109/28.464536>
180. Jamil MA, Khanam S (2024) Influence of One-Way ANOVA and Kruskal–Wallis Based Feature Ranking on the Performance of ML Classifiers for Bearing Fault Diagnosis. Journal of Vibration Engineering and Technologies 12:3101. <https://doi.org/10.1007/S42417-023-01036-X>
181. Attoui I, Oudjani B, Boutasseta N, Fergani N, Bouakkaz MS, Bouraiou A (2020) Novel predictive features using a wrapper model for rolling bearing fault diagnosis based on vibration signal analysis. International Journal of Advanced Manufacturing Technology 106:3409–3435. <https://doi.org/10.1007/S00170-019-04729-4>
182. Jamil M, Vibration SK-IJ of A&, 2022 undefined (2022) Fault Classification of Rolling Element Bearing in Machine Learning Domain. International Journal of Acoustics & Vibration 27:77–90. <https://doi.org/https://doi.org/10.20855/ijav.2022.27.21829>
183. Taha Jijo B, Mohsin Abdulazeez A (2021) Classification Based on Decision Tree Algorithm for Machine Learning. Journal of Applied Science and Technology Trends 2:20–28. <https://doi.org/10.38094/jastt20165>
184. Lee HH, Nguyen NT, Kwon JM (2007) Bearing Diagnosis Using Time-Domain Features and Decision Tree. Lecture Notes in Computer Science (including subseries Lecture Notes in Artificial Intelligence and Lecture Notes in Bioinformatics) 4682 LNAI:952–960. https://doi.org/10.1007/978-3-540-74205-0_99
185. James G, Witten D, Hastie T, Tibshirani R (2021) Support Vector Machines. 367–402. https://doi.org/10.1007/978-1-0716-1418-1_9

186. Rojas A, Nandi AK (2005) Detection and classification of rolling-element bearing faults using support vector machines. 2005 IEEE Workshop on Machine Learning for Signal Processing 153–158. <https://doi.org/10.1109/MLSP.2005.1532891>
187. Wang M, Chen Y, Zhang X, Chau TK, Ching Iu HH, Fernando T, Li Z, Ma M (2022) Roller Bearing Fault Diagnosis Based on Integrated Fault Feature and SVM. *Journal of Vibration Engineering and Technologies* 10:853–862. <https://doi.org/10.1007/S42417-021-00414-7>
188. Nayana BR, Geethanjali P (2017) Analysis of Statistical Time-Domain Features Effectiveness in Identification of Bearing Faults from Vibration Signal. *IEEE Sens J* 17:5618–5625. <https://doi.org/10.1109/JSEN.2017.2727638>
189. James G, Witten D, Hastie T, Tibshirani R, Taylor J (2023) An Introduction to Statistical Learning. <https://doi.org/10.1007/978-3-031-38747-0>
190. Feurer M, Methods FH-A machine learning:, 2019 undefined Hyperparameter optimization. [library.oapen.org](https://library.oapen.org/handle/document/44444)M Feurer, F HutterAutomated machine learning: Methods, systems, challenges, 2019•[library.oapen.org](https://library.oapen.org/handle/document/44444)
191. Skelsey P (2021) Forecasting risk of crop disease with anomaly detection algorithms. *Phytopathology* 111:321–332. <https://doi.org/10.1094/PHYTO-05-20-0185-R/ASSET/IMAGES/LARGE/PHYTO-05-20-0185-RF7.JPEG>
192. Wang Z, Hutter F, Zoghi M, Matheson D, De Freitas N (2016) Bayesian Optimization in a Billion Dimensions via Random Embeddings. *Journal of Artificial Intelligence Research* 55:361–387. <https://doi.org/10.1613/JAIR.4806>
193. Bergstra J, Bardenet R, Bengio Y, Kégl B (2011) Algorithms for Hyper-Parameter Optimization. *Adv Neural Inf Process Syst* 24:
194. Liu H (2015) Comparing Welch ANOVA, a Kruskal-Wallis test, and traditional ANOVA in case of heterogeneity of variance

LIST OF PUBLICATIONS AND THEIR PROOFS

The work conducted in this research has resulted in the following major publications:

Research Papers Published/ Accepted in Journals

- 1) Ansari, Abdul Khaliq, and Paras Kumar. "Vibration and acoustics analyses of tapered roller bearing." *Journal of Vibration Engineering & Technologies* 12.2 (2024): 2467-2484. <https://doi.org/10.1007/s42417-023-00991-9> (SCIE, IF-2.7).
- 2) Ansari, Abdul Khaliq, and Paras Kumar. "Experimental investigation of the static and dynamic damping behaviour of antifriction bearings." *Nondestructive Testing and Evaluation* (2024): 1-22. <https://doi.org/10.1080/10589759.2024.2322658> (SCIE, IF-4.2).
- 3) Ansari, Abdul Khaliq, and Paras Kumar. "Vibro-acoustic analysis of defective taper roller bearings." *Tribology International*. 199 (2024): 110044. <https://doi.org/10.1016/j.triboint.2024.110044> (SCIE, IF-6.9).
- 4) Ansari, Abdul Khaliq, and Paras Kumar. "Enhancing Machine Learning Classifier Performance in Bearing Fault Diagnosis through Feature-Based Ranking." *Mesurement*. 257 (2025): 118661 <https://doi.org/10.1016/j.measurement.2025.118661> (SCIE, IF- 5.6).

Research Papers Presented in International Conferences

- 1) Ansari, A.K., Kumar, P. and Rastogi, V., 2022. Dynamic behavior of aluminium matrix composite rotor on bearing vibration. *Materials Today: Proceedings*, 62, pp.233-238. <https://doi.org/10.1016/j.matpr.2022.03.026> "International Conference on Advances in Materials and Mechanical Engineering (ICAMME – 2022) held on 18th -19th Feb 2022 at AKJEC, UP, India. (Scopus Index)
- 2) Ansari, A.K., Kumar, P. and Rastogi, V., 2024. Machine Learning Algorithms for Multi-Defect Bearing Analysis. "International Conference on Manufacturing, Material Science and Engineering (ICMMSE-2024), held on 16th -17th August 2024 at Vignan Institute of Technology, Hyderabad, Telangana, India. (Scopus Index) (AIP conference proceedings)

Your Submission JVET-D-22-01387R1 - [EMID:5994dc76709e0755] External



Journal of Vibration Engineering & Technologies (JVET) <em@editorialmanager.com>

Fri, Apr 21, 2023, 2:21 PM ★ ↩ ⋮

to me ▾

Dear Mr. Ansari,

We are pleased to inform you that your manuscript, "Vibration and acoustics analyses of tapered roller bearing", has been accepted for publication in Journal of Vibration Engineering & Technologies.

You will receive an e-mail in due course regarding the production process.

Please remember to quote the manuscript number, JVET-D-22-01387R1, whenever inquiring about your manuscript.

With kind regards,
S.K. Lai
Associate Editor
Journal of Vibration Engineering & Technologies

Comments to the author (if any):

Your article has been accepted for publication DOI - 10.1080/10589759.2024.2322658 External

GNTF-production@journals.tandf.co.uk
to me ▾

Wed, Feb 21, 2024, 6:19 AM ★ ↩ ⋮



Dear Abdul Khaliq Ansari,

Congratulations! We are pleased to share that your article "Experimental investigation of the static and dynamic damping behaviour of antifriction bearings" has been accepted for publication in Nondestructive Testing and Evaluation.

To move forward with publication, we need you to review your Open Access options and accept the terms and conditions of an author publishing agreement.

We'll start with some questions that will inform the details we include in your agreement.

[START AGREEMENT PROCESS](#)

If you have questions about publishing your article, don't hesitate to contact us directly at GNTF-production@journals.tandf.co.uk

We look forward to seeing your article published, and we are pleased to have you in our authorship community.

Kind regards,

Nondestructive Testing and Evaluation Production Team



Your Submission External

Tribology International <em@editorialmanager.com>
to me ▾

Thu, Jul 25, 2024, 12:45 PM ☆ ↶ ⋮

Ms. Ref. No.: **TRIBINT-D-24-01762R2**
Title: Vibro-acoustic analysis of defective taper roller bearings
Tribology International

Dear Dr. Mr. Abdul Khaliq Ansari,

I am very pleased to be able to tell you that the above paper has now been accepted for publication in Tribology International and has been sent to our publishers for processing. You should be receiving proofs and copyright forms in due course.

We appreciate and value your contribution to Tribology International. We regularly invite authors of recently published manuscript to participate in the peer review process. If you were not already part of the journal's reviewer pool, you have now been added to it. We look forward to your continued participation in our journal, and we hope you will consider us again for future submissions.

We encourage authors of original research papers to share the research objects – including raw data, methods, protocols, software, hardware and other outputs – associated with their paper. More information on how our open access Research Elements journals can help you do this is available at https://www.elsevier.com/authors/tools-and-resources/research-elements-journals?dgcid=ec_em_research_elements_email.

Yours sincerely,

Benyebka Bou-Said, Prof.
Editor-in-Chief

Comments from the Editors and Reviewers:

[MEAS-D-25-04374R2] – Congratulations, your paper has been accepted! External Inbox x Updates x

Measurement <em@editorialmanager.com>
to me ▾

Tue, Aug 5, 7:06 PM (5 days ago) ★ ↶ ⋮

Ms. Ref. No.: **MEAS-D-25-04374R2**
Title: Enhancing Machine Learning Classifier Performance in Bearing Fault Diagnosis through Feature-Based Ranking
Measurement

Dear Mr. Abdul Khaliq Ansari,

I am pleased to confirm that your paper "Enhancing Machine Learning Classifier Performance in Bearing Fault Diagnosis through Feature-Based Ranking" has been accepted for publication in Measurement.

Comments from the Editor and Reviewers can be found below (if available).

Thank you for submitting your work to this journal.

What happens next?

1. Our production department will create a proof of your article, which will be shared with you for approval.
2. We will send you a link to your post-acceptance online author forms. These forms include the publishing agreement for you to complete as well as confirming whether your article is to be published open access or subscription. We kindly request you complete the forms as soon as possible upon receipt of the link.

If we need any further information from you during the typesetting process, we will let you know.

For further information about the proofing process, please click this link: https://service.elsevier.com/app/answers/detail/a_id/6007/p/10592/supporthub/publishing/related/

CURRICULUM VITAE/BRIEF PROFILE

JOB EXPERIENCE

- **Designation: Application Engineer, Simulation**

Institute Name: Prolim Solutions India Pvt. Ltd., Bangalore

Duration: From July 2024 to Present.

Responsibilities:

- Develop and build 1D simulation models to simulate and analyze dynamic systems, including hydraulic, pneumatic, thermal, or mechatronic systems.
- Assist in coordinating and executing all technical activities throughout the sales opportunity such as technical discovery, product presentations, demonstrations, evaluations, POCs.
- Provide technical expertise and support to teams, troubleshooting simulation-related issues, and proposing innovative solutions.

- **Designation: Guest Faculty**

Institute Name: Delhi Technological University (DTU), New Delhi.

Duration: From Aug. 2022 to June 2024.

Responsibilities:

- Teaching at Bachelors Level (Subjects: Kinematics of Machines, Operational Research & Engineering Graphics in AutoCAD).
- Demonstrating experiments to students in engineering labs.

- **Designation: Guest Faculty**

Institute Name: Jamia Millia Islamia (JMI), New Delhi.

Duration: From Aug. 2016 to May 2018.

Responsibilities:

- Teaching at Bachelors Level (Subjects: Basic Mechanical Engineering, Engineering Mechanics, Engineering Graphics).
- Demonstrating experiments to students in engineering labs.

- **Designation: Guest Faculty**

Institute Name: Zakir Hussain College of Engineering & Technology (ZHCET), AMU Aligarh.

Duration: From Sept. 2014 to May 2015.

Responsibilities:

- Teaching at Bachelors & Masters Level (Subjects: Engineering Drawing, Strength of Materials, AutoCAD).
- Demonstrating experiments to students in engineering labs.
- Making examination papers and conducting exams.

ACADEMIC PROFILE

- 2018 to Present
Doctor of Philosophy in Mechanical Engineering (Mechanical Engineering) with course work CPI of **9.0** (on scale of 10) with 1st division (Honours) from Delhi Technological University with Institute fellowship.
Dissertation: *Modeling and Experimental Analysis of Multifaults in a Tapered Roller Bearing System.*
Work brief:
 - Research involvement in the field of Multifaults analysis and system damping of rotor bearing system.
 - Developed a condition monitoring system to predict bearing component failure and classify defect using machine learning based on sensor data.
 - Knowledge of DAQ, vibration measurement and Impact hammer test.
 - Machine condition monitoring.
- 2012 to 2014
Master of Technology in Mechanical Engineering (Machine Design) with CPI of **8.778** (on scale of 10) with 1st division (Honours) from Aligarh Muslim University with MHRD Scholarship.
Dissertation: *Experimental Study of Balancing of Rotor Bearing-System Using Machinery Fault Simulator-Lite.*
Project: *Study the Effect of Coupling Misalignment on Vibration Signature Using MFS-Lite.*
- 2007 to 2011
Bachelor of Technology in Mechanical Engineering from Aligarh Muslim University with CPI **7.241** (on scale of 10) with 1st division.
Project: *Design of roller conveyor assembly for HFIW TUBE MILL.*
Summer Training: Four weeks of training in Diesel Bogie Section at Training Center, Northern Railway, Charbagh, Lucknow, U.P.
- **XII** Standard from Senior Secondary School, AMU Aligarh in 2006 (1st division).
- **X** Standard from City High School, AMU Aligarh in 2004 (1st division).

ACADEMIC ACHIEVEMENTS AND DISTINCTIONS

- Delivered a Lecture on a series of 5 days “HANDS-ON TRAINING ON AUTOCAD FOR FIRST-YEAR STUDENTS in the Department of Mechanical Engineering, DTU Delhi in Four consecutive semester of sessions 2021-2022

and 2022-2023.

- Organising member in One-day seminar on “NOISE FUNDAMENTALS, MEASUREMENT AND ANALYSIS” in the Department of Mechanical, Production & Industrial and Automobile Engineering, Delhi Technological University, Delhi in OFFLINE MODE on 26th May 2023.
- Organising member in One Week Short Term Training Program on “ROBOTICS & ARTIFICIAL INTELLIGENCE” in the Department of Mechanical, Production & Industrial and Automobile Engineering, Delhi Technological University. Delhi from 17 to 21 MAY, 2022 in physical mode.
- 2012: Scored a percentile of 93.8 in the Graduate Aptitude Test in Engineering (GATE) 2012 conducted by the IIT. Eligible for the assistantship governed by the MHRD, Government of India.
- Qualified all India Exam Gate in 2012,2013 and 2015

COMPUTER SKILLS

- AutoCAD, SolidWorks, MATLAB, AMESim
- MS Office, HAP

WORKSHOPS AND FDP

- Successfully participated in SERB sponsored National High-End workshop on “Statistical Tools: Modeling and Optimisation” (STMO-2022) organised by Department of Industrial and Production Engineering, NIT-Jalandhar from 18th -24th July 2022.
- Participated and completed successfully one-week Online FDP on “Recent Advancements in Design and Manufacturing (RADM-2022)” from 22th- 26th March 2022 at Mechanical Engineering Section, University Polytechnic, AMU, Aligarh.
- Participated & completed successfully AICTE Training and Learning (ATAL) Academy Online Elementary FDP on "Advanced MATLAB for Scientific Computing" from 13th-17th September 2021 at University Polytechnic, AMU Aligarh.
- Participated & completed successfully AICTE Training and Learning (ATAL) Academy Online Elementary FDP on "Computational techniques in Engineering" from 2th-6th August 2021 at University Polytechnic, AMU Aligarh.
- Attended the online Faculty Development Programme on “Vibration Analysis & Condition Monitoring for Rotating Machines” Organized at Indira

Gandhi Institute of Technology, Sarang, Dhenkanal, Odisha, India during 05-09 October, 2020 under TEQIP-III.

- Attended the short-term course on “Vibration Analysis of Rotor Bearing Systems” under TEQIP-III held at IIT Delhi from 02nd Mar. to 06th Mar., 2020.
- Successfully completed E-Recourses: A Gateway for research (2019) organised by central library, DTU, Delhi from 2th-6th September 2019.
- Participated in the TEQIP-III sponsored One-week international lecture series on Bondgraph Modelling and Simulation (BMS-2018) organized by Mechanical Engineering Department DTU, Delhi from 1st to 5th October 2018. (One Week).

PERSONAL DETAILS

Name:	Abdul Khaliq Ansari
Father's Name:	Mr. Abdul Razzaq
Date of Birth:	24th Sept, 1989
Passport No.:	B7802283 (Indian)
Marital Status:	Married
Hobbies & Interests:	Reading & listening ghazals, Calligraphy, Computer Savvy.
Languages Known:	English, Urdu & Hindi.

I hereby declare that the given above information are true to the best of my knowledge.

Place: Delhi

Abdul Khaliq Ansari